DOCTORAT MATIERE BRETAGNE MOLECULES LOIRE ET MATERIAUX

UNIVERSITÉ DE NANTES

THESE DE DOCTORAT DE

L'UNIVERSITE DE NANTES
COMUE UNIVERSITE BRETAGNE LOIRE

ECOLE DOCTORALE N° 596
Matière, Molécules, Matériaux
Spécialité : Chimie Analytique et Radiochimie

Par
« Corentin JACQUEMMOZ »

ULTRAFAST MULTIDIMENSIONAL NMR FOR THE MONITORING OF CHEMICAL REACTIONS

Thèse présentée et soutenue à Nantes, le 21 septembre 2020
Unité de recherche : Laboratoire CEISAM

Rapporteurs :

Stéphane Viel — Professeur des universités, Aix-Marseille Université, ICR
Marc-André Delsuc — Directeur de recherche, Université de Strasbourg, IGBMC

Composition du Jury :

Président :	Denis Merlet	Professeur des universités, Université Paris-Saclay, ICMMO
Examinatrice :	Laura Castanar	Reaserch Fellow, University of Manchester, Chemistry department
Dir. de thèse :	Jean-Nicolas Dumez	Chargé de recherche, Université de Nantes, CEISAM

Remerciements

Dans un premier temps, je tiens tout d'abord à remercier Angela Marinetti ainsi que Jean-Michel Bouler pour m'avoir accueilli respectivement au sein de l'ICSN à Gif-sur-Yvette et du CEISAM à Nantes.

Je tiens également à remercier tous les membres du jury, Marc-André Delsuc, Stéphane Viel, Laura Castanar et Denis Merlet pour avoir pris le temps d'évaluer le travail de ces trois ans de thèse.

Ensuite, j'aimerais dire un immense merci à mon directeur de thèse Jean-Nicolas Dumez pour m'avoir donné la chance de travailler sur cette thèse, pour son temps, ses nombreuses explications et conseils ainsi que son soutien pendant la totalité de la thèse.

Je tiens également à exprimer ma reconnaissance à tous mes collègues de l'ICSN et du CEISAM. J'aimerais remercier tout particulièrement Louise et Ludmilla pour leur aide et leur soutien pendant mon année à l'ICSN, mais aussi Camille, Claire-Marie, Anaïs, Luiza, Ghanem, Maria-Grazia et même Florian, pour tous les bons moments passés en pauses café. Je remercie également tous les permanents que j'ai pu côtoyer à l'ICSN et qui ont contribué à la bonne ambiance du laboratoire tels que Nelly, Véronique, Alda, Guillaume, Nadine, Carine, Ewen et Christina. J'adresse un grand merci à François pour ses nombreux conseils et son aide concernant les (nombreux) problèmes que l'on a eus sur notre pompe HPLC. Je voudrais également remercier tous mes collègues de l'équipe EBSI, Dylan, Achille, Rituraj, Célia, Virginie, Sophie, Lenny, Thomas, Shrikant, Mathilde, Estelle, Arnab, Patrick, Benoit, John, Anne-Marie, Illa, Serge et Gérald pour leur bonne humeur. Je remercie particulièrement Virginie et Benoit pour leur aide concernant les spectromètres.

Enfin, j'aimerais remercier ma famille et en particulier mes parents pour leur soutien au cours de ces trois ans.

Résumé de la thèse

Introduction

La spectroscopie de résonance magnétique nucléaire (RMN) est très utilisée pour le suivi de réactions chimiques. En général, le suivi se fait à l'aide de spectres 1D. Cependant, en raison de la faible dispersion des signaux en proton, il y a un fort risque de recouvrement. Pour limiter ce problème, il est possible de séparer les signaux grâce à l'introduction d'une ou plusieurs autres dimensions. Cependant, pour créer ces dimensions, il est nécessaire d'incrémenter un délai un grand nombre de fois, ce qui amène à des durées d'expériences trop longues pour pouvoir les utiliser pour un suivi de réaction. Dans un premier temps, nous allons voir les méthodes déjà existantes qui permettent de faire du suivi de réaction, et certaines façons d'accélérer l'acquisition d'expériences multidimensionnelles. Dans un second temps, nous nous intéresseront à la façon dont l'encodage spatial permet d'accélérer deux expériences particulièrement utiles pour l'analyse de mélanges : la DOSY (Diffusion Ordered SpectroscopY) et les expériences multi quanta. Ensuite, la possibilité de faire un suivi de réaction en flux à l'aide d'expériences spatialement encodés sera étudiée. Finalement, nous verrons comment l'encodage spatial peut également permettre l'accélération d'expériences 3D DOSY.

Résumé de la littérature

Afin de pouvoir comprendre les mécanismes de réaction et développer de nouvelles méthodes de synthèse, il est nécessaire de pouvoir suivre la façon dont les réactions se passent. Pour cela plusieurs techniques analytiques peuvent être utilisées et la RMN est l'une d'entre elle.

Le suivi de réactions peut se faire directement dans un tube RMN, par exemple en synthèse organique, pour des réactions enzymatiques, de transformation de biomasse ou bien diverses réactions électrochimiques. Cependant, effectuer la réaction dans un tube RMN peut amener à des résultats assez différents comparés à une réaction faite dans des conditions plus classiques. Pour cette raison, différentes méthodes de suivi de réaction en flux ont été développées. Dans ce cas la réaction est faite dans un réacteur classique et une fraction du mélange réactionnel est continûment prélevée et envoyée vers un spectromètre. Ce type de suivi peut être combiné avec plusieurs autres types d'analyses tels que la chromatographie liquide ou la spectroscopie infra rouge.

L'utilisation de spectres 1D pour le suivi de réactions atteint ses limites lorsque des mélanges un peu trop complexes sont analysés, en raison du recouvrement des signaux. Une façon de limiter ce recouvrement est d'utiliser des méthodes multidimensionnelles. Ces expériences multidimensionnelles reposent sur le schéma :

Préparation – Evolution (t_1) – Mixage – Acquisition (t_2)

Avec une répétition de ce schéma pour échantillonner une grille de valeurs de t_1. Le résultat de ce genre d'expérience est une matrice 2D sur laquelle on applique une transformée de Fourier 2D de manière à obtenir un spectre.

Il existe de nombreuses expériences multidimensionnelles telles que les expériences COSY (COrelation SpectroscopY), HSQC (Heteronuclear Single Quantum Correlation), ou J-résolue et certaines d'entre elles sont particulièrement adaptées à l'analyse de mélanges tel que la DOSY (Diffusion Ordered SpectroscopY) ou la MQS (Multiple Quantum Spectroscopy). Cependant, en raison de la durée nécessaire pour acquérir des spectres 2D, ceux-ci sont rarement utilisés tels quels pour le suivi de réactions.

Au fil des années plusieurs méthodes ont été suggérées de manière à accélérer l'acquisition de spectres 2D. On peut citer par exemple les méthodes d'impulsions rapides qui consistent à réduire le temps entre deux incréments tel que la SOFAST (band-Selective Optimized Flip-Angle Short-Transient heteronuclear multiple quantum coherence) qui repose sur l'excitation sélective des protons amides de protéines pour diminuer le temps de relaxation effectif. Une autre méthode utilisée est l'échantillonnage non uniforme dans lequel l'incrémentation des délais t_1 se fait différemment par rapport à des expériences conventionnelles.

L'approche qui permet l'accélération la plus importante est l'encodage spatial ; développé par Frydman en 2002. Cette méthode consiste à réaliser tous les incréments en parallèle dans des régions différentes du tube RMN. Grâce à ce type d'expérience, il est possible d'acquérir un spectre 2D en moins d'une seconde, ce qui lui a valu le nom d'expérience ultrarapide. Il est possible en utilisant cette méthode d'encoder le déplacement chimique pour des expériences de type COSY ou HSQC, mais aussi l'information de diffusion pour la DOSY. Cette approche a été utilisée pour différentes applications et notamment pour le suivi de réactions mais aussi pour l'analyse de mélanges hors équilibres tels que des échantillons hyperpolarisés (échantillons dont la polarisation diminue très rapidement au cours du temps).

Caractérisation de la DOSY spatialement encodée

Parmi les expériences RMN particulièrement adaptées à l'analyse de mélanges, on peut citer la DOSY (Diffusion Ordered SpectroscopY) qui est souvent comparée à une chromatographie virtuelle car elle permet de séparer les signaux de différentes molécules en fonction du coefficient de diffusion de ces dernières. Cette méthode repose sur l'acquisition successive de plusieurs spectres 1D dans lesquels l'intensité d'une paire de gradients est augmentée progressivement. Cela permet d'encoder le mouvement aléatoire translationnel des molécules. Le résultat de cette expérience est une série de spectres 1D dans lesquels l'intensité des signaux décroit d'un facteur lié au coefficient de diffusion de la molécule en question. Cette atténuation peut être exprimée grâce à l'équation de Stesjkal Tanner. À partir de cette équation, il est possible d'extraire les coefficients de diffusion pour chaque signal et d'en

faire une représentation graphique 2D dans laquelle la première dimension correspond au déplacement chimique et la seconde correspond au coefficient de diffusion.

Cette méthode a montré sa pertinence pour l'analyse de mélanges dans de nombreux cas. Cependant, puisqu'il est nécessaire d'incrémenter la valeur de l'intensité des gradients, cela peut mener à des expériences relativement longues, d'où l'idée d'utiliser l'encodage spatial pour l'accélérer. Cette méthode a déjà été utilisée dans plusieurs cas, mais une caractérisation précise des paramètres utilisés n'a pas encore été faite.

Pour transformer les expériences DOSY en une version spatialement encodée, nous nous sommes appuyés sur les travaux de Frydman et Keeler. De manière à réaliser l'encodage spatial, deux blocs d'encodage spatial doivent être introduits dans la séquence (nous nous sommes limités à différentes variations de l'écho stimulé). Ces blocs sont composés d'une impulsion balayée en fréquence, que l'on nommera par la suite impulsion chirp, appliquée en même temps qu'une impulsion de gradient. Dans le cas de la DOSY, les deux blocs sont espacés d'un délai, appelé délai de diffusion, et le gradient d'encodage dure deux fois plus longtemps que l'impulsion chirp. De plus, le signe des gradients d'encodage est le même durant les deux blocs. Cette combinaison chirp et gradient a pour effet de faire subir une aire de gradient différente en fonction de la position des spins dans le tube. Les différents incréments nécessaires à la DOSY conventionnelle sont donc ici faits à différentes positions dans le tube. Enfin, afin de pouvoir récupérer l'information spectrale et spatiale, l'acquisition classique est remplacée par une acquisition de type EPSI (Echo Plannar Spectroscopic Imaging). Ce type d'acquisition consiste en un train d'impulsions de gradient positif et négatif. Grâce à l'encodage spatial et à l'acquisition EPSI, il est possible d'acquérir une expérience DOSY en moins d'une seconde.

Dans un premier temps, nous nous sommes intéressés à l'effet que pouvait avoir plusieurs paramètres de la DOSY spatialement encodés sur le résultat final. Le premier paramètre étudié est le choix des paramètres d'encodage. Pour une DOSY conventionnelle, si le délai de diffusion (usuellement appelé Δ) est laissé constant, la décroissance de l'intensité des signaux dépend de l'aire du gradient d'encodage. Dans sa version spatialement encodée, ce qui contrôle l'aire maximale de gradient subie est le produit de la durée de l'impulsion chirp par la gamme de fréquence balayée. Plusieurs expériences ont été faites en augmentant la durée du chirp de 1 à 5 ms tout en gardant le produit mentionné précédemment constant. L'échantillon modèle sur lequel les expériences ont été faites contient du DMSO, du méthanol, de l'acétate d'éthyle ainsi que de la caféine à une concentration de 100 mM dans du D_2O. Les coefficients de diffusion ont été calculés à partir de tous les signaux du mélange pour toutes les expériences. Dans tous les cas, le coefficient de diffusion reste similaire quel que soit le chirp utilisé. Le rapport signal sur bruit du DMSO, qui est le pic le plus intense du spectre, a également été calculé pour les 5 expériences. Dans tous les cas le rapport signal sur bruit est comparable d'une expérience à l'autre. Il y a de petites variations, mais aucune tendance nette ne se dégage.

De la même façon, l'effet de l'intensité du gradient d'acquisition a été étudié. Comme précédemment, une série d'expériences DOSY a été acquise avec différentes valeurs pour le gradient d'acquisition. Les coefficients de diffusion ont été calculés pour toutes ces expériences et une tendance semble se dégager. Lorsque le gradient d'acquisition augmente, le coefficient de diffusion calculé augmente. Ce résultat n'est pas expliqué pour le moment. De plus la comparaison des rapports signal sur bruit a été faite et, comme prévu, ce dernier décroit lorsque le gradient d'acquisition augmente.

Enfin, le dernier paramètre étudié est la durée de l'acquisition. Encore une fois, une série d'acquisition a été réalisée avec différentes durées d'acquisition. La comparaison des coefficients de diffusion n'a pas mis en avant de tendance particulière et la comparaison des rapports signal sur bruit a également été faite et a montré que plus l'acquisition est longue, plus le rapport signal sur bruit augmente.

Un des problèmes des expériences DOSY est qu'elles sont très sensibles à la convection. En effet, si le tube est soumis à un gradient de température, un mouvement de convection va s'installer dans le tube ce qui interfèrera avec les mesures de coefficient de diffusion. Dans le cas d'expériences conventionnelles, ce problème peut être corrigé en utilisant un double écho stimulé. Nous avons montré que cette stratégie peut également être appliquée aux expériences spatialement encodées.

Enfin, il a pu être démontré que la DOSY spatialement encodée pouvait être implémentée sur une sonde n'ayant qu'un seul axe de gradient si certaines précautions sont prises.

Résonance magnétique nucléaire multi quanta et maximum quanta ultrarapide

En RMN du proton, les déplacements chimiques sont souvent dans la gamme 1-10 ppm, ce qui mène à un fort risque de recouvrement des signaux. Le fait d'ajouter une ou plusieurs autres dimensions permet de créer des spectres multidimensionnels dans lesquels les signaux sont mieux séparés. Cependant, pour créer cette autre dimension, il est nécessaire de répéter plusieurs fois une acquisition en incrémentant un ou plusieurs délais, ce qui mène à des temps d'expériences qui peuvent être relativement longs, empêchant leur utilisation pour l'analyse d'échantillons qui évoluent rapidement. Différentes stratégies ont été développées au fil des années de manière à accélérer l'acquisition de ces expériences multidimensionnelles. Celle à laquelle nous allons nous intéresser a été développée en 2002 par Frydman et repose sur l'encodage spatial du déplacement chimique. Pour transformer une expérience 2D conventionnelle en son équivalent encodé spatialement, il faut remplacer le délai incrémenté t_1 par une paire de blocs d'encodage spatial. Tout comme pour la DOSY, le bloc d'encodage spatial est composé d'une impulsion chirp appliquée en même temps qu'un gradient d'encodage. Cependant, cette fois les deux blocs sont accolés l'un à l'autre, le gradient est de la même durée que l'impulsion chirp et les deux gradients d'encodage sont de signes opposés. L'acquisition est remplacée par un bloc EPSI comme pour la DOSY.

Dans le cadre de l'analyse de mélanges, un type d'expérience particulièrement bien adapté est la famille des expériences multi quanta. Lorsque des mélanges de composés aromatiques sont analysés,

l'utilisation d'expériences multi quanta permet de grandement simplifier les spectres. En effet, lorsque l'ordre de cohérence maximal (appelé par la suite MaxQ) d'un système de spin est atteint, son spectre 2D ne comporte qu'une seule ligne. Cela est particulièrement bien adapté à l'analyse de composés aromatiques puisque leur MaxQ est de 5 pour un cycle aromatique mono-substitué.

Il a déjà été montré qu'il était possible d'encoder spatialement des cohérences double quanta, mais la question se posait de savoir s'il était possible d'encoder spatialement des cohérences d'ordre supérieur. Pour vérifier cela, nous avons utilisé un mélange de différents composés aromatiques dont les MaxQ allaient de 3 à 5.

Dans un premier temps, nous avons pu démontrer qu'il était possible d'utiliser la séquence d'impulsion en version spatialement encodée de manière à encoder des ordres de cohérence 3, 4 et 5 quanta. Deux séquences ont pu ensuite être comparées et les délais ont pu être optimisés démontrant que cette étape était cruciale.

Enfin, pour démontrer que ce type d'acquisition pouvait être utilisé pour faire du suivi de réactions, nous avons étudié une réaction d'hétéro Diels-Alder dans laquelle la transformation d'un cycle aromatique le fait passer d'un MaxQ de 5 à 4. Le suivi a été fait avec des acquisitions de type ultrarapide et des spectres 1D ^{1}H. Les courbes d'évolution des signaux obtenus avec les deux techniques sont en accord. Cependant, la sensibilité des spectres ultrarapides est beaucoup plus faible que pour les spectres 1D.

Encodage spatial sur un échantillon en flux

Le suivi de réaction est un outil important pour les chimistes organiciens qui ont parfois besoin de savoir comment se déroule leur réaction. Pour cela, la RMN est un outil très intéressant grâce à son caractère non destructif et non invasif. Deux méthodes sont principalement utilisées pour suivre une réaction par RMN. La première est de faire la réaction dans des conditions classiques, en utilisant un ballon ou un réacteur dans un bain d'huile par exemple. Au cours de la réaction, plusieurs échantillons seront prélevés pour être analysés par RMN. Cependant, le suivi ne se fera pas en temps réel. De plus, il ne sera pas possible d'observer des espèces dont les durées de vie sont courtes tels que les intermédiaires réactionnels. L'autre façon de suivre une réaction qui est souvent utilisée (et qui a été utilisée dans le chapitre précédent pour suivre la réaction de Diels-Alder) est de faire la réaction directement dans un tube RMN. L'avantage principal est que le suivi se fera en temps réel et qu'il sera possible d'observer des composés dont la durée de vie est courte. En revanche, un des inconvénients est que la réaction ne se déroulera pas dans des conditions « réalistes ». Il a été montré que les deux méthodes peuvent amener à des résultats assez différents.

Une façon de combiner les deux méthodes, est de faire la réaction dans des conditions normales et de faire le suivi en flux. Différentes façons de le faire ont été développées au fil des années, par exemple en utilisant des sondes en flux tel que celle utilisés pour la combinaison chromatographie liquide avec la RMN. Cependant, dans ce cas il est nécessaire d'acheter une sonde spécifiquement

pour le suivi de réaction. Le suivi de réaction en flux a été facilité par le développement et la commercialisation de cellules en flux ou tubes en flux. Un système InsightMR, commercialisé par Bruker, a été acheté par le laboratoire dans le cadre de ce projet. Ce système est composé de plusieurs éléments. Premièrement une pompe HPLC est utilisée pour prélever une fraction du mélange réactionnel pour l'envoyer vers le spectromètre. Une ligne de transfert est ensuite utilisée pour transférer le mélange réactionnel depuis la pompe vers le spectromètre. Cette ligne de transfert peut être régulée en température grâce à un bain thermostaté. Enfin, le flowtube est un tube RMN renforcé dans lequel le capillaire plonge pour transférer le mélange réactionnel avant que celui revienne par un autre capillaire. De cette façon, le suivi peut se faire en temps réel tout en faisant la réaction dans des conditions « réalistes ».

L'utilisation de ce type d'équipement a déjà été proposée pour faire du suivi de réactions, mais principalement en utilisant des spectres 1D ^{1}H. Nous avons donc voulu savoir s'il était possible de faire du suivi de réactions en flux en utilisant des expériences ultrarapides. Le principal défi que cela soulève est de savoir s'il est possible de faire de l'encodage spatial sur un échantillon qui est en mouvement.

Dans un premier temps, il a été montré avec des expériences d'imagerie 1D que le fait d'utiliser une pompe HPLC créait des variations de vitesse du fluide circulant dans le tube. Dans un second temps, les conséquences du flux sur une expérience de type ufCOSY ont été étudiées sur un échantillon modèle n'évoluant pas au court du temps. Les expériences ont été répétées plusieurs fois à plusieurs débits. Les résultats ont révélé plusieurs phénomènes ; (i) lorsque le débit augmente, l'intensité des pics décroit, (ii) l'intensité des pics est sujet à des variations lorsque le débit est élevé (iii) les points (i) et (ii) dépendent fortement du déplacement chimique du pic observé dans la dimension spatiale : plus le déplacement chimique est élevé, plus les pertes sont importantes. Les tests faits ensuite ont révélé que ces pertes étaient liées à l'étape d'encodage et en particulier au sens dans lequel l'impulsion chirp balaye les fréquences. Un second bloc d'encodage spatial a ensuite été utilisé pour vérifier si ce dernier pouvait être immunisé contre l'inhomogénéité des pertes d'intensité. Malheureusement, avec ce second bloc, les pertes d'intensité étaient toujours inhomogènes. Le fait de doubler le nombre de blocs d'encodage spatial a également été testé, mais n'a pas mené à un résultat convenable.

Jusqu'à présent, toutes les expériences décrites ont été faites en utilisant un encodage spatial selon l'axe Z, soit le même axe que celui selon lequel le flux circule. Afin de vérifier si le fait d'avoir un encodage spatial perpendiculaire au flux permettait de limiter les pertes, les expériences précédentes ont été réitérées avec un encodage spatial selon l'axe X. Dans ce cas, les pertes d'intensités des pics ont été beaucoup plus faibles et ne dépendaient pas du déplacement chimique du pic en dimension spatiale.

Après avoir montré qu'il était possible d'utiliser des expériences basées sur l'encodage spatial sur un échantillon n'évoluant pas, nous avons utilisé ces expériences pour faire un suivi de réaction

modèle : la saponification de l'acétate d'éthyle. Dans un premier temps, les suivis en utilisant des encodages suivant l'axe X et Z ont été comparés. Les courbes obtenues grâce au suivi avec un encodage en Z étaient bien plus bruitées qu'avec un encodage en X. Dans un second temps, des mesures de cinétiques obtenues avec des expériences de type 1D ^{1}H et UF avec encodage en X ont été comparées et elles mènent à des résultats très similaires.

Enfin, des premiers tests ont été faits avec la DOSY avec encodage spatial, mais aucun résultat répétable n'a pu être obtenu à ce jour.

Accélération d'expériences 3D-DOSY par l'encodage spatial du déplacement chimique

Comme il a été montré dans la partie 3, l'expérience DOSY est un outil très intéressant pour l'analyse de mélange puisqu'elle permet de séparer les spectres des différents composants d'un mélange. Le plus souvent, la DOSY est utilisée pour séparer des spectres 1D. Cependant, puisque les déplacements chimiques du proton se concentrent principalement entre 0 et 10 ppm, le risque des recouvrements est relativement important, ce qui peut compliquer l'extraction des coefficients de diffusion sur laquelle est basée la séparation des spectres. Pour remédier à cela, une solution consiste à utiliser des méthodes multi-variées pour extraire les informations de diffusion. Une autre solution est d'augmenter le nombre de dimensions des spectres à séparer. La DOSY peut être utilisée pour séparer des spectres de n'importe quelle dimension. Cependant, cela peut mener à des expériences très longues puisqu'il faut incrémenter les délais nécessaires aux dimensions supplémentaires ainsi que les gradients de diffusion. Une façon d'accélérer ces expériences est d'utiliser l'encodage spatial. Il a déjà été montré qu'il est possible d'utiliser l'encodage spatial de l'information de diffusion pour accélérer l'expérience, et nous allons montrer ici que l'encodage spatial du déplacement chimique permet une accélération encore plus importante. Deux expériences ont été étudiés ici en version 3D DOSY : la COSY et la DQS (double quantum spectroscopy).

Deux types de séquences d'impulsion ont été étudiées dans ce chapitre. La première consiste à faire se succéder la séquence d'impulsion de la DOSY et la séquence de la 2D voulue. Dans un premier temps, nous avons étudié la 3D DOSY-COSY. Il a été montré sur un mélange modèle de composés concentrés à 100 mM que cette séquence permet d'obtenir un spectre 3D en environ 3 minutes, soit une accélération de plus d'un ordre de grandeur par rapport à la version conventionnelle. Dans un second temps, une autre séquence d'impulsion a été étudiée. Il est possible de transformer une séquence pour une expérience 2D en son équivalent 3D DOSY en utilisant certains gradients déjà présents dans la séquence et en les incrémentant pour créer la dimension de diffusion supplémentaire. Cette approche est généralement appelée iDOSY. Cette approche peut être intéressante car elle ne mène pas à une perte de sensibilité d'un facteur 2 comme l'écho stimulé. La séquence 3D COSY-

iDOSY avec encodage spatial a été mise en place et a bien fonctionné, une fois prises en compte les possibles interférences entre codage spatial et diffusion.

Dans un second temps, l'expérience DQS fut aussi transformée en son équivalent 3D DOSY. Dans ce cas, les deux méthodes DOSY et iDOSY menèrent à de bons résultats, mais en raison de leur faible sensibilité, elles durent être faits sur un échantillon modèle d'alcool concentré à 1M.

Enfin, il a pu être montré que la non-uniformité des gradients de l'axe Z des sondes avec gradient trois axes avait une grande importance dans le calcul des coefficients de diffusion. En effet, une apodisation spatiale est effectuée lors du traitement des spectres encodés spatialement, de manière à leur donner un meilleur aspect. En raison de la non-uniformité des gradients, les spins au centre du tube subissent des gradients plus importants que ceux aux extrémités du tube et l'apodisation spatiale donne un poids plus important à ces spins. Pour corriger cela, il faudrait soit une sonde qui a des gradients uniformes, soit faire une carte des gradients de manière à faire une correction en fonction de l'apodisation spatiale utilisée.

Conclusions

Au cours de cette thèse, nous nous sommes intéressés à différentes expériences spatialement encodées qui pouvaient être intéressantes pour l'analyse de mélanges, et à l'utilisation de l'encodage spatial sur un échantillon en flux.

L'influence de plusieurs paramètres d'acquisition de la DOSY spatialement encodée a pu être mise en avant. La possibilité d'encoder des ordres de cohérences supérieurs à deux à l'aide d'encodage spatial a pu être démontrée et a été utilisée pour suivre une réaction d'hétéro Diels-Alder. L'influence du flux et des variations de vitesse a pu être caractérisée, mais ce résultat n'est pas complètement expliqué à ce jour. Malgré cela, il a été montré qu'il était possible de faire un suivi de réaction réaliste en utilisant les méthodes spatialement encodées. Enfin, il a également été montré que l'encodage spatial pouvait être utilisé de manière à accélérer certaine expériences 3D-DOSY, même si dans certains cas, la sensibilité décroit de façon significative.

Table des matières

Notations and abbreviations

^{13}C: Carbon

^{15}N: Nitrogen

1D: One-dimensional

^{1}H: Proton

2D: Two-dimensional

^{2}H: Deuterium

^{31}P: Phorsphorus

3D: Three-dimensional

ASAP: Acceleration by Sharing Adjacent Polarization

B_0: Main magnetic field

BW: BandWidth

COSY: Correlation Ordered SpectroscopY

CT: Constant-Time

CTP: Coherence Transfert Pathway

D: Diffusion coeffcient

DECRA: Direct Exponential Curve Resolution Algorithm

DOSY: Diffusion-Ordered SpectroscpY

DQS: Double Quantum Spectroscopy

DSTE: Double Stimulated Echo

EPSI: Echo-Planar Spectrocopic Imaging

EXSY: Exchange SpectroscopY

FID: Free induction

FLASH: Fast Low Angle SHot

FOV: Field Of View

FT: Fourier Transformation

HMBC: Heteronuclear Multiple Bond Coherence

HMQC: Heteronuclear Multiple Quantum Coherence

HPLC: High Performance Liquid Chromatography

HSQC: Heteronuclear Single Quantum Coherence

J-Res: J-Resolved

LC: Liquid Chromatography

MaxQ: MAXimum Quantum

MRI: Magnetic Resonance Imaging

MQS: Multiple Quantum Spectroscopy

ND: Multi-Dimensional

NMR: Nuclear Magnetic Resonance

NOESY: Nuclear Overhauser Effect SpectroscopY

NUS: Non Uniform Sampling

PFG: Pulsed Field Gradient

PHIP: ParaHydrogen-Induced Polarization

RF: Radio Frequency

SABRE: Signal Amplification By Reversible Exchange

SE: Spin Echo

SMART: SMAll Recovery Times

SNR: Signal to Noise Ratio

SOFAST: band-Selective Optimized Flip-Angle Short-Transient

SPEN: SPatially ENcoded

STE: STimulated Echo

SW: Spectral Width

T_1: Longitudinal relaxation time

T_2: Transverse relaxation time

TOCSY: Total Correlation SpectroscopY

UF: UltraFast

UV: UltraViolet

Introduction

Nuclear magnetic resonance (NMR) spectroscopy is a powerful tool for mixture analysis, as it provides structural and quantitative information, and because of its non-destructiveness. In the majority of cases, the information sought by chemists are the structure of their newly synthetized molecule or the quantification of a molecule in a mixture. NMR can also be used in order to monitor reactions thanks to its simple sample preparation. Its usefulness for reaction monitoring has already been shown for numerous applications from electrochemical reactions to biological and organic reactions.

One dimensional NMR experiments can provide useful information on mixtures. However, due to its limited resolution, especially for ^{1}H spectra, structural analysis can greatly benefit from higher dimensionality experiments. It was shown that several experiments are particularly suited for complex mixture analysis such as multiple quantum spectroscopy, that allow to separate compounds based on the number of spins in their spins system, or diffusion-ordered spectroscopy (DOSY) that separates molecules' signals according to their diffusion coefficients. The main advantage of these experiments is that it is not necessary to separate compounds before analysis, leading to great time saving.

Despite being very useful for structural analysis, multidimensional experiments have a drawback: their long durations compared to 1D experiments. Hence, they cannot be used to observe samples that evolve too quickly. For example, 2D NMR cannot be used in order to monitor reactions whose durations are less than a few minutes or samples whose polarization decay quickly such as hyperpolarized ones. Over the years, several methods have been developed in order to reduce durations of multidimensional experiments, such as fast pulsing techniques,[1] Hadamard spectroscopy[2–4] or Non-Uniform Sampling[5] to cite only a few. The one that lead to the highest acceleration was developed in 2002 and relies spatial encoding of the sample in order to parallelize the increments needed to build up the different dimensions.[6,7]

In this work, we will describe several spatially encoded experiments that are useful for the analysis of mixture and for reaction monitoring. Moreover, we will study the possibility to spatially encode a flowing sample in order to do online reaction monitoring.

In the first part of this work, we will focus on an experiment that is particularly suited for complex mixture analysis: Diffusion Ordered SpectroscopY. This experiment allows to separate compounds' signals based on the diffusion coefficient of the associated molecules.[8] It is often compared to a virtual chromatography, but in this case, there is no physical separation of the components of the mixture. It was shown that the sequence could be spatially encoded to accelerate it.[9] However, other questions remained such as the influence of different parameters that will be studied. Despite being very useful, this method is very sensitive to convection. When the tube is submitted to a gradient of temperature, a convection motion occurs that lead to meaningless DOSY experimental results. It will be shown that

the method used in order to compensate for the convection in the conventional experiments[10] can also be used in spatially encoded experiments.

Then, another experiment that is useful for mixture analysis will be studied: multiple quantum spectroscopy. These experiments have been used a lot to study complex aromatic mixtures as the method allow to drastically simplify spectra.[11] It was shown that it was possible to spatially encode double quantum coherences[12] and we wondered if it was possible to encode higher coherence orders. The monitoring of aromatic reactions could greatly benefit from this acceleration for example. After proving that 3, 4 and 5 quantum coherences can be spatially encoded, an optimization of the method will be shown on a stable sample. Finally, as an example, a hetero Diels-Alder reaction will be monitored using a series of spatially encoded multiple quantum experiments.

In the third part of this document, we will focus on use of spatially encoded experiments with a flowing sample. To monitor reactions with NMR, one solution is to do it in conventional conditions: in a reactor or a round bottom flask with heating bath for example, and to regularly collect fraction of the reaction mixture to analyze it by NMR. However, with this method, the information collected do not always give a real time representation of the reaction course. For example, if short life-time compounds are created during the reaction (such as intermediate), they will probably not survive the time needed to collect the sample, prepare it and go to the spectrometer for the analysis. Another way to monitor reaction that allow to get around the previously mentioned problem, is to do the reaction inside the NMR tube. With this method, the reaction will be monitored in real time. However, the conditions in which the reaction is done do not mimic well the batch reaction. For example, it was shown that the kinetic of the reaction could be different from the 'realistic' reaction because it is not possible to stir the sample inside the magnet or because the heat transfer is different.[13] One solution to combine the advantages of each method is to run the reaction in realistic conditions and to continuously take a fraction of the reaction mixture thanks to a pump to send it to the spectrometer to be analyzed thanks to a flow tube of flow cell.[14,15] This online solution has shown to be useful for several situations, but until now, the spatially encoded experiments were never used to monitor a reaction in flow conditions at high field. The main challenge this method raises is to know if it is possible to spatially encode information on a sample that is flowing or if there are interferences between the encoding and the flow. If such interferences exist, several solutions can be contemplated such as adapting the pulse sequences to cancel the interferences or changing the spatial encoding axis.

In the last part of the document, a multidimensional experiment will be studied: 3D DOSY. The 2D version of the experiments allows to separate signals from 1D spectra. However due to the low resolution of 1D experiments, especially for ^{1}H nuclei, signals can easily overlap leading to a degradation of the analysis. One solution to this problem would be to use multivariate processing. Another solution, the one on which we chose to use , is to add a new dimension in order to reduce the probability of overlapping signals, leading to 3D experiments. The problem with such experiments is that they are very long and could not be used on evolving samples. It was already shown that they

could be accelerate using spatial encoding of the diffusion dimension.[9] However, with this acceleration, the experiment is as long as conventional 2D experiments. We will show here that it can be even more accelerated through the spatial encoding of the chemical shift.

1 Fast multidimensional NMR for reaction monitoring.

1.1 Introduction

Nuclear magnetic resonance (NMR) spectroscopy is a powerful analytical method that provides structural and quantitative information on chemical samples. Thanks to the simple sample preparation needed, it is used on many kinds of samples ranging from isolated compounds in solution to very complex mixtures, such as biofluids or food matrices as schematized in Figure 1. Most of the time, NMR spectroscopy is used on non-evolving samples for applications that include structure elucidation, quantification or conformation analysis. There are also many reasons to study out-of-equilibrium samples such as chemical reactions, to gather information about their kinetics, flowing samples or hyperpolarized mixtures, and this motivates the development of fast multidimensional NMR methods. For example, for fast chemical reactions, it can be hard to obtain details on reaction intermediates without fast acquisition methods. Also, hyperpolarization gets more and more attention these days as a way to drastically increase NMR sensitivity, but magnetization usually drops very quickly. Hence, more and more developments are made in order to extract as much information as possible before the loss of all signal. In this chapter, the use of 1D NMR to collect information while a chemical reaction

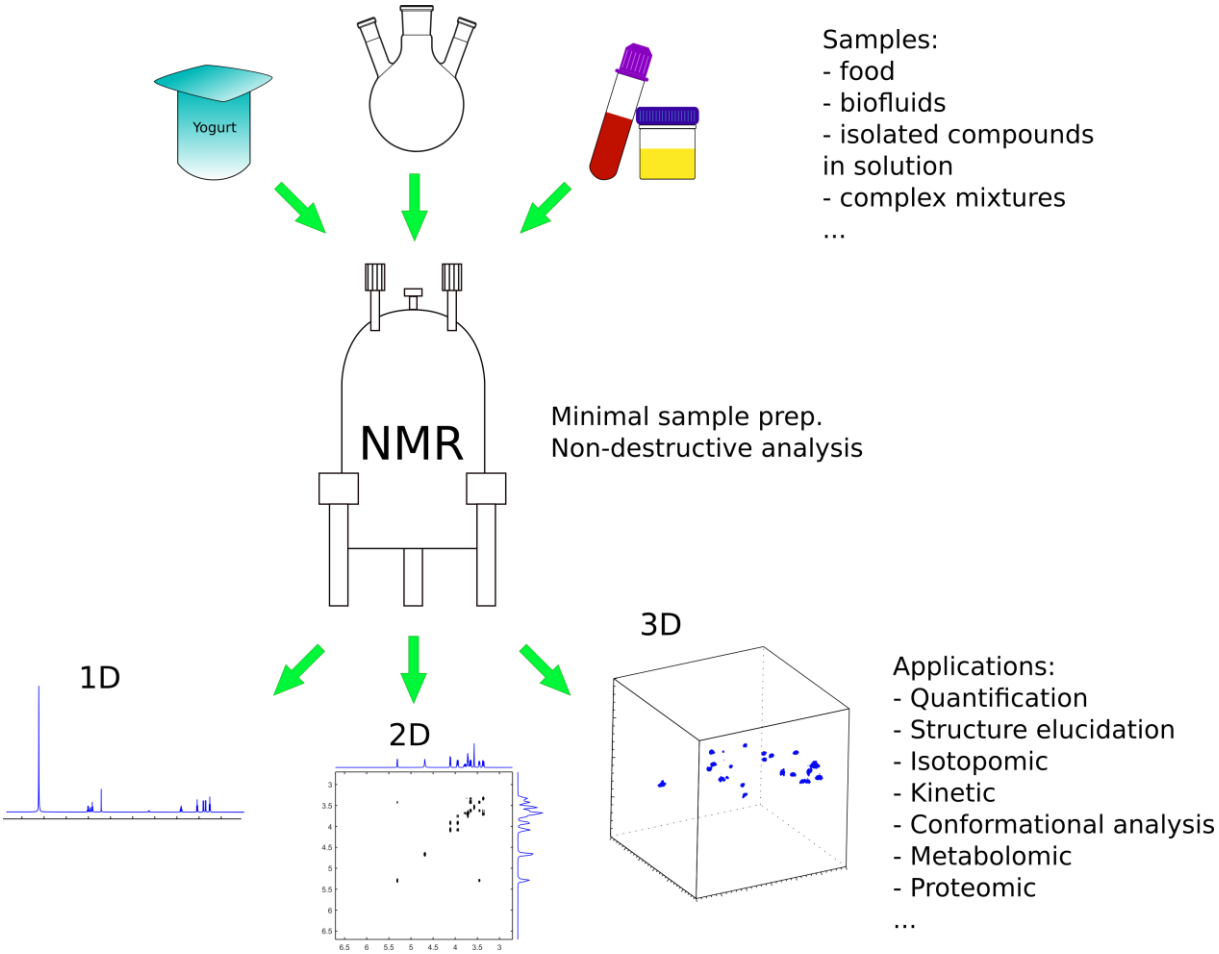

Figure 1: Examples of samples analyzable by NMR and of applications of this analytical technique.

is occurring will first be described. Then, the principles of multidimensional NMR will be detailed and it will be shown how the addition of a second dimension makes it possible to decrease the overlap between signals and, however, comes with a limitation in terms of experimental duration. Then, several methods to accelerate the acquisition of multidimensional spectra will be developed, before finally reaching the fastest one and its applications in numerous fields including reaction monitoring.

1.2 NMR for reaction monitoring

1.2.1 Principle

Reaction monitoring is an important component of chemical science, to be able to understand reaction mechanisms, develop new methods in chemical synthesis (more efficient, or "greener" for example) and to optimize reactions and processes. Being able to gather information on the order of a reaction or the kinetic profiles is very important in the process to better understand it, and several analytical methods can be used as tools for mechanistic studies.[16]

The simplest experiment in NMR consists in a 90° radiofrequency pulse followed by the acquisition of a signal (FID) as shown on Figure 2. Then a Fourier transform generates the spectrum that can be interpreted. The approach can be used for reaction monitoring as follows: the reaction mixture is introduced into an NMR tube and the reaction is performed in the magnet while repeated acquisitions are performed. Note that real-time monitoring can be used solely for reactions that are slow compared to the acquisition of an NMR experiment. Indeed, if a chemical modification, that produce a chemical shift change, occurs during the acquisition, the resulting spectrum will contain artifacts. For samples at equilibrium, information can be gathered on phenomenon on shorter timescales, for example analyzing lineshapes. Here we will focus on the analysis of out-of-equilibrium samples.

1.2.2 Applications

Reaction monitoring with a succession of 1D NMR spectra can be done in a simple NMR tube or rotor, as will be shown in the first part of this section. Recently, efforts have been made to develop methods that make it possible to perform the reaction in a classical reaction vessel, using more realistic conditions, while a flow of reaction mixture is sent either to a modified NMR probe or to a classical probe through specific equipment to achieve 'on line' monitoring.

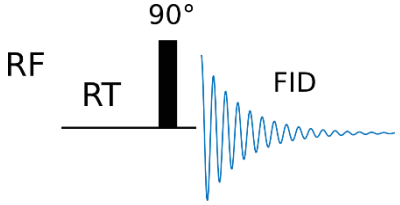

Figure 2: Pulse acquire experiment. The black rectangle represents a 90° hard pulse. RT corresponds to the relaxation time.

1.2.2.1 Without flow

Protons are the most studied nuclei in NMR spectroscopy as they are very abundant and also one of the most sensitive stable isotopes in NMR. Countless examples of reaction monitoring were done thanks to ^{1}H NMR. For example, it has been used in order to monitor aerobic biotransformation,[17] biomass transformation[18] or enzymatic reactions.[19] It was shown that it was possible to study biocatalytic polymerization in order to understand mechanisms.[20] Other complex reactions can be studied such as oscillatory reactions as the Bray-Liebhafsky reaction that involve water periodic chemical shift changes[21] or photocatalyzed reaction.[22] It was also shown that NMR reaction monitoring could be very useful for electrochemistry in order to highlight magnetoelectrolysis effect[23] or to study the structure of unstable intermediates.[24] All the previous reactions were done in NMR tube, sometimes with modification to inject air, or electric current, but it is also possible to monitor reaction on solid state.[25]

However, due to the poor spectral resolution and small signal dispersity of 1D ^{1}H NMR spectra, it can be complicated to extract information from them for reaction monitoring. That is the reason why other nuclei have been used, such as carbon-13, that benefit from a wider spectral dispersion and sharper peaks as ^{1}H-^{13}C couplings can be decoupled.[26]

The other nuclei that are typically observed in NMR because of their high gyromagnetic ratio and abundance, such as ^{19}F and ^{31}P, can also be used for reaction monitoring.[27–29] The use of these nuclei is interesting as they are more sensitive than 13C and their signals are distributed on a wider range than ^{1}H. Other, more exotic, nuclei also may be used, such as ^{195}Pt to probe organometallic compounds and monitor complex in vivo reactions such as the one of the anticancer drugs cis-platin and trans-platin binding to DNA as shown in Figure 3.[30] Through NMR reaction monitoring, it is also possible to

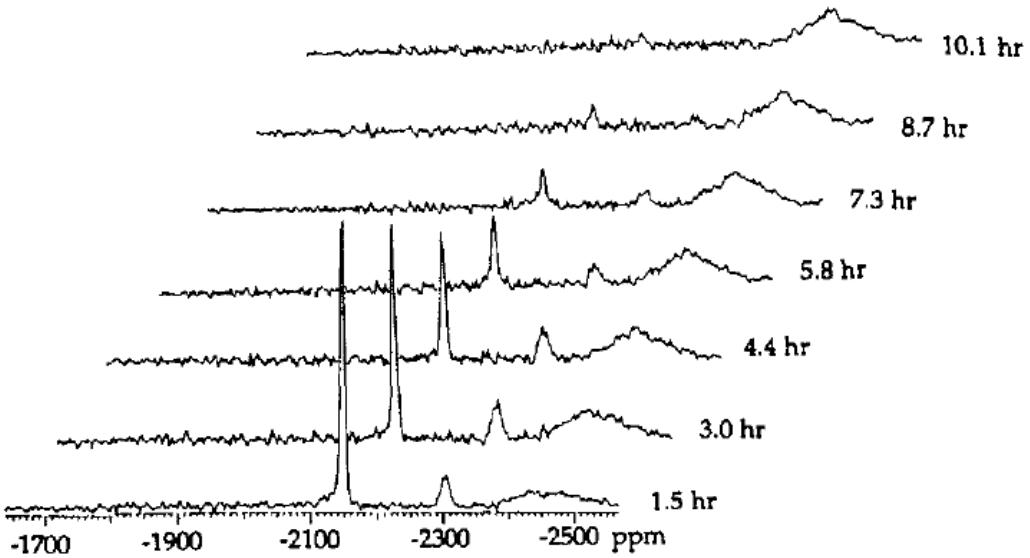

Figure 3: Time-dependent ^{195}Pt NMR spectra of the reaction between m-DDP and chicken erythrocyte DNA at 37 °C in 3 mM NaCl, 1 mM NaH_2P0_4, at a drug-to-nucleotide ratio (D/N) of 0.07. Reproduced from reference 30. Copyright American Chemical Society.

extract very important information such as the association rate of the complex with the solvent or mechanistic insight. It is also possible to use much less abundant nuclei such as ^{2}H in particular conditions, in aqueous chiral liquid crystals, to access enzymatic reaction rates in chiral liquid crystals.[31]

1.2.2.2 With flow

The previous results were obtained on reactions that were performed in the NMR tube and in the magnet, leading to several limitations in terms of quantities or temperature range. The inability to stir the reaction mixture or the incompressible dead time needed to lock and shim the sample between the beginning of the reaction and the first acquired spectrum are also important drawbacks. This dead time problem can be limited by shimming on a similar sample, but (i) there will always be some data points loss at the beginning of the reaction and (ii) due to the different conditions in terms of heat transfer and stirring, it is expected that the reaction will behave differently in the magnet and in more "realistic" conditions. The comparison between three methods (online, periodic inversion and motionless tube) was done by Foley & al[13] on several reactions showing that the NMR monitoring technique has a significant effect on the results as shown in Figure 4.

Hyphenation between NMR and HPLC is also a good combination of analytical methods, and has shown to be effective in the understanding of pharmaceutical reaction processes. Data obtained from both of these methods were compared and the results were very similar.[32] Moreover, it was shown that, unlike UV detector, NMR spectroscopy provides quantitative data simplifying kinetic analysis as the calculation of relative response factor is unnecessary. Finally, the use of NMR allows to collect more precise structural information than UV detector.

When the reaction is to be monitored at high field, several methods have been proposed over the years to be able to investigate the reaction in realistic conditions, but they often need specific equipment, such as a flow probe, that makes it possible to circulate a fluid circulate through the probe. This solution is often used for hyphenation with HPLC and can also be used for online reaction

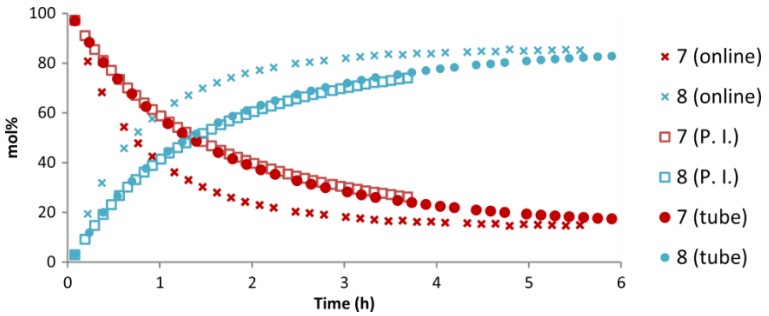

Figure 4 A summary of all methods used to study the aniline and 4- fluorobenzaldehyde coupling reaction to form the imine in 1:1 methanol: acetonitrile at 25 °C. Online nuclear magnetic resonance (NMR) (×) initial concentrations were 64mM each reactant. Periodic inversion (□) and NMR tube (●) reactions' initial concentrations were 69mM for each reactant. Reproduced from reference 13. Copyright Wiley

monitoring,[33–35] but necessitate to buy or build a dedicated probe. Another solution is to develop flow tubes that can be inserted in classical NMR probes. Different designs of such flow tubes have been proposed in the literature[15,36] and some of them are now commercially available as the one that will be used further in this work.[14] This system is composed of a pump that circulates a fraction of the reaction, of a thermally insulated capillary that goes from the pump to the magnet and of a modified NMR tube that can be introduced in any 5 mm probe, as shown in Figure 5.

This kind of setup has proven to be robust and has been adopted by academic researchers to study reactions that would not be feasible with classical equipment,[37,38] and different reaction conditions,[39] or by pharmaceutical industries to optimize reaction performance[40] on reaction volumes much higher that what is feasible in the classical NMR tube (60 mL vs 600 µL). Moreover, with such setup hyphenation with other analytical methods are possible such as Near Infra-Red (NIR) for example as shown in Figure 6.

High-field NMR is very powerful but has major drawbacks. First, it is expensive, due to the need of superconducting magnets that necessitate specific alloys and periodic cryogenic fluid refill. Then, it often needs dedicated infrastructure and staff to operate the system. The recent years have seen an increasing interest in the development and use of low field (1–2 T) benchtop spectrometers, which use cheaper and cryogen free permanent magnets and are transportable. The design of some low field NMR magnets has been developed so that a glass tube could be inserted through the magnet to make it possible analyze a flowing sample, for, e.g., reaction monitoring applications. It has been shown that inline NMR analysis at low field is useful for flow synthesis thanks to its easier implementation, compared to high field, while off line analysis was performed at high field afterwards to benefit from the higher resolution.[41] As with high-field NMR, other nuclei can be used for reaction monitoring at low field.[42]

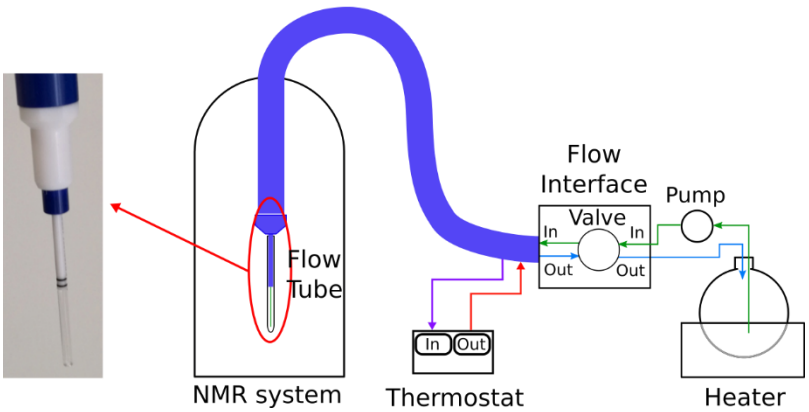

Figure 5: Schematic representation of the Bruker InsightMR flow unit that will be used in this work.[43] Reproduced with permission from reference 43. Copyright Royal Society of Chemistry

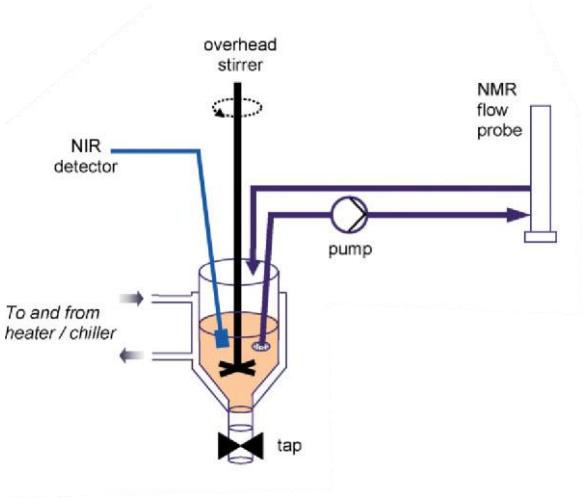

Figure 6: The flow-reactor apparatus shown (A) as a schematic reproduced with permission from reference 40. Copyright Wiley.

Methods have been developed over the years to monitor chemical reactions on even shorter timescales, with reaction time constants down to 20 ms.[44] One of these solutions is to use an approach known as stop flow, introduced by Chance in 1940 for light absorption analysis,[45] which was then used for NMR measurement.[46] It consists in rapidly injecting two solutions in a spectrometer, stopping the flow when the mixture is in the coil of the probe and analyzing while the reaction takes place. This powerful method has been used to measure polymerization kinetics[47] and for mechanistic studies.[48] A second solution was proposed by McGarrity in 1981: a sample is already in an NMR tube in the magnet and a reactant is rapidly injected, hence the rapid injection name[49]. The equipment used has been improved since then[50] and the methodology has been used to study chemical reactions[44,51,52] and to identify reaction intermediates.[49,53]

Flow NMR has also been used together with miniaturized detection devices in microfluidics. The purpose of this approach is to analyze very small quantities. Due to the reciprocity theorem, decreasing the size of a coil increases its mass sensitivity.[54] This drives the development of smaller and smaller coil, down to the microliter or even nanoliter scale,[55,56] to reach the lowest limit of detection possible. Moreover, due to the nowadays relatively easy access to 3D printers allow to develop cheap printable devices.[57]

The use of flow NMR also leads to the possibility to study cells or proteins in vivo conditions[58,59] but this aspect will not be discussed here.

1.3 Multidimensional NMR experiments for complex mixture analysis

NMR spectroscopy is a powerful analytical method that provides information on molecules and their structure through chemical shifts, coupling constants and other NMR parameters. It is not limited to the analysis of a single compounds, and in many cases the sample is a mixture. However, when complexity of the mixture increases, 1D spectra are insufficient as signals overlap, especially for nuclei that do not have wide dispersion in chemical shifts, such as ^{1}H. One solution is to separate the

analytes prior to NMR analysis thanks to chromatography, but for very complex mixtures (biological samples for example), it can be too long or result in sample degradation. Hence, instead of physically separating compounds it is possible to separate signals by spreading them along more than one dimension. The principle of 2D (and by extension nD) NMR was introduced by Jean Jeener in 1971[60] and relies on the scheme:

Preparation – Evolution (t_1) – Mixing – Acquisition (t_2)

with a repetition of this scheme to sample a regular grid of t_1 values that fulfills the Nyquist criterion. The experiment results in a 2D matrix on which a double Fourier transform is applied to provide the spectrum. Other experiments were imagined incrementing a delay or a gradient but that do not involve a double Fourier transform at the end. This last family is often called "pseudo-2D" spectra. Out all of these experiments, we will focus on one in particular: Diffusion Ordered Spectroscopy.

1.3.1 Correlation spectroscopy

1.3.1.1 Homonuclear correlations

The first correlation experiment is the COSY (Correlation SpectroscopY) experiment, that was introduced by Ernst in 1976.[61] This experiment makes it possible to visualize the coupling between different nuclei, thus greatly simplifying the analysis. Since then, countless experiments were proposed and some of them are widely used. One of the advantages of these experiments is that the information is spread over two or more dimensions. It is especially useful for nuclei that suffer from peak overlapping due to poor signal dispersion, ^{1}H being one of the worst cases. One of the experiments that has become widely used for the analysis of mixtures is Total COrrelation SpectroscopY (TOCSY) initially named HOmonuclear HArtman Hahn spectroscopy (HOHAHA),[62] which was introduced by Davis and Bax in 1985. In this experiment, the correlation between the entire spin system will be seen, helping to differentiate them from each other.

The COSY experiment relies on the encoding of single-quantum coherences. Experiments to indirectly observe higher coherence orders have been introduced, for example to measure ^{13}C-^{13}C coupling constants[63] but also was adapted for different cases and used for ^{1}H experiments.[64] One of the big advantages of Multiple Quanta (MQ) experiments is that the diagonal peaks, that can be very strong in COSY spectra, disappear, hence simplifying the spectrum as shown in Figure 7. It has also been shown that MQ experiments could be very useful to analyze mixture of aromatic compounds,[65–67] especially using the MAXimum Quantum (MaxQ) idea. It corresponds to the maximum quantum order of a spin system and was also used for polyphenols, flavonols, secoiridoids or lignans mixtures analysis.[68]

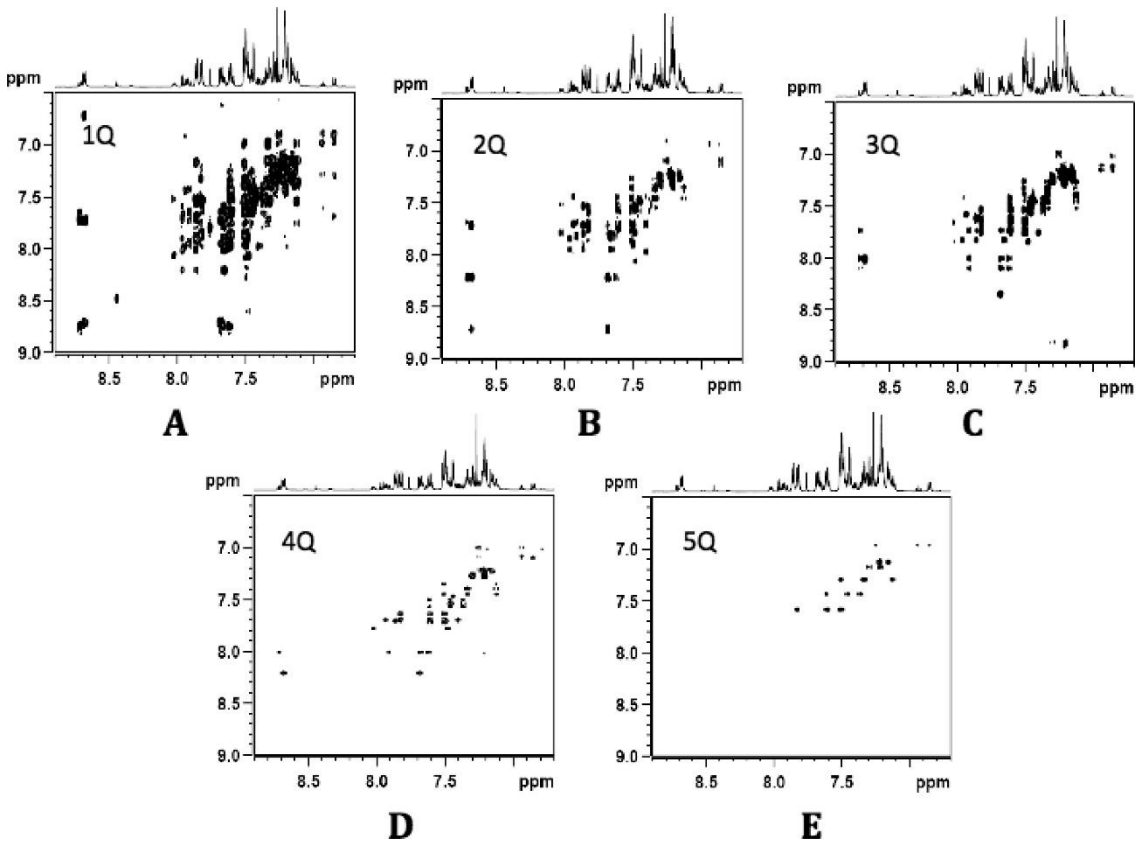

Figure 7: Series of MQ-1Q correlation spectra of the test mixture, with the coherence order p ranging from 1 to 5 (A-E). The MQ dimension uses a reduced frequency scale δ1 R equals to δ1/p, with p as the coherence order. In this reduced scale, the MaxQ signal appears at the average of the resonance values of the protons that contribute to its creation. The spectral complexity reduces with the number of quanta, due to a progressive simplification of the spectrum in the MQ dimension and to the filtering out of some molecular fragments. Reproduced from reference 66. Copyright American Chemical Society.

The identification of J couplings is useful to elucidate the chemical structure of a molecule, and is at the heart of correlation spectroscopies. The value of these couplings can also bring information on the geometry of the compounds. J-resolved spectroscopy was introduced by Aue & al in 1976 to measure coupling constant values.[69] J-resolved spectra also provide a way to obtain ^{1}H 1D spectra with homonuclear decoupling, so this experiment has been improved and its modification was used in for complex mixtures analysis in the field of metabolomics.[70]

Another class of 2D experiments concerns the transfer of longitudinal magnetization through the Nuclear Overhauser Effect (NOESY), which provides information on internuclear distances,[71] or chemical exchange (EXSY).[72]

1.3.1.2 Heteronuclear correlations

Correlation experiments between several different nuclei have also been developed. One of the first 2D heteronuclear correlation was introduced by Maudsley & Ernst[73] in 1977 and relies on the coherent transfer of transverse magnetization from a nucleus S to I. It allows the indirect detection of the S nucleus and its correlation with I with increased sensitivity. This work was used several years later by Bodenhausen in 1980 to develop the Heteronuclear Single Quantum Correlation (HSQC) experiment.[74] This time a double transfer was used in order to gain even more in term of sensitivity for nuclei with low gyromagnetic ratio. This method is still widely used today with ^{13}C for organic

chemical analysis or with ^{15}N in structural biology applications and are the foundations of numerous other experiments that will be not detailed here.

1.3.2 Diffusion ordered spectroscopy

In this part, we describe examples of multidimensional NMR experiments that do not establish correlations between nuclear spins. These experiments do not rely on Fourier transform to extract information but on curve fitting or Laplace transform. Here we will focus on diffusion NMR, which is one of most useful non-correlation experiments for the analysis of mixtures. Molecules in solution experience translational diffusion. This Brownian motion is characterized by a diffusion coefficient, which is qualitatively linked to the size and shape of the molecule. For "big" particles that are only subjected to collisions with smaller particles (usually solvent molecules), the diffusion coefficient D is linked to the size of the particle through the Stokes-Einstein relationship:

$$D_{ij} = \frac{k\,T}{6\,\pi\,r_i\,\mu_j}$$

with D_{ij} the diffusion coefficient of i in solvent j, k the Boltzman constant, T the absolute temperature, r_i the hydrodynamic radius of i and μ_j the dynamic viscosity of j. This relationship is however not valid as such for most small molecules in solution, and it tends to underestimate diffusion coefficients. The qualitative relationship is however still useful for data interpretation, and several modifications of the Stokes-Einstein equation have been proposed for quantitative analysis.[75]

The measurement of diffusion coefficients by NMR was introduced by Stejskal and Tanner in 1964 using a Spin Echo (SE) pulse sequence.[8] The approach was modified several years later[76] to introduce the Stimulated Echo (STE), which remains today one of the most widely used sequence for diffusion NMR. These experiments rely on incrementing the intensity of a pair of gradients separated by a delay as shown on Figure 8.[77] The spins are defocused by the first gradient pulse and only partially refocused by the second gradient pulse, leading to a decay of the signal intensity as a function of the gradient intensity. This decay can be fitted with the Stejskal-Tanner equation to access the diffusion coefficient information:

$$S(q) = S_0 e^{-[Dq^2\Delta']},$$

where S_0 is the initial amplitude of the signal, D is the diffusion coefficient, Δ' is the diffusion delay corrected to account for finite pulses and q corresponds to the pitch of the phase helix shown in Figure 8. It is proportional to the area of the gradient and can be expressed as:

$$q = \gamma\delta g,$$

where γ is the gyromagnetic ratio of the observed nucleus, δ is the duration of the gradient and g is the intensity of the gradient. This equation assumes the gradient is rectangular. Otherwise, a correcting actor has to be applied.

This relies on the hypothesis that no translational motion other than diffusion occurs during the delay Δ. If this condition is not fulfilled (flow or convection for example), additional dephasing can appears as shown in Figure 8.

Diffusion NMR experiments for the analysis of mixtures are often referred to under the name diffusion-ordered NMR spectroscopy (DOSY). This term was introduced in 1992 by Morris and Johnson Jr and was first a processing method to create the 2D spectra on which correlation was made between each peak and its corresponding diffusion coefficient.[78] For each chemical shift, a diffusion coefficient was calculated and represented on the 2D spectrum by a gaussian in the diffusion dimension whose width corresponds to the fit standard deviation (representation that will be also used later in this work). As this 2D spectra is a convenient way to represent diffusion data (see Figure 9), the term Diffusion Ordered Spectroscopy has now become a generic name for diffusion experiments.

One of the problems encountered in DOSY experiments is that the use of intense currents in the gradient coils leads to distortion of the spectra. One solution to circumvent this problem was to introduce a small delay to the STE experiment[79] to let eddy currents vanish. A second proposition to avoid such current has been suggested a few years later by making the global gradient null using bipolar (BP) gradient.[80]

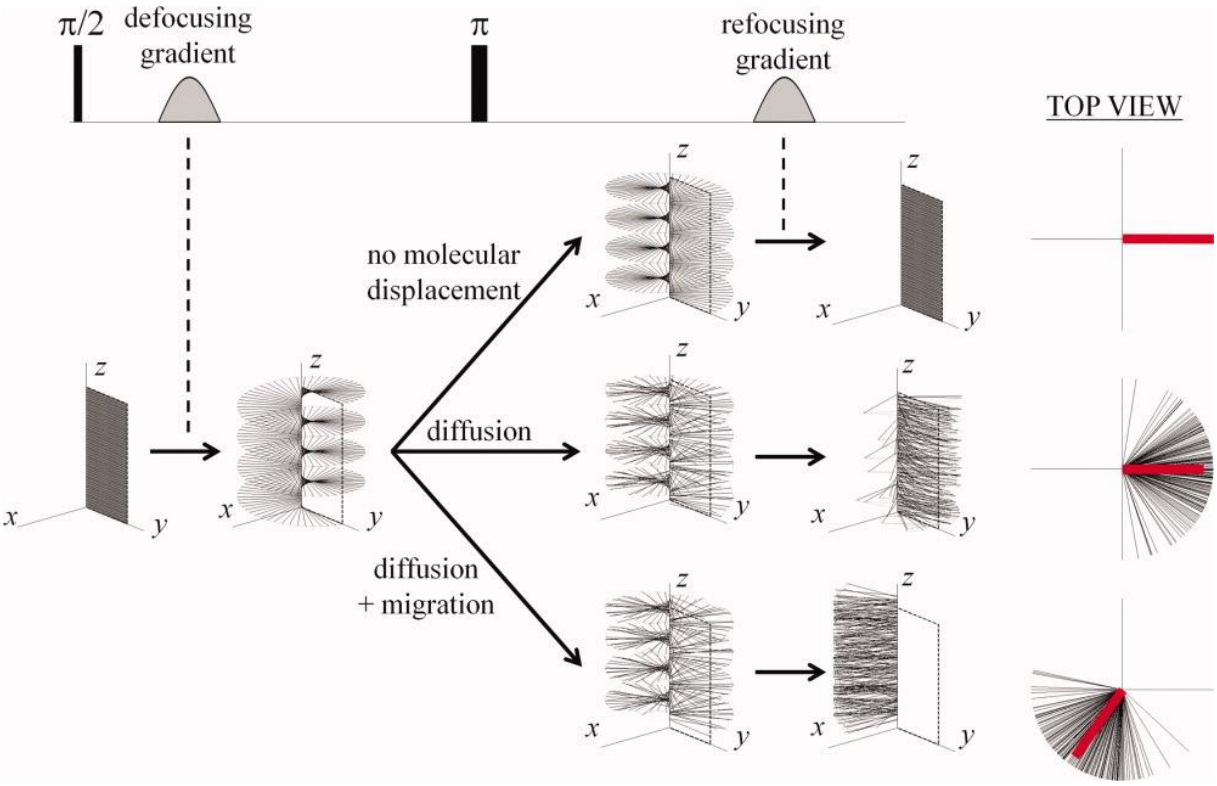

Figure 8: Principle of the DOSY experiment illustrated with the SE pulse sequence. Reproduced from reference 77. Copyright Wiley.

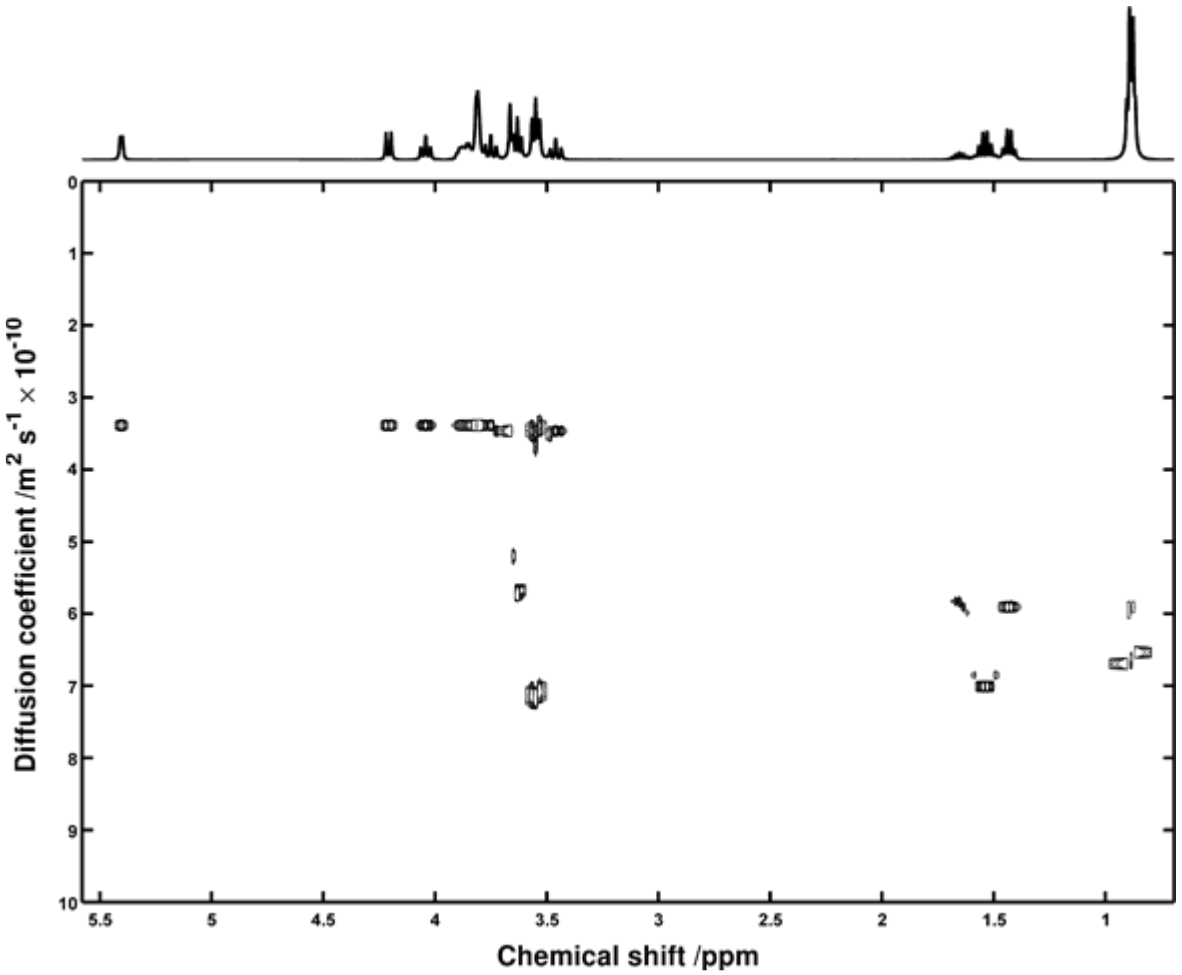

Figure 9: DOSY spectrum resulting from biexponential fitting of the demonstration data. The signals originate from sucrose (diffusion coefficient 3.410.10^{-10} m².s^{-1}) isopentanol (diffusion coefficient 5.910.10^{-10} m².s^{-1}), and n-propanol (diffusion coefficient 7.010.10^{-10} m².s^{-1}). Reproduced with permission from reference 96. Copyright Elsevier.

As said earlier, DOSY pulse sequences are designed to measure diffusion coefficients of molecules in a motionless solution. However, if the solution is submitted to a temperature gradient, a second movement will add-up to the Brownian motion: convection. This phenomenon, that will actually always occur to some degree,[81] can lead to artifacts preventing the acquisition of good quality data. One of the most effective solutions to this problem was introduced by Jershow & Muller and consists in combining two consecutives stimulated echoes, where diffusion effects will add-up while convection will cancel.[10,82]

As DOSY is a powerful way to separate signals from different compounds, which is however hampered by overlap in crowded 1D spectra, it has naturally been combined with correlation experiments to obtain 3D datasets. To combine the pulse programs, two different approaches have been used. The first is to follow the classical STE pulse sequence by the pulse sequence of the selected correlation, experiment such as COSY,[83] Jres[84] or HMQC.[85] The other possibility is to use a delay in the correlation experiment to introduce the diffusion attenuation. This method is usually called interleaved DOSY (iDOSY) and has been used for COSY,[86] DQS,[87] Jres,[88] HMQC[89] experiments, and others. This 3D method combining high signal separation thanks to chemical shift correlations and

diffusion information was used for complex mixture analysis[90] such as carbohydrates mixtures[91] or formulation control.[92]

Several methods have been developed to process the data of diffusion NMR experiments. Indeed, unlike for the Fourier transform, there is not a unique and well-defined way to achieve a Laplace transform. The choice of method depends, among other things, on whether the sample contains a continuum of diffusion coefficients (as for a polymer) or a discrete set of well-defined values,[93–96] as for small molecule mixtures. For this last kind of mixture, it is usually preferred to use a single exponential fit that provide good quality data as long as there are no overlapping signals.

1.4 Acceleration of multidimensional NMR experiments

The separation power of multidimensional NMR experiments comes at the cost of long experiment durations. Indeed, as they rely on the step-wise incrementation of a parameter, either a delay or a gradient intensity, the experiment duration is much longer than for the acquisition of 1D spectra. Correlation experiments usually require at least 64 to 128 and up to more than 1000 increments, depending of the resolution needed, leading to experiment durations of at least 5 minutes for the most sensitive ones, assuming a relaxation delay of the order of 2.5 s is used. The number of increments is usually less for diffusion experiments, but phase cycling is needed leading to durations of the same order of magnitude as for correlation experiments. In this section, we will describe several methods that have been proposed over the years in order to reduce the duration of multidimensional experiments, including fast-pulsing methods and non-uniform sampling. Ultrafast 2D NMR based on spatial encoding will be described in the next section.

1.4.1 Fast-pulsing methods

A family of methods are based on reducing the effective longitudinal relaxation time of nuclear spins, thus allowing to pulse faster providing either a better SNR per unit of time, or, what will interest us here, a faster acquisition. One solution that was introduced by Schanda and Brutscher for protein NMR is known as band-Selective Optimized Flip-Angle Short-Transient heteronuclear multiple quantum coherence (SOFAST-HMQC).[1] The principle is that selective excitation will be used to flip only amide proton spins, while leaving the others along longitudinal axis. Thanks to cross-relaxation and solvent exchange, the apparent longitudinal relaxation time will shorten allowing to pulse much faster. Figure 10 show a ^{1}H-^{15}N spectrum acquired in only 5 seconds. This concept has then been used to accelerate 3D acquisition and allowed to decrease the experiment duration to a few minutes.[97]

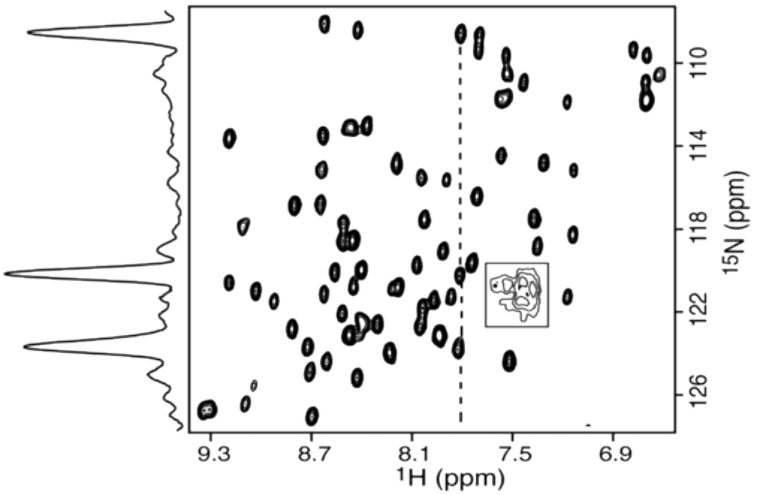

Figure 10: ^{1}H-^{15}N correlation spectrum (central part) of ubiquitin (2 mM, pH 4.7) recorded at 800 MHz in only 5 s using the SOFAST-HMQC sequence. The peak pattern surrounded by a box arises from Arg side chain resonances. Reproduced from reference 1. Copyright American Chemical Society.

Moreover, The SOFAST method is compatible with an excitation at the Ernst angle θ_E that can be defined as:

$$\cos(\theta_E) = \exp\left(-\frac{T_R}{T_1^{eff}}\right),$$

with T_R is the repetition time between the beginning of two successive acquisitions and T_1 is the effective longitudinal delay of the observed spin. With a ratio $\frac{T_R}{T_1} = 3$, the relaxation is almost complete and the optimum angle is close to 90°. However, if it is chosen to work with faster pulsing, the angle has to be adapted according to the formula above.

Other methods have been developed to allow fast pulsing such as the Acceleration by Sharing Adjacent Polarization (ASAP).[98] In this ^{1}H-^{13}C correlation experiment, the relaxation delay is shortened to several tens of millisecond and a Hartmann-Hahn block is introduced. The possibility to pulse faster relies on the small abundance of the ^{13}C. Spins are categorized in two groups: the donors that are bonded to ^{12}C and acceptors that are bonded to ^{13}C. The pulse sequence will transfer the acceptors polarization to ^{13}C for observation while donors' polarization remains untouched. The Hartmann-Hahn block introduced during the relaxation delay will transfer polarization from donors to acceptors allowing to pulse again almost immediately after. This method allows the acquisition of 2D experiments in less than one minute with a significant SNR increase. However, it is limited to the experiments where ^{1}H are in vast minority linked to low abundant NMR active nucleus while the others are bounded to non-active nuclei.

A last interesting method that can be noted is the SMAll Recovery Times (SMART) one.[99] When no fast-pulsing method is used, it is usually recommended to work with a relaxation delay between one and five times the maximum T_1. For small compounds in solution that have long relaxation times, this leads to long experiments. Usually, this long duration is driven by the need of a good resolution rather than increasing the signal to noise ratio. Indeed, in a lot of cases if the relaxation delay is

reduced way below the maximum T_1, the problem will not be the signal to noise ratio but the rise of artifacts coming from unsuppressed coherences between scans. To decrease this kind of artifacts, the SMART method consists in decreasing the recovery delay and to introduce a pulsed field gradient during it. This method was originally used in MRI experiments such as in the Fast Low Angle SHot (FLASH) method.[100] The area of this gradient changes at every scan in such a way that the angle between any two directions is the highest possible. It allows decreasing the relaxation delay to a few tens of milliseconds while having artifact free data. However, in order to implement SMART experiments, a triple axis gradient probe is needed, an equipment that is not so common in most laboratories.

1.4.2 Non-Uniform Sampling

The incrementation of an evolution delay required for multidimensional correlation experiments is usually performed using a Cartesian 1D grid: the duration is incremented linearly from its minimum to its maximum value with enough points to fulfil the Nyquist criterion. Several early studies had suggested that sampling along a non-uniform grid could make it possible to obtain the same information with shorter experiment duration.[101,102] Instead of recording the full set of points on the grid, only part of it was actually recorded. Different methods have been proposed over the years to allow it. Some of them rely on the acquisition of specific time points such as the Projection-Reconstruction that acquire 2D projection data sets and use them to build the 3D spectra,[103] or the simultaneous sampling of the indirect dimensions spanning a subspace of a conventional experiment before a processing that uses a combination of G-matrix and Fourier Transform (GFT).[104] Other methods exist that allow to process experiments that have been obtained recording essentially arbitrary evolution times such as MUlti-dimensional NMR spectra Interpretation (MUNIN), that relies on automated interpretation of data through decomposition of time domain data that describe a single peak or related peaks[105] or Fourier transform of arbitrarily sample data that relies on the calculation of pairs of frequencies.[106] Processing of non-uniformly sampled experiments can also be done using maximum entropy theorem and have shown to be useful for different 2D spectra processing.[107–109] The use of non-uniform sampling (NUS) has become more widespread with the advent of so-called compressed sensing algorithm, which were originally introduced in the field of magnetic resonance imaging.[5,110]

The non-correlation experiments by themselves, such as diffusion measurement, do not highly benefit from NUS. Indeed, in this case as the indirect dimension does not correspond to a spectral dimension, the Nyquist criterion does not apply. Nothing forces the gradient to be sampled linearly and for some applications it is necessary to sample the gradient intensity quadratically such as for DECRA processing.[111] However, it has been shown that a conjointly non uniform sampling in time and gradient domain could be used to accelerate 3D experiments[112] as shown in Figure 11 that illustrate haw the NUS was done.

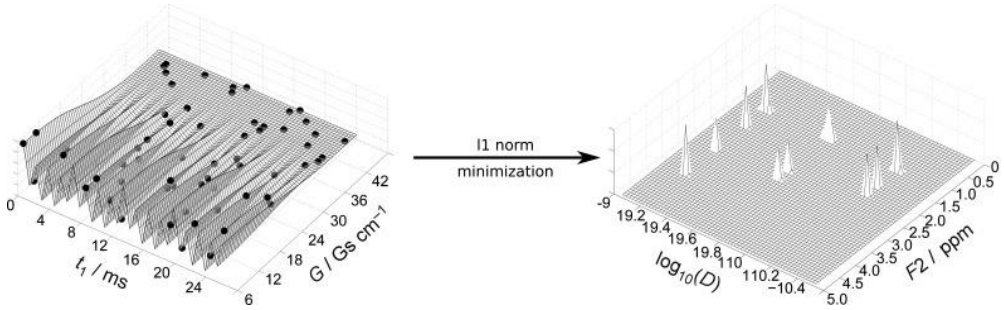

Figure 11: Joint sparse sampling of the time and gradient domains in diffusion-ordered NMR spectroscopy. Reproduced from reference 112. Copyright Wiley

1.4.3 Other methods

A solution to accelerate 2D acquisition was introduced by Kupče in 2002 using Hadamard matrices.[2–4] They are matrices whose coefficients are all 1 or -1 and whose rows are all orthogonal to each other. Instead of sampling randomly as previously, a number of scans is performed using selective radiofrequency pulses whose phases are set according to the selected Hadamard matrix. This makes it possible to decrease the experiment duration by more than one order of magnitude, but has two limitations. First, the number of scans must be larger than the number of signals observed, so it cannot be used on too complex mixtures. Then, the operator has to know the number of signals and their position to setup the experiment.

As mentioned in the introduction, one of the reasons for the long duration of DOSY experiments is the phase cycle required by the STE pulse sequence. A solution to get rid of this phase cycle was suggested under the name “one-shot” DOSY.[113] It is a modification where the two lobes of the bipolar gradient used for diffusion encoding are slightly unbalanced avoiding the need of phase cycling, allowing experiment duration of less than one minute. However, this modification changes the partial refocusing experienced by the spins, leading to the need to adapt the fitting equation used to extract the diffusion information. When a triple-axis gradient probe is available, coherence selection can be achieved with gradient pulses applied on an orthogonal axis, with no need to modify the fitting equation.

1.5 Spatial encoding

The fastest approach to record 2D NMR spectra is ultrafast 2D NMR based on spatial encoding. The central concept of spatial encoding is the parallelization of sub-experiments. Instead of being done one after the other, all the sub-experiments are done at the same time in different regions of the tube as illustrated by the Figure 12.

In this section we will describe how it was used for correlation spectroscopy as well as for diffusion.

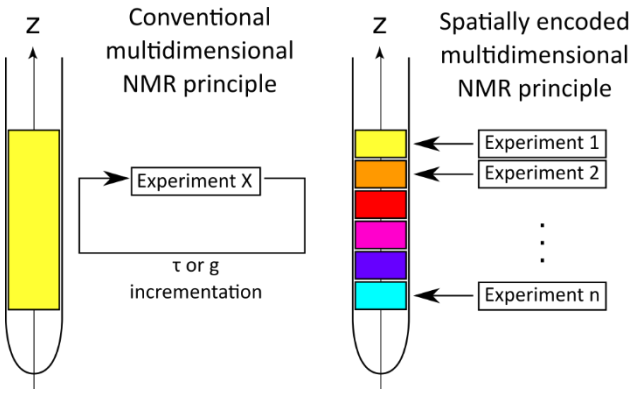

Figure 12: Principle of the parallelization through spatial encoding.

1.5.1 Chemical shift

1.5.1.1 Principle

The concept of chemical-shift spatial encoding has been introduced by Frydman[6,7] and consists in having the different evolution time t_1 in different slices in the NMR tube.

This concept was first implemented with of train of spatially selective pulses, as shown in Figure 13.[6] With this scheme, each slice is excited at a different time, and corresponds to a different value of the evolution time of the 2D experiment. The acquisition scheme also has to be modified compared to a conventional experiment, in order to extract simultaneously spectral and spatial information. The method chosen by Frydman is Echo Plannar Spectroscopic Imaging[114] and consists in a train of bipolar gradient pulses. Such procedure allows a reduction of the experimental duration by more than one order of magnitude: COSY or TOCSY spectra can be recorded in 200 ms. The encoding scheme proposed by Frydman was then improved by Pelupessy.[115] In this new form, the encoding is performed in a continuous rather than discrete manner, with adiabatic frequency-swept chirp pulses rather than a succession of spatially-selective excitation or refocusing pulses, leading to the effective spin evolution shown in Figure 14.

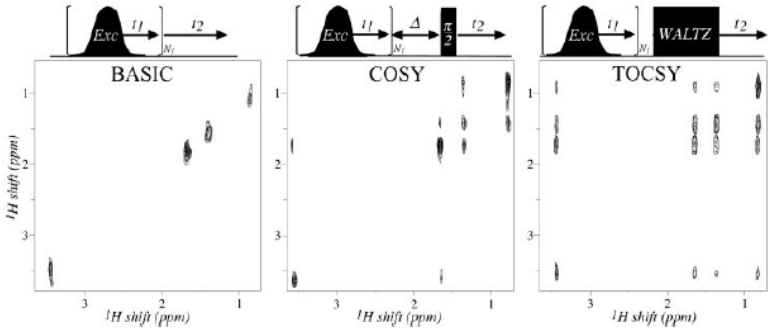

Figure 13: Phase-sensitive single-scan 2D ^{1}H NMR spectra recorded within ≈ 0.22 s on a 20% (vol/vol) solution of n-butylchloride, $CH_3CH_2CH_2CH_2$-Cl, dissolved in CDCl3. The pulse sequences used for acquiring these spectra are shown (Upper), with Δ set to 20 ms in the COSY and a 74-ms-long WALTZ sequence used for the TOCSY. The selective pulses are applied together with a gradient to produce spatial selective pulses. Data were acquired with N1 = 40 initial Gaussian pulses being applied at 4-kHz offset increments, while in the presence of γ_H Ge= 150 kHz/cm, and an acquisition involving 256 gradient echoes of the same magnitude with Ta = 340 μs long and 10-μs dwell times. All remaining pulses were applied nonselectively. Reproduced from reference 6. Copyright Proceedings of the National Academy of Sciences.

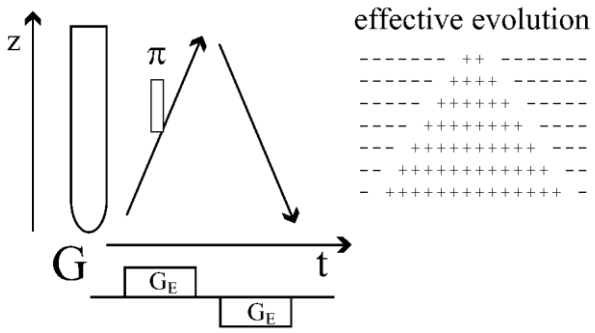

Figure 14: The effect of the two adiabatic pulses can be represented by two instantaneous ð pulses that occur when the frequency of the adiabatic sweep passes through the resonance frequency of the spins. Hence the spins near the bottom of the sample are refocused first while the ones at the top are affected last. For the second pulse the situation is time-reversed since the sign of the gradient is inverted. This results in differential evolution throughout the sample, as shown on the right of the figure. Reproduced from reference 115. Copyright American Chemical Society.

This acceleration can be useful in cases where a long acquisition would not be possible, for example to monitor fast chemical reaction or as a detector after a chromatography separation where substrates do not stay in the detector for a long time.

1.5.1.2 Limitations and method improvement

This significant gain in experiment duration comes with limitations. First of all, due to the high bandwidth needed for the acquisition of such experiment, the amount of noise is higher, leading to a high decrease of Signal to Noise Ratio (SNR). A problem all the more important considering that NMR is already not very sensitive. Another problem, that is due in part to the short acquisition times, is that resolution will drop compared to a conventional acquisition. Another limitation arises from the particular acquisition scheme. To obtain both spectral and spatial information, the acquisition chosen by Frydman is the Echo Planar Spectroscopic imaging (EPSI).[114] It consists in a train of bipolar gradients as shown in Figure 15.

This acquisition scheme, unlike 1D acquisitions, is very demanding and cannot be maintained for more than 100-200 ms on most probes. Then, the spectral width and resolution in the spatial dimension are both limited by the maximum acquisition gradient intensity and, for most probes, the values typically used for conventional acquisitions cannot be attained.

Strategies have been developed to increase the spectral width in the spatial dimension and will be developed later here. To increase the spectral width in the spectral dimension Frydman proposed to

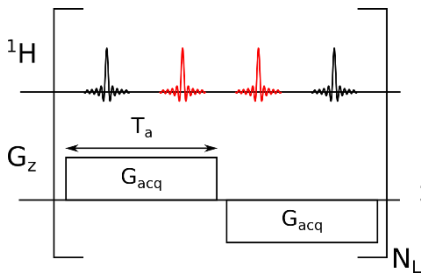

Figure 15: Representation of the EPSI pulse sequence (a) and the resulting trajectory in kt space in 2D (b) and 3D (c).

perform *N*' acquisitions with an incremented delay $2T_a/N$'. He also showed that single scan multidimensional NMR was not specific to ^1H NMR and performed other experiments such as HSQC of 3D TOCSY-HSQC.

Over the years, many other developments of this method have been made to improve it and work around its limitations.

About the encoding and evolution part of the pulse sequence, Shapira suggested to use symmetrical spatial encoding[116] that leads to better lineshapes hence enhancing the resolution. Still about the evolution part of the sequence, Pelupessy & al suggested to modify it to fold peaks, which would otherwise appear outside of the acquisition window, back into the spectrum using a band selective pulse surrounded by a bipolar gradient.[117] Finally, other improvements of the spatial encoding that must be noted are the ones proposed by Shrot & Frydman based on nonlinear encoding that allow to observe chemical site that are too far away from each other to be seen with linear encoding.[118]

About the acquisition part, a modification of EPSI was suggested by Giraudeau & Akoka in order to be able to obtain ultrafast J-res spectra.[119] Instead of a train of bipolar pulses their acquisition step consisted in a succession of positive gradient followed by a 180° hard pulse. However, this method is specific to J-res as the chemical shifts are refocused while homonuclear scalar couplings evolve. A limitation about the acquisition, as said earlier, is that the spectral width in the spatial dimension is limited by the maximum acquisition gradient intensity.

Finally, the last step of the ultrafast NMR method is the processing. As points are not equally spaced, a classical Fourier transform would not lead to the desired results. A first choice would be to process odd and even echoes separately and then combine them.[120] This approach is simple to carry out, but it can be problematic if odd and even echoes are not perfectly mirror images of each other. A second is to use a modified version of the Fourier transform[121] to process at once interleaved odd and even echoes leading to an increase of spectral width and resolution in the spectral dimension by a factor of two. Other suggestions have been made to improve the quality of spectra. For example, Giraudeau and Akoka proposed to perform apodisation along the spatial dimension to improve peak lineshape.[122] This can be done by applying a Fourier transform along the spatial dimension, followed by an adequate window multiplication, such as cosine or Gaussian, and an inverse Fourier transform. This modification can have consequences that will be discussed in section 5.5.

1.5.1.3 Applications

Due to the significant acceleration obtained by using spatial encoding, examples of ultrafast 2D NMR experiments have been reported in several fields, especially for cases where conventional acquisitions were not an option because of their length. First, we will see that it can be used for quantitative analysis, and then, that it is especially useful when conventional experiments are not feasible.

One of the powers of NMR analysis is that, in the right conditions, it is quantitative.[123] In simple pulse-acquire experiments, if relaxation is complete, peak integrals are proportional to the number of spins they integrate for and all peaks have the same proportionality constant. For multidimensional spectra, this is not as simple. Peak integration will also be proportional to the number of spins but the proportionality constant will be different from one peak to another, except for very specific cases. However, quantification is still possible through calibration methods with external or internal reference or with standard addition. It was demonstrated that ultrafast 2D NMR experiments could be used for quantification. This method was used to measure the concentration of a small molecule in a complex mixture[124] through ufDQS or to measure isotopic enrichment in biological mixture.[125] These results show how despite the limitations in terms of SNR, SW or resolution, ultrafast experiments allow to probe complex sample and extract useful information.

NMR spectroscopy is sometimes used as a detector following a separation step by liquid chromatography. While hyphenation of liquid or gas chromatography with mass spectrometry is widespread, it is less so for NMR. LC-NMR requires a specific probe, and proximity between a pump and a magnet. Moreover, as the residence time of the sample inside the probe is short (due to the flow), long experiments, especially the ones needing incrementation and/or phase cycling, are prohibited, limiting the range of feasible experiments to 1D spectra. Thanks to the acceleration power provided by spatial encoding methods, the feasibility of hyphenation of liquid chromatography with UF2DNMR was illustrated. LC-UF2DNMR combines the separation power of chromatography to the specificity of 2D NMR. It was first demonstrated on a custom chromatography setup for the separation of aromatic compounds[126] and was then done on a commercial HPLC-NMR equipment for the separation of natural products.[127]

With their very short duration, ultrafast 2D NMR experiments have opened new perspectives for reaction monitoring. For real-time monitoring, the duration of each NMR experiment should be short compared to the reaction time, in order to sample enough time points for kinetic analysis, and to avoid artifacts or "t_1 noise". The use of UF2DNMR for reaction monitoring was first illustrated by Frydman, whose group showed that it was possible to monitor real-time H-D exchange in proteins, or the first step of an aromatic nucleophilic substitution.[128] This kind of approach was then used by Herrera to study different reactions such as the one between ketones, triflic anhydride and nitrile through TOCSY,[129] or tandem TOCSY/HMBC.[130] It was even possible to identify the presence of reaction intermediates as shown in Figure 16.

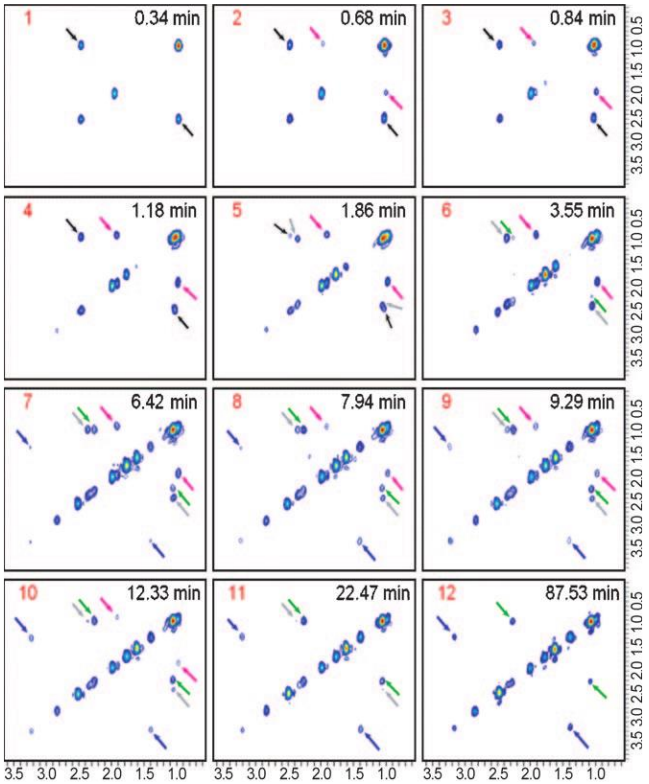

Figure 16: A series of two-dimensional TOCSY NMR spectra taken at different times throughout the reaction (scale is in ppm). 525 TOCSY experiments were acquired. Data were collected at 37C at approximately every 10 s. Time points are shown within each window. Pink and grey arrows show reactional intermediate signals. Reproduced reference 129. Copyright Wiley.

Other information on reactions were obtained thanks to ultrafast 2D NMR of other nuclei such as ^{31}P for example.[130] Reaction monitoring was also performed on electrochemical reactions under particular conditions to identify unstable reaction intermediates.[131]

All the experiments described here were performed at high field, but with the implementation of pulsed-field gradients on low field spectrometer, it became also possible to use ultrafast monitoring on benchtop NMR. It was shown by Gouilleux that it was possible to monitor a Heck-Matsuda reaction at low field despite the limitations of SNR, gradient intensity and gradient axis (as the system is equipped with gradient perpendicular to the tube).[132]

Ultrafast 2D NMR is also particularly useful to collect 2D spectra from hyperpolarized substrates. With single shot hyperpolarization methods such as dissolution dynamic nuclear polarization, magnetization does not reappear once it has been excited, and incrementation cannot be done to create the second dimension. This problem is resolved by spatial encoding as spectra are recorded with a single excitation. Frydman and Blazina demonstrated that it was possible to perform ultrafast HSQC on hyperpolarized sample and compared the results to conventional one.[133] This methodology was studied more in detail[134] and then also used in combination with a "shifting" method to fold peak that rely outside the acquisition window bas in the acquisition range.[135] Another hyperpolarization technique that provides liquid sample is Signal Amplification By Reversible Exchange (SABRE)

relies on the exchange of para-hydrogen, and showed promising results when coupled with ultrafast experiments.[136]

1.5.2 Diffusion

1.5.2.1 Principles

1.5.2.1.1 Encoding considerations

Spatial encoding also allows to encode diffusion information using similar methods. The key idea was introduced in 2001 by Keeler[137,138] and was then also used by Frydman.[139] The encoding scheme was the same in both articles using a combination of chirp pulses and pulsed field gradients. The main difference with the chemical shift encoding is that both gradients have the same sign canceling the chemical shift encoding and a diffusion delay is introduced between them in order to let Brownian motion effect takes place. The principle of this spatial encoding will be more detailed in section 2.2.

1.5.2.1.2 Acquisition considerations

In the aforementioned publications the diffusion spatial encoding is similar but the acquisitions are very different. In Keeler's work, a small gradient is applied while the FID is acquired, that will broaden the peaks and reveal the spatial profile that encodes the diffusion information (due to the previous encoding) as shown on Figure 17. Each diffusion curve can then be fit to the Stejskal-Tanner equation to extract the diffusion coefficient. The major drawback of this method is that, as peaks broaden, the risk of overlapping signals increases. Moreover, for multiplets, the analysis becomes very complicated. The acquisition scheme used by Frydman is the same than for chemical shift encoding: EPSI. This time, as there is no chemical shift encoding, there is only one echo during a gradient lobe. A Fourier transform along the spatial axis will yield a spatial profile that encodes diffusion. It is then possible to fit the spatial profile to obtain the diffusion coefficient. This 2D method has a lower risk of overlapping signals than Keeler's one, but has similar limitation as for chemical shift encoding, namely a limited spectral width in the spectral dimension and harsh acquisition conditions for the probe.

1.5.2.2 Applications

Spatial encoding can also be used to accelerate higher-dimensional experiments. It was demonstrated that a 3D COSY-DOSY with a spatial encoding of the diffusion dimension could be recorded in about 11 min,[9] where the conventional experiment needed about 17h.

Spatially encoded diffusion NMR spectroscopy was used to monitor a chemical reaction. With the example of an imination reaction,[140] Hamdoun et al. showed that the use of spatial encoding allowed to correct the diffusion coefficient of one of the reactants measured with the conventional DOSY that was artificially increased because of the signal decay induced by the chemical reaction.

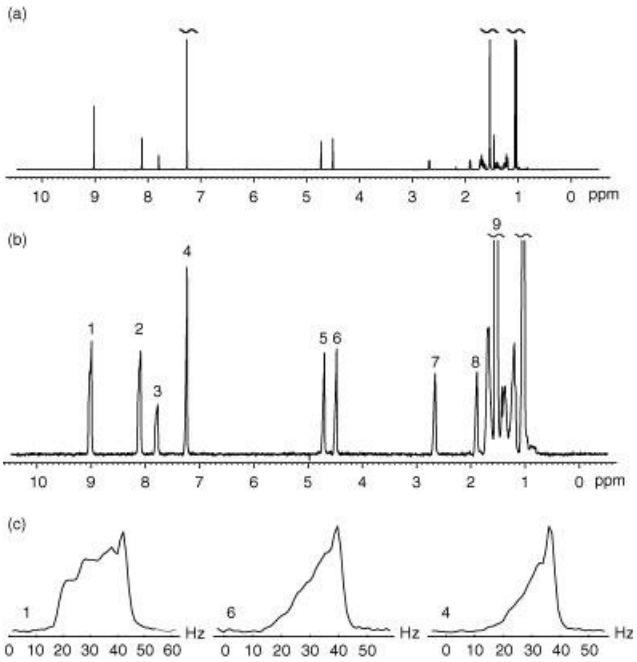

Figure 17: (a) Conventional 1D proton spectrum of a sample containing camphene, a zinc(II) porphyrin and chloroform in CDCl3. (b) 1D DOSY spectrum of the same sample; the diffusion coefficient for each resonance is encoded in its lineshape. (c) Expansions of the 1D DOSY spectrum, showing a zinc(II) porphyrin (1), camphene (6) and chloroform (4) peak. Visual inspection of the peaks gives a qualitative indication of the relative diffusion rates of the three molecules and a quantitative analysis of the lineshapes yields estimates of the diffusion coefficients. Reproduced from reference 137. Copyright Wiley.

Spatially encoded DOSY was also used for hyperpolarized samples in different ways. The proof of concept was done on compounds hyperpolarized through ParaHydrogen-Induced Polarization (PHIP) with ultrafast multidimensional Laplace NMR that was used to obtained D-T_2 maps in less than one second.[141] It was shown that a double diffusion encoding experiments was very effective to reduce the artifacts coming from the rapid injection after dissolution.[142] The same group demonstrated the feasibility of SPEN DOSY on SABRE hyperpolarized mixture, but encountered turbulence problems, coming from the tube shaking. Their solution was to perform the spatial encoding along a perpendicular axis, that lead to good results.[143] Finally, it was also show that ultrafast Laplace NMR could be done on hyperpolarized xenon gas adsorbed on mesoporous materials with standard liquid NMR probe.[144]

1.6 Conclusions

NMR spectroscopy is a powerful analytical method. 1D NMR provides quantitative, structural and conformational information and is very powerful to monitor chemical reactions. On the other hand, multidimensional NMR helps gathering information on the structure or help analyzing mixtures thanks to the addition of the second dimension, reducing overlap between signals. However, the need to record many increments leads to long experiment duration and limits its use for reaction monitoring. Over the years, several methods have been developed to accelerate multidimensional experiments, such as non-uniform sampling and fast-pulsing methods. The fastest scheme was introduced by

Frydman in 2002 and relies on spatial encoding. It was used in several applications where conventional 2D experiments were not possible such as reaction monitoring.

Until now, ultrafast 2D NMR was mostly used for reaction monitoring in an NMR tube, using pulse sequences that were not specifically designed for mixture analysis. An important question is: is it possible to combine flow NMR with spatial encoding for reaction monitoring purposes at high field? It can also be wondered which experiment is the best in this context as several have been shown to provide interesting information about mixtures in their conventional form, such as DOSY or multi quanta spectroscopy, or even a combination of both.

2 Characterization of spatially encoded DOSY

2.1 Introduction

Nuclear magnetic resonance[145] (NMR) spectroscopy is used in diverse fields such as metabolomics or chemical synthesis as it provides a non-destructive and non-invasive analysis of solution mixtures. Diffusion Ordered SpectroscopY (DOSY) is especially well suited for the analysis of mixtures. It can be compared to a virtual chromatography, as it separates the molecules' spectra based on their diffusion coefficients. This method relies on the acquisition of a succession of 1D experiments with increasing intensity for a pair of gradient pulses, which will encode molecules' stochastic translational motion. The resulting data set consists in a series of 1D spectra in which each signal is attenuated by a factor linked to the diffusion coefficient of the molecule of interest. This attenuation can then be fitted to the Stejskal-Tanner equation[8] (see Eq (2.1)) to extract the diffusion coefficient D for each signal. Finally, a graphical representation of the data can be done in a 2D fashion, in which one dimension correspond to the chemical shift, and the second dimension corresponds to the diffusion coefficient.

This method is powerful but the need to increment gradient intensities leads to long acquisition durations that make challenging its use to study out-of-equilibrium samples, such as reaction mixtures or hyperpolarized samples. Over the years, several methods have been developed in order to accelerate the acquisition of DOSY experiments, such as the One Shot method[113] or sparse sampling.[112]

The fastest approach to collect a complete DOSY dataset was developed by Frydman and co-workers[6] and is achieved through Spatial Encoding (SPEN), that leads to acceleration of more than one order of magnitude. A similar method was developed by Keeler also based on spatial encoding, but with a different acquisition method.[138] Since then SPEN DOSY has shown to be very useful and led to several applications.[9,140,142,143]

2.2 Theory

In this chapter, the theory and the basic principles of the SPEN DOSY are described. Then, the setup of the experiment is described in the cases of single-axis-gradient and triple-axis-gradient probes. Then, the influence of encoding and acquisition parameters is analyzed. We discuss the effect on the signal to noise ratio of the chosen encoding block, and of the gradient intensity and the duration of the acquisition. Finally, we show how the effect of convection, which can lead to unphysical results, can be mitigated.

2.2.1 Principle of diffusion experiments

2.2.1.1 Conventional experiments

In conventional DOSY experiments, Brownian motion is encoded through the repetition of 1D sub-experiments with incremented gradient intensity. These gradients are separated by a delay Δ usually called the diffusion delay. Several pulse programs have been developed for this, and the most used is the Stimulated Echo (STE) developed by Tanner.[76] The pulse sequence of the stimulated echo with bipolar gradients can be seen in Figure 18.

The result of this experiment is a series of 1D spectra in which the intensity of each peak decreases. This decay can be fitted to the Stejskal-Tanner equation whose expression is:

$$S(q) = S_0 e^{-[Dq^2\Delta']}, \tag{2.1}$$

where S_0 is the amplitude of the signal in the absence of diffusion attenuation, D is the diffusion coefficient, Δ' the diffusion delay corrected to account for finite pulses, and q is an incremented variable that corresponds to the area of the diffusion-encoding gradient multiplied by the gyromagnetic ratio. This variable is given by the following equation:

$$q = \gamma \int_0^{\delta} G(t')dt', \tag{2.2}$$

with G the time dependent Pulsed Field Gradient (PFG), γ the gyromagnetic ratio of the investigated nuclei. The fitting of the Stejskal-Tanner equation allow to extract a diffusion coefficient for each signal.

The attenuation described by Eq. (2.1) finds its origin in the fact that diffusion mixes volume elements in which the spin's magnetization has different phases. Assuming that the diffusion-encoding gradients are applied along the z axis, during the first gradient pulse the spins acquire a spatial phase that depends on their position along the z-direction. The spins' phase evolution is given by the equation:

$$\Phi(t,z) = \int_0^{t} \gamma G(t')dt' \; z, \tag{2.3}$$

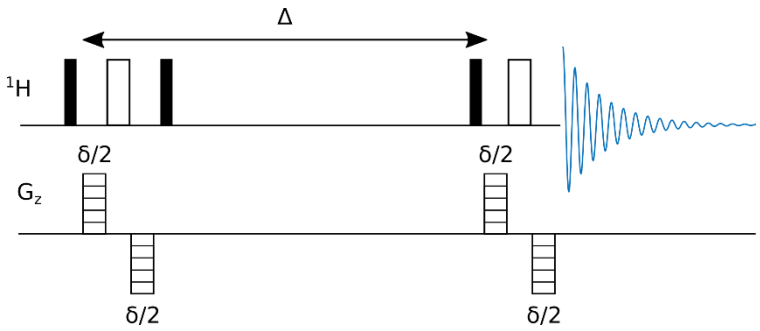

Figure 18: Stimulated echo pulse sequence using bipolar gradient pulses.

where G is the time dependent field gradient, γ the gyromagnetic ratio of the investigated nuclei and z the spins' position in the sample. It can be shown, by solving the Bloch Torrey equation, that the effect of diffusion on the transverse magnetization is given by:

$$\left|M_{xy}(t)\right| = \left|M_{xy}(0)\right| \times \exp\left(-\frac{t}{T_2}\right) \times \exp\left(-D\int_0^t \left(k(t')\right)^2 dt'\right), \tag{2.4}$$

where

$$k(t) = \gamma \int_0^t G(t')dt', \tag{2.5}$$

M_{xy} is the magnetization in X-Y plane, T_2 is the transversal relaxation time and D is the diffusion coefficient of the observed molecule.

When the second gradient pulse is applied, the spins will undergo a spatial phase evolution opposite to the one generated by the first gradient pulse. The net spatial phase evolution will be zero, to produce an observable signal. However, the signal obtained will be attenuated because of diffusion; using Eq. (2.4) and (2.5) for the stimulated echo pulse sequence using rectangular gradients, Eq (2.1) is obtained with $q = \gamma g \delta$ and $\Delta' = \left(\Delta - \frac{\delta}{3}\right)$.

2.2.1.2 Spatially encoded experiments

As explained above, the conventional version of the DOSY experiment requires several increments in order to have enough point to fit the peak decays with the Stejskal-Tanner equation. In this section, the tools to obtain the same information in only one scan, as shown in Figure 19, will be explained.

In conventional experiment, the effective gradient area that spins experience is the same in the entire sample, meaning that the spatial phase created by the diffusion gradients varies linearly across the whole sample, and changes for each gradient increment. With a spatial encoding of the diffusion information, the effective gradient area the spins experience depends on the position as schematized in Figure 19. On triple gradient axis probes, the diffusion encoding is done on the center part of the coil due to gradient inhomogeneity on coil edges as shown with the 1D images on Figure 19.

The Stejskal-Tanner equation (Eq. (2.1)) that was used for conventional experiment with linear spatial phase can be generalized to arbitrary phase variation as:

$$S(z) = \mathrm{S}_0 e^{-\left[\mathrm{D}\Delta'\left(K(\tau,z)\right)^2\right]}, \tag{2.6}$$

where τ is the duration of the spatial encoding block, and K is the first spatial derivative of the spins' phase:[146]

$$K(t,z) = \frac{\partial\phi(t,z)}{\partial z}. \tag{2.7}$$

For conventional DOSY experiments, the values of gradient intensities that are sampled can be chosen arbitrarily, and, usually, linear, quadratic or exponential sampling is used. In this document, we focus only on spatial encoding with a linear variation of the effective gradient area along the NMR tube. Given the Eq. (2.7), a linear variation of the effective gradient area means that a quadratic spatial phase needs to be created. Such quadratic phase can be achieved using a combination of frequency swept chirp pulses and pulsed field gradients.[139] The resulting pulse sequence used derives from the standard STimulated Echo (STE) DOSY and is shown in Figure 20. We will now recall the derivation of the phase created by a chirp + gradient block.

Chirp pulses have a frequency that evolve over time as:

$$\omega_c(t) = O_i + Rt\,, \tag{2.8}$$

where R is the rate of the sweep, t the chirp pulse duration, and O_i is the initial frequency. When the chirp pulse is applied together with a gradient G_e, the pulse sweeps over a region of length:

$$L = \frac{2\,\pi BW}{\gamma G_e}, \tag{2.9}$$

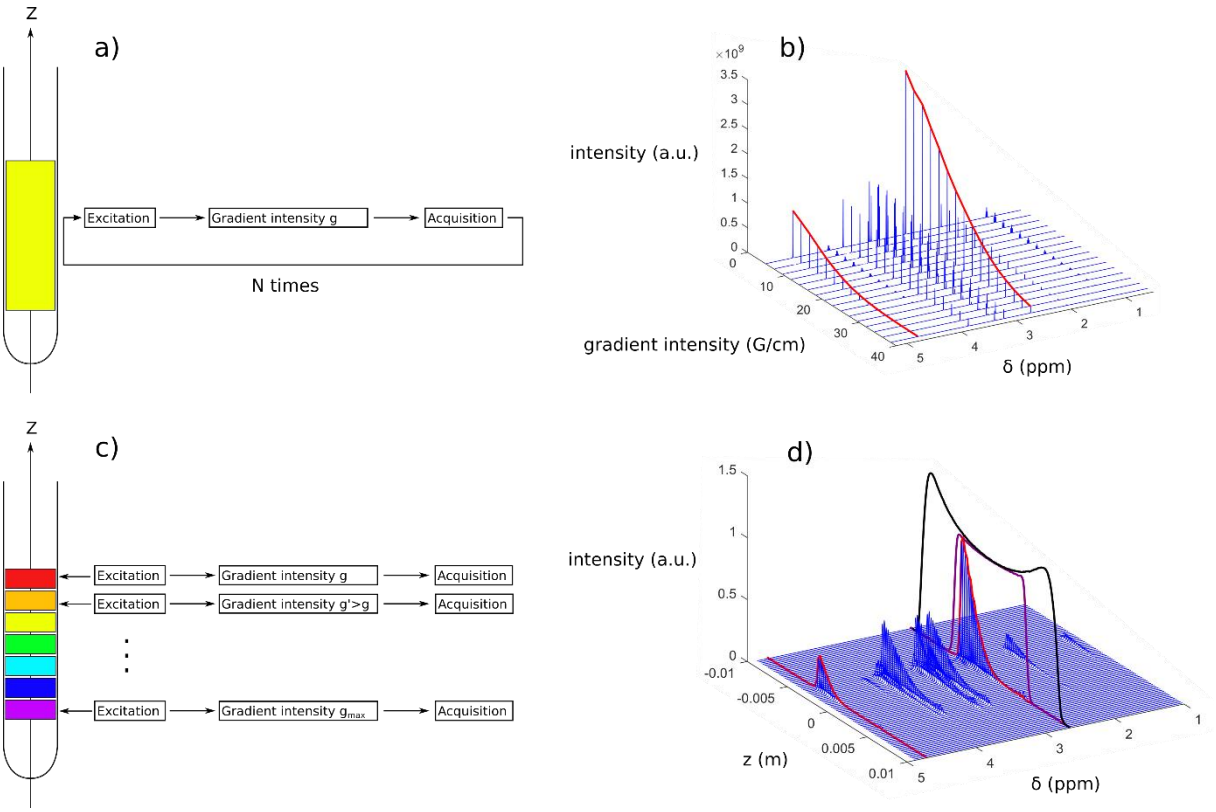

Figure 19: Concept of the conventional DOSY experiment (a) and obtained 2D data set corresponding to a series of 1D ^{1}H spectra decaying as the gradient intensity increases (b). Concept of the parallelization of the gradient intensities as a function of the position of spins in the NMR tube (c) and obtained 2D dataset in which one dimension correspond to the chemical shift while the second dimension correspond to the position (d). In the figures b) and d) the red lines correspond to the data used for the fit and the calculation of diffusion coefficients. The black line corresponds to an unrestricted image of the tube and the purple line correspond to an image with a restriction of 10 mm that have been obtained through similar pulse sequence than SPEN DOSY without diffusion delay and using only one reading gradient.

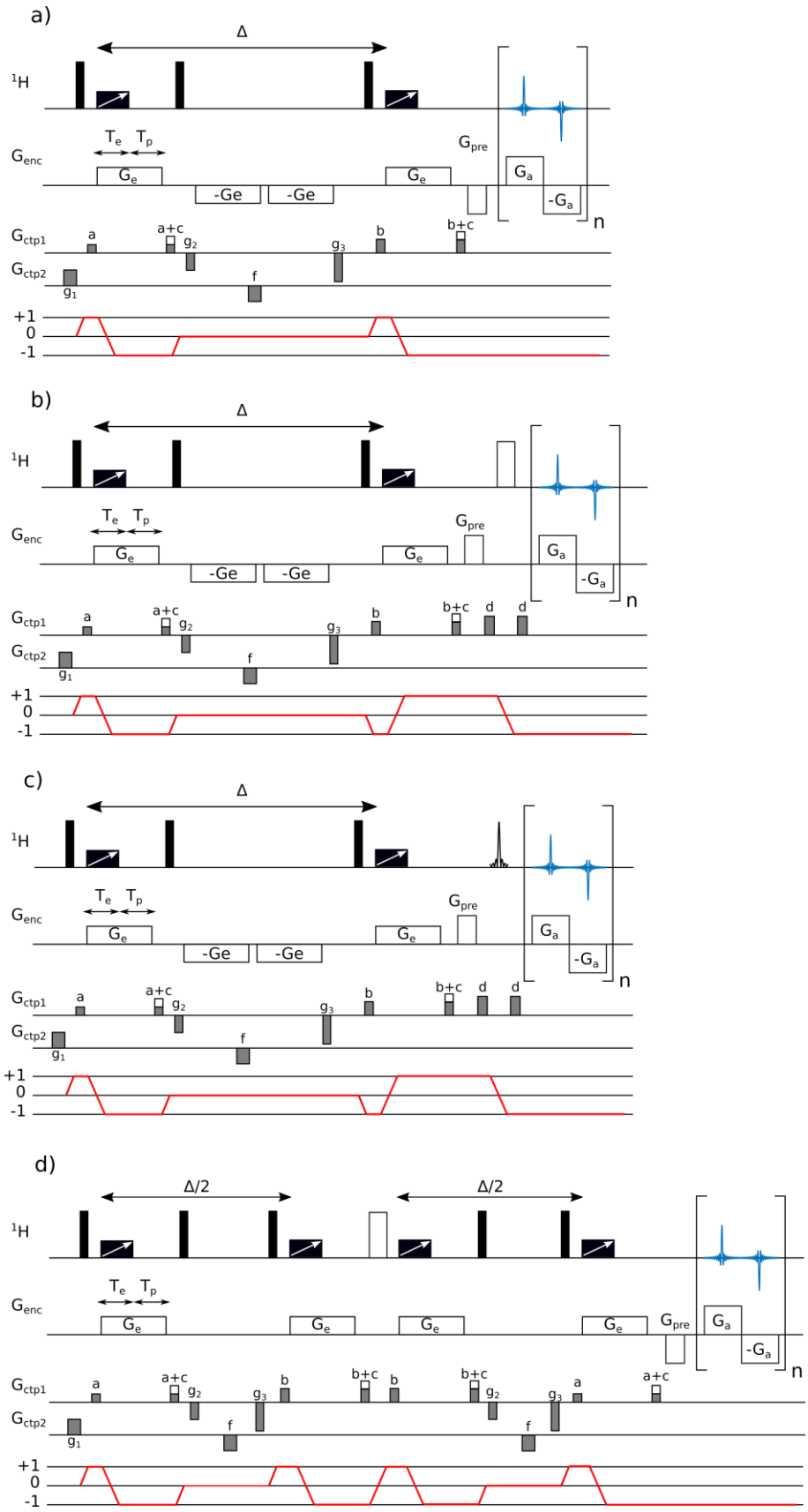

Figure 20: SPEN DOSY pulse sequences. (a) SPEN STE DOSY for magnitude processing. (b) SPEN STE DOSY for pure-aborption processing, (c) SPEN STE DOSY for pure-absorption processing, with spectral selection. (d) SPEN DSTE DOSY. Black rectangles correspond to 90° hard pulses, White filled rectangles correspond to 180° hard pulse. Black rectangles with white arrow correspond to frequency sweeping chirp pulses. Diffusion encoding gradient and CTP (Coherence Transfer Pathway) gradients are displayed on different lines. Red lines correspond to coherence pathways.

where BW is the bandwidth of the chirp pulse and $G_e$is the intensity of the gradient applied with the chirp pulse. When the magnetic field gradient is applied along z, the pulse acts on the sample progressively along z. If it is assumed that spins flip instantaneously under the effect of the pulse[139,147] when their frequency matches that of the pulse, the spins at position z will flip when the condition $\omega_{spins}(z) = \omega_c(t)$ is fulfilled, with

$$\omega_{spins}(z) = \Omega + \gamma G_e z, \tag{2.10}$$

where Ω is the spins' Larmor precession frequency. From these equations, it is possible to extract the moment t_z when the spins will flip:

$$t_z = \frac{\gamma G_e z + \Omega - O_i}{R}. \tag{2.11}$$

Then, it is possible to calculate the phase acquired by the spins during the first chirp pulse can be expressed as

$$\Phi_1(t,z) = (\Omega + \gamma G_e z)t \qquad 0 < t < t_z \tag{2.12}$$

$$\Phi_1(t,z) = -\Phi_1(t_z,z) + 2\Phi_c(t_z) + (\Omega + \gamma G_e z)(t - t_z) \qquad t_z < t < \tau \tag{2.13}$$

with $\Phi_c(t) = \int_0^t \omega_c(t')dt' = O_i t + \frac{Rt^2}{2}$ and τ being the duration of the spatial encoding block. In the case of the SPEN DOSY, the gradient is typically applied for an additional duration T_p after the end of the chirp pulse, leading to the expression $\tau = T_e + T_p$. At the end of the spatial encoding block (t = τ) and after substituting t_z and Φ_{rf} in Eq. (2.13), the spatially dependent phase acquired after the chirp swept is spatially quadratic, and of the form:

$$\phi_1^{(q)}(z) = -\left(\frac{\gamma G_e T_e}{L}\right) z^2 + \left(\gamma G_e T_p - \frac{2T_e\Omega}{L}\right) z^1 + \left(\Omega T_p - \frac{\gamma G_e T_e L}{4} - \frac{T_e\Omega^2}{\gamma G_e L}\right) z^0. \tag{2.14}$$

Finally, taking the derivative of Eq. (2.14), one has

$$K(z) = -\frac{2\gamma G_e T_e}{L} z + \gamma G_e T_p - \frac{2T_e\Omega}{L}, \tag{2.15}$$

that can be simplified assuming $\gamma G_e \gg \Omega$:

$$K(z) = -\gamma G_e T_e \left(\frac{2z}{L} - \frac{T_p}{T_e}\right). \tag{2.16}$$

As expected, thanks to the spatial encoding block, the effective gradient area is position dependent.

The phase given by Eq (2.14) is plotted in Figure 21 in two cases, together with its tangent in two points. It becomes apparent on the figure why the gradient is applied for an additional delay T_p. If T_p = 0, the spins that experience the lowest effective gradient area are at the center of the tube while the ones that experience the highest effective gradient area are at the edges. It means that the diffusion profile will be symmetrical and will contain twice the same information. However, if $T_p = T_e$, the spins that experience the lowest gradient will be at one edge while the ones that experience the highest effective gradient area will be at the other edge.

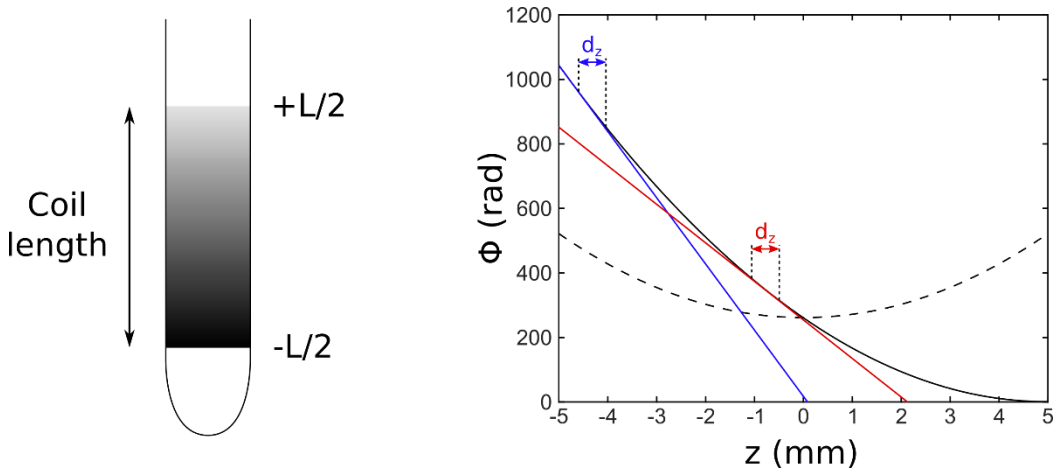

Figure 21: Phase and attenuation: Phase after the first chirp pulse with Tp = 0 (dashed line) and Tp = Te (solid line) and the tangent of the case Tp = Te in two arbitrary points (blue and red straight lines)

Using an equation analogous to Eq. (2.4), with k(t) replaced by K(z,t), Eq. (2.6) may be derived. The full derivation is given in Ref. 146, and results in $\Delta' = \Delta - \frac{\tau}{2}$. In practice, for data analysis, *K* is calculated by numerical integration using the chirp pulse profile.[9] With this model systematic errors are reduced as we no longer consider the 'instantaneous' flip of the chirp and also because we take into consideration the diffusion attenuation occurring during the chirp pulse.

2.2.2 Acquisition considerations

After the diffusion information has been spatially encoded, it has to be decoded, for each peak in the NMR spectrum. This requires the acquisition of a 1D spatial profile for each peak, in a single scan. This can be achieved with Echo Planar Spectroscopy Imaging (EPSI)[114] that is an acquisition scheme frequently used in spectroscopic imaging experiments. Here we will first describe 1D imaging with gradient echoes, then spectroscopic imaging with EPSI.

One of the simplest NMR imaging experiment is the gradient echo, whose pulse sequence is shown in Figure 22. This pulse sequence is composed of a first RF pulse of the desired angle, followed by a prephasing gradient, that create a spatially linear phase, and an acquisition gradient during which the acquisition is done. In such experiment, instead of obtaining a FID, the resulting signal is called an echo (see Figure 22.c). Then, a Fourier transform is done on the echo to obtain a 1D image of the sample along the axis of the gradient as shown in Figure 22.d. Imaging experiments, are usually described by considering the signal not as a function of time (as it is for spectroscopy) but in the k-space, in which k corresponds to the gradient area multiplied by the gyromagnetic ratio, as defined in the Eq (2.5). It corresponds to the spatial frequency that is sampled. In the gradient echo sequence (and in many other, including EPSI), the prephasing gradient is chosen so its area is half the one of the acquisition gradient. This way, it is possible to explore symmetrically from $-k_{max}$ to k_{max} as shown in Figure 22.c.

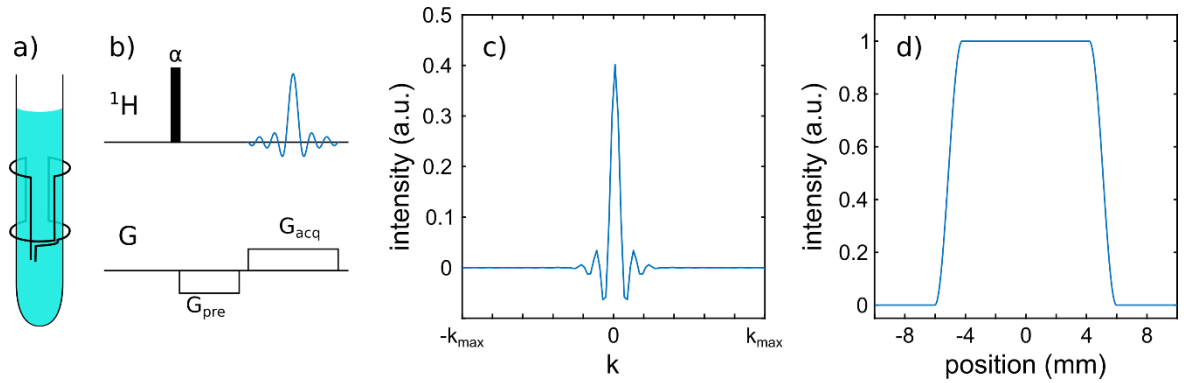

Figure 22: Example of a sample of water in NMR tube to be imaged (a). Pulse sequence of a gradient echo (b), simulation of the signal obtained with a gradient along Z-axis (c) and the image of the sample obtained after Fourier transform of the echo (d).

In the case of the SPEN DOSY experiment, additional encoding blocks, composed of chirp pulses applied together with encoding gradient (named G_e on Figure 20), have been introduced between the acquisition and the detection in order to encode the diffusion information on the desired length. In this particular case, the image obtained will not be solely representative of the spin distribution in the sample, but will be a product of this distribution by a Stejskal-Tanner curve, as shown in Figure 23.

This acquisition method would be adequate to measure the diffusion coefficient of a species if there were only one signal in the NMR spectrum. In order to be able to use this method to analyze mixtures, it is mandatory to have one curve by NMR signal. One solution to obtain such result in only one scan is to use the EPSI method. In such acquisition scheme, after the prephasing gradient, instead of having only one gradient pulse, there is a train of bipolar gradient pulses of duration T_a each. This method allows to observe the signal not only in the k space as it was shown earlier for the simple gradient echo, but in the k-t space. The result consists in a succession of echoes. In order to be processed, the linear succession of echoes is reshaped in a 2D matrix as shown in Figure 24. A first Fourier transform along the t dimension will generate the NMR spectrum, and a second Fourier transform along the k dimension provides the spatial profiles, in which the diffusion information is encoded in the SPEN DOSY case.

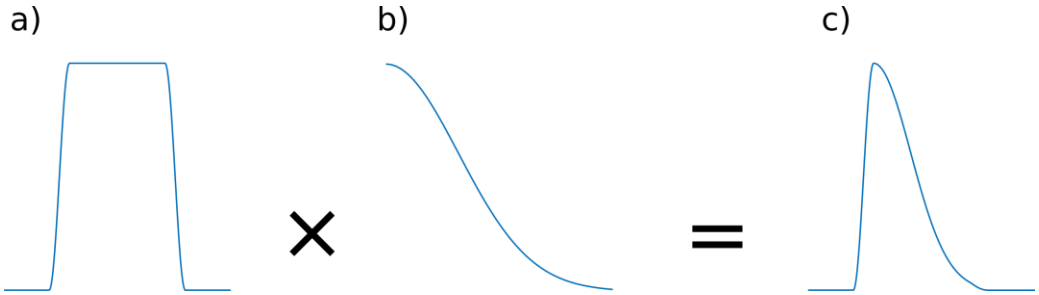

Figure 23: Scheme of a classical 1D image (a), of a Stejskal-Tanner diffusion curve (b), and an example of a diffusion profile obtained after encoding diffusion information (c).

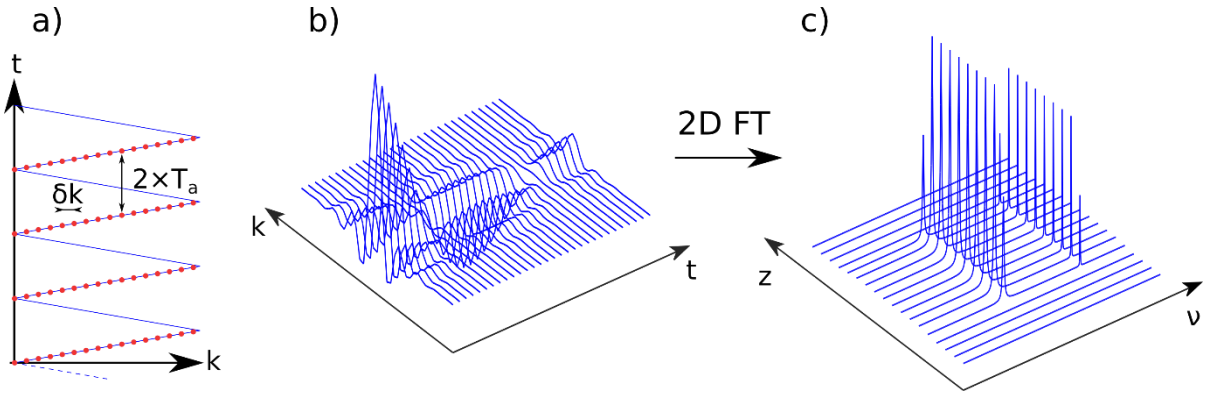

Figure 24: Trajectory in k-t space using EPSI acquisition scheme (a), resulting signal obtained with EPSI acquisition after reshaping (b) and spectroscopic image obtained after double Fourier transform of the echoes in k-t space (c).

Usually, only odds or even echoes are selected to be processed. The duration between two successive odd echoes will then be $2T_a$, allowing to calculate the spectral width in the spectrum dimension:

$$SW^{spec} = \frac{1}{2T_a}, \tag{2.17}$$

Since the EPSI acquisition is performed with a filter bandwidth chosen to accommodate the gradient-induced frequency dispersion γGL, peaks that are out of the region of width SW are folded into the window of interest through translation by an integer multiple of SW^{spec}. In the spatial dimension, the region of space observed, or Field Of View (FOV) detected by the acquisition is:

$$FOV = \frac{1}{\gamma G_a dw}, \tag{2.18}$$

with G_a the intensity of the acquisition gradient and dw the duration between two complex points. The Field Of View is not a constraint as dw can be chosen to be small enough so that FOV > L. Usually, the FOV is set to be several times the size of the observed object. The spatial resolution depends on the area of the readout gradient, as:

$$\Delta r = \frac{1}{\gamma G_a T_a}, \tag{2.19}$$

The higher the acquisition gradient, the better the resolution. For SPEN DOSY, the gradient intensity has to be chosen to have enough resolution to have a well-defined fitting curve while keeping the highest SNR possible. Spatial resolution indeed comes at the cost of a loss in signal to noise ratio. As stated above, the acquisition bandwidth is larger than for conventional experiments. As noise is proportional to $\sqrt{BW}$, the SNR of spatially encoded experiment is lower than that of conventional ones.[148] The losses in sensitivity per square root of measurement duration is proportional to $\sqrt{N_p}$, where N_p is the number of pixels into which the diffusion profile is sliced.

In the case of the SPEN DOSY, EPSI is used similarly as in MRI experiments to obtain one spatial profile for each signal in the NMR spectra. It differs from its use in the ultrafast COSY (UFCOSY) experiments were there are multiple echoes according to the number of signal in the NMR spectrum,

and where the Fourier transform is done only in the time dimension. Note that, in contrast to UFCOSY that will be developed in the next chapter the maximum gradient strength is typically not a limitation for SPEN DOSY.

2.2.3 Convection in diffusion measurement

Additional challenges exist for diffusion experiments when there is motion other than translational molecular diffusion in the sample. When the solvent is very fluid or has low ebullition point, or when the sample temperature is away from room temperature, convection phenomenon will occur. It is due to the temperature gradient in the NMR tube that causes the hotter part of the solution to rise while the colder part moves in the opposite direction. It means that the molecules will acquire an additional motion and velocity to the one due to the Brownian motion as shown in the Figure 25.

During DOSY experiments, convection usually leads to sensitivity losses, faster decay and in some cases spurious oscillations in the data. There are several solutions to avoid the problems caused by convection. The first one is to work in conditions less suitable for convection to appear,[81] such as changing the diameter or the material of the NMR tube, increasing the gas regulation flow to homogenize temperature within the sample, restraining sample length using Shigemi tubes, or spinning the sample. Another one is to use gradient pulses along a transversal axis, in order to encode diffusion in a direction perpendicular to convection. However, it requires a triple axis gradient probe, and for SPEN DOSY the small diameter of the tube is a limitation as the encoding has to be done on less than 4 mm (compared to 10 mm on Z-axis) and as a reference profile is needed for the processing.[143]

The last solution, the one we chose to use, was proposed by Jershow and Muller[82] and consists in using a specific pulse sequence composed of two symmetrical steps that will cause the effect of the velocity to cancel out while the effect of the diffusion adds up. This method gives good results for conventional DOSY, and the convection-compensated SPEN DOSY pulse sequence has been designed by analogy (see Figure 20 d)) for the SPEN DOSY convection compensated pulse sequence).

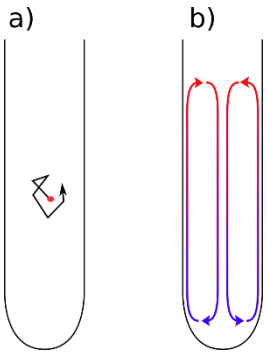

Figure 25: Scheme of a particle submitted to the random Brownian motion (a) and global motion created by thermal convection (b).

In order to compensate for the effect of the velocity, it is needed to evaluate the additional phase shift caused by the flow that can be calculated using the following formula

$$\Phi_v(t) = \gamma G \delta t v_z \,, \tag{2.20}$$

with δ the duration of the gradient and v_z the component in the z-axis of the fluid velocity v. The signal attenuation is hence modified to become:[10]

$$S(q) = S_0 e^{-\left[Dq^2\left(\Delta-\frac{\delta}{3}\right)\right]} e^{[iv_z q\Delta]} \,. \tag{2.21}$$

By analogy, we can assume that in the case of SPEN DOSY Eq. (2.21) becomes

$$S(z) = S_0 e^{-\left[DK(z)^2\left(\Delta-\frac{\tau}{2}\right)\right]} e^{[iDK(z)v_z(\Delta-\tau)]}, \tag{2.22}$$

where τ is the duration of the diffusion encoding block that can be expressed as $\tau = T_e + T_p$: If we consider p as the coherence order that change to select the desired CTP one can define

$$K^*(z) = pK(z). \tag{2.23}$$

The Stejskal-Tanner equation for the DSTE becomes

$$S(z) = S_0 e^{-\left[DK_1^*(z)^2\left(\Delta''-\frac{\tau}{2}\right)\right]} e^{[iDK_1^*(z)v_z(\Delta''-\tau)]} e^{-\left[DK_2^*(z)^2\left(\Delta''-\frac{\tau}{2}\right)\right]} e^{[iDK_2^*(z)v_z(\Delta''-\tau)]}, \tag{2.24}$$

with $\Delta'' = \frac{\Delta}{2}$ so that the result can be compared with the single STE.

Compensation of the velocity induced phase term is obtained for $K_1^*(z) = -K_2^*(z)$ in a way that the diffusion effect is cumulative at the end of the pulse sequence. However, because of the second STE block, the sensitivity will drop by 50% compared to a classical STE experiment.

2.3 Experimental

2.3.1 Spectrometers

The experiments with a single-axis gradient probe (section 2.4.7) were carried out on a Bruker Avance III spectrometer operating at a ^{1}H Larmor frequency of 500.13 MHz and equipped with a 5 mm dual ^{1}H/^{13}C cryo-probe with single-axis gradients.

The other experiments (sections 2.4.2 to 2.4.6) were carried out on a Bruker Avance III spectrometer operating at a ^{1}H Larmor frequency of 500.13 MHz and equipped with a room-temperature 5 mm TXI ^{1}H/^{13}C/^{15}N probe with triple-axis gradients.

In both cases, the gradients were calibrated along each axis using a Shigemi tube filled with doped water (1% H_2O + 0.1% $CuSO_4$ in D_2O) and a restricted sample length of 10 mm. The temperature inside the probe was calibrated with a standard methanol sample and then set to a value of 298 K with airflow of 535 L/h. All the experiments were done without sample rotation.

2.3.2 Samples

Several model samples were prepared.

The first model mixture (M1) for setting up the experiment was prepared according to the following procedure. 7.2 of L-valine was dissolved into 590 µL of D_2O. Then, 2.4 µL of methanol, 3.4 µL of ethanol and 4.5 µL of n-propanol were added to the solution. The solution was shaken until complete dissolution of valine and filtered to remove any solid particles. The concentration is near 100 mM for each compound.

The second model mixture (M2) for setting up the experiment was prepared according to the following procedure. To 600 µL of D_2O was added 24.3 µL of methanol, 35.0 µL of ethanol and 44.9 µL of propanol. The concentration is near 1 M for each compound. The sample was well shaken and poured into a 5 mm NMR tube.

The third model mixture (M3) was prepared according to the following. In a vial was weighted 14.8 mg of caffeine, which was dissolved in 750 µl of D_2O. The solution was shaken until complete dissolution. In that solution was added 7.2 µL of ethyl acetate, 5.3 µL of DMSO and 3.0 µL of methanol. The concentration of each molecule is about 100 mM. 600 µL of this solution was withdrawn and introduced into a 5 mm NMR tube.

The fourth model mixture (M4) of pyridines was prepared according to the following. 10.9 mg of N,N-dimethyl-nicotinamide and 11.5 mg of 4.4-bipyridyl were weighted and dissolved in 750 µL of $CDCl_3$. The solution was shaken until complete dissolution. To that solution was added 8.6 µL of 3-ethylpyridine and 6.1 µL of pyridine. The concentration of each molecule is about 150 mM. 600 µL of this solution was withdrawn and introduced into a 5 mm NMR tube.

The fifth model mixture (M5), used for convection-compensated experiments, was prepared according to the following. In a vial was weighted 14.6 mg of caffeine, which was dissolved in 750 µl of $CDCl_3$. The solution was shaken until complete dissolution. In that solution was added 7.2 µL of ethyl acetate, 5.3 µL of DMSO and 3.0 µL of methanol. The concentration of each molecule is about 100 mM. 600 µL of this solution was withdrawn and introduced into a 5 mm NMR tube.

2.3.3 Processing

All the experiments were processed using a custom MATLAB code shown in the annexes. First data are read from Bruker format. The data are stored as 1D fids, so they are first reshaped as 2L x M matrices,

where L is the number of loops in the EPSI train and M the number of points acquired during each readout gradient. Then apodisation in the time dimension is done: for data processed in pure absorption, apodisation consists in a cosine window, while for data processed in magnitude, a sine window is used. If necessary, apodisation can be done using a Hamming window in the spatial dimension, but it is not done here. At this point only odd echoes are selected to be processed. Next, zero filling in the time dimension is applied prior to double Fourier transform. Similarly, although it can be done, no zero filling is applied on spatial dimension. Then, peaks are selected on a 1D spectrum (in order to obtain the value of the non-folded chemical shift) and on a slice of the data (possibly including folding). A correction of their chemical shift displacement during encoding and acquisition is performed. For each peak the diffusion curve is plotted and fitted to the modified Stejskal-Tanner equation to extract the corresponding diffusion coefficient. Finally, a DOSY map is created regrouping for each peak the selected region, the diffusion coefficient and the standard deviation of the fit (illustrated in Figure 26).

2.4 Results at high field and discussion

The proof of concept of SPEN DOSY has already been shown and used for several applications.[142,143,149] As said previously, it consists in encoding the Brownian motion to obtain a map in which one dimension is the classical chemical-shift axis in ppm while the second one is a diffusion coefficient axis as shown in Figure 27 a). In our case the calculation of the diffusion coefficient is done fitting the diffusion curve with the modified Stejskal Tanner equation (Eq.(2.6)) as shown in Figure 27 b-f). Here we will focus on how robust and sensitive the measurement of diffusion coefficient is to modifications of different parameters, such as encoding and acquisition ones. It will also be shown how the use of experiment that can be processed in pure absorption enhances resolution. Finally, the efficiency of the DSTE to cancel convection effect will be shown.

2.4.1 Classical parameters

Here we will describe examples of classical parameters and results that can be obtained on a single axis gradient probe, using sample M1. First, we choose to induce a decay on 20 mm. Note that this number must be adapted depending on the probe the experiment is done on: on single axis gradient direct probe, a value up to 20 mm can be chosen, but on inverse probe, the maximum value is around 15 mm (as the coil is shorter). On triple axis gradient probe (that will be used further) it is preferred to keep a maximum value of 10 mm because of the non-uniform gradient further away from the center of the coil. For a given length of the region used for spatial encoding, the maximum effective gradient area is given by the product $T_e \times BW$. Its value should be selected by trial-error as it would be done for conventional DOSY with the aim of having a diffusion curve that have a good attenuation. Usually we try to set parameters so that a peak from the acquisition with the highest gradient amplitude have

an intensity of about 5% of the intensity of the same peak from the acquisition with the lowest gradient amplitude. In this case the resulting parameters are a chirp of duration (T_e) 2.5 ms sweeping over 200 kHz (BW) applied with a gradient of 35.3 % (23.5 G/cm) of the maximum gradient intensity. The acquisition consists in a series of 310 pairs of echoes of 190 points each separated by a dwell time of 1.25 µs. This leads to a Ta = 250 µs corresponding to SW = 2000 Hz. If a peak does not fit in the window, it will be folded. For the sample we studied (M1), the spectral width is wide enough to avoid folding. The results of a SPEN DOSY obtained with such parameters and several diffusion curves can be seen in Figure 27 a).

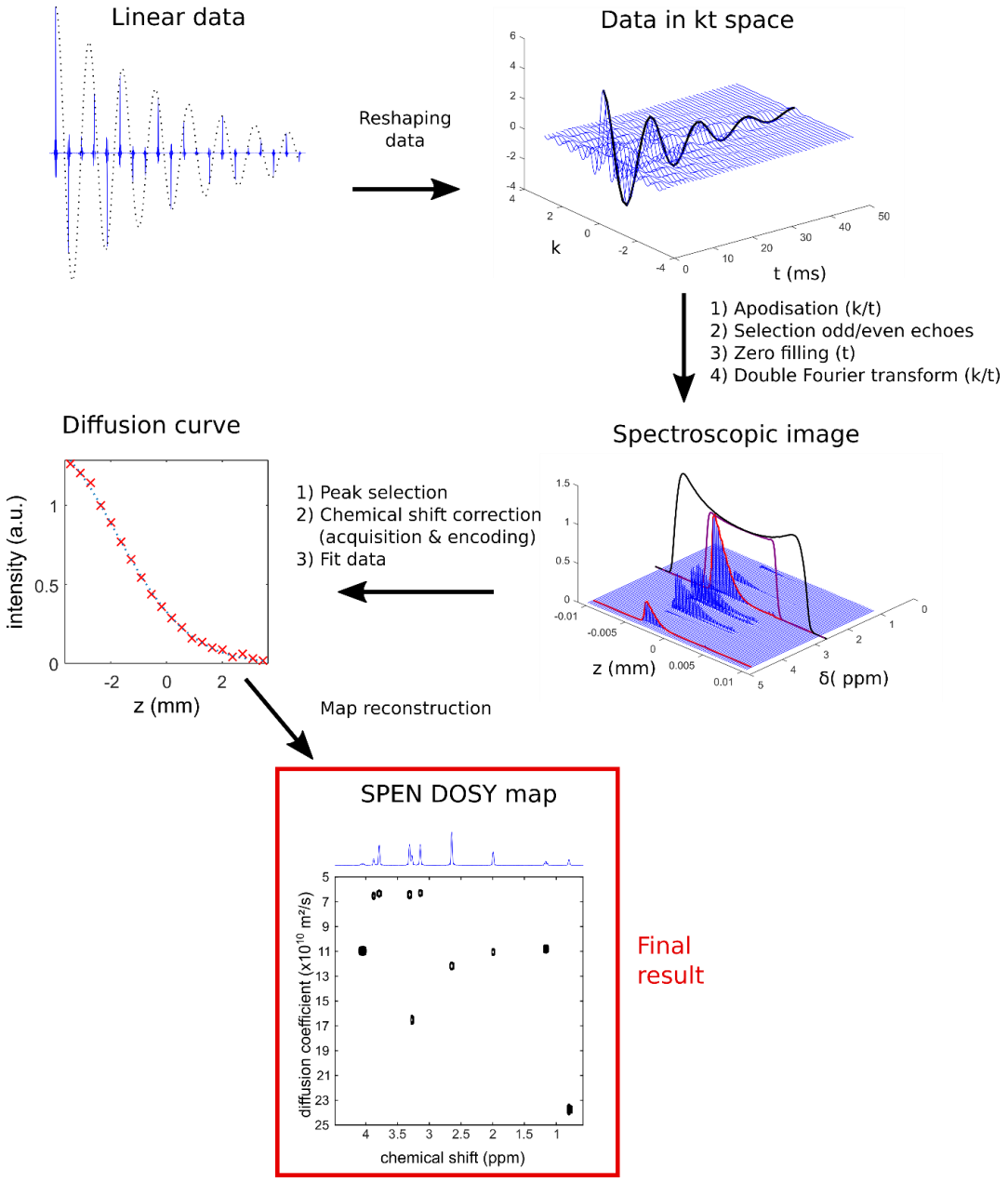

Figure 26: Workflow for SPEN DOSY processing

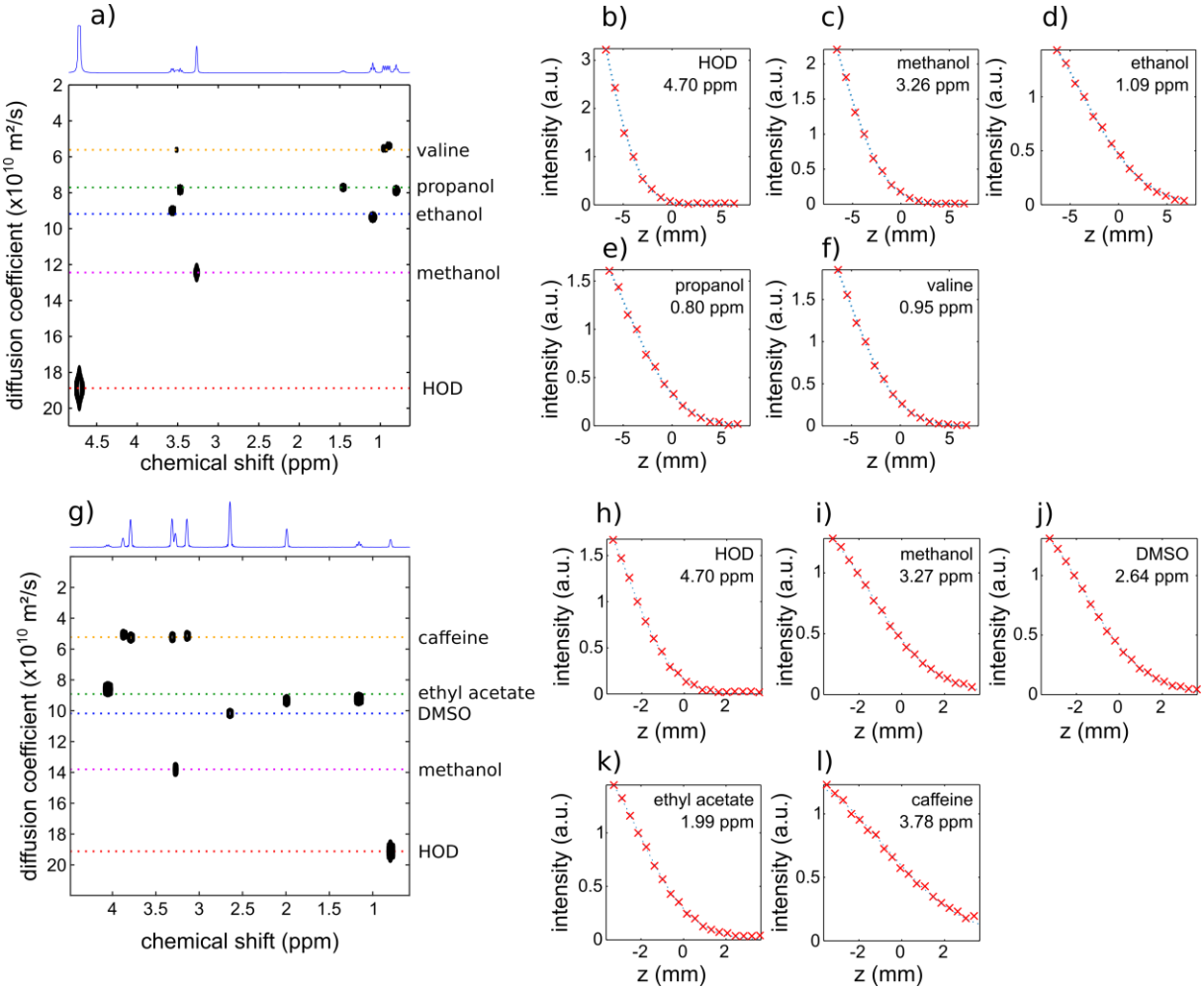

Figure 27: Example of a SPEN DOSY 2D map obtained on the model mixture 1 (a) and 3 (f). Examples of diffusion curves for compounds in mixtures 1 (b-e) and 3 (g-k) The blue dotted lines correspond to the fit and the red crosses correspond to the experimental points

In this case, gradient named “c” (see Figure 20 a)) was not used for reasons that will be explain in section 2.4.7. Gradient “g_2” corresponds to twice the “a” gradient and the “g_3” gradient corresponds to twice the “b” gradient. The gradient “f” is a spoiler to cancel all magnetization left after the second 90° hard pulse and the ”g_1” gradient is a compensation gradient that is the opposite of “f".

For triple gradient axis probe, different parameters have been used for the following sections. For the encoding part, the decay was induced on 10 mm with a variety of chirp pulses that will be detailed in section 2.4.2. The acquisition consists in a series of 256 pairs of echoes of 128 points each separated by a dwell time of 1 µs. This leads to a Ta = 256 µs corresponding to SW = 1953 Hz. The acquisition gradient was set to 35% (22.1 G/cm). For the acquisition gradient and the acquisition length parts, a 1.5 ms chirp pulse with a bandwidth will be used in combination with an encoding gradient of 41 % (25.7 G/cm) and the acquisition parameters were modified according to was is explain in these parts. On the triple gradient axis probe, the “c” gradient has been used with gradients along orthogonal axis.

2.4.2 Influence of encoding parameters

In the next parts we will focus on how the modification of certain parameters influences the measurement and the signal to noise ratio of SPEN DOSY. All the experiments in this section were carried out on a triple-axis gradient probe.

SPEN DOSY relies on spatial encoding of the diffusion information. While with conventional experiment the parameters to choose are the gradient ramp and the duration of the gradient pulses, with SPEN DOSY the critical ones are the duration of the chirp pulses and their bandwidth. For a given length of the spatial region used for encoding, the product of the duration by the bandwidth of the pulses will determine the maximum gradient area the spins will experience. They can be jointly modified to increase or decrease the duration of the chirp while keeping the same product $T_e \times BW$. The goal is to keep the chirp duration T_e as short as possible while having a reasonable maximum B_1. In order to verify that experiments with different chirp duration while keeping the product $T_e \times BW$ constant would yield the same results, a series of SPEN DOSY experiments were done with various encoding parameters on a model sample composed of ethyl acetate, DMSO, methanol and caffeine in D_2O (sample M3). These parameters are displayed in Table 1. As the pulse sequence allows it, the experiments were processed in magnitude and in pure absorption and the diffusion coefficients measured for each peak are displayed in the Figure 28 a). Except for the methanol and water peaks, the results are very similar from one experiment to another. The variations of methanol and HOD diffusion coefficients could come from the fact that the maximum gradient area was set to observe diffusion of heavier compounds, leading to results with larger uncertainties. One ethyl acetate peak also shows some variations and larger uncertainties from other signals. It corresponds to the CH_2 peak (4.05 ppm) that is the peak with the lowest SNR of the spectrum, hence usually the one that lead to the worst fit. Then a comparison in SNR was done between all encoding parameters that were used here. Out of simplicity, only the SNR of the DMSO peak was taken into consideration. For each experiment DMSO, SNR was calculated for magnitude and absorption processing and were plotted in the Figure 30 a). In each case the SNR is better with absorption processing by a factor around $\sqrt{2}$. All the experiments have SNR of the same order of magnitude and no clear tendency seems to appear even if punctual changes can be seen.

2.4.3 Influence of acquisition parameters

In order to have a better understanding on how the parameters of the EPSI acquisition impact the measurement of the diffusion coefficient, two parameters were studied: the intensity of the acquisition gradient and the duration of the acquisition (the number of loops of the EPSI acquisition).

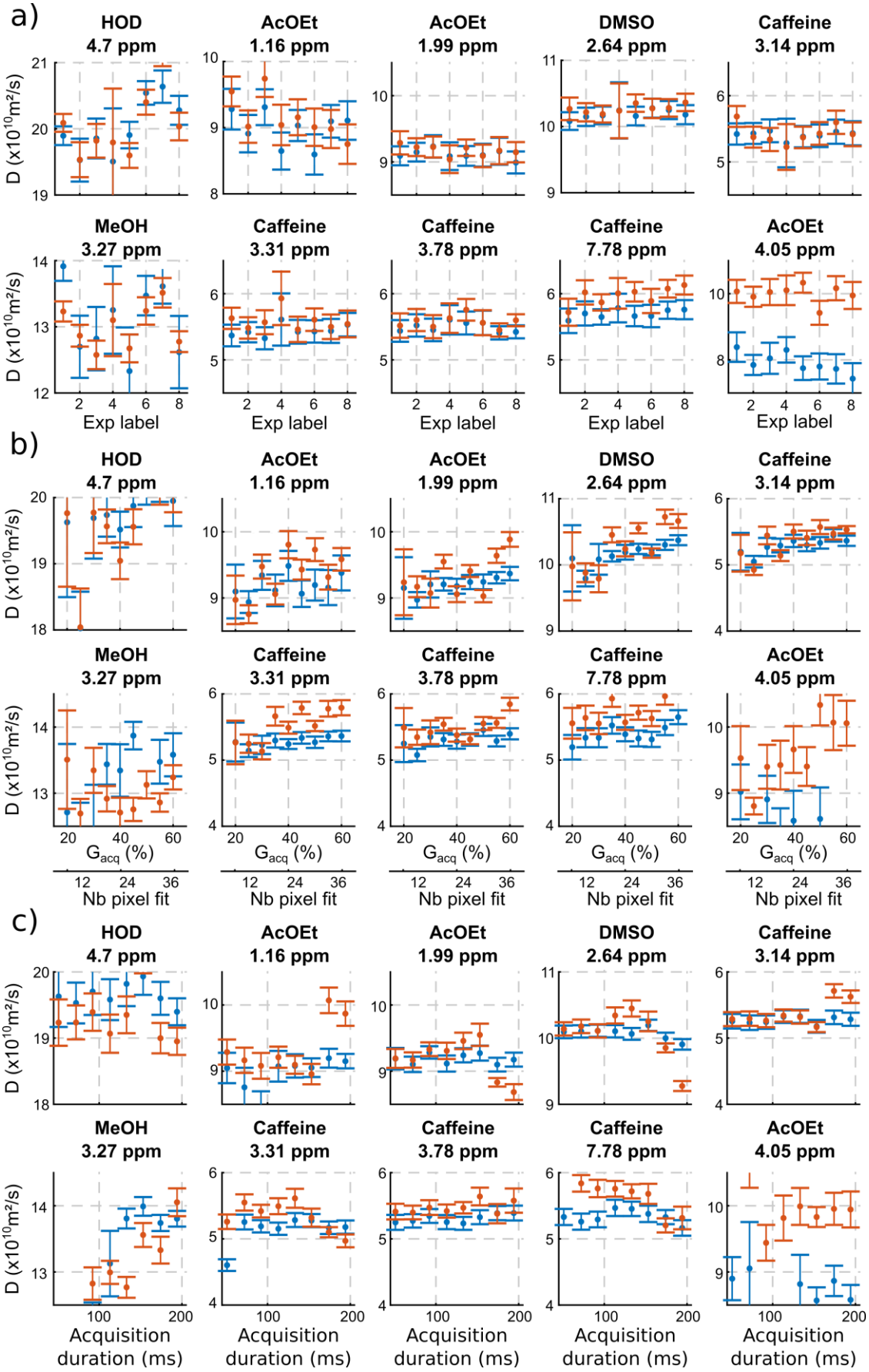

Figure 28: Diffusion coefficient of each peak of the mixture depending of the encoding parameters a) used (see Table 1), the acquisition gradient intensity (b) and the acquisition duration (c), processed in magnitude (blue) or in absorption (red).

Table 1: Duration and bandwidth of the chirp pulses used for the study of the spatial encoding effect.

Exp label	T_e (ms)	BW (kHz)	G_{enc} (G/cm)
1	1.5	91.0	21.38
2	2.0	68.3	16.04
3	2.5	54.6	12.83
4	3.0	45.5	10.69
5	3.5	39.0	9.16
6	4.0	34.1	8.02
7	4.5	30.3	7.13
8	5.0	27.3	6.42

2.4.3.1 Acquisition gradient

For a given duration of a readout gradient pulse, its intensity determines the resolution of the image. In order to determine the influence of the intensity of the acquisition gradient on the measured diffusion coefficient, a series of experiments were acquired with increasing acquisition gradients on the same model sample as previously (M3). For each experiment, the diffusion coefficient calculated for each signal and the standard deviation of the fit were extracted and compared on Figure 28 b). The diffusion coefficient measured with absorption and magnitude processing are compared as a function of the gradient intensity that can also be expressed as the number of points on which the fit is done. The data seems to show that the calculated diffusion coefficient is increasing with the gradient intensity. This phenomenon is not fully understood yet. Another important effect that must be noted is the modification of the signal to noise ratio as a function of the acquisition gradient intensity. As the gradient intensity increases, the frequency dispersion increases too, leading to a lower signal to noise ratio and higher resolution, hence a higher number of points on the fitting curve. For each experiment, the signal to noise ratio of the DMSO peak was calculated as a function of the acquisition gradient intensity and the results are plotted on Figure 30 b). As expected, the signal to noise ratio decreases when the gradient intensity increases. A choice has to be done between signal to noise ratio and number of points for the fit. As shown previously, the acquisition gradient also has an impact on the resolution hence the number of points of the fit as shown with the second axis on Figure 28 b) and Figure 30 b).

2.4.3.2 Acquisition duration

The second parameter that was investigated was the acquisition duration. A series of experiments were acquired with an increasing number of loops for the EPSI block, keeping the duration of a single readout gradient pulse constant, still on the same model sample (M3). The diffusion coefficients were extracted and compared in the Figure 28 c) as a function of the acquisition duration. For most peaks,

the results are similar regardless of the acquisition duration. However, the methanol and one of the caffeine peaks are noticeably affected when the acquisition is too short. This phenomenon is due to the loss of resolution when the acquisition duration is not long enough, and can also come from the apodisation in the case of magnitude processing. The window used in this case is a sine function and can lead to small modification of the peaks position as shown on Figure 29. For caffeine and methanol peaks, counter intuitively, resolution seems to be better with acquisition duration of 52 ms than with 92 ms. This is due to sine apodisation. This anomaly disappears if cosine apodisation or no apodisation used, but in the first case peaks becomes too broads and in the second, truncation artifacts make the processing very complicated.

As the peaks are close to each other, poor spectral resolution yields meaningless fitting curves and diffusion coefficients values. As previously, the effect of the acquisition duration on the signal to noise ratio was investigated. For each experiment, the signal to noise ratio of the DMSO peak was calculated and plotted in the Figure 30 c). Except for the last point (probably due to hardware difficulties to acquire for 200 ms) the longer the acquisition is the higher the signal to noise ratio becomes. Of course, this effect will occur only if the acquisition is short compared to the transverse relaxation time: if acquisition duration grows too much, relaxation will take place hence limiting the phenomenon.

2.4.4 Resolution enhancement through pure absorption experiments

The initial implementation of the SPEN STE DOSY experiment (see pulse sequence in Figure 20 a)), is not designed for pure-absorption processing, and the resulting data is processed in magnitude mode. In order to gain in resolution, it would be interesting if the data could be processed in pure absorption. A hard 180° pulse was thus added between the end of the second encoding gradient and the beginning of the acquisition in order to obtain a full refocusing of the chemical-shift evolution at the time of the first gradient echo of the EPSI train, hence producing pure absorption peaks (see Figure 20 b)).

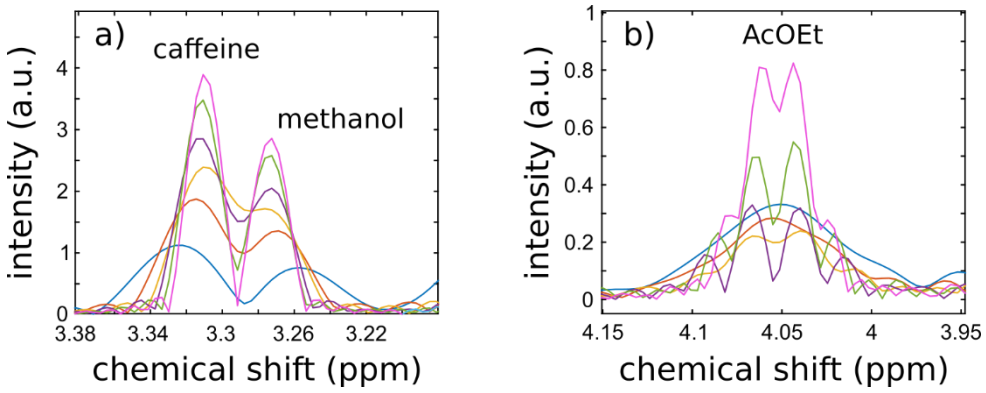

Figure 29: Zoom on caffeine and methanol (a) and ethyl acetate (b) extracted from 2D datasets after processing. These results have been obtained with acquisition duration of 52 (blue), 72 (red), 92 (yellow), 113 (purple), 133 (green) and 153 ms (pink).

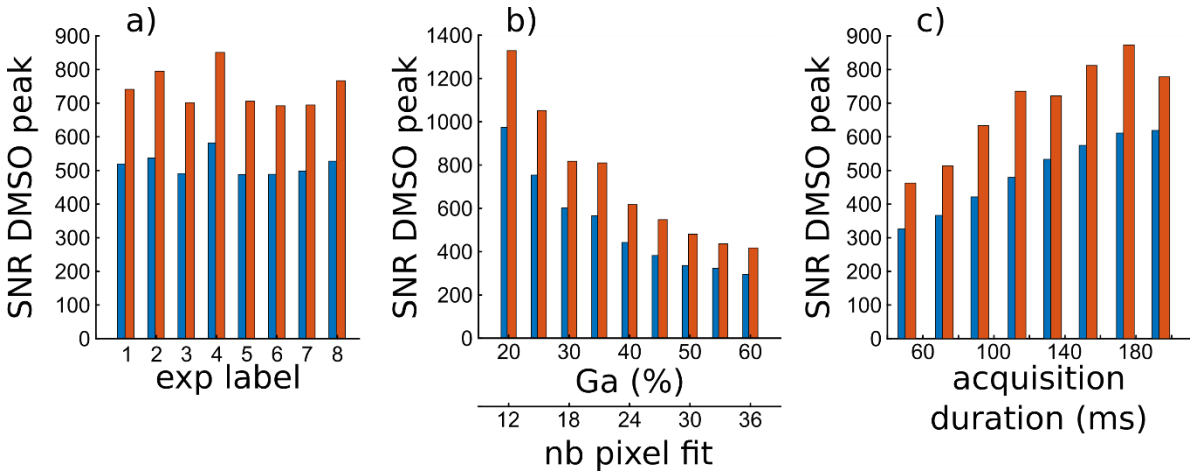

Figure 30: Signal to noise ratio of the DMSO peak measured after EPSI processing as a function of the encoding parameters (a) (see Table 1 for detail of the parameters), acquisition gradient intensity (b) and of the acquisition duration (c). Red bars correspond to pure absorption data and blue bars correspond to magnitude data.

The gain in resolution is illustrated on a mixture of pyridine derivatives: N,N-dimethylnicotinamide, 4,4-bipyridyl, 3-ethylpyridne and pyridine (sample M4). The crowded part of the spectrum in the aromatic region represents a challenge for SPEN DOSY. A spectrally selective SPEN DOSY experiment, replacing the hard 180° pulse by a spectrally selective 180° pules (see Figure 20 c)), was used on the previously mentioned sample to eliminate folding of aliphatic signals. The data obtained were processed in pure-absorption mode and in magnitude mode and the final 2D maps obtained were compared. The results are displayed in Figure 31. While no useful information can be obtained from the magnitude-mode processed data, because of peak overlap, pure-absorption processing makes it possible to distinguish the four compounds of the mixture. This illustrates the advantage of the pure absorption processing, even if, in this case, the separation between the four compounds is not perfect and overlap remains in the diffusion dimension.

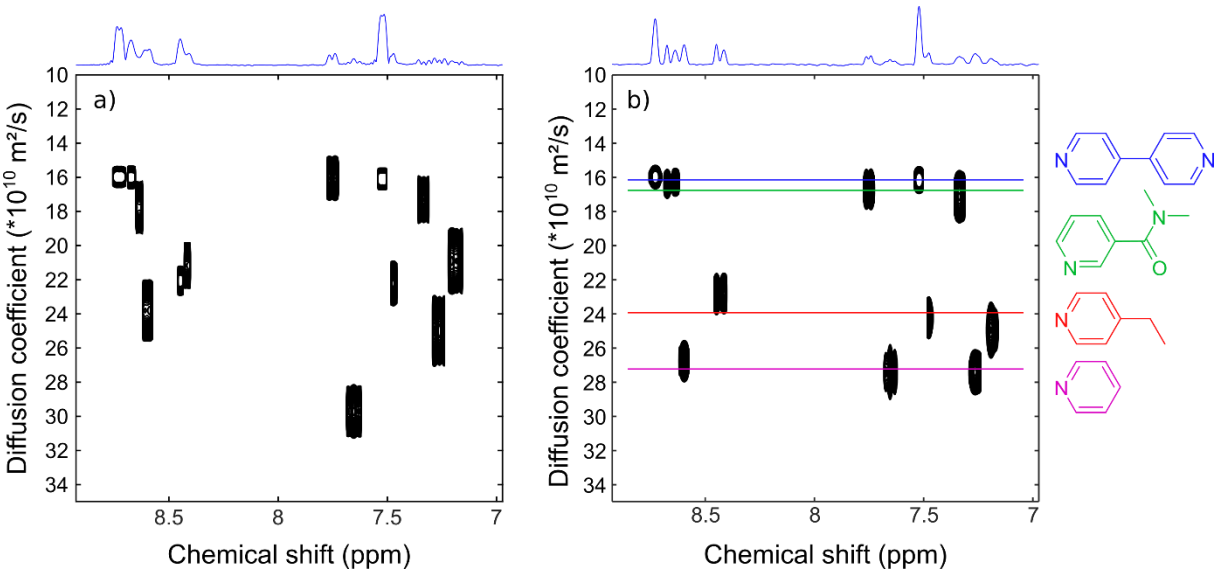

Figure 31: 2D SPEN DOSY spectra obtained for the model mixture 3 processed in magnitude-mode (a) and in absorption-mode (b). The corresponding molecules are displayed on the right to illustrate the separation according to the diffusion coefficient.

2.4.5 Signal to noise considerations

2.4.5.1 SPEN DOSY vs conventional DOSY

One of the limitations of the SPEN DOSY experiment is that because of spatial parallelization, the sensitivity is lower than for conventional experiments. In order to have an idea of how much loss spatial encoding leads to, a comparison was done between conventional DOSY and SPEN DOSY. It was chosen to do a conventional DOSY with 16 increments and 8 scans per increment. To obtain comparable results with the SPEN DOSY, 128 scans were done and the acquisition gradient was chosen so that the fit of 8 mm would lead to a curve with 16 points. The other parameters were the same (recovery time, gain…). The FID in conventional DOSY was truncated during the processing to simulate an acquisition of the same duration as for the SPEN DOSY, and the apodisation was done the same way in both experiments. Moreover, the SNR in conventional DOSY was corrected to take into account the fact that the SPEN experiments only uses 8 mm of the sample, while the conventional experiment is done on the full sample. Finally, the SNR was compared on the DMSO peak. The results are displayed in Table 2. The $\sqrt{2}$ factor between magnitude-mode and absorption-mode processing is once again founded here for the SPEN experiment but is lower for the conventional one. In this case, the cost in SNR due to the spatial encoding is between 5 and 6, close to the theoretical estimate that is around 4 with these parameters. As a reminder, the losses in sensitivity per square root of measurement duration is proportional to $\sqrt{N_p}$, where N_p is the number of pixels in which the diffusion profile is sliced into. In this case, the parameters were set in order to have 16 pixels in the profile in order to mimic the 16 increments of the conventional experiment, leading to a theorical loss in SNR of about 4.

2.4.5.2 Acquisition scheme

An alternative to EPSI for spatially encoded DOSY experiments is the use of a single weak gradient pulse during the acquisition, as shown in Figure 32.[137]

In the resulting 1D spectrum, each peak is broadened and reveals the spatial profile in which the diffusion coefficient is encoded. We wondered if the two methods were similar in terms of sensitivity. In order to answer the question, two experiments were done: the first is a SPEN DOSY experiment as shown previously in Figure 20 a), and the second is the same with the EPSI replaced with an acquisition with a single gradient shown in Figure 32. The encoding step was the same for both experiments and the acquisition was as similar as possible: same acquisition time and number of points, and equivalent spatial resolution (the total gradient area in the second acquisition is the same as

Table 2: SNR of the DMSO peak as a function of the experiment type and the processing mode

Processing	Conventional corrected	SPEN
Magnitude	48 360	8105
Absorption	55 671	10797

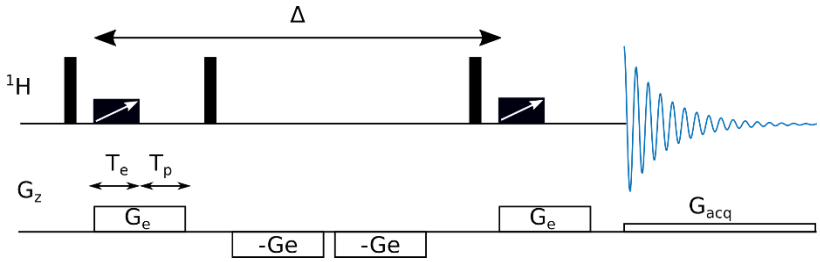

Figure 32: SPEN DOSY using another acquisition scheme where a weak gradient is applied continuously during the acquisition.

that of the first lobe of the EPSI acquisition). To avoid overlapping signals due to widening signal, it was decided to run the experiment on a sample of doped water. The acquisition done with EPSI give SNR_{EPSI} = 3522 while the acquisition done with the single gradient leads to SNR_{1D} = 7575 hence a factor a 2.15 in favor of the 1D acquisition. A $\sqrt{2}$ factor was expected as for the 2D processing, half of the echoes are discarded. The additional difference may come from imperfections of the EPSI acquisition.

2.4.6 Compensation of the convection

A common problem with DOSY experiments is convection. If the sample is too fluid, convection can occur in the NMR tube as a result of temperature gradients. The motion observed with the DOSY experiments will not be solely directed by the Brownian motion, leading to erroneous results. As shown in section 2.2.3, a solution to this problem is to use a DSTE pulse sequence to cancel out the effect of the velocity term. The sample M5 was used to obtain SPEN DOSY in two conditions: two sets of data were recorded with STE and DSTE pulse sequences. On Figure 33 is shown the DMSO diffusion curve for the two data sets. While the influence of the convection lead to fast decay and oscillation in the case of the STE experiment, the one recorded using DSTE show good quality data thus allowing a precise measurement of the diffusion coefficient. However, the cost of cancelling the convection is a loss in signal to noise ratio by a factor of 2 compared to single STE.

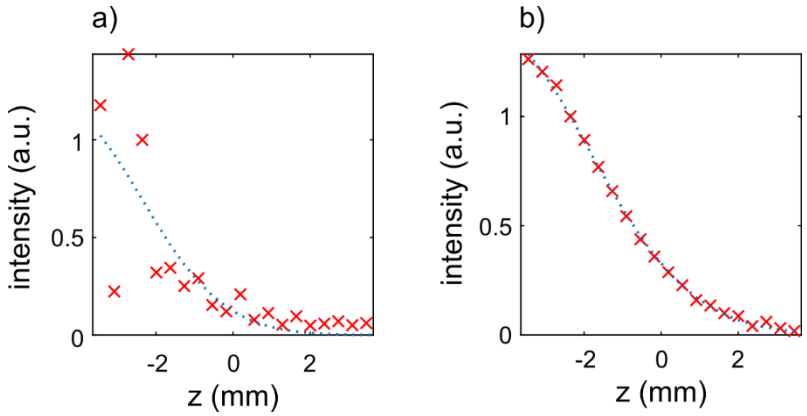

Figure 33: Fitting curve of the DMSO signal at 313 K obtained with an ufSTE experiment (a) and with an ufDSTE experiment (b). The dotted blue lines correspond to the fit and the red crosses correspond to the experimental points.

2.4.7 Implementation on single axis setup

In most facilities, NMR probes are equipped with single axis gradient and it can be wondered if the spatial encoding and CTP gradients can interfere. First, a SPEN DOSY experiment was done on mixture M2 and reference diffusion coefficients were calculated. To answer the question about the CTP gradients, several experiments on the same sample changing different CTP gradients were done and the resulting diffusion coefficients measured were plotted in the Figure 34. The first experiment corresponds to a reference SPEN DOSY experiment. In the experiments 2 and 3, the gradient "a" and "b" were respectively modified leading to no drastic modification of the diffusion coefficient. However, if the "c" gradient is modified in a way or another (experiments 4 and 5), the diffusion coefficient measured changes significantly. This phenomenon is due to the fact that the "c" gradient is not taken into account into the model used for the diffusion coefficient calculation, leading to biased results. Hence, the use of the "c" gradient should be avoided on systems using single axis gradient probes, and on system with triple-axis gradient probe, "c" should be along transversal axis.

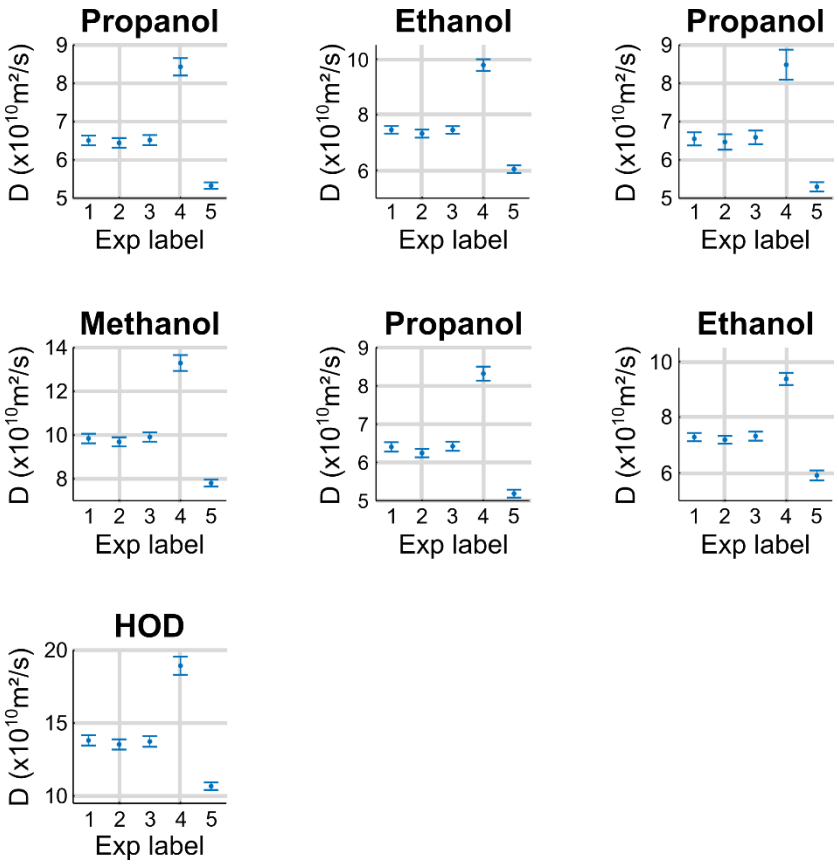

Figure 34: Influence of the CTP gradient on the measurement of diffusion coefficient on a single gradient axis probe. For each signal the diffusion coefficient was calculated in 5 conditions: reference conditions (label 1), with gradient a (see Figure 20) increased by 30% (label 2), with gradient b increased by 30 % (label 3), with gradient c increased by 30 % (label 4) or decreased by 20 % (label 5).

2.4.8 Conclusions

We have given here a detailed explanation of how spatial encoding of diffusion is performed. First, we have shown that using a pulse sequence compatible with pure-absorption processing leads to a gain in resolution. Then it has been shown that the acquisition gradient intensity has an unexpected effect on the diffusion coefficient measurement and has to be carefully selected to make a choice between having enough points on the curve and good SNR. One thing that can be done to improve SNR is to increase the acquisition duration, but in this case the instrumentation will be the limitation. The parameter used for spatial encoding and the duration of the acquisition do not seem to affect the diffusion coefficient, it can be chosen freely within hardware limitations. Finally, the relevance of using a DSTE pulse sequence in order to cancel the effect of convection has been illustrated.

2.5 Preliminary results at low field

2.5.1 Introduction

NMR spectroscopy is very effective in numerous fields of analytical chemistry. However, its range of application is limited by the cost of superconductive magnets, and then the need of a dedicated infrastructure to operate them. These drawbacks have fueled to the development of benchtop NMR spectrometer that are less expensive, portable, and can be operated in diverse environments including, for example, under a fume hood. While their resolution and sensitivity is necessarily more limited than that of high-field systems, these "benchtop" NMR spectrometers are becoming more and more popular, for applications such as reaction monitoring and quality control. Recently, pulsed field gradients have been implemented on benchtop spectrometers, opening the possibility to implement spatial encoding experiments. It has for example been shown that spatial encoding of chemical shifts was possible.[150] The fast acquisition of DOSY data on benchtop spectrometers would be particularly useful for quality control and monitoring applications. Here we describe our work on the implementation of the SPEN DOSY pulse sequence on a Spinsolve system.

2.5.2 Experimental

The experiments were carried out on a Magritek Spinsolve spectrometer operating at a ^{1}H Larmor frequency of 60 MHz and equipped with a 5 mm dual $^{1}H/^{13}C$ probe with single-axis gradients. The default calibration was used (G_{max} = 16 G/cm). All the experiments were done without sample rotation.

The model mixture used at low field (M6) for setting up the experiment was prepared according to the following procedure. 30.4 µL of methanol, 13.5 µL of non-deuterated water and 53.2 µL of DMSO were dissolved in 503 µL of D_2O. The concentration is near 1 M for each compound.

2.5.3 Results and discussions

The theory of the spatial encoding is the same than at high field. In practice however, there is an important difference: the gradient axis is perpendicular to the tube. As a result, the spatial profile of

the object, shown on Figure 35, has to be taken into account in the processing of spatially encoded DOSY experiments.

To begin with, we decided to work on a simple model mixture containing compounds that have a single NMR peak and that are highly soluble in water. We chose methanol and DMSO that have non-overlapping signals and have high diffusion coefficients differences.

First, conventional DOSY experiments were recorded at low and high field in order to have a reference to compare the SPEN DOSY values with. The values obtained are displayed in Table 3.

The values are different from those obtained at high field, but stay in the same range. This is mainly due to the fact that the gradient were not calibrated yet. Second, the SPEN DOSY data was recorded using the pulse sequence described in Figure 20 a). As explained earlier, in order to obtain sensible values for diffusion coefficient, a correction by the reference profile is needed. Indeed, without profile correction, the observed diffusion curve is a multiplication between the actual diffusion decay caused by the Brownian motion and the spatial profile in the absence of diffusion. Moreover, in this particular case, the fit of data cannot be done on 8 mm as the tube is only 5 mm wide. To obtain optimum results, it was decided to fit data on 2 mm. An example of the obtained data is illustrated in Figure 36.

Table 3: Diffusion coefficients and standard deviation of the fit for the conventional DOSY experiment for the M6 model mixture.

	Low field		High field	
Compound	D x 10^{10} ($m^2.s^{-1}$)	Fit STD x 10^{10} ($m^2.s^{-1}$)	D x 10^{10} ($m^2.s^{-1}$)	Fit STD x 10^{10} ($m^2.s^{-1}$)
HOD	17.98	0.03	17.0	0.1
Methanol	12.67	0.04	11.91	0.06
DMSO	9.27	0.01	8.64	0.03

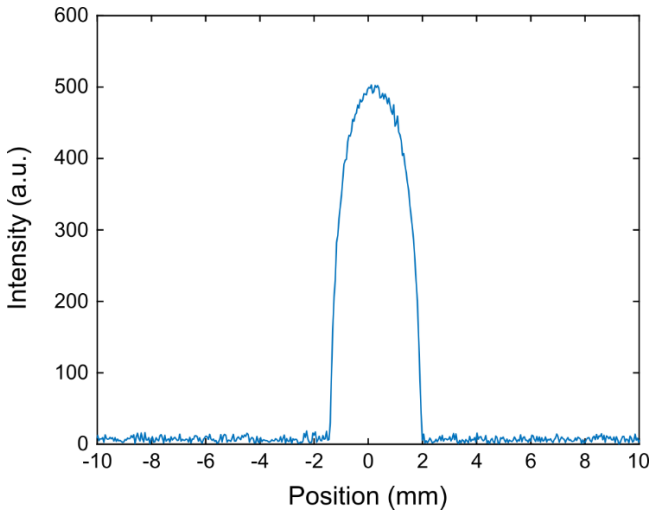

Figure 35: Tube spatial profile along the X-dimension obtained on a H_2O/D_2O 90/10 tube using a gradient echo.

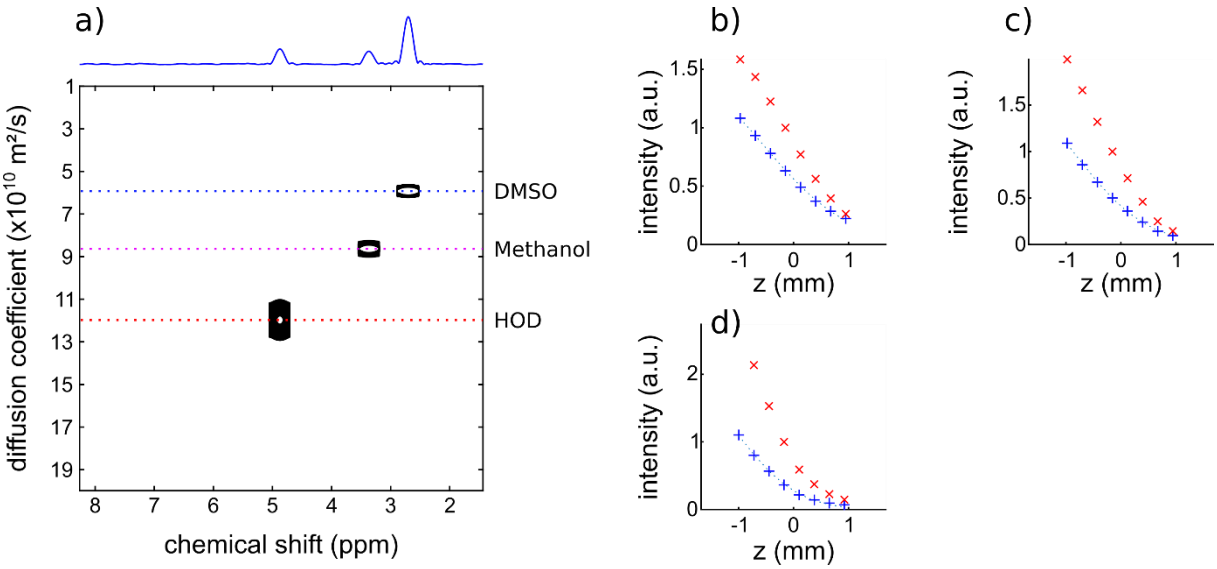

Figure 36: Example of a SPEN DOSY 2D map obtained on the model mixture 6. Diffusion curves obtained for DMSO (b), methanol (c) and water (d). The red crosses correspond to the initial raw data, the blue crosses correspond to the corrected data and the dotted lines correspond to the fit.

It can be seen on the figure above that the fits are very good; the separation is clear on the final map and that the processing that had to be adapted for Magritek data works well. However, the diffusion coefficients calculated show a systematic difference compared to those obtained with conventional DOSY. In order to understand if the problem was coming from the data and the acquisition or from the processing step, the acquisition with a spatial encoding on the transversal axis was done on the high field spectrometer. Good results were obtained with conventional DOSY while similar differences appeared with SPEN DOSY. It seems that the problem is coming from the processing step. However, to this day, the error was not identified yet.

Another problem that arises from the use of spatial encoding at low field is a spectral width problem. Indeed, the spectral width in the spectral dimension is calculated as

$$SW^{conv} = \frac{1}{2T_a} . \qquad (2.15)$$

A typical value at high field of T_a of 256 µs leads to a spectral width of 1953 Hz. It corresponds to 3.9 ppm on a 500 MHz, but 32 ppm on a 60 MHz, that is clearly unnecessary for most applications. If the spectral width has to be reduced, it led either to a longer acquisition, that is not always possible due to demanding acquisition scheme, or to a loss of resolution in the spatial dimension, meaning fewer point to fit. Finally, as expected, the last drawback is that the sensitivity is very low. Indeed, the combination low field and spatial encoding is a real problem.

The feasibility of spatial encoding of diffusion information on a benchtop spectrometer has been proven and showed good quality data. The next steps are to work on more complicated mixtures and one way to overcome the sensitivity issues could be to work on hyperpolarized substrates.

2.5.4 Conclusions

It has been shown here that the spatial encoding of the diffusion could be adapted on low field spectrometer. Good quality data and a good separation between compounds were obtained but the processing method seems to lead to biased values due to an error during the processing step. The sensitivity loss is more problematic than at high field because of the already poor sensitivity at low filed. One interesting way to solve this issue would be to work on hyperpolarized samples.

3 Ultrafast multiple-quantum and maximum-quantum NMR

3.1 Introduction

NMR spectroscopy is a powerful analytical method, but the resolution of ^{1}H 1D spectra can be a limitation for the analysis of complex mixtures. Indeed, as most ^{1}H signals are in the range 0-10 ppm, the risk of overlap becomes very high when the complexity of the mixture increases. In order to resolve signals that overlap in 1D spectra, one solution is to spread them over two dimensions. In the previous chapter we described how this second dimension could be used to separate signals according to the diffusion coefficient of the corresponding molecules and how it was possible to accelerate the experiment using spatial encoding. In this chapter we will describe a different way to build up the second dimension using correlations between spins, and how to accelerate it, also using spatial encoding. First the principle of chemical-shift spatial encoding will be explained as it differs in several ways from diffusion spatial encoding and an example of ultrafast COSY experiment will be shown. Second, we will show how spatial encoding, that has proven to be effective for single- and double-quantum coherences, can also be used for higher coherence orders. Finally, it will be shown how, thanks to the acceleration provided by spatial encoding, reaction monitoring can be performed.

3.2 Principles of chemical shift encoding

3.2.1 Introduction

In the previous part we described how the combination of frequency-swept chirp pulses with gradient pulses can be used in order to spatially encode diffusion information. In this part we will see how a similar spatial encoding scheme can be used to encode chemical shift information, as shown in Figure 37. First the theory will be explained as it differs slightly from the previous one, then examples of experimental parameters will be shown, and finally an example of how it can be used to obtain ultrafast COSY spectra in less than one second will be shown.

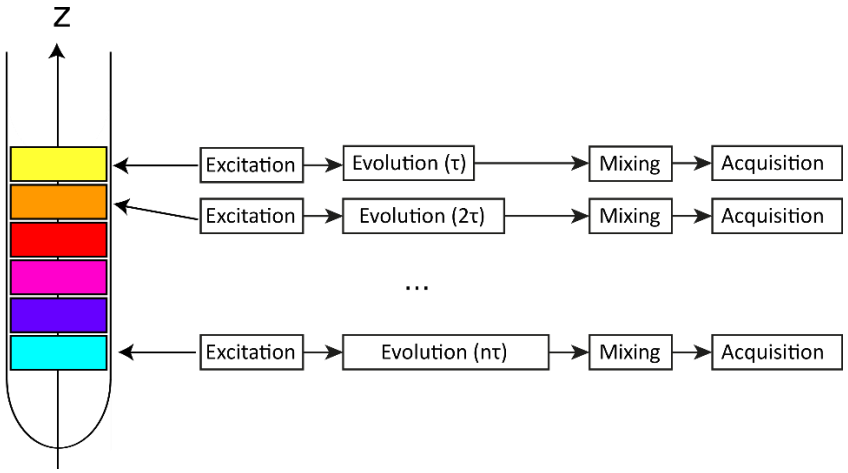

Figure 37: Schematic principle of chemical shift spatial encoding

3.2.2 Theory

3.2.2.1 Spatial encoding

The basic principle of chemical-shift encoding is the same as the one for diffusion encoding as it is based on using chirp pulses and pulsed field gradients. Several spatial encoding schemes have been described, using different flip angles for the chirp pulses. Phase Modulation (PM) uses a combination of two 90° chirp pulses, Amplitude Modulation (AM) uses first a 90° chirp pulse, followed by a 180° one and Constant Time (CT) uses a pair of 180° pulses after an adequate excitation. All these spatial encoding have been extensively described in the literature.[151] We will focus here only on the constant time encoding.

The goal of the chemical shift spatial encoding is to obtain an evolution time t_1 proportional to the spins' position in the NMR tube:

$$t_1(z) = Cz\,, \tag{3.1}$$

with C a constant depending on how long the maximum t_1 has to be. The way to reach this experimentally is similar to what has been developed previously for diffusion experiments using chirp pulses and gradients. As a reminder (see section 2.2.1.2), the spins' phase after the first chirp pulse with gradient can be written as:

$$\phi_1^{(q)}(z) = -\left(\frac{\gamma G_e T_e}{L}\right) z^2 + \left(\gamma G_e T_p - \frac{2T_e\Omega}{L}\right) z^1 + \left(\Omega T_p - \frac{\gamma G_e T_e L}{4} - \frac{T_e\Omega^2}{\gamma G_e L}\right) z^0, \tag{3.2}$$

where γ is the gyromagnetic ratio of the observed nucleus, G_e is the intensity of the encoding gradient, T_e is the duration of the chirp pulse, L is the length of the encoded region and Ω is the offset.

As previously, in order to cancel the quadratic phase, a second encoding block is applied. However, this time the two blocks are not identical: the sign of the gradient during the second encoding block is opposite to the one during the first block. Moreover, as diffusion information are not sought here, the two chirp pulses will be applied one directly after the other leading to the pulse sequence shown in Figure 38 (here diffusion only results in a modest loss of sensitivity). With this spatial encoding scheme, the spatially quadratic phase is canceled out, but the bilinear term proportional to both z and the chemical shift offset remains. This means that signals with different chemical-shift offsets Ω will have different spatial phases, which can be represented as winding as shown in Figure 38.

As most probes are equipped with a gradient coil along the Z-axis only, spatial encoding is usually done along this axis. However, if the laboratory is equipped with a triple-axis gradient probe, transversal axis can be used as it will be seen in the next chapter.

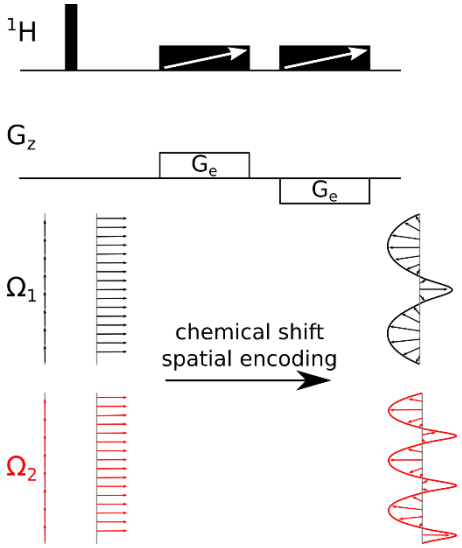

Figure 38: Constant Time spatial encoding block used for this work.

3.2.2.2 Acquisition

After chemical shifts are encoded, they have to be decoded to be able to obtain a two-dimensional spectrum. As previously, this is done using EPSI. However, in this case, more than one echo will be obtained. Indeed, as the chemical shift were encoded through a spatial phase, each chemical shift will have a different winding as shown in Figure 38. The acquisition gradient will unwind each helix, producing several echoes at different times as shown in Figure 39 a). It will create the first dimension, which will be called 'spatial dimension' here, even if there are no Fourier transform to retrieve the sample image. A second acquisition gradient, with an opposite sign, is then applied. This pair of bipolar gradients is repeated numerous times in order to observe echo evolution over time that will consist in the spectral dimension leading to a similar trajectory in the kt space than for the SPEN DOSY but with several echoes this time as shown in Figure 39 b-c.

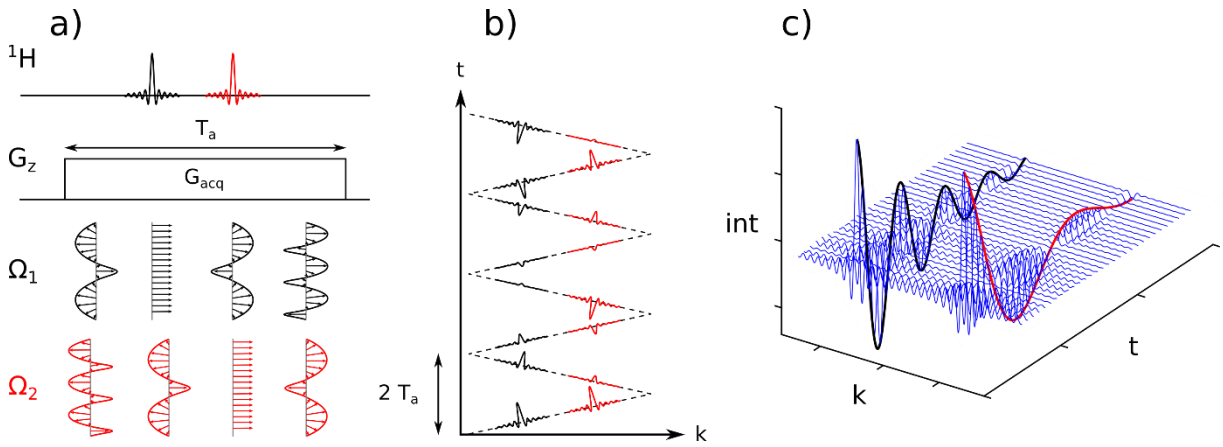

Figure 39: Visual representation of how several echoes are formed during the acquisition gradient (a), acquisition trajectory in kt space (b) and the resulting dataset (c).

Odd and even echoes are usually processed separately, and the spectral width in spectral dimension can be calculated as:

$$SW^{conv} = \frac{1}{2\,T_a}, \tag{3.3}$$

with T_a the duration of one acquisition gradient lobe. The resolution in the spectral dimension is given by:

$$\Delta\nu_{conv} = \frac{1}{2\,T_a N_L}, \tag{3.4}$$

with N_L, the number of loops. In the spectral dimension, the calculation of the parameters SW and Δν can differ depending on the encoding scheme that is used. Here we will only take into consideration the Constant Time (CT) encoding that consists of a pair of adiabatic refocusing pulses applied together with a bipolar gradient pulse, as it is the only one that will be used in this work. The spectral width in the spatial dimension is then:

$$SW^{spatial} = \frac{\gamma\,G_a\,T_a\,L}{4\,T_e}, \tag{3.5}$$

with γ the gyromagnetic ratio of the observed nucleus, G_a, the intensity of the acquisition gradient, L the length on which the spatial encoding is performed and T_e the duration of a chirp pulse.

The resolution in the spectral dimension depends of the total acquisition duration as for 1D spectrum. Then the maximum gradient of the probe limits the maximum spectral width as shown by Eq(3.5). For high-resolution probes, this maximum is typically between 50 and 65 G/cm. These values do not permit do have spectral width and resolution as good as conventional acquisitions.

3.2.3 Experimental part

3.2.3.1 Spectrometers

The experiments on unreacting samples were carried out on a Bruker Avance III spectrometer operating at a ^{1}H Larmor frequency of 600.13 MHz equipped with a 5 mm triple $^{1}H/^{13}C/^{15}N$ room temperature probe with triple-axis gradient. The temperature inside the probe was calibrated with a standard methanol sample and then set to a value of 298 K with airflow of 535 L/h. All the experiments were done without sample rotation.

The experiments for the hetero Diel-Alder reaction monitoring were carried out on a Bruker Avance III spectrometer operating at a ^{1}H Larmor frequency of 600.33 MHz equipped with a 5 mm triple $^{1}H/^{13}C/^{15}N$ cryo-probe with single-axis gradient. The temperature inside the probe was calibrated with a standard methanol sample and then set to a value of 298 K with airflow of 535 L/h. All the experiments were done without sample rotation.

3.2.3.2 Samples

The first model mixture (M1) for the ultrafast COSY example was prepared according to the following procedure. 7.2 mg of L-valine was dissolved into 590 µL of D_2O. Then, 2.4 µL of methanol, 3.4 µL of ethanol and 4.5 µL of n-propanol were added to the solution. The solution was shaken until complete dissolution of valine and filtered to remove any solid particles. The concentration is near 100 mM for each compound.

The second model mixture (M2) for multiple-quantum experiments was prepared according to the following procedure. 16.2 mg of caffeic acid, 17.5 mg of ferulic acid, 15.1 mg of vanilic acid, 16 mg of anthracene, 11.5 mg of naphthalene and 8.5 mg of phenol were dissolved in 600 µL of deuterated DMSO and was shaken until complete dissolution of all compounds. The concentration is near 150 mM for each compound.

The first reaction monitoring solution was prepared according to the following procedure. 36.1 mg of imine I ((E)-N,1-diphenylmethanimine) and 39.3 mg of dieneophile DP (benzyl N-[(E)-1-methylprop-1-enyl]carbamate) was dissolved in 500 µL of $CDCl_3$. A first spectrum of this solution without catalyst was done. Then 1.9 mg of catalyst (BINOL-phosphoric acid) was added to the solution. The solution was introduced in the magnet, tuned, locked and shimmed. The spectra acquisition began 3 minutes and 45 seconds after the introduction of the catalyst. A series of experiments were acquired during 2 hours interleaving 1D ^1H and ultrafast 2D acquisitions.

The second reaction monitoring solution was prepared according to the following procedure. 32.3 mg of imine I and 34.8 mg of dieneophile DP was dissolved in 500 µL of $CDCl_3$. A first spectrum of this solution without catalyst was done. Then 1.7 mg of catalyst was added to the solution. The solution was introduced in the magnet, tuned, locked and shimmed. The spectra acquisition began 3 minutes and 30 seconds after the introduction of the catalyst. A series of experiments were acquired during 3 hours and 40 minutes interleaving 1D ^1H and conventional 2D acquisitions.

3.2.3.3 Acquisitions

For ultrafast COSY experiments with alcohols and valine mixture in D_2O, bipolar encoding gradients of ± 1.04 $G.cm^{-1}$ were used in combination with 15 ms chirp pulses with 12 kHz bandwidth. The acquisition consisted of a train of bipolar gradient pulses, of ± 45.5 $G.cm^{-1}$, with 128 loops and a duration of 256 µs for each gradient pulse. A relaxation delay of 10 s was used.

For ultrafast DQS experiments with alcohols and valine mixture in D_2O, bipolar encoding gradients of ± 0.65 $G.cm^{-1}$ were used in combination with 15 ms chirp pulses with 12 kHz bandwidth. The acquisition consisted of a train of bipolar gradient pulses, of ± 52 $G.cm^{-1}$, with 128 loops and a duration of 256 µs for each gradient pulse. The delay for J-coupling evolution τ (as shown in Figure 43) was set to 250 ms and a relaxation delay of 10 s was used.

For ultrafast 3,4 and 5Q spectra experiments with aromatic mixture in D_2O, bipolar encoding gradients of respectively ± 0.78, 0.65 and 0.26 $G.cm^{-1}$ were used in combination with 15 ms chirp

pulses with 12 kHz bandwidth. The acquisition consisted of a train of bipolar gradient pulses, of ± 26 $G.cm^{-1}$, with 80 loops and a duration of 428 µs for each gradient pulse. The delays τ, for J-coupling evolution, and τ' for conversion of anti-phase coherences into in-phase coherences (as shown in Figure 43) were respectively set to 200/80/100 ms and 180/60/60 ms for 3, 4 and 5Q spectra. A relaxation delay of 10 s was used.

For the optimization of ultrafast 3,4 and 5Q spectra experiments with aromatic mixture in D_2O, bipolar encoding gradients of respectively ± 0.78, 0.65 and 0.26 $G.cm^{-1}$ were used in combination with 15 ms chirp pulses with 12 kHz bandwidth. The acquisition consisted of a train of bipolar gradient pulses, of ± 26 $G.cm^{-1}$, with 80 loops and a duration of 428 µs for each gradient pulse. For non-refocused experiments (Figure 43.a), a series of experiments were done incrementing τ value from 20 to 300 ms. For refocused experiments (Figure 43.b), the best τ value was then selected and used for a series of experiments incrementing τ' from 20 to 300 ms. A relaxation delay of 10 s was used.

For ultrafast 4-quanta spectra experiment with reaction monitoring, bipolar encoding gradients of ± 0.45 $G.cm^{-1}$ were used in combination with 15 ms chirp pulses with 12 kHz bandwidth. The acquisition consisted of a train of bipolar gradient pulses, of ± 32.5 $G.cm^{-1}$, with 80 loops and a duration of 428 µs for each gradient pulse. The delays τ and τ' were respectively set to 100 ms and 80. A relaxation delay of 10 s was used and 8 scans were acquired for each experiment.

3.2.3.4 Processing

The processing of conventional experiments consists first in importing the data into MATLAB. Then zero filling in indirect dimension is done. For the sensitivity comparison, the number of points in direct dimension were reduced to mimic an acquisition length similar to the corresponding ultrafast acquisition length. Apodisation is done in both dimensions using a sine window. Finally, data are double Fourier transformed and plotted.

The processing of data obtained through chemical-shift spatial encoding consists in reshaping the linear data to 2D data. Apodisation for the time dimension is performed as in conventional experiments. Apodisation for the spatial dimension, which was shown to lead to better lineshapes,[122] is done as follows: first, an inverse Fourier transform is done along the k dimension, then apodisation is done in the spatial domain, finally, the data is Fourier transformed back to the k domain. This process is illustrated on Figure 40. Processing of reaction monitoring experiments consisted in first processing a spectrum on which the integration regions were defined. The other spectra were then processed and integration was performed using the same regions.

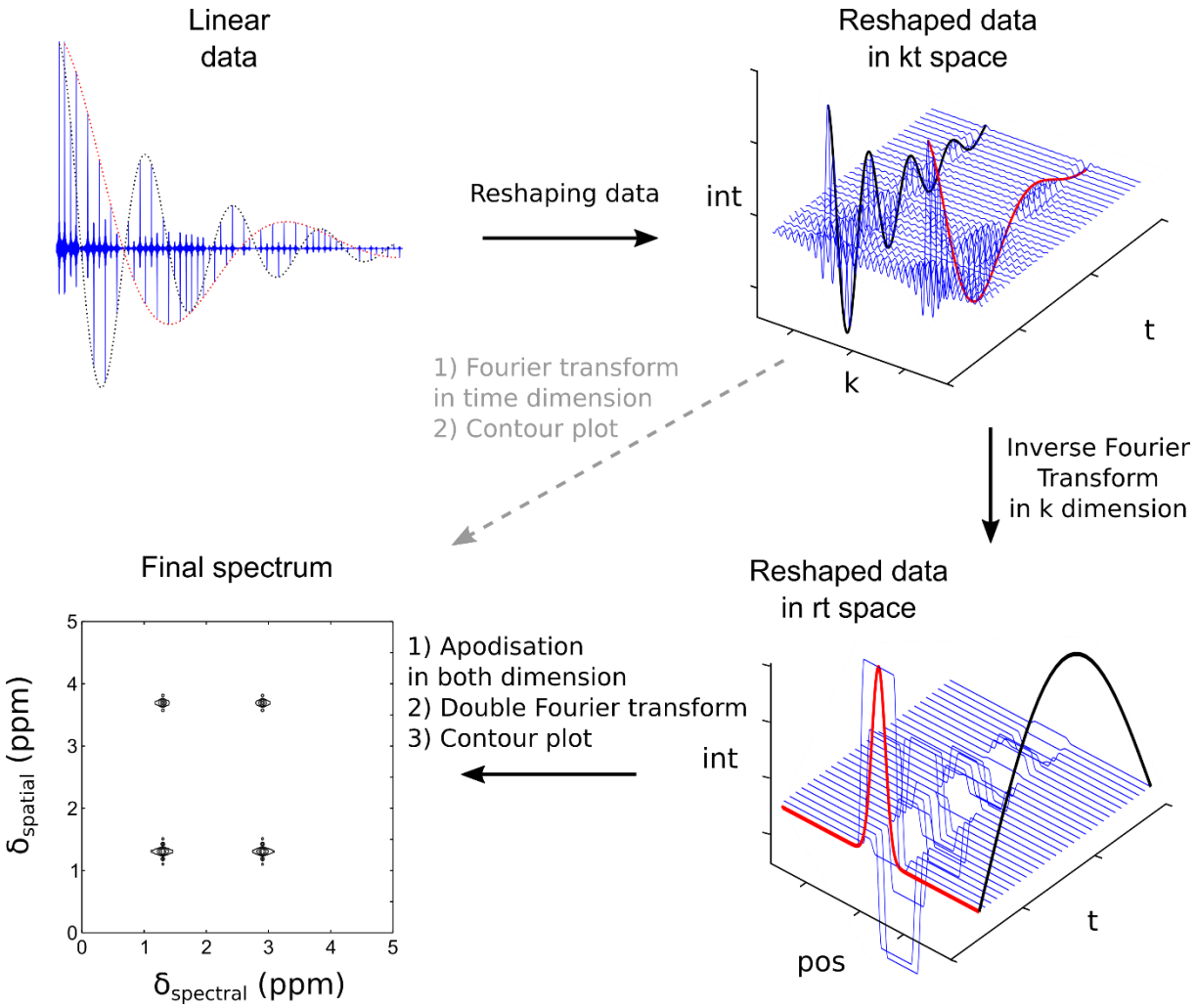

Figure 40: Schematic representation of processing used for ultrafast multidimensional NMR experiments.

3.2.4 Example of the ultrafast COSY experiment

First, we will show how spatial encoding can be used in order to accelerate a simple COSY experiment. In this case, and for all following ultrafast experiments, we will only consider the constant time version of the pulse sequence that is shown in Figure 41 a). An example of ultrafast COSY spectrum is shown in Figure 41 b). It was recorded with a pair of chirp pulses whose duration is 15 ms and bandwidth 12 kHz combined with gradient of 1.04 G/cm. For spatially encoded DOSY, the chirp pulses were only encoding a part of the sample (between 8 and 20 mm depending of the probe used). For chemical shift spatial encoding, chirp pulses sweep over more than the length of the coil. In this case it is possible as, contrary to SPEN DOSY, the gradient non-uniformity does not lead to dramatic consequences.

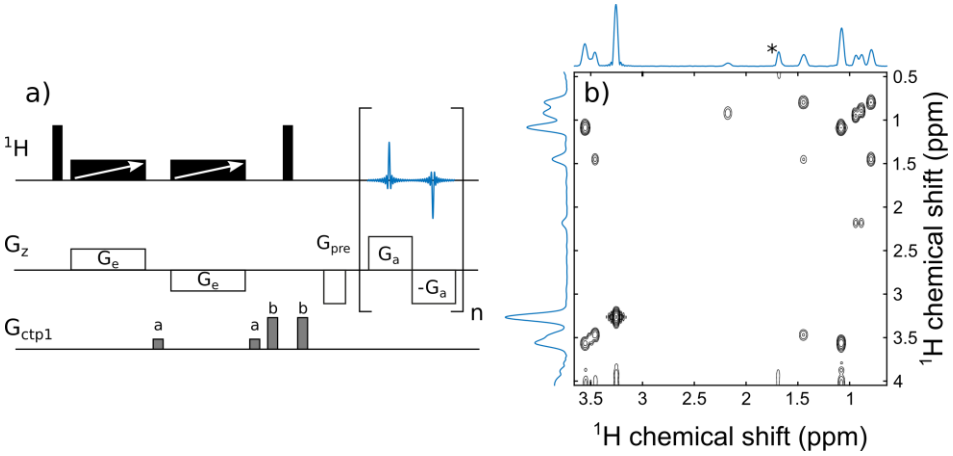

Figure 41: ultrafast COSY pulse program (a) and spectrum obtained on a sample containing methanol, ethanol, n-propanol and valine in D_2O (b). Peak with an asterisk correspond to an unsuppressed water folded peak.

3.3 Spatial encoding of higher coherence order

3.3.1 Example of the DQS experiment

It was illustrated with the ultrafast COSY spectrum how spatial encoding of single-quantum coherences is achievable. One may wonder if it is possible to spatially encode higher coherence orders. The conventional pulse sequence to acquire Double (or higher) Quantum Spectrum (DQS) is shown in Figure 42. It consists in a first spin echo to build up antiphase coherences by letting homonuclear J-coupling evolve, followed by a 90° pulse to convert them into multiple-quantum coherences. These coherences evolve during an incremented delay before a last 90° pulse to convert them back into observable single-quantum coherences. The selection of the coherence number observed is done thanks to a pair of gradient pulses around the last pulse. Their relative area defines the coherence order observed.

This experiment has proven to be very useful in the case of ^{13}C NMR with the INADEQUATE experiment. For ^{1}H NMR it is also useful as it results in a diagonal-free spectrum that is less crowded than COSY, allowing easier analysis. As was done for COSY, a single-scan version of this experiment based on spatial encoding has been implemented, with the pulse sequence as shown in Figure 43 a). Its usefulness has been illustrated with the quantification of taurine in energy drinks.[124]

The pulse sequence will be the same for the observation of higher coherence orders. The gradient ratio for the coherence selection will be adapted each time though. Pulse programs for the ultrafast acquisition is the same as the one presented in Figure 42a) with the t_1 evolution replaced by the chemical shift spatial encoding block used earlier as shown in Figure 43.

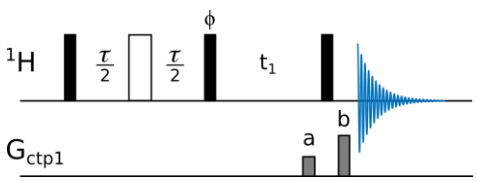

Figure 42: Pulse sequence used for conventional multiple quantum spectra. The coherence order is defined by the ratio b/a. The phase ϕ is x for the observation of even coherences and y for the observation of odd coherences.

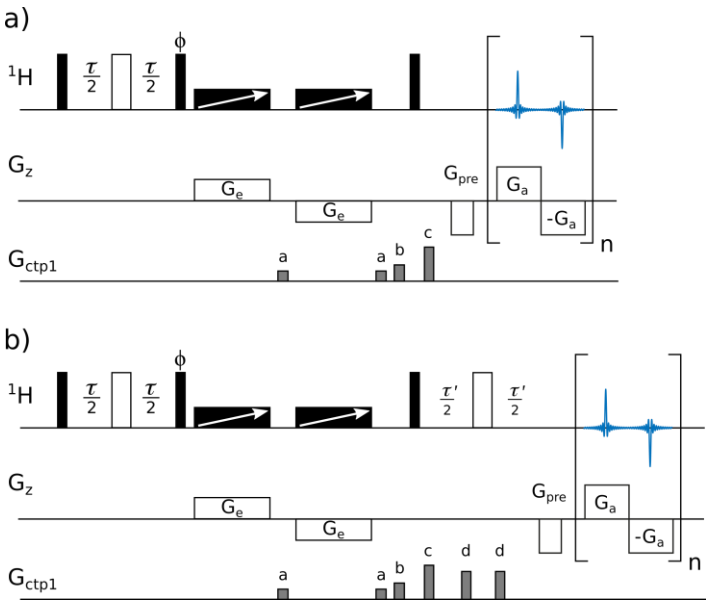

Figure 43: Ultrafast multiple quantum spectra pulse sequence without (a) and with (b) refocalization step.

An example of DQS spectrum of the same mixture as previously can be seen in Figure 44. As expected, the spectrum is less crowded than the COSY one, and peaks are further apart from each other. Hence, one may wonder until when increasing the observed coherence order will lead to a simplification of the spectrum.

3.3.2 Higher coherence orders (MQS) and maximum order (MaxQ)

Until the present work, no spatial encoding of coherence orders higher than two had been reported. First, we will see why the observation of such coherences can be interesting. Then, it will be shown how such experiment can be spatially encoded and how it can be used for the analysis of aromatic mixtures. It will also be shown how this experiment can be optimized before being used in order to monitor a hetero Diels alder reaction.

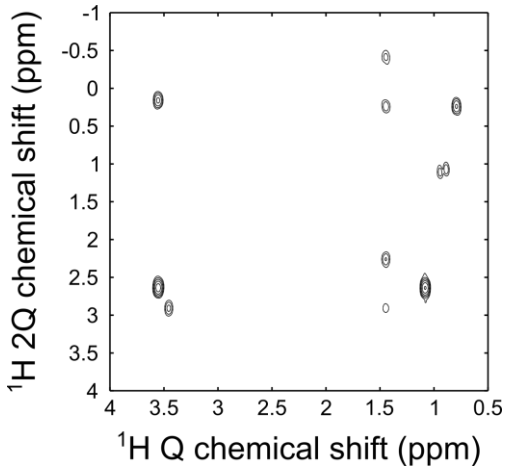

Figure 44: Ultrafast double quantum spectra of the mixture methanol, ethanol, n-propanol and valine in D_2O.

3.3.2.1 Why look at higher coherence orders?

For aromatic compounds, increasing the observed coherence order leads to a simplification of the spectrum. The Multiple-Quantum Spectrum (MQS) of a spin system can be simplified until the observed coherence order corresponds to the maximum order of this spin system, i.e., to the number of spins that it contains. For example, ethanol has a Maximum-Quantum order of 5 (if it is considered that the OH is not taken into account). It can be quite complicated to use MaxQ for mixture of molecules with alkyl chains as the spin system can have too many spins to be observable with the MQS method. Indeed, counter intuitively, the multiple quantum spectra of alkyl chains can actually become more crowded than simple COSY spectra. If we take the example of an ethyl chain, the COSY spectrum will be composed of 4 peaks, as shown in Figure 45 a), while the DQS spectra will be composed of 5 peaks as shown in Figure 45 c). Moreover, the longer the chain will be, the more complex DQS spectra will be as shown with the example of a linear propyl chain in Figure 45 d). Moreover, the higher coherence order is observed, the lower the sensitivity will be[67], so even for a short chain as propyl, the maximum-quantum spectra of 7Q would lead to high SNR losses.

The aromatic compounds on the other hand are much more interesting to study with such methods as their MaxQ is very simple to calculate depending on their substitutions. Conventional MaxQ Experiments were used for the analysis of phenolic mixture.[11] The reason MaxQ is so useful is that when the maximum coherence order of a spin system is observed, its spectrum in the indirect dimension consists in a single line whose normalized chemical shift is the mean of the spin system spins' chemical shift. To illustrate the possibility to use spatial encoding on coherence orders higher than two, we decided to use a mixture of aromatic compounds whose MaxQ are 3 (caffeic acid, vanilic acid and ferulic acid), 4 (naphthalene and anthracene) and 5 (phenol). The structure of the selected compounds is shown in Scheme 1.

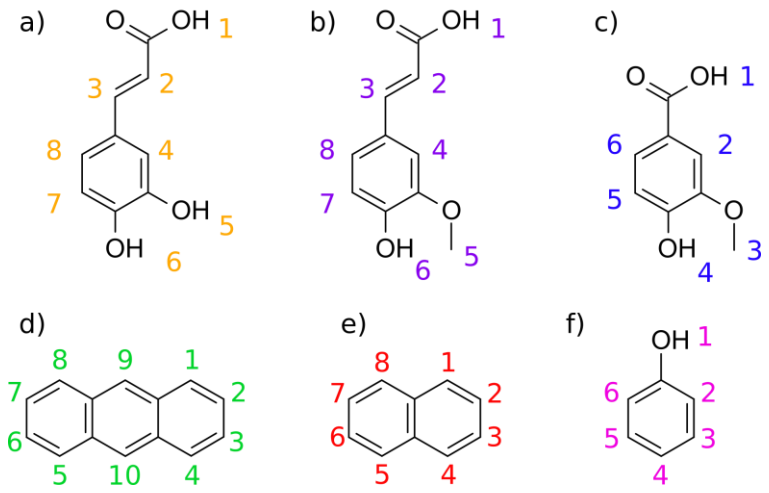

Scheme 1: Structure of caffeic acid (a), ferulic acid (b), vanilic acid (c), anthracene (d), naphthalene (e) and phenol (f).

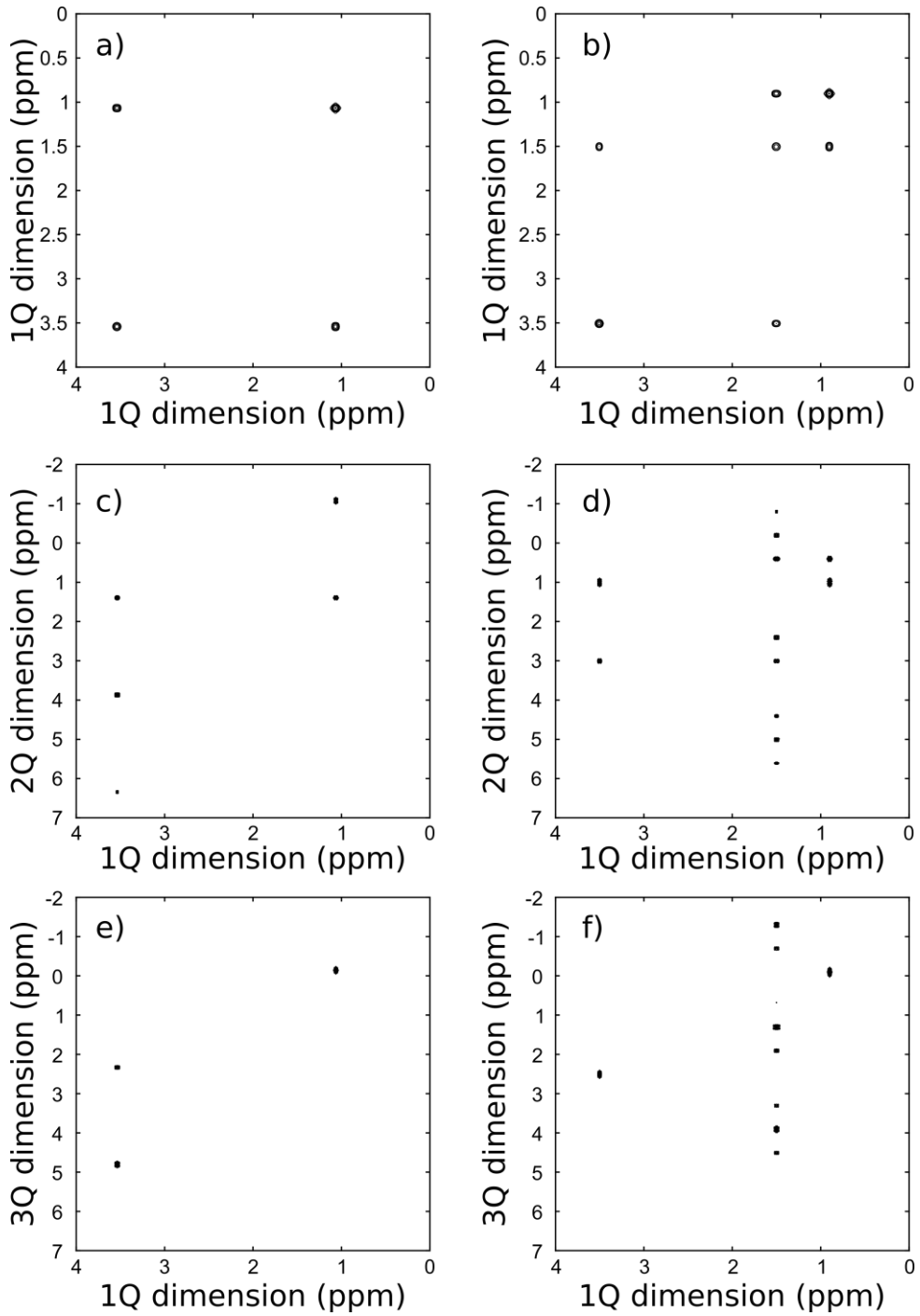

Figure 45: Simulated COSY, DQS and TQS spectra for ethyl chain (a,c,e) and linear propyl chain (b,d,f). Simulation have been obtained using Spinach

Conventional and ultrafast 3, 4 and 5Q spectra of these molecules' mixture were done and are displayed on Figure 46.

First, it can be seen that good spectra were obtained, confirming that the possibility to spatially encode coherence order higher than two. Ultrafast spectra are very similar to conventional ones despite the lower sensitivity. The higher the observed coherence order, the higher the sensitivity drop. This phenomenon is not specific to ultrafast spectra, but is more problematic in this case as the SNR is already impacted by the loss due to the EPSI acquisition.

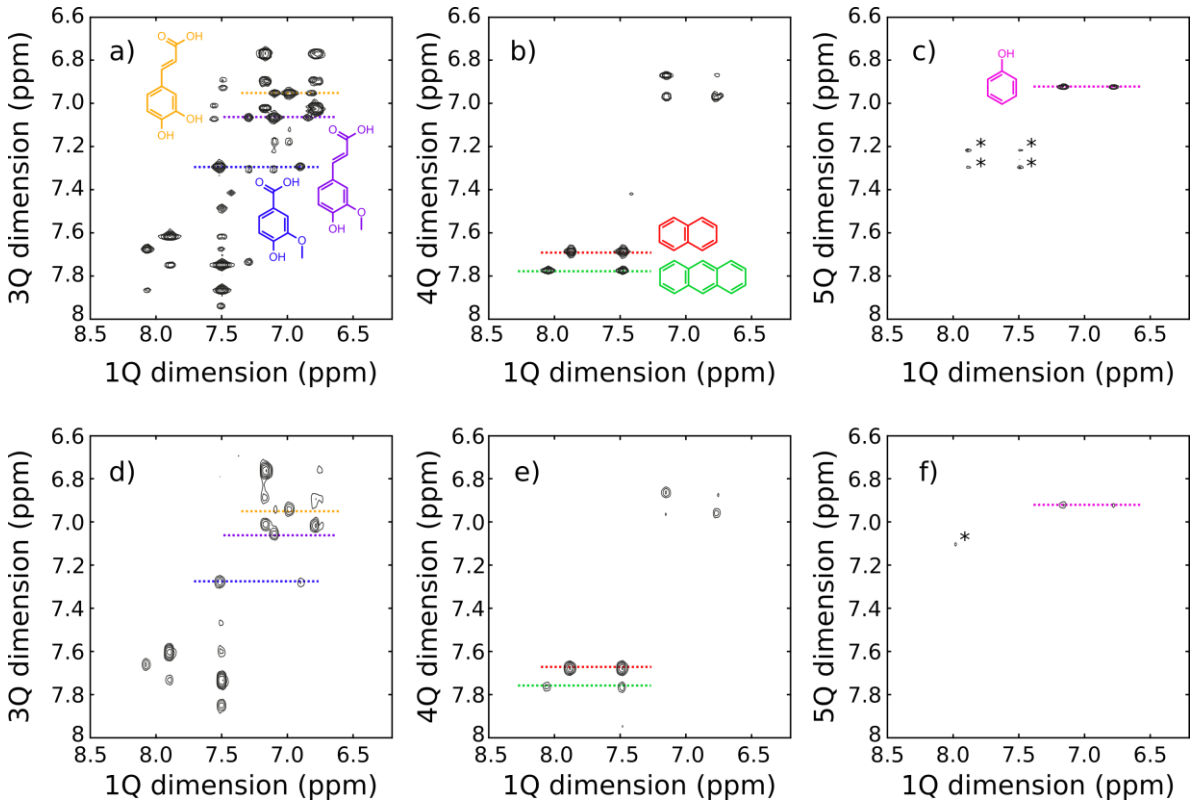

Figure 46: Conventional 3Q (a), 4Q (b) and 5Q (c) of the aromatic mixture. Ultrafast 3Q (a), 4Q (b) and 5Q (c) of the aromatic mixture. Dashed lines identify the slice for each compounds whose MaxQ is reached. The MQ spatial dimension uses a reduced frequency scale $\delta_1^R = \delta_1/p$ with p as the coherence order.

3.3.2.2 Optimization as a function of the coherence order.

The ultrafast MQ-NMR spectra shown in Figure 46 have actually been obtained using the pulse program shown in Figure 43 b). For ultrafast 2D NMR spectra, the acquisition duration is limited by the robustness of the probe and the gradient amplifier. It is usually recommended to avoid too long acquisitions to preserve hardware. For this kind of experiments, the acquisition duration is usually lower than 100 ms. This delay does not always allow antiphase coherences to convert into observable in-phase coherences before the end of acquisition, leading to important sensitivity losses. In order to increase sensitivity, it was suggested to add a spin echo between the last 90° pulse and the acquisition as shown in Figure 43 b), as in the refocused inadequate experiment.[63] An example of why the optimization is so important is illustrated with phenol and naphthalene compounds. Several conventional and ultrafast 3, 4 and 5Q spectra were done on the aromatic mixture sample with different values of τ and τ'. The average integration for all phenol and naphthalene peaks were then measured and plotted in the Figure 47.

In most cases, even if there are some slight differences, the global tendency for ultrafast spectra is the same as with conventional spectra. Moreover, it can be seen that the delays τ and τ' can have significant influence on peak integration. For example, if a τ' of 240 ms is used for the 3Q spectra, phenol and naphthalene integration will decrease to only 10% of their maximum value. This example

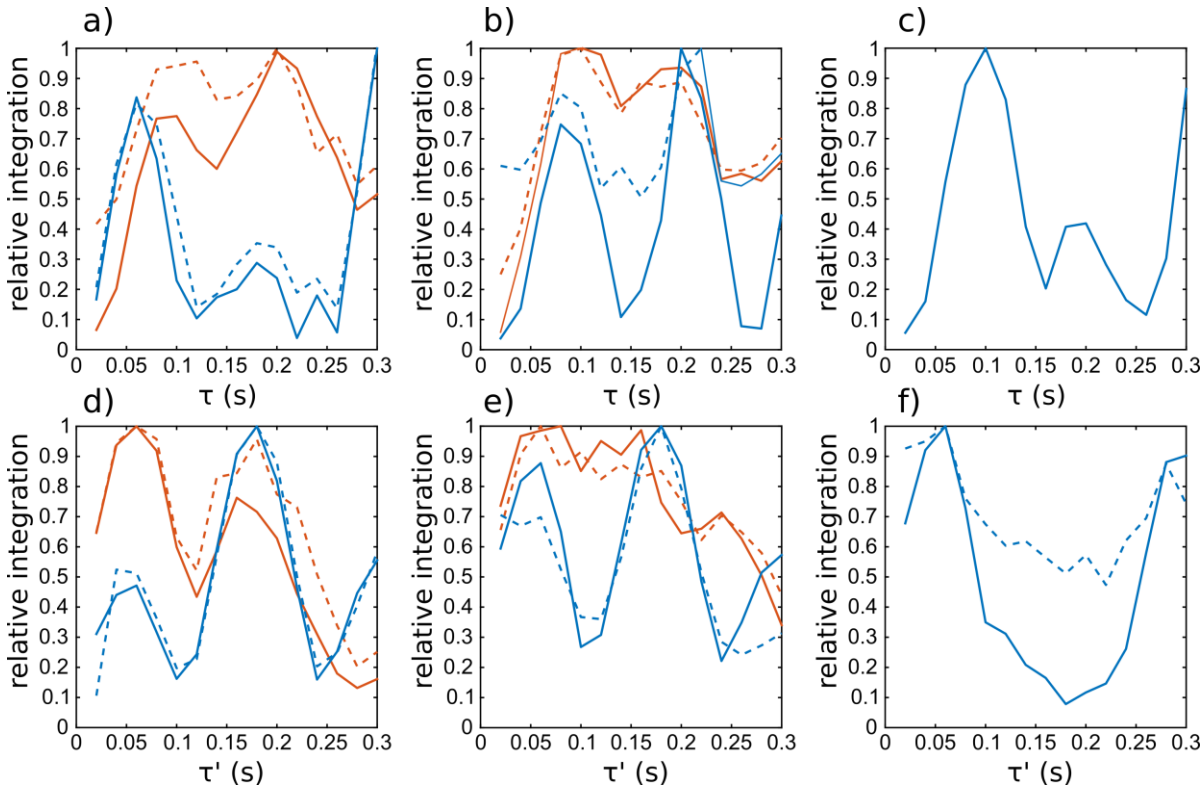

Figure 47: Relative evolution of phenol (blue) and naphthalene (red) peaks for 3, 4 and 5Q for conventional (straight lines) and ultrafast (dashed lines) as a function of τ (a, b and c) or τ' (d, e and f). Refocalized spectra used for d, e and f were done with τ = 200 ms for 3Q, 100 ms for ultrafast 4Q, 80 ms for conventional 4Q and 100 ms for 5Q spectra.

illustrates how τ and τ' can influence the spectra. With two compounds it is rather simple to reach a good compromise, but when the mixture becomes more complex, the optimization becomes difficult. Moreover, the effect of τ and τ' can be peak selective, leading to an even more complex optimization.

3.3.2.3 Sensitivity consideration

Ultrafast 2D NMR experiments, although allowing great acceleration, suffer from poor sensitivity. It is mainly due to the acquisition bandwidth that must be significantly higher than for conventional acquisition because of the EPSI step. We wanted to quantify here the loss induced by the use of spatially encoded experiments. To do so, conventional and ultrafast experiments were done with the same parameters (gain, relaxation delay, τ, τ'…) and the same total experiment duration. In this case the number of sub-experiments of the conventional experiments was set the number of scans for the ultrafast acquisition. Finally, the FIDs of conventional experiments were truncated to simulate the same acquisition duration. Ultrafast and conventional processing were as similar as possible including a sine apodisation in temporal / t_2 and spatial / t_1 dimensions and zero filling to 1024 in both dimensions. Then for each compound, the SNR was measured for the most intense peak and the results are displayed in the following tables.

Table 4: SNR comparison between conventional and ultrafast 3Q spectra

SNR	Caffeic acid	Ferulic acid	Vanilic acid	Naphthalene	Anthracene	Phenol
Conventional	1 600	1 759	1 288	8 881	2 235	3 521
Ultrafast	220	217	311	193	743	978

Table 5: SNR comparison between conventional and ultrafast 4Q spectra

SNR	Naphthalene	Anthracene	Phenol
Conventional	1 430	342	296
Ultrafast	522	168	172

Table 6: SNR comparison between conventional and ultrafast 5Q spectra

SNR	Phenol
Conventional	1 613
Ultrafast	132

In terms of SNR, the difference between conventional and ultrafast experiments are between 1.7 and 46 depending of the peaks and the compounds studied. In addition to the $\sqrt{2}$ loss factor due to the processing of only half of the echoes, it was shown that the SNR losses of spatially encoded experiments were proportional to $\sqrt{N_i}$ where N_i is the number of virtual increments in the ultrafast experiment[148,151] This number of increments is defined by:

$$N_i = L_e k_{max}, \tag{3.6}$$

where L_e is the length encoded by the spatial encoding block and k_{max} is the maximum k-value explored by the EPSI acquisition. It is defined as:

$$k_{max} = \gamma G_a T_a, \tag{3.7}$$

where G_a is the intensity of the acquisition gradient and $T_a$is the duration of an acquisition gradient. In our case can be calculated as $\sqrt{N_i} = 13$. This value is in the range of the losses measured experimentally. However, the comparison that is made here may not be the best as conventional and ultrafast are not completely equivalent. Indeed, the ultrafast experiments that were done here are done with a constant time encoding. To make the comparison more meaningful, the conventional experiment too should also have been done in the constant time fashion.

3.3.3 Reaction monitoring using ufMQS

One interesting application of ultrafast 2D NMR experiments is its use to monitor chemical reactions. Indeed, it can be used for reactions that are too fast to be monitored by conventional 2D NMR and when 1D spectra are too complicated. We will show here how ultrafast MQ spectra can be used to monitor a Hetero Diels-Alder reaction. This kind of NMR experiment is particularly adapted to this

experiment as the MaxQ of the reactants is different from the one of the product. Both reactants have MaxQ of 5 while the product has two rings with a MaxQ of 5 and one of 4 as shown in Scheme 2.

The reaction was carried out in a classical NMR tube. An ultrafast 4Q spectrum was acquired and optimized before the catalyst was introduced, in order to have a reference spectrum that can be seen on Figure 48 a). Then after addition of the catalyst, a series of interlaced 1D and ultrafast acquisitions were used for reaction monitoring. Unfortunately, the SNR was too low to be able to monitor the reaction on the spectrometer that was used for the optimization. To circumvent this problem, it was decided to work on spectrometer equipped with a cryo-probe and to do 8 scans for each ultrafast experiment. The integration of three peaks were monitored, two coming from a reactant and one from the product. No signal could be monitored for the dienophile as its signal to noise is too low. The product signal used for monitoring is the phenyls ones as they overlap, giving strong signal. Unfortunately, the signals coming from the product's ring with a MaxQ of 4 have a too weak signal to noise ratio to be used for monitoring as shown in Figure 48 c).

To confirm that the signal of the 4Q ring is not an artifact, several spectra at the end of the reaction were added and compared to a conventional one. These spectra are displayed in Figure 49.

As ultrafast experiments were interleaved with 1D ^{1}H spectra, and as the spectrum contain isolated peak, the reaction monitoring done with ultrafast spectra was compared with the one done using 1D experiments. Integration curves can be seen on Figure 50 b).

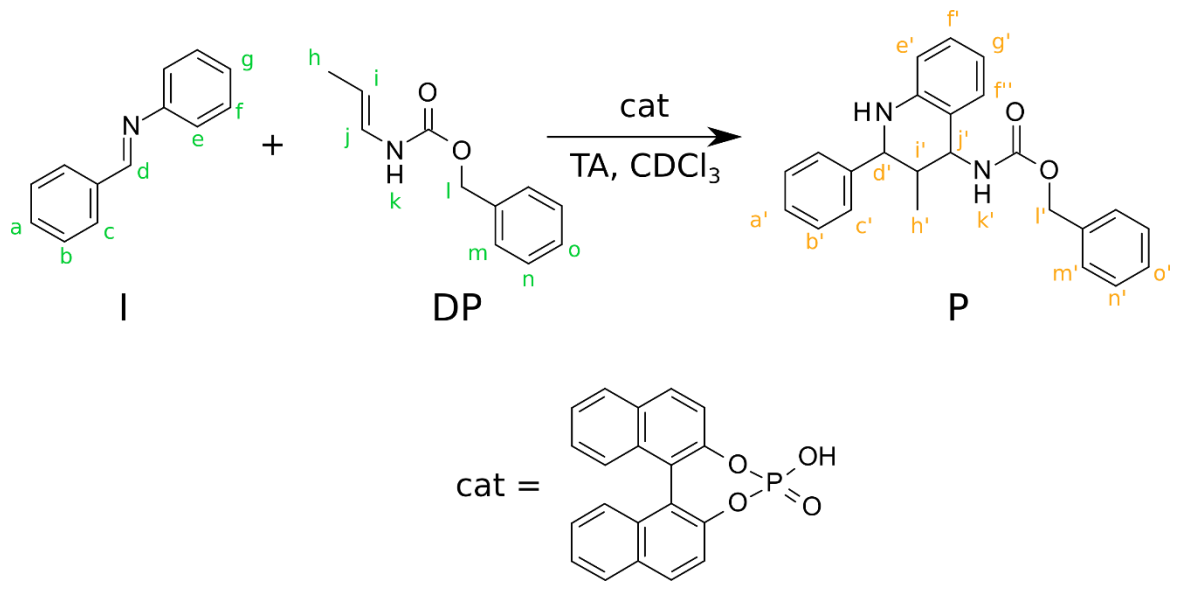

Scheme 2: Reaction of Hetero Diel Alder between the Imine I and the Dieneophile DP to yield the product P. The reaction is catalyzed by BINOL-phosphoric acid.

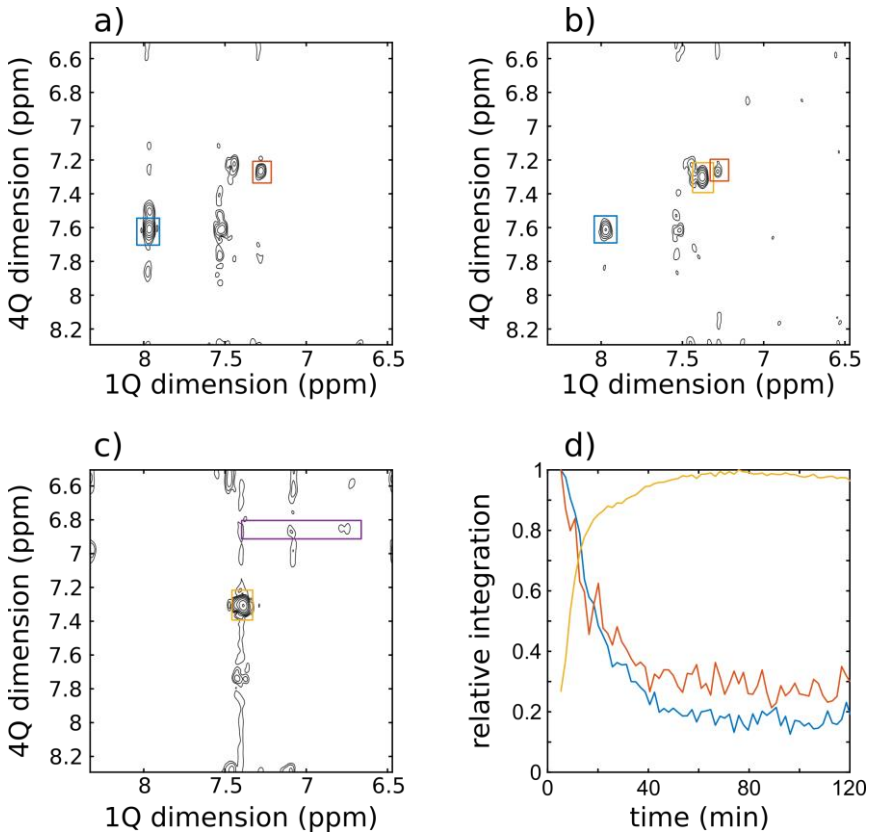

Figure 48: Ultrafast 4Q spectra before the addition of the catalyst (a), 3 min 45 sec after the addition of the catalyst (b) and 2 hours after the beginning of the reaction (c). Evolution of peak integration as a function of time (d). Signal surrounded by blue and red rectangles corresponds to the imine I and signals surrounded by yellow and purple rectangle correspond to the product signal.

Curves obtained by 1D NMR are very similar to those obtained by ultrafast confirming the validity of using such experiments for reaction monitoring. Moreover, 1D ^{1}H spectra have a much better SNR than ultrafast acquisition. In this case it was possible to isolate peaks of interest in the 1D spectrum allowing an easy monitoring, however, it may not be always possible. Ultrafast acquisition will be helpful to be able to fetch structural information thanks to the simplification provided by MaxQ and for cases with more crowded spectra that cannot be monitored with only 1D experiments.

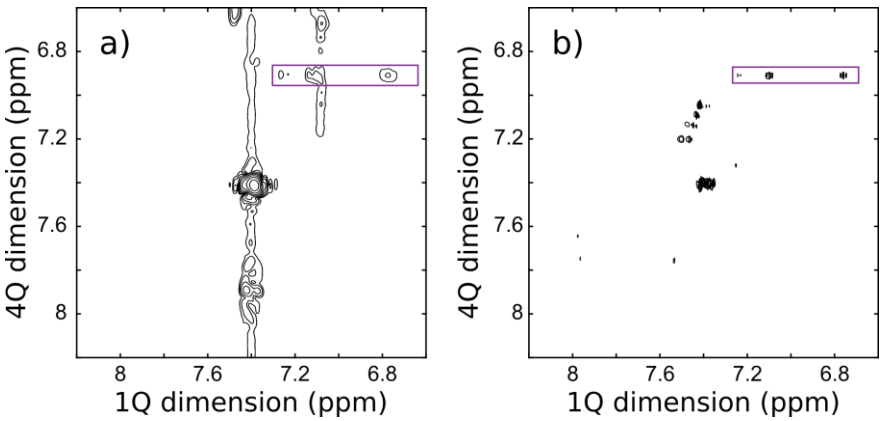

Figure 49: Ultrafast (a) and conventional (b) 4Q spectra after the end of the hetero Diels-Alder reaction. To increase signal to noise ratio in ultrafast spectrum, that last 30 spectra of the reaction monitoring have been added.

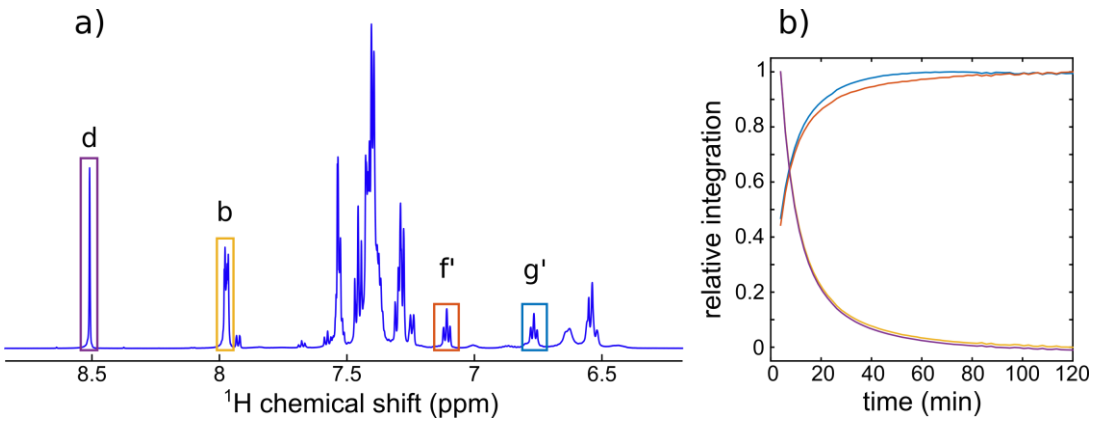

Figure 50: 1D ^{1}H spectrum during the reaction (a) and evolution of relative peak integration (b). Letters above integrated peaks correspond to the attribution that can be seen in Scheme 2.

3.4 Conclusion

It was shown here how it was possible to spatially encode chemical shifts. It was already used for single and double quantum coherences for different applications. We showed here that it was also possible to spatially encode higher coherence order allowing to simplify spectra and analysis and it was demonstrated on an aromatic mixture. The importance of the optimization of this pulse sequence was also demonstrated. However, we also showed that the major drawback of this method is its sensitivity.

We have also shown how MQS could be used for reaction monitoring thanks to the simplification it brings and to the structural information that can be extracted from the spectra. The possibility to monitor a chemical reaction was illustrated with the example of a hetero Diels-Alder reaction.

4 Spatial encoding on a flowing sample

4.1 Introduction

Reaction monitoring is an important topic for chemical synthesis. The evolution of component concentrations, the nature of reaction intermediates, and reaction kinetics are examples of information that chemists need in order to understand and optimize reactions. This information can be accessed through different methods of reaction monitoring. Among all these methods, NMR is a very powerful technique thanks to its non-destructiveness and to all the structural information that it can bring. For these reasons it is widely used for reaction monitoring.[16,152,153]

Reaction monitoring with NMR is usually done by sampling the reaction mixture several times during the reaction and then analyzing these fractions. However, in these conditions, short lifetime species cannot be observed. It is also possible to carry out the reaction inside the spectrometer. However, as magnetic stirring cannot be used and heat transfer is different from a heating bath, the conditions will probably differ from doing the reaction in a round bottom flask, leading to different kinetics. Moreover, reactions that necessitate specific atmospheres or temperatures cannot be done in the spectrometer.

One solution that can be used is online monitoring. The reaction is carried out in realistic conditions and a fraction of the reaction mixture is continuously sent to the spectrometer through a capillary[58,59,154,155] Initially, this kind of setup necessitated dedicated flow probes such as the ones used for hyphenation between HPLC and NMR. Recently, "flowtubes" and "flow cells" have been developed and commercialized,[14,15] that can be inserted in the majority of standard probes, allowing laboratories not equipped with flow probes to carry out online reaction monitoring. However, this equipment cannot be used to monitor very fast reaction whose duration are less than a few seconds. For fast reactions, other equipment has to be used such as stop flow[46–48] of rapid injection devices.[44,50–53]

The efficiency of reaction monitoring depends on the amount of information that can be extracted. Usually, reaction monitoring is done with fast repetition of 1D experiments of sensitive nuclei such as ^{1}H, ^{31}P or ^{19}F. Multidimensional experiments are rarely used because of their durations. A 2D experiment for example needs at least 5 to 10 min minutes to finish. If the reaction is too fast it can lead to artifacts. Indeed, if peak intensities vary due to the reaction, t_1 noise will appear. As said in section 1.4, many developments have been done over the years in order to reduce the duration of multidimensional experiments such as non-uniform sampling,[156] Hadamard spectroscopy[2] or accordion experiments.[157] The method that provide the highest acceleration is spatial encoding, developed by Frydman and coworkers.[6,7,115] So-called "ultrafast" experiments have already been used for reaction monitoring[128–131,145,158,159] and as detector after a chromatographic separation,[126,127] but not yet for online reaction monitoring at high field.

In this chapter, we will show how spatially encoded experiments can be used to monitor a sample that evolves over time under flow conditions, using a commercial flowNMR system on a high-field magnet. First, imaging experiments will be described in order to characterize the interference between gradient pulses and flow. Then, ultrafast 2D experiments under flow conditions will be analyzed, and their use to monitor a saponification reaction will be demonstrated. Finally, preliminary results of DOSY experiments will be shown.

4.2 The Flow Unit setup

The flow unit that is in the laboratory was purchased from Bruker Biospin (Billerica, MA). It is composed of several pieces that are shown in Figure 51 and in a schematic way in Figure 52. First, a HPLC pump that circulates a fraction of the reaction mixture through a PEEK (PolyEther Ether Ketone) capillary that goes from the reaction vessel to the NMR tube and comes back. A thermostatic bath is also used in order to cool or heat the capillary and its content during the transfer to the spectrometer. The flow interface is used to connect the thermostatic fluid to the capillary and to select the direction of the flow. It can either be used in bypass mode, in which the fluid returns to the reaction vessel without going through the spectrometer, or in online mode, in which the reaction mixture circulates through the entire circuit before returning to the reaction vessel.

Finally, the flowtube is the part that is inserted in the magnet. It corresponds to an NMR tube fixed on a support that is equivalent to a spinner to hold the tube on the probe. The tube is a reinforced glass tube that is meant to handle pressure up to 10 bars in which a capillary is inserted. The capillary in which the reaction mixture circulates goes down to the bottom of the tube to avoid the formation of air bubbles.

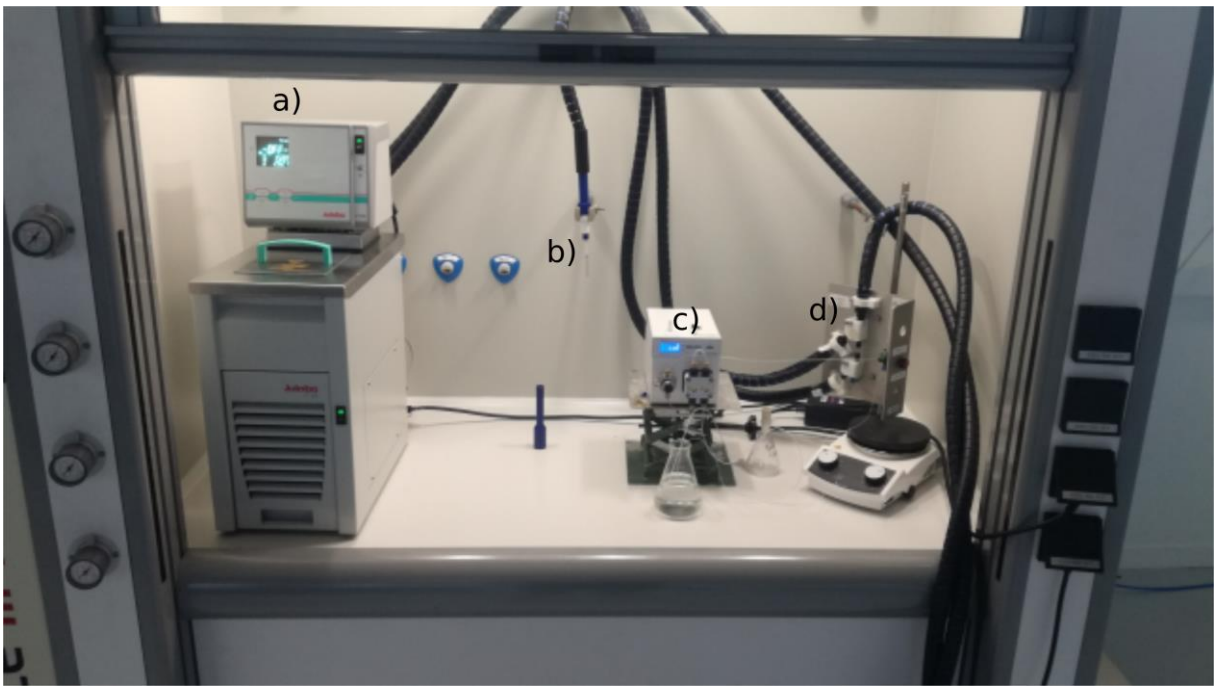

Figure 51: Picture of the Flow Unit setup including a thermostatic bath (a), the flowtube (b), the HPLC pump (c) and the flow interface (d) under a ductless fume hood.

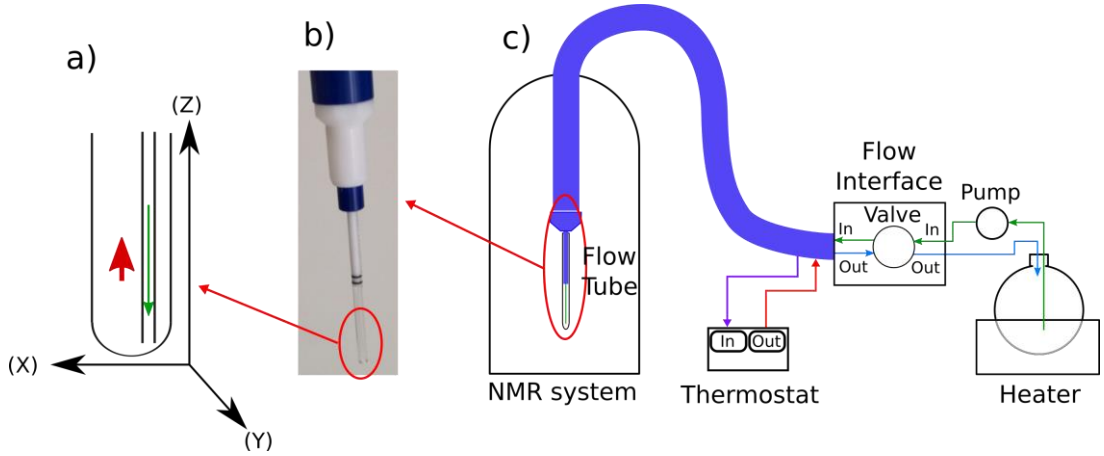

Figure 52: Scheme of the bottom of the flowtube (a), picture of the flowtube (b) and scheme of the complete Flow Unit (c).

The Flow Unit is intended to be under a fume hood to protect the user from potentially dangerous chemicals as shown in Figure 51. However, the ductless fume hood was not available until the last year of this PhD. Hence, the reactions that will be described were done without the use of a fume hood and were selected accordingly.

4.3 Experimental part

4.3.1 Samples

Unreacting mixture 1 was prepared according to the following procedure. 203 µL of methanol, 292 µL of ethanol, 376 µL n-propanol and 463 µL 2-butanol were dissolved in 25 mL of purified and degassed water. The concentration is near 200 mM for each compound.

Unreacting mixture 2 was prepared according to the following procedure. 203 µL of methanol, 292 µL of ethanol, 376 µL n-propanol, 463 µL 2-butanol and 370 µL of acetone were dissolved in 25 mL of purified and degassed water. The concentration is near 200 mM for each compound.

Unreacting mixture 3 was prepared according to the following procedure. 81 µL of methanol, 116 µL of ethanol, 150 µL n-propanol and 186 µL 2-butanol were dissolved in 10 mL of acetonitrile. The concentration is near 200 mM for each compound.

The first saponification reaction was prepared according to the following procedure. The temperature of the probe was set to 25°C, but that of the reaction mixture was not monitored. In a flask equipped with a magnetic stirrer, 125 µL of 10 M NaOH (1eq. 25 mM) was dissolved into 50 mL of purified and degassed water. The solution was fed to the flow tube with a flow rate of 3 mL/min until the solution returned to the flask. The dead time before the system equilibrates is about 1 min and 40 seconds. The probe was tuned on the solution flowing at 3 mL/min. A series of acquisitions were repeated every 15 s interlacing ufCOSY experiments with spatial encoding on Z-axis and on X-axis. This 15 s delay is chosen to avoid any damage to the probe, and provides a repetition time that is still much shorter than with conventional (non-UF) experiments. After the end of the fourth UF experiment

with spatial encoding on X-axis, 119 µL of ethyl acetate (1eq, 25 mM) was added in the reaction mixture. The acquisitions continued for about 40 min.

The second saponification reaction for kinetic measurement was prepared according to the following procedure. First, temperature regulation of the probe was set to the desired temperature (25, 35 or 45°C) and the probe was tuned on a tube containing ethanol and sodium acetate at 25mM in purified undeuterated water. At room temperature, in a 100 mL round-bottom flask with magnetic agitation, 50 mL of purified and degassed water were used to dissolve 119 µL of ethyl acetate (1eq, 25 mM). The flask was heated to the selected temperature (25, 35 or 45°C) in a bain-marie. The solution was fed to the flow tube with a flow rate of 3 mL/min until the solution returned to the flask while the transfer line was heated to the desired temperature using a thermostatic water bath. With this setup, the dead time before the system equilibrates is about 1 minute and 40 seconds. A series of acquisition were repeated every 15s interlacing 1D ^{1}H and ufCOSY experiments with spatial encoding on X-axis. This 15 s delay is chosen to avoid any damage to the probe, and provides a repetition time that is still much shorter than with conventional (non-UF) experiments. After the end of the fourth UF experiment, 125 µL of 10 M NaOH (1eq, 25 mM) was added in the reaction mixture. The acquisitions continued for about 40 min.

4.3.2 Acquisitions

All the experiments described below were carried out on a Bruker Avance III spectrometer operating at a ^{1}H Larmor frequency of 600.13 MHz equipped with a 5 mm triple ^{1}H/^{13}C/^{15}N room temperature probe with triple-axis gradient. The temperature inside the probe was calibrated with a standard methanol sample and then set to a value of 298 K with airflow of 535 L/h. All the experiments were done without sample rotation.

For 1D imaging on water, a small tipping angle of about 6° was used. Prephasing and acquisition gradients were set to ± 6.7 G/cm. 50 experiments of 512 complex points were recorded during the acquisition. The field of view of the experiment if about 3.5 cm. The echo delay was set to about 20 ms and a repetition time of 55 ms was used. After each acquired echo, an 800 µs sinusoidal gradient of respectively -12.0, 6.7 and -4.7 G/cm on Z, X and Y-axis. Note that in order to have a better control of the delay between images, the 1D imaging experiments were recorded in a pseudo-2D fashion.

For 2D imaging experiments on water, a 1 ms 90° selective pulse was used to excite a 0.5 mm thick slice. 64 increment of phase encoding gradient were used ranging from -8.7 to +8.7 G/cm. An acquisition gradient of 27.3 G/cm was used to acquire 256 complex points. With these parameters, the field of view in both dimensions is about 7.5 mm. The echo time was set to 3.9 ms, and the repetition time was set to 5s.

For UFCOSY experiments with unreacting mixtures in water, bipolar encoding gradients of ± 1.04 (for theZ-axis) or ± 0.85 (for the X-axis) G/cm were used in combination with 15 ms chirp pulses with

12 kHz bandwidth. The acquisition consisted of a train of bipolar gradient pulses, of ± 45.50 (for Z-axis encoding) or ± 35.00 (X-axis encoding) G/cm, with 128 loops and a duration of 256 μs for each gradient pulse. A relaxation delay of 10 s was used including 5 s of presaturation. The excitation sculpting block (see Figure 61) was composed of a pair of 2 ms trapezoidal pulses and a hard π pulse surrounded by a pair of 1 ms gradient pulses (on the X and Y-axis for Z-SPEN experiments and on the Y axis for X-SPEN experiments).

For UFCOSY experiments with unreacting mixtures in acetonitrile, bipolar encoding gradients of ± 1.07 (for Z-axis encoding) or ± 0.083 (X-axis encoding) G/cm were used in combination with 15 ms chirp pulses with a 12 kHz band-width. The acquisition consisted of a train of bipolar gradient pulses of ± 45.5 (for the Z-axis) or ± 35.0 (for the X-axis) G/cm, with 128 loops and a duration of 241 μs for each gradient pulse. A relaxation delay of 10 s was used including 5 s of presaturation. The WET block (see Figure 68) was composed of four 20 ms sinc1 pulses with optimized power, each one followed by a 1 ms gradient pulse (on the X and Y-axis for Z-SPEN experiments and on the Y-axis for X-SPEN experiments).

For UFCOSY experiments with unreacting mixtures in water with a double spatial encoding block, bipolar encoding gradients of ± 1.04 G/cm on Z-axis were used in combination with 7.5 ms chirp pulses with 12 kHz bandwidth. The acquisition consisted of a train of bipolar gradient pulses, of ± 45.50 G/cm on Z-axis, with 128 loops and a duration of 256 μs for each gradient pulse. A relaxation delay of 10 s was used including 5 s of presaturation. The excitation sculpting block was composed of a pair of 2 ms trapezoidal pulses and a hard π pulse surrounded by a pair of 1 ms gradient pulses (on the X and Y-axis for Z-SPEN experiments and on the Y axis for X-SPEN experiments).

For UFCOSY experiments with reacting mixtures, bipolar encoding gradients of ± 1.04 (for Z-axis encoding) or ± 0.80 (X-axis encoding) G/cm were used in combination with 15 ms chirp pulses with a 12 kHz bandwidth. The acquisition consisted of a train of bipolar gradient pulses of ± 45.5 (for the Z-axis) or ± 35 (for the X-axis) G/cm acquisition gradient, with 128 loops and a duration of 241 μs for each gradient pulse. A relaxation delay of 10 s was used including 5 s of presaturation. The excitation sculpting block was composed of a pair of 2 ms trapezoidal pulses and a hard π pulse surrounded by a pair of 1 ms gradient pulses (on the X and Y axis for Z-SPEN experiments and on the Y axis for X-SPEN experiments).

4.3.3 Processing

All processing was performed using a custom MATLAB code.

For 1D imaging, data are imported in MATLAB and then rearranged into a 2D matrix. The first dimension corresponds to the k dimension in which echoes are acquired, the second dimension is the increment dimension. Echoes are Fourier transformed along the k dimension. Magnitude spectra were used. The selection of integral region was done on the first image and used for all the other ones.

For 1D imaging, data are imported in MATLAB and then rearranged into a 2D matrix. Zero filling to 1024 points was used prior to Fourier transformation

The UF2DNMR data are imported in MATLAB, and then rearranged into a 2D matrix. Odd and even echoes are separated, and only odd echoes are processed here for simplicity. Along the spatial dimension, the data are inverse Fourier transformed, apodised with a Gaussian window, zero-filled and Fourier transformed. Along the spectral dimension, the data are apodised with a sine window, zero-filled and Fourier transformed. Magnitude spectra are used in all cases. For the build-up curves, the integration range of peaks were selected on the first spectrum and were used for integration on the following spectra.

4.4 Imaging with flowtube

Theory and practice of imaging are well known for motionless and flowing samples. However, because of some results obtained with conventional DOSY (see section 4.7) on a flowing unreacting mixture, it was decided to observe the behavior of the flow using imaging. First, we did series of 1D imaging along Z-axis on a flowing water sample. Results showed good results and almost identical profiles from one experiment to another. After several tests, it appears that the problem could be seen only if the experiments were repeated faster and with a higher echo time. The results obtain with an echo time of 20 ms and a repetition time of 55 ms are displayed in the Figure 53.

It can be seen that the image periodically suffers high integral losses. The frequency of these losses is about 2.2 Hz. This frequency corresponds to the oscillation of the pump's pistons. The HPLC pump we use relies on a motor that moves two pistons in a synchronized way as shown in the Figure 54. At

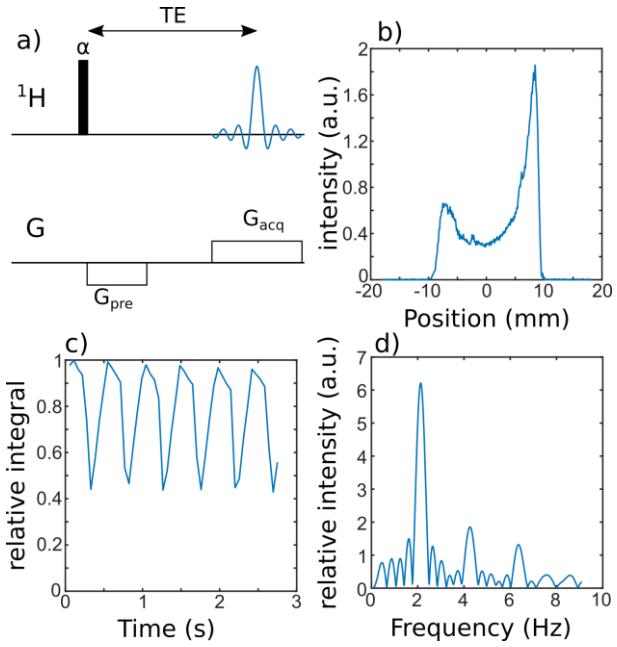

Figure 53: Pulse sequence used for 1D imaging (a) and an example of a 1D profile obtained with it (b). Evolution of the relative integral of the profile with a flow rate of 3 mL/min (c) and Fourier transform of the evolution (d). α correspond to a tipping angle of 6°.

one point, the pistons have to stop to then move in the opposite direction. It creates velocity variations of the fluid, hence leading to changes in profile integral. Indeed, if a volume element moves during the gradient echo experiment, it results in an additional velocity-dependent phase term. Since, as will be seen later on, the fluid does not circulate as a whole, there are velocity distributions, that result is partial refocusing and intensity losses. If the velocity distribution changes over time, these losses will also change.

In addition to this velocity changes, another problem we dealt with was the non-repeatability of the pump's behavior. On Figure 55 are shown the integrals of series of 1D images recorded one day apart.

The frequency of the velocity changes stays the same, but intensity losses are not the same from one day to another.

In the flowtube, the direction of the flow is mainly along the Z-direction. We wanted to see if the velocity changes would lead to the same integral losses if the imaging was done along X-axis. The comparison of the evolution of image integral with encoding along Z and X-axis is shown on Figure 56.

There are still intensity losses when imaging is done along an axis transversal to the flow, but they are highly reduced. In this case, the losses are about 5% of the initial while it was almost 40 % when the imaging was done along the Z-axis. In addition, a progressive intensity loss can be seen in both cases. This is mainly due to the fact that experiments are repeated quickly and it led to saturation.

One solution to avoid the velocity variations would be to use another kind of pump. Peristaltic pumps are known to be able to provide a way more regular flow than the piston pump used for HPLC. However, these pumps cannot sustain the pressure needed to circulate the fluid through the 14 m of capillary with a decent flowrate. The pressure generated by the HPLC pump to circulate the fluid with a flowrate of about 3 mL/min is between 5 and 6 bars. This pressure cannot be generated by laboratory peristaltic pumps.

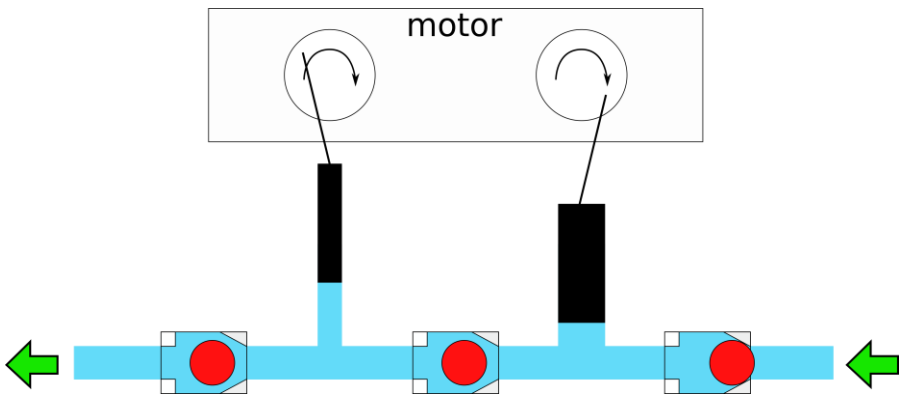

Figure 54: Scheme of a HPLC piston pump. Blue lines correspond to the fluid, black rectangles correspond to the pistons and red circles correspond to the balls used to create the anti-return flow valves.

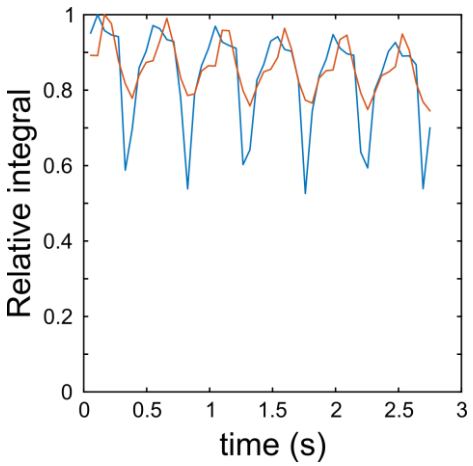

Figure 55: Integral of 1D imaging series done one day apart. In both cases, the flow rate was set to 3 mL/min.

Another solution is to add a backpressure regulator. On HPLC system, the velocity variations are not such a problem as the column usually generates a lot of backpressure that smoothens oscillations. A backpressure regulator is a device that maintains a defined pressure upstream of itself (at its own inlet). It was considered to use one of these devices to decrease fluid velocity variations. However, the pressure that should be used to smooth the variation is too high. Indeed, Bruker recommends not to exceed 10 bars in the flowtube to avoid breaking the glass limiting the use of back pressure regulator.

One last option to completely remove the velocity variations would be to completely stop the pump each time an experiment has to be done. In order to evaluate how long it takes for the fluid to stop after the pump has been stopped, the same kind of image series was done, but the pump was stopped in the middle of the experiment. As previously, the profile integrals were monitored, and the result is displayed in the Figure 57.

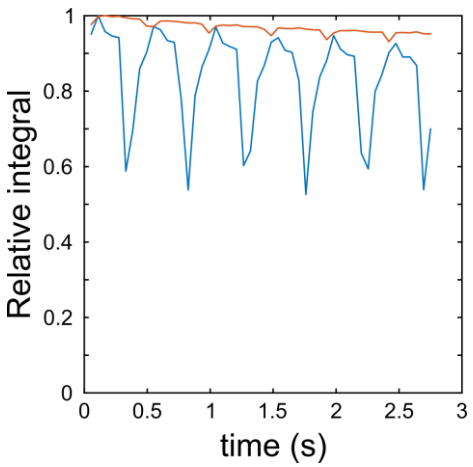

Figure 56: Evolution of the relative intensity of image integral for image of the flowtube along Z (blue) and X-axis (red). Flow rate was set to 3 mL/min.

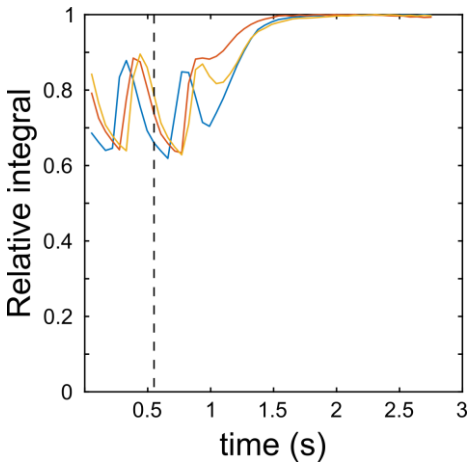

Figure 57: Evolution of the relative integral of a series of 1D images along Z-axis. Dashed lines correspond approximately to the moment the pump was stopped (pressing on the stop button). The three colors represent three repetitions of the experiment.

It can be seen that after the button is pressed on the pump, the variation of intensity takes about 1 second to stop. As the repetitions delays that are used for ultrafast experiment are usually longer than this (usually never lower than 10s to let the acquisition gradient rest between two acquisitions), the solution consisting in stopping the pump before each experiment could work. Moreover, there is a way to connect the pump to the console, opening the possibility to control the pump through the pulse programs. However, it was decided to keep this solution as the last on to use if nothing else works.

A last question that can be asked is about the different flow in the flowtube. Indeed, the velocity of the fluid will not be the same in the capillary than in the rest of the flowtube. In order to have an idea of how the velocity in the capillary affects the experiment, 1D imaging experiments were done. The capillary cannot be seen on the Z-profiles as the capillary is all along the tube. It can be seen on profiles along X or Y-directions as it can be seen on Figure 58.

The position of the capillary can clearly be seen on the Y-axis, but not as much on the X-axis one. This is mainly due to the fact that the capillary is not perfectly straight in the flowtube. Moreover, it will depend on how the flowtube is inserted inside the magnet. To have a better visualization of the

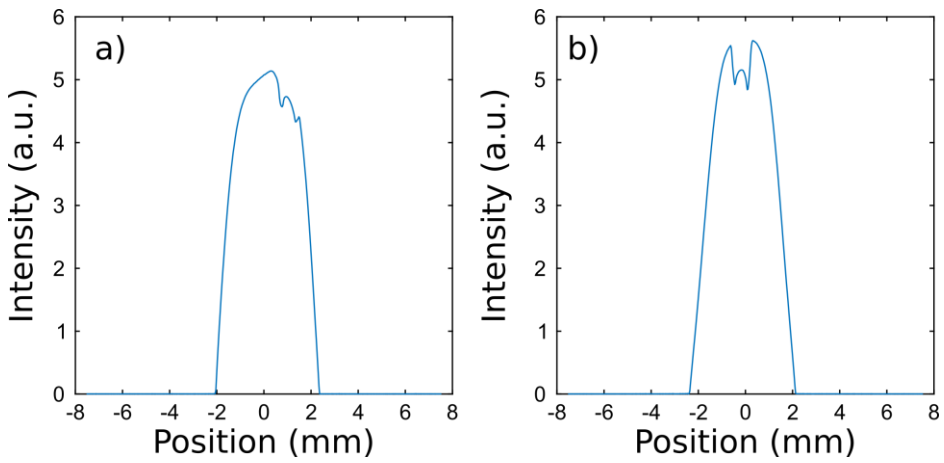

Figure 58: 1D profiles along X (a) and Y-axis (b).

position of the capillary in the tube, it was decided to do 2D imaging. Several imaging experiments were done at several flow rates and the images of displayed in Figure 59.

In these 2D images, the position of the capillary in the tube is really clear. The image of the water inside the capillary is visible when there is no flow, but it disappears when the flow rate increases. Indeed, the velocity of the fluid inside the capillary is much higher than in the rest of the flowtube. Based on measurement made on 2D imaging, the capillary interior radius is about 0.3 mm and the tube interior radius is about 2.2 mm. As the flow rate inside the capillary has to be the same than in the rest of the flowtube, it results that the velocity of the fluid inside the capillary is about 60 times higher than in the tube. As we plan to do reaction monitoring with a high flow rate, in order to keep the delay the fluid takes to go from the reaction vessel to the flowtube to a minimum, the capillary will be neglected in the rest of this chapter.

The velocity in the rest of the tube was also calculated. Based on the previous measurement, flow rate between 0 and 3 mL/min correspond to velocities between 0 and 0.33 cm/s. However, this value corresponds to the mean velocity. The actual velocity depends on the position of the fluid in the tube.

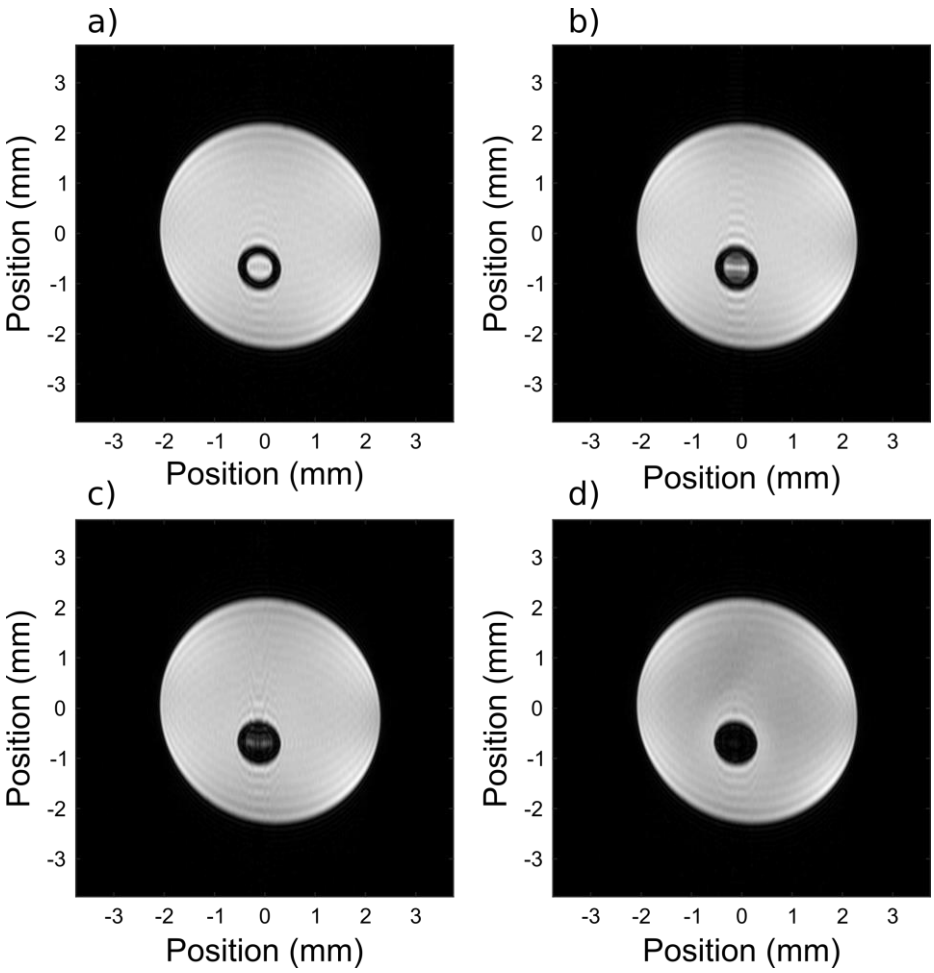

Figure 59: 2D images of the flowtube without flow (a) and with flow rates of 0.5 (b), 1 (c) and 2 mL/min (d).

As the velocity profile could be useful for future work, calculations were made for three flow rates for a sample of water, assuming a laminar flow. The resulting profiles are displayed in the Figure 60.

These velocity profiles have been calculated assuming the flowtube is a perfect cylinder and without taking into account the capillary. These profiles will be used later on (see section 4.5.1.1) for numerical simulations.

4.5 Case study of the ufCOSY of a non-evolving sample

It was seen that the velocity changes created by the pump lead to important intensity losses on imaging experiments. We will see in this chapter the effect they have on experiments relying on spatial encoding of the chemical shift. First, we will see what happens if the encoding is done along the Z-axis with several spatial encoding blocks, and then what happens when it is done along the X-axis.

4.5.1 Spatial encoding along the longitudinal axis

4.5.1.1 Single spatial encoding block

The effect of velocity variations on chemical-shift spatial encoding block were not known when this work was started. It was shown in the previous section that for 1D imaging it leads to integral losses, so we wanted to know what were the effects for ultrafast 2D NMR experiments. 20 mL of a mixture of alcohols was prepared in non-deuterated water in order to identify the best solvent suppression in these conditions. It was found that excitation sculpting combined with presaturation offers very good results so it was incorporated in the ultrafast COSY pulse sequence as shown in Figure 61.

A series of ultrafast COSY experiments were acquired with the sample flowing in the flow unit with of flow rate of 0, 1 and 2.5 mL/min. Examples of spectra obtained at the three flow rates are displayed in Figure 62 a-c). In each case, it can be seen that good quality spectra are obtained, that there are no artifacts or important peak distortions, and that the water peak is well suppressed. On Figure 62 d), the volume of a selection of peaks in the ufCOSY spectrum is shown, as a function of repetition number, concatenated for three different flow rates. It can be seen that the average peak

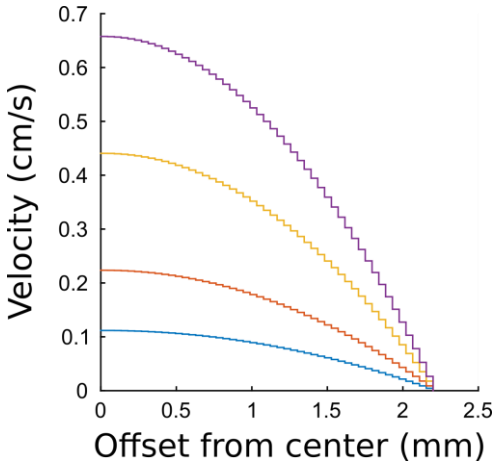

Figure 60: Velocity profile as a function of the offset from the center of the tube for flow rates of 0.5 (blue), 1 (red), 2 (yellow) and 3 mL/min (purple).

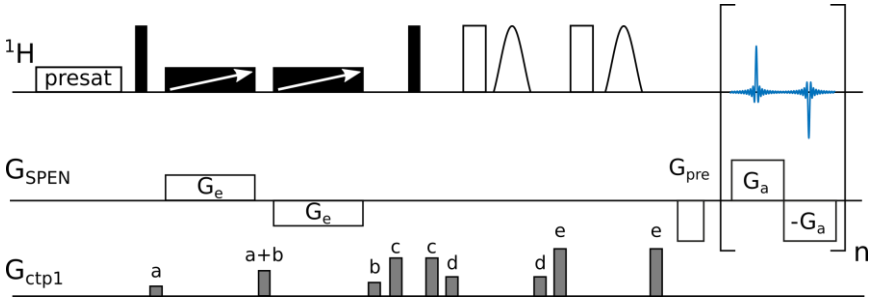

Figure 61: Pulse sequence for ufCOSY with excitation sculpting. Black filled rectangles correspond to 90° pulses and empty ones correspond to 180° hard pulses. Black filled rectangles with arrows correspond to the 180° adiabatic chirp pulses. All pulses have the same phase. For convenience, CTP and SPEN gradients are displayed on different lines. They may be applied on orthogonal axes. Shaped pulses correspond to soft 180° pulses used for excitation sculpting (2 ms trapezoidal pulses).

integral decreases when the flow rate increases. Moreover, the peak integrals display important variations that can go up to 70 % of their initial value. These two phenomena seem to be linked to the peak's chemical shift in the spatial dimension. Peaks with high chemical shift in the spatial dimension are highly affected while peak with low spatial chemical shift are much less affected.

In order to understand where this phenomenon could come from, a series of ufCOSY were done, with several encoding parameters. First, a series of experiments was repeated with the same conditions

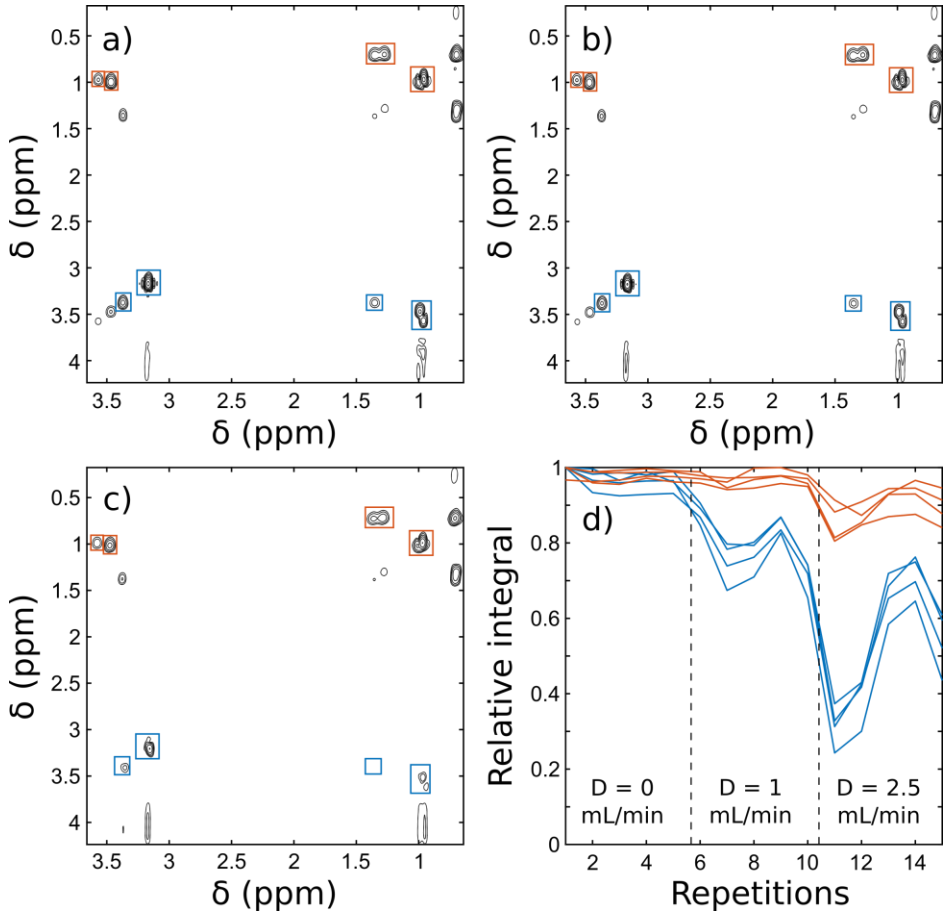

Figure 62: ufCOSY spectra obtained of the alcohols mixture with a flow rate of 0 (a), 1 (b), and 2.5 mL/min (c). Evolution of selected peak integral as a function of the repetition concatenated for three flow rate (d). Colored squares correspond to the integral regions.

to have a confirmation of the previous results and to have a reference. Then a second one was done in which the sign of the acquisition and prephasing gradient were changed. In the third series of experiments, it was the sign of the encoding gradient that was changed. Finally, a series of experiments was done in which the chirp pulse was sweeping from low to high frequency, contrary to all previous experiments that were using a chirp pulse that was sweeping from high to low frequency. Two ethanol peaks were selected, one with different chemical shift in the spatial dimension. The series of experiments were obtained with different flow rates and the selected peak intensity was monitored. The results are displayed in the Figure 63.

For the three first set of experiments that consisted in changing gradient signs, the results are always the same. On the series of experiments on which the chirp sweeping way was modified, the behavior of the peaks changes. In this case, it is the peaks that have a low chemical shift that suffer from high integral variations and losses. The previous experiment was done on only two peaks. In order to confirm the results, the average integral of all peaks was monitored. On Figure 64 are presented the average peaks integral over the 5 experiments at 2.5 mL/min compared to the initial integral without flow as a function of their chemical shifts in the indirect dimension. The y value of each point corresponds to the peak average integral while the error bar corresponds to the standard deviation the values used for the averaging.

This result confirms what was seen earlier: the integral variations and losses are linked to the chemical shift in the spatial dimension and to the way the chirp sweeps in frequency. The ways the chirp sweep in space do not seem to have any importance as changing the encoding gradient sign do not have any effect.

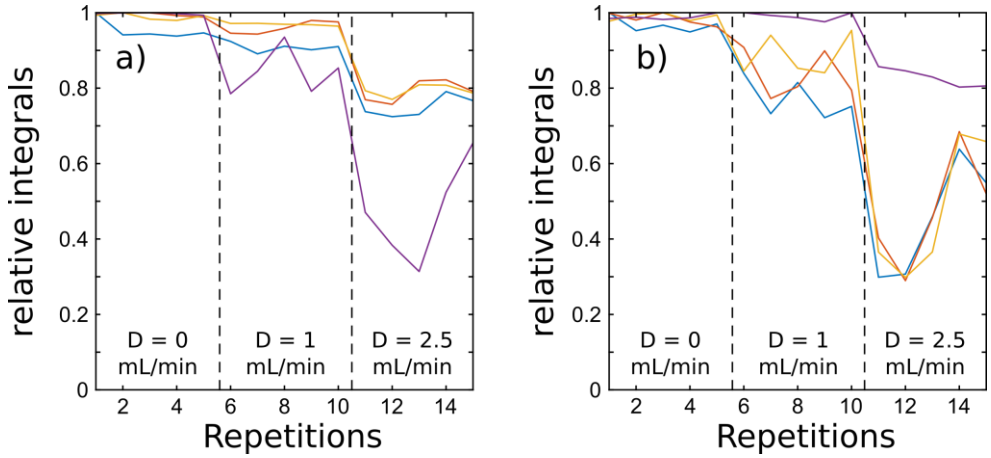

Figure 63: Evolution of two ethanol peak integrals with low (a) and high (b) chemical shift in the spatial dimension. Blue lines correspond to the reference (same conditions than the Figure 62), red correspond to the experiment with the prephasing and acquisition gradient with an opposite sign, yellow correspond to the experiment with the encoding gradient with an opposite sign and the purple lines correspond to the experiments where the chirp pulse was sweeping from low to high field.

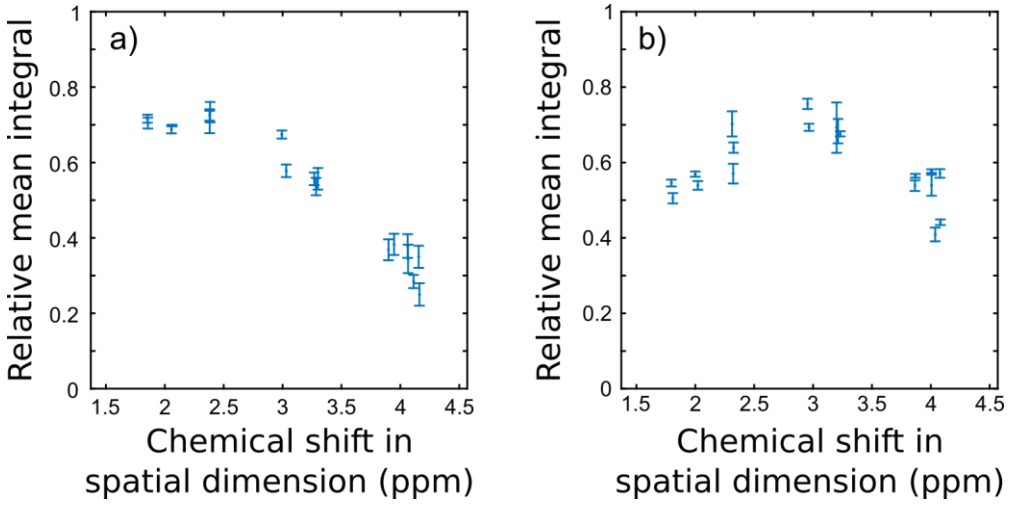

Figure 64: Average peak integral and standard deviation for all peaks of the ufCOSY spectra recorded at 2.5 mL/min with chirp sweeping from high to low (a) or low to high (b) frequencies. Peaks y values correspond to the average and error bars correspond to the standard deviation.

This phenomenon of peak integral that vary depending on the chemical shift can be a real problem for reaction monitoring as signal integral would not reflect the evolution of compounds concentration.

We wanted to know if other approaches to spatial encoding would avoid the chemical shift dependency, and the spatial encoding block shown in Figure 65 was tested.[118,160] It still consists in a pair of frequency sweeping chirp pulses applied with encoding gradient. The two differences compared to the previous spatial encoding block are (i) the two chirp pulses are separated by a hard 180° pulse and (ii) chirp pulses sweep in opposite ways.

As it was done for the first spatial encoding block, series of experiments were acquired at different flow rates and the integral of several peaks with different spatial chemical shifts were monitored. Resulting curves are displayed in the Figure 66.

With this second spatial encoding block, the variations are very similar for all selected peaks. There are still important variations and the frequency seem to be different from what was obtained with the first spatial encoding.

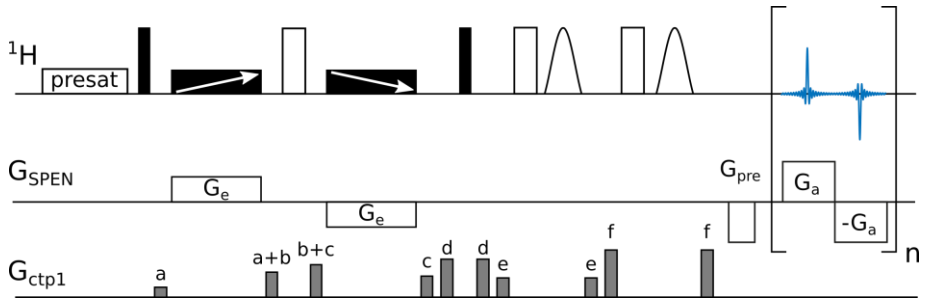

Figure 65: Pulse sequence for ufCOSY using the "alternative" spatial encoding block with excitation sculpting and presaturation.

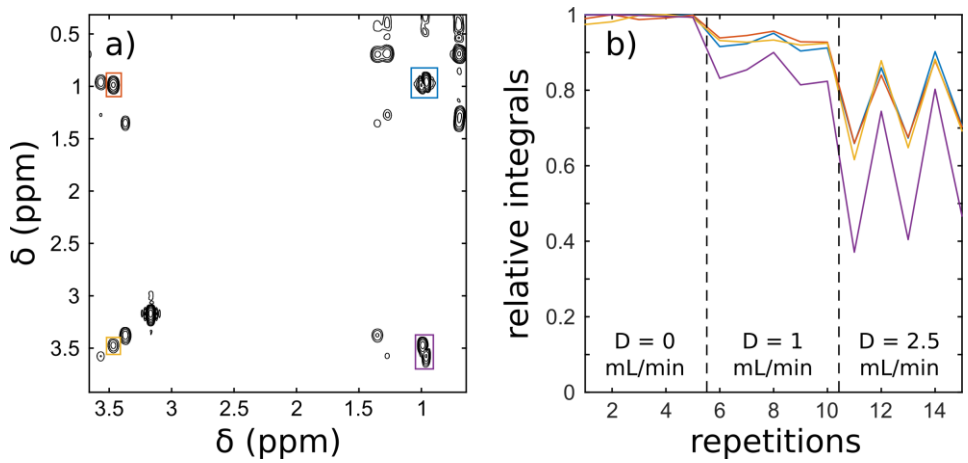

Figure 66: ufCOSY spectrum obtained with the "alternative" spatial ending block shown in Figure 65 a) and relative integral of 4 peaks as a function repetitions and flow rate.

It is worth noting here that the pattern that is seen is a stroboscopic effect. From the results obtained with 1D imaging experiments, the velocity variation has a frequency of about 2.2 Hz at 3 mL/min. It was possible to observe it with fast imaging acquisition: the repetition time for these experiments was 55 ms. With ultrafast 2D NMR experiments, in order to preserve the probe and gradient amplifier, it is not possible to repeat acquisition this fast. Hence, as the frequency of the acquisition (one every 15 seconds) is lower than the velocity variations frequency, the monitoring of peaks integral results in stroboscopic effect. As the duration of the pulse sequence using the second spatial encoding is different from the one using the first encoding block, the apparent frequency of the integral losses is different. The relaxation delay of the pulse sequence could have been optimized so that the two pulse sequences would have the exact duration. This, in combination with a good management of the stroboscopic effect, could lead to acquiring the ultrafast experiments when the losses would have been minimum. However, the connection between the pump and the NMR console could not be used to trigger the acquisition as it can be done for hyperpolarization for example, limiting the potential of this method. Moreover, it would necessitate to have a very precise value for the velocity variations frequency for each flow rate. Unfortunately, 1D imaging did not provide precise enough values.

The previous series of experiments showed a uniform loss for the selected peaks. However, there are no peaks on the ufCOSY spectrum near the center, all the peaks are at the edges. To confirm the previous results, two series of experiments were done on another sample. The selected sample was the same mixture of alcohols in which a small amount of acetone was added so its concentration is about 200 mM. The same experiments were done with both spatial encoding blocks at different flow rates and several peak integrals were monitored. The resulting curves are displayed in the Figure 67. Several phenomena can be observed on these curves. First, there is still an integral loss on average when the flow rate increases for all peaks. However, the fluctuations almost completely disappeared. One explanation would be that adding acetone in the solution modified slightly its viscosity or compressibility, hence changing the solution's response to the pump's oscillations.

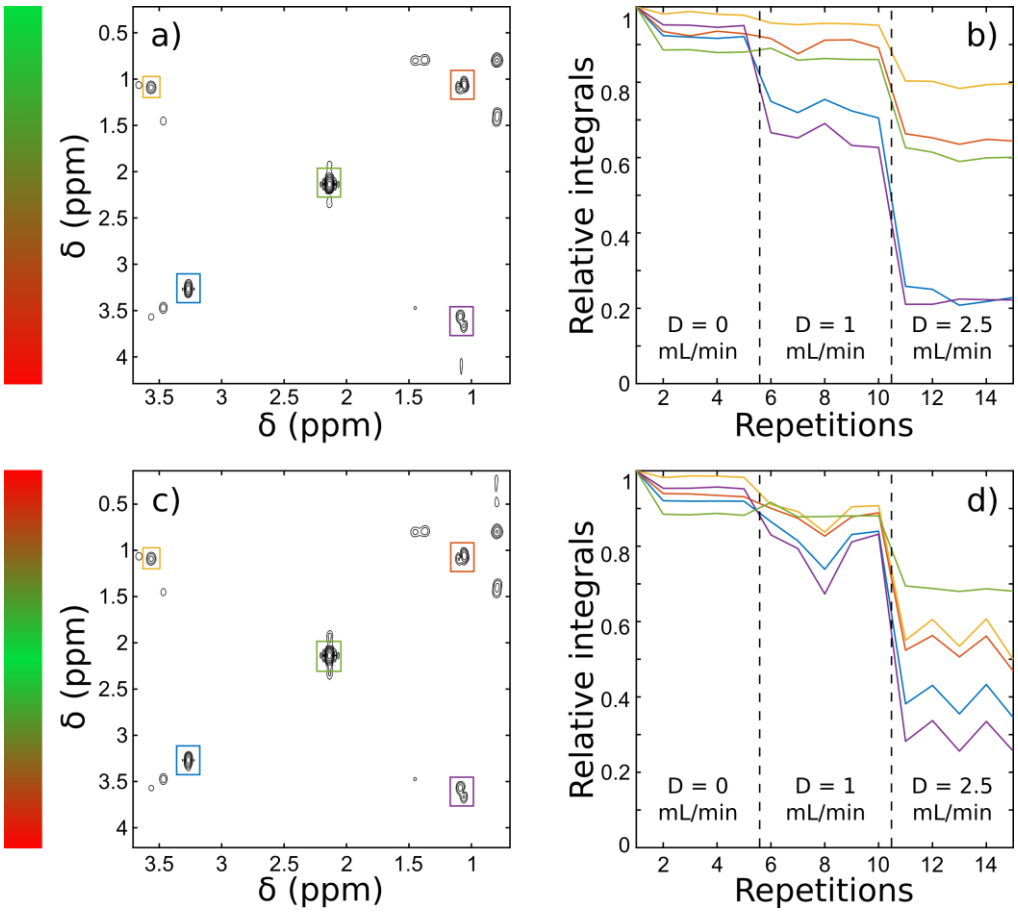

Figure 67: Ultrafast COSY spectra of unreacting mixture 2 with the classical (a) and the alternative (c) spatial encoding block and monitoring of several peak integral as a function of repetition concatenated for three flow rates for classical (b) and alternative (d) spatial encoding block. The red and green bars symbolize which peaks are affected by integrals losses.

The link between integral losses and chemical shift in the spatial dimension is confirmed. For the classical spatial encoding block, the previous result is also confirmed: peaks with a high spatial chemical shift suffer more intense integral losses than peaks with low spatial chemical shift. For the alternative spatial encoding block though, it is clear that the integral losses are not homogeneous for all peaks. In this case the peak that display the smallest losses is the acetone peak that is in the center of the spectrum, while peaks at the edges are more affected.

In order to have a more complete description of how peaks integrals are affected by the interaction between spatial encoding and flow, it was decided to do the same experiment on a last sample with more peaks more evenly distributed in the observed spatial chemical shift range. The sample chosen was the same mixture of alcohols that previously, but in acetonitrile in order to makes the OH signals appear. The choice of sample leads to the need of changing the solvent suppression method. Indeed, excitation sculpting is not selective enough to suppress only the acetonitrile peak and not others. Moreover, a ^{13}C decoupling had to be added in order to suppress satellites peaks of acetonitrile. The chosen method was the WET method. The resulting pulse sequences for both spatial encoding blocks are displayed in the Figure 68.

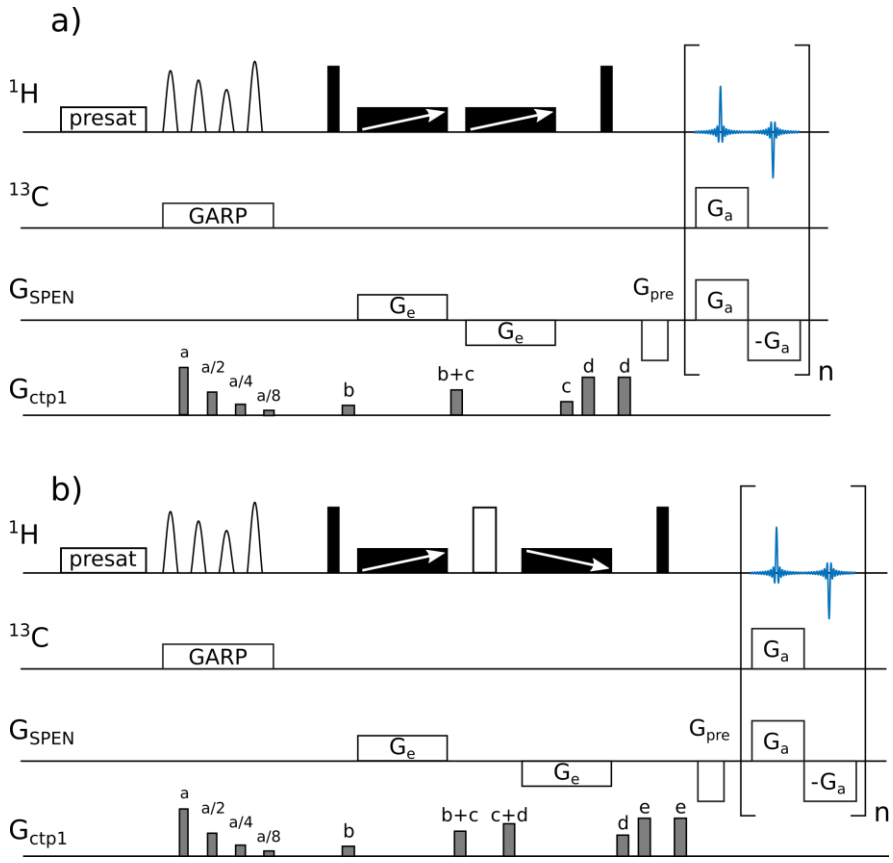

Figure 68: Ultrafast COSY pulse sequence for first (a) and second (b) spatial encoding block including WET solvent suppression method and ^{13}C decoupling.

Once again, the series of experiment were done at several flow rates with these pulse sequences and several peak integrals were monitored. Resulting curves are displayed in the Figure 69. In addition, this time, the average loss experienced by every peak was measured, and is reported in the Figure 69 as a function of their chemical shift in the spatial dimension.

Once again, the previous results are confirmed; depending of the spatial encoding block used, there are discriminations in integrals losses according to the spatial chemical shift of the observed peak.

In order to see if these losses of intensity could be predicted, simulations were made using Spinach. First, a set of ufCOSY spectra were simulated with mean fluid velocity from 0 to 1 cm/s with the two spatial encoding blocks. The velocity profile was then used. Another schematic representation of the velocity profile under the form of the cross section is shown on Figure 70. Of course, in the tube the velocity evolution is continuous, but for calculations, discretization had to be done.

The circulation of the fluid in the Flowtube can be schematically represented as an ensemble of hollow cylinders in which the fluid circulates at different velocities. The simulations that were mentioned earlier were assuming the fluid velocity was the same everywhere. In order to have a more realistic approximation of the spectrum that would be obtained, composite spectra were calculated for

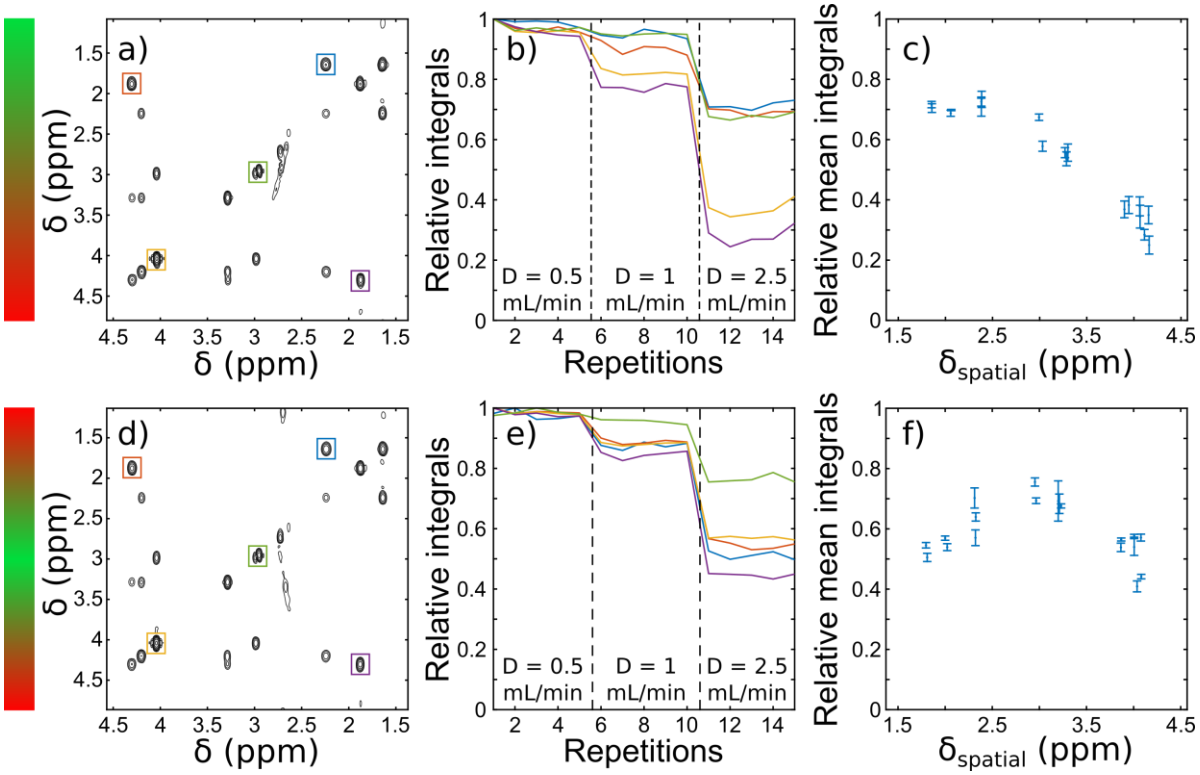

Figure 69: Ultrafast COSY spectra obtained with the first (a) and second (d) spatial encoding block on unreacting mixture 3. Relative integral for five peaks as a function of the repetition for three flow rates obtained for the series with the first (b) and the second (e) spatial encoding block. Relative integrals at 2.5 mL/min compared to integrals at 0.5 mL/min for every peaks of the spectrum as a function of their chemical shift in spatial dimension for spectra obtained with the first (c) and second (f) spatial encoding block.

each mean velocity using the following formula:

$$sp_{final} = \sum_{i=v_{min}}^{i=v_{max}} \frac{sp(i) \times S_{cylinder}(i)}{S_{tube}}, \tag{4.1}$$

where sp(i) if the spectrum associated to the velocity i, $S_{cylinder}$ is the surface of a cross section of a hollow cylinder for a fluid velocity and S_{tube} is the total surface of the cross section of the tube. An example of one of these composite spectra is displayed in Figure 71 a). The integrals of four peaks was monitored as a function of the mean velocity and were plotted on Figure 71 b) and c).

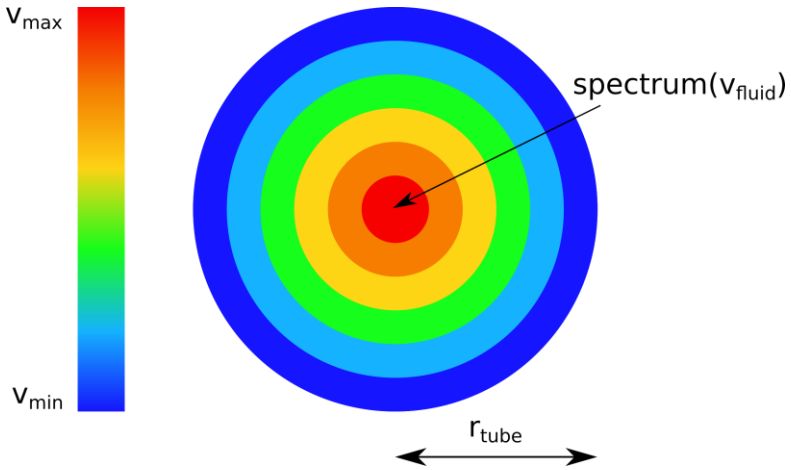

Figure 70: Cross section of a tube in which a fluid circulates. Each color corresponds to a velocity calculated previously (see Figure 60) and to each velocity corresponds a simulated spectrum.

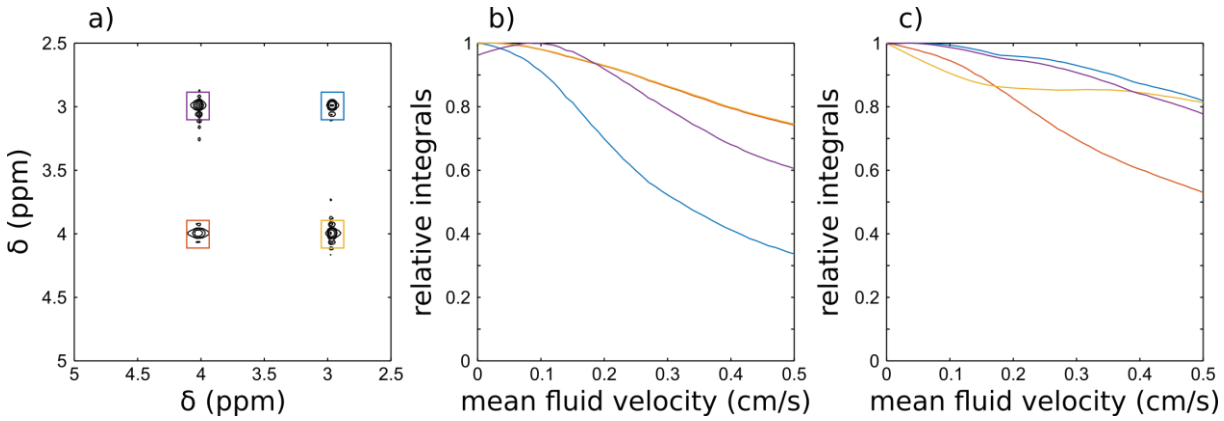

Figure 71: Example of a simulated spectrum after correction (a) and evolution of peak integral as a function the mean velocity for standard (b) and alternative (c) spatial encoding blocks.

With both of the spatial encoding blocks, peak integral losses can be observed when the velocity of the fluid increases and as for the experimental values, it seems that there is a link between losses and chemical shift in the spatial dimension. However, the evolution differs from the experiments. Indeed, in the simulations, peaks with the same chemical shift in the indirect dimension do not always have the same evolution in contrary to what is experimentally observed.

This phenomenon was until now never observed nor characterized. Few examples of ultrafast experiments on flowing samples have been reported in the literature. Two of them were using NMR as a detector after a chromatographic separation, either with a homemade column[126] in combination with an HPLC system.[127] In the first case, a system using compressed air was used to make the fluid circulate through the column leading to a pulse-free flow, in the second case, the flow was much lower that we used and, in both cases, they were using signal averaging, that was smoothing the variations. Another example of ultrafast experiments under flowing conditions for reaction monitoring have been reported at low field.[132] However, on low field benchtop spectrometers, the gradient is orthogonal to the flow, so the phenomenon described earlier was not observed.

4.5.1.2 Double spatial encoding block

The use of a single spatial encoding block has shown to produce discrimination of peaks as a function of their spatial chemical shift. We wondered if using a double spatial encoding block could cancel this discrimination. In the previous pulse programs, single spatial encoding has been replaced with double blocks. To do so, chirp pulses for single blocks have been replaced with chirp pulses twice shorter but with the same bandwidth. For the classical spatial encoding block, using twice the same encoding block works well. However, for the alternative spatial encoding block there are an additional 180° hard pulse, so the second block have to be the opposite of the first one in order to avoid cancelling the encoding made by the first block. The resulting pulse sequences are displayed in the Figure 72. This time, only a series of experiments were done at 2.5 mL/min in order to observe the discrimination of peak integral as a function of their spatial chemical shift. Two peaks were selected,

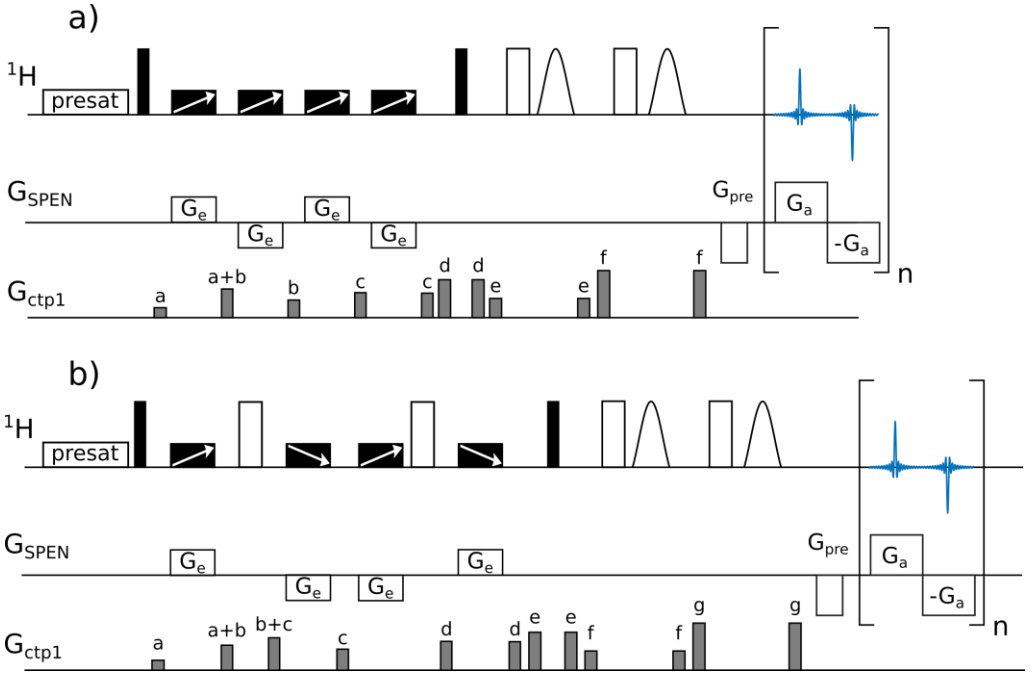

Figure 72: Ultrafast COSY pulse sequence using double classical (a) or alternative (b) spatial encoding blocks.

one with a high spatial chemical shift and one with a low one. Their integrals were monitored and displayed on Figure 73.

The previous results are once again confirmed. With the double classical spatial encoding block, the peaks with high spatial chemical shift suffer lower integral losses while the other peaks suffer higher losses.

It was shown that using one spatial encoding block led to heterogeneous losses. With two shorter spatial encoding blocks, it was shown that the losses were slightly more homogeneous. One could wonder if continuing to add shorter and shorter SPEN blocks could lead to completely homogeneous losses. However, at one point, the condition for successive excitation ($BW_{chirp} \times D_{chirp} > 50$)[161] would not be fulfilled anymore.

4.5.2 Spatial encoding along a transversal axis

It was seen with imaging experiments that the velocity variation had much less effect on the images when the observed axis was transversal to the flow. We wondered if the same would apply to chemical-shift spatial encoding.

As previously, series of experiments with two samples (alcohols mixtures in water and in acetonitrile) were done with spatial encoding along X-axis at several flow rates, and relative integrals were monitored for different peaks. The results obtained with the classical spatial encoding block are displayed in Figure 74.

The first noticeable thing is that when spatial encoding is done along a transversal axis, the resolution in the spatial dimension drops. There are two reason for this. First, the length of the tube is higher in the Z-direction than in the X direction. Second, on triple-axis gradient probes, the maximum gradient intensity along the X and Y-axes is lower than that along the Z-axis. Usually these values are

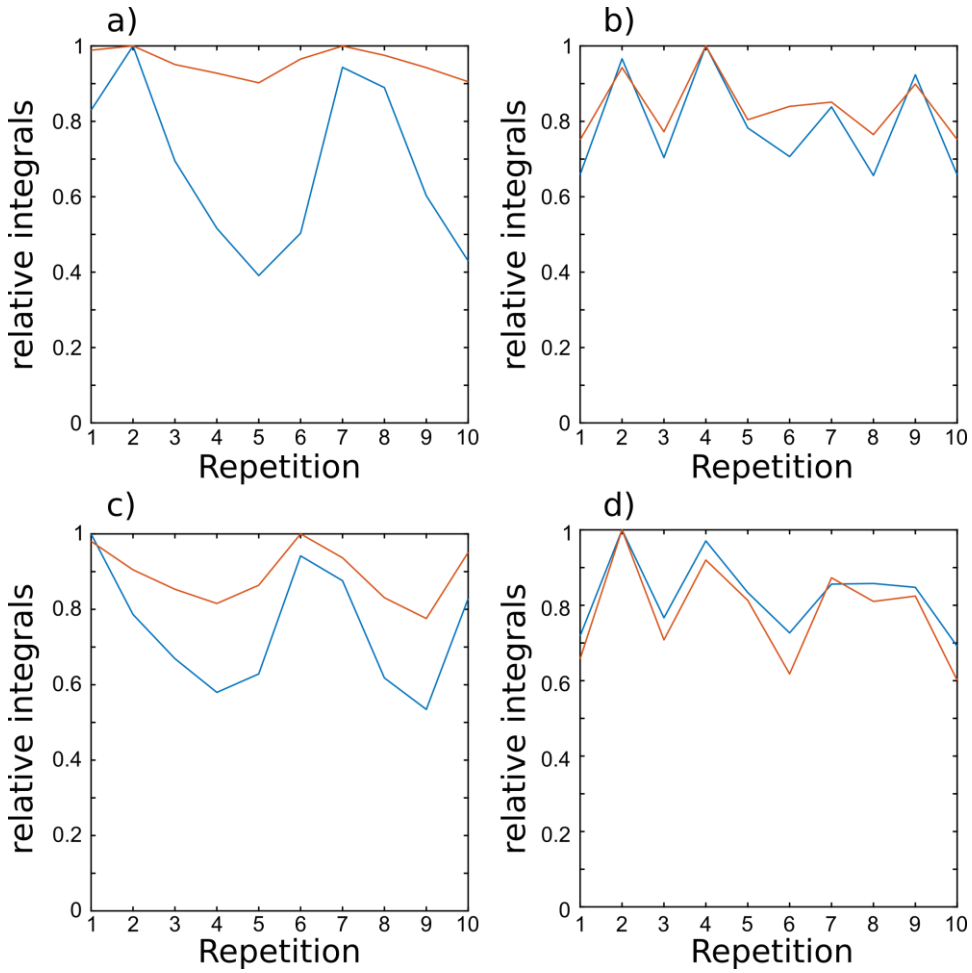

Figure 73: Relative integral of ethanol peaks that have high (blue) and low (red) spatial chemical shift. The integrals correspond to data obtained with single (a) and double (c) classical encoding block or single (b) and double (d) alternative spatial encoding block.

respectively around 50 and 65 G/cm for X/Y and Z axis. Hence, the number of "virtual" slices is lower, leading to a loss of resolution.

The integral losses observed with transverse encoding are very different from those observed with longitudinal encoding. In both aqueous and organic solutions, the average loss is smaller than when spatial encoding is done along the Z-axis. Moreover, the losses seem to be the same for all peaks, and there is no more any discrimination of peaks as a function of their spatial chemical shift.

This solution seems to be an interesting alternative to the spatial encoding along Z-gradient for reaction monitoring as it provides peaks whose evolution would only reflect the evolution in concentration of the compounds (if the parameters are kept identical). However, in order to work well, it was found that the spatial encoding along transversal conditions requires that the gradients for coherence selection pathways are set also along a transversal axis. Series of experiments have been done with increasing flow rate. For the first series, the CTP gradients around the chirp pulses were set along the Z-axis, while for the second series, they were set along the Y-axis in order to be orthogonal to the flow and to the spatial encoding. Then, as previously the relative integrals of several peaks were monitored. The curves are displayed in Figure 75.

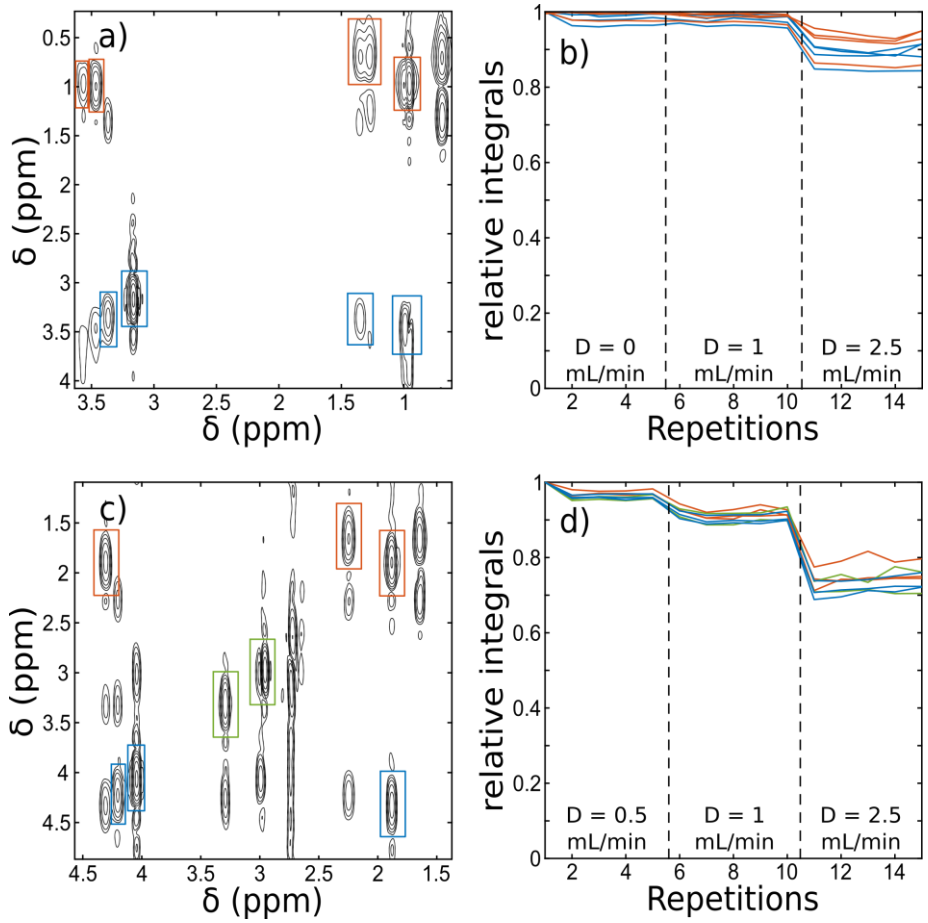

Figure 74: Ultrafast COSY spectra with a spatial encoding along the X-axis of alcohols mixture in water (a) and acetonitrile (c) and relative integral of selected peaks for both cases (b and d).

When the CTP gradient around the chirp pulses are set along Z-axis, it leads to dramatic loss in integral when the flow rate increases. Note that it is not limited to chirp pulses, this is also true for other CTP gradients such as the ones used for excitation sculpting. If they are set along the Z axis, the solvent suppression is less effective and can vary from one acquisition to another. The effect is more marked for chirp pulses as the delay between the dephasing and rephasing is longer, due to the longer duration of chirp pulses, that for excitation sculpting that uses here 2 ms long pulses.

4.6 Case study of reaction monitoring

4.6.1 Saponification reaction

In order to validate that spatial encoding can be used for reaction monitoring under flow conditions it was decided to use a well-known reaction. Moreover, as, at that moment, the ductless fume hood was not installed yet, the reaction had to be done in non-toxic conditions. Hence, it was decided to study the reaction of ethyl acetate saponification as shown in Scheme 3.

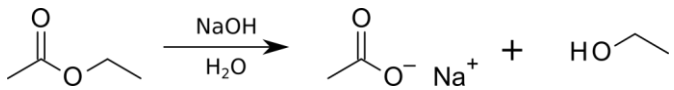

Scheme 3: Saponification reaction of ethyl acetate.

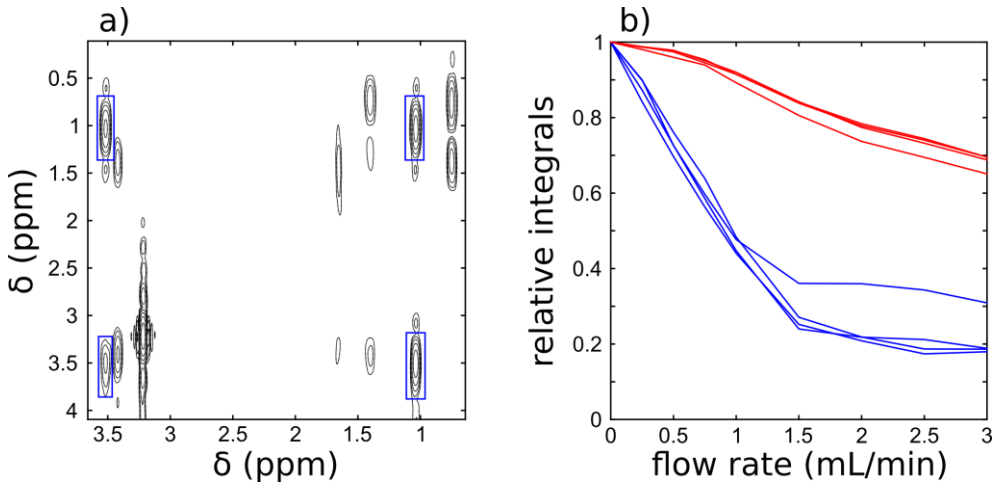

Figure 75: Ultrafast COSY spectrum (a) and relative peak integral as a function of the flow rate. Blue lines correspond to the series of experiments that were done with CTP gradient along Z-axis and red one correspond to the series with the CTP gradients along Y-axis.

First, the reaction was done circulating a solution of NaOH in the flowtube and adding ethyl acetate after launching a series of acquisition. In order to compare longitudinal and transversal spatial encoding, ultrafast experiment with Z-axis and X-axis encoding were interlaced. Example of spectra

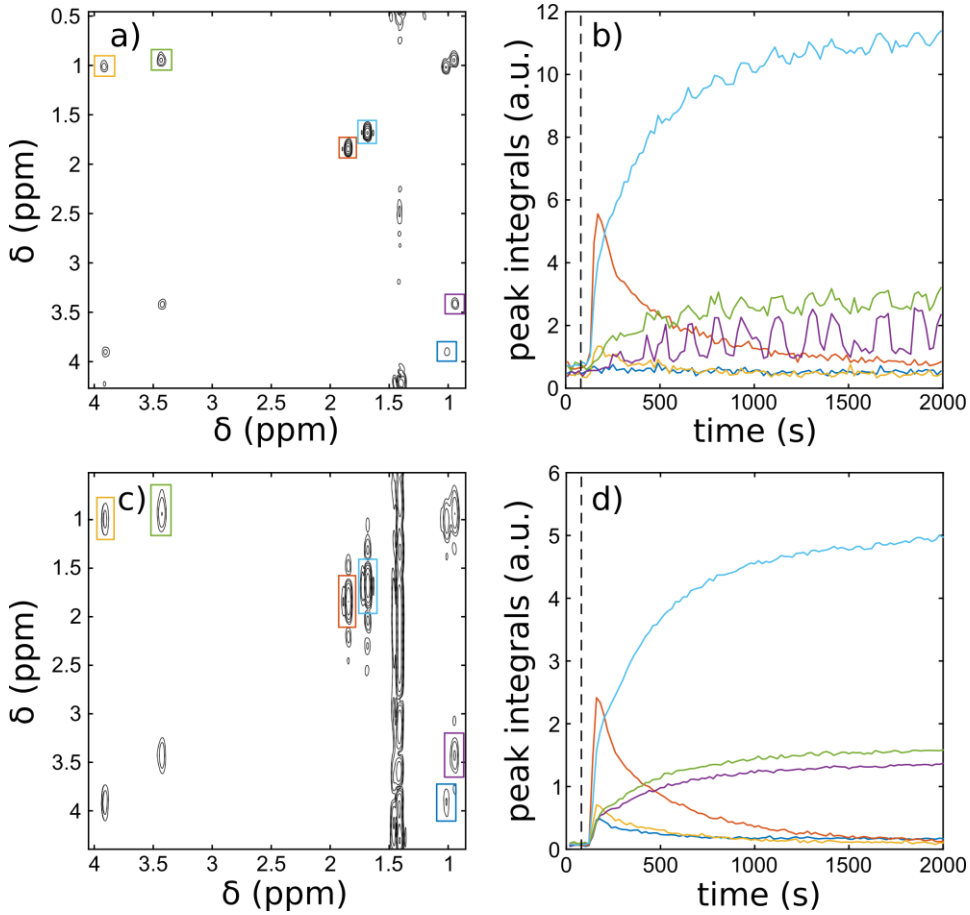

Figure 76: UFCOSY spectra with Z-axis (a) and X-axis (c) encoding and evolution of the peak integral for selected signals (b and d) during a saponification reaction (ethyl acetate: red, yellow and blue; acetic acid: cyan; and ethanol: green and purple). UFCOSY spectra were recorded every 10 s, alternating X and Z-spatial encoding. The dashed line indicates when ethyl acetate was introduced into the reaction mixture.

obtained during the course of the reaction can be seen in the Figure 76 a) and c). In both case, good quality data are obtained.

The integrals of several signals were monitored all along the course of the reaction. The delay between the introduction of ethyl acetate, shown by the dashed line, and the apparition of the signal corresponds to the 'dead time' that the reaction mixture takes to reach the flowtube. In these conditions it is about 1 min 40 second. The evolution of peak integrals is displayed in Figure 76 b and d. In both cases the trend of the curves is the same. However, the curves obtained with spectra done with spatial encoding along Z-axis are much noisier, and two signals of the reactant are almost not visible.

Then, in order to see if kinetic information could be extracted from reaction monitored by ultrafast experiment, ethyl acetate saponification monitoring was reiterated at several temperatures. In order to be able to extract kinetic information, the initial ethyl acetate integral is needed. Hence, the order of introduction of reactant was changed. This way, the integral of ethyl acetate signal can be used for kinetic calculations. The saponification of ethyl acetate is known to be a reaction of order 2. In order to evaluate the kinetics of the reaction, the saponifications were done with equal quantities of ethyl acetate and NaOH, so that [AcOEt] = [NaOH]. Then the decay of the concentration of ethyl acetate can be fitted to the equation:

$$\frac{1}{[AcOEt](t)} = at + b, \tag{4.2}$$

where t is the reaction time. The reaction rate constant is then equal to a. Peak volumes can be converted to concentrations by using the known initial concentration of ethyl acetate:

$$[AcOEt](t) = [AcOEt]_0 \frac{I(t)}{I_0}, \tag{4.3}$$

where I(t) is the peak volume at time t, I_0 is the peak volume before the reaction starts, and $[AcOEt]_0$ is the initial concentration in ethyl acetate.

For kinetic measurement, the acetate solution was initially fed to the flowtube and the NaOH solution was then added. Moreover, instead of interleaving Z and X-axis encoding experiments, 1D ^{1}H experiments were interleaved with X-axis spatially encoded experiments. Reactions were done at 25, 35 and 45°C. Examples of 1D ^{1}H and ufCOSY spectra with spatial encoding on X-axis and evolution of integrals as function of time at the three temperature are displayed on Figure 77 and Figure 78.

Then, the integrals of ethyl acetate CH_3(CO) signal for 1D ^{1}H and ufCOSY, plotted in the Figure 79, were used in order to calculate the kinetics of the reaction. The evolution of the ratio $\frac{I}{I_0}$ and $\frac{I_0}{I}$ were plotted, and fitting of the latter curve allowed to calculate the rate of the reaction. The results obtained with 1D ^{1}H and with ufCOSY are displayed and compared in Table 7 for the three temperatures. For the three cases, the results obtained with the two methods are very similar. The differences may be explained by the fact that at 25°C and 45°C there are small variations of the initial integral in ufCOSY

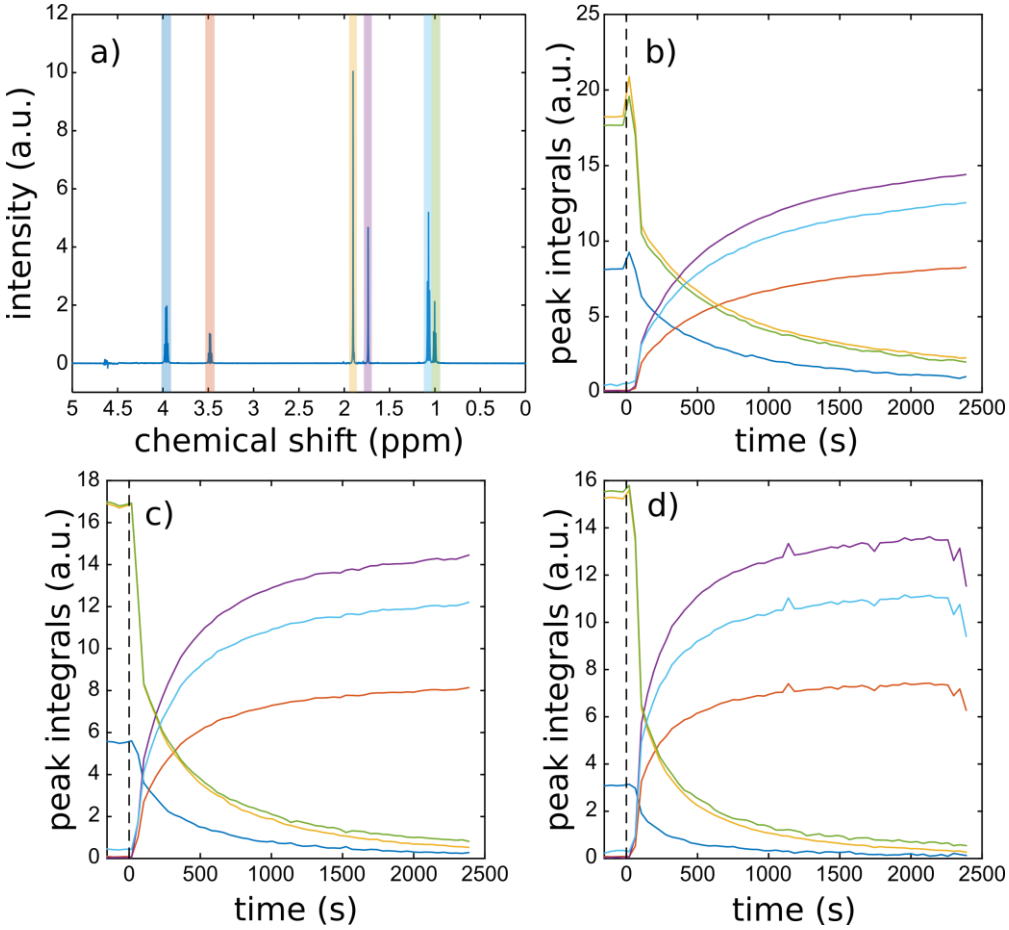

Figure 77: Example of 1D ^{1}H spectrum during the course of the reaction (a) and evolution of selected peak integrals as a function of reaction time for reaction temperature of 25 (b), 35 (c) and 45°C (d). Dashed lines correspond to the moment of the NaOH solution was introduced.

spectra. The signals stay the same for the four first experiments, and just after the addition of NaOH, they increase. This phenomenon is unexplained for now.

These results show that spatially encoded experiments can be used in order to monitor chemical reactions under flow conditions.

4.6.2 Other reactions

After the saponification reaction, other reactions were tested. As the ductless fume hood was not ready at that time, the reactions had to be non-dangerous and had to be doable in a non-toxic solvent. The chosen solvent was acetonitrile because of its harmlessness and because it has only one ^{1}H signal to suppress. We chose to observe the reaction of benzaldehyde that leads to a reduction of the aldehyde function that will produce a noticeable change in the aromatic signals.

The first reaction that was tested was the aldolization of propanal by benzaldehyde as shown in Scheme 4. Both reactants, propanal and benzaldehyde, are not toxic by inhalation allowing their use with only individual protection equipment. Propanal is harmful and will be always be manipulated in small quantities (< 1 mL). Moreover, as benzaldehyde does not have only enolysable proton, only one product should be produced. The reaction can be done in highly basic or acidic conditions. Usually for basic conditions, an alcoolate such as methanolate is used. However, it could not be used in this case

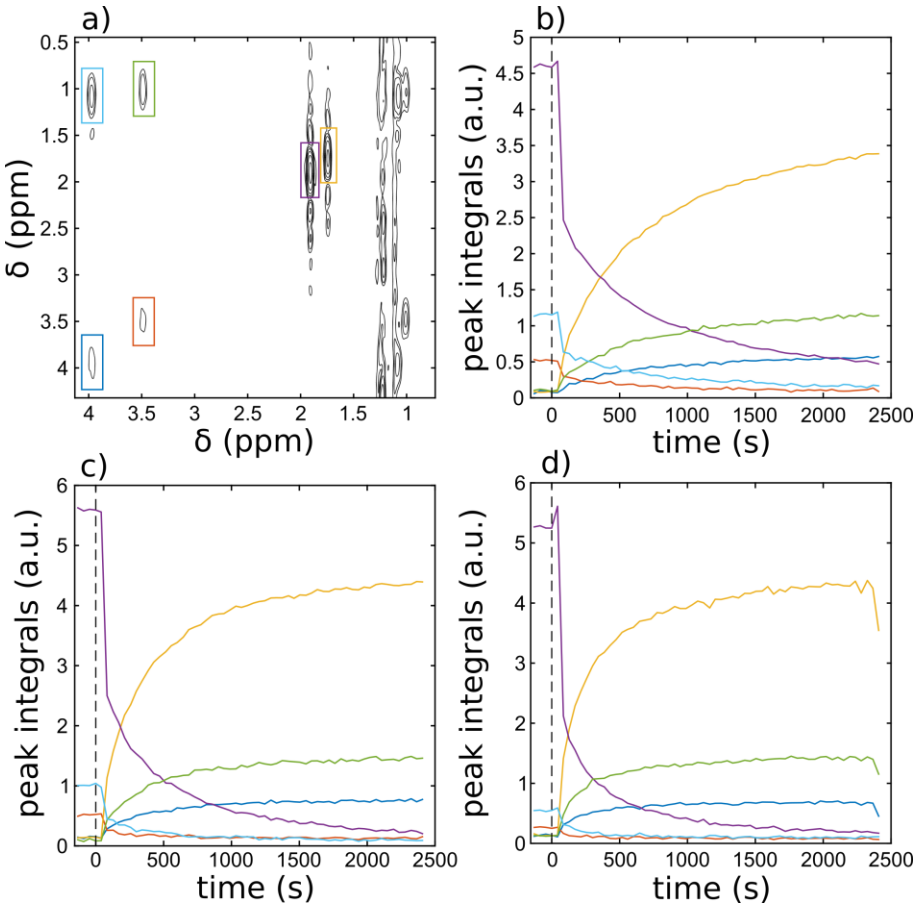

Figure 78: Example of ufCOSY spectrum with spatial encoding on X-axis during the course of the reaction (a) and evolution of selected peak integrals as a function of reaction time for reaction temperature of 25 (b), 35 (c) and 45°C (d). Dashed lines correspond to the moment of the NaOH solution was introduced.

because it would damage the pump, hence mild acidic conditions were used with trifluoroacetic acid (TFA).

A solution of benzaldehyde with TFA in acetonitrile was fed to the flowtube, and propanal was then added. Unfortunately, no sign of reaction was observed. It is probably due to the too mild acidic condition.

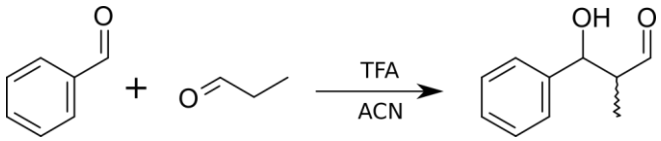

Scheme 4: Aldolisation of propanal by benzaldehyde in presence of trifluoroacetic acid in acetonitrile.

The second reaction that we wanted to observe was the Cannizzaro reaction of benzaldehyde shown on Scheme 5. It is a dismutation of cetone or aldehyde that do not have enolisable proton. The reaction is usually done in presence of base such as NaOH or KOH. As previously, a solution of benzaldehyde was fed to the flowtube, and the solution of NaOH was then added. However, a precipitation quickly appeared, so the pump was stopped to avoid damaging it or blocking the capillary. The precipitation actually corresponds to the oxidation of acetonitrile by NaOH if water is

Table 7: Reaction rates determined by fitting the data shown in Figure 79, obtained with 1D ^{1}H NMR experiments and UFCOSY for saponification at 25°C, 35°C and 45°C.

Experiment	k at 25°C (L.mol^{-1}.s^{-1})	k at 35°C (L.mol^{-1}.s^{-1})	k at 45°C (L.mol^{-1}.s^{-1})
1D ^{1}H NMR	0.11	0.28	0.47
ufCOSY	0.13	0.30	0.48

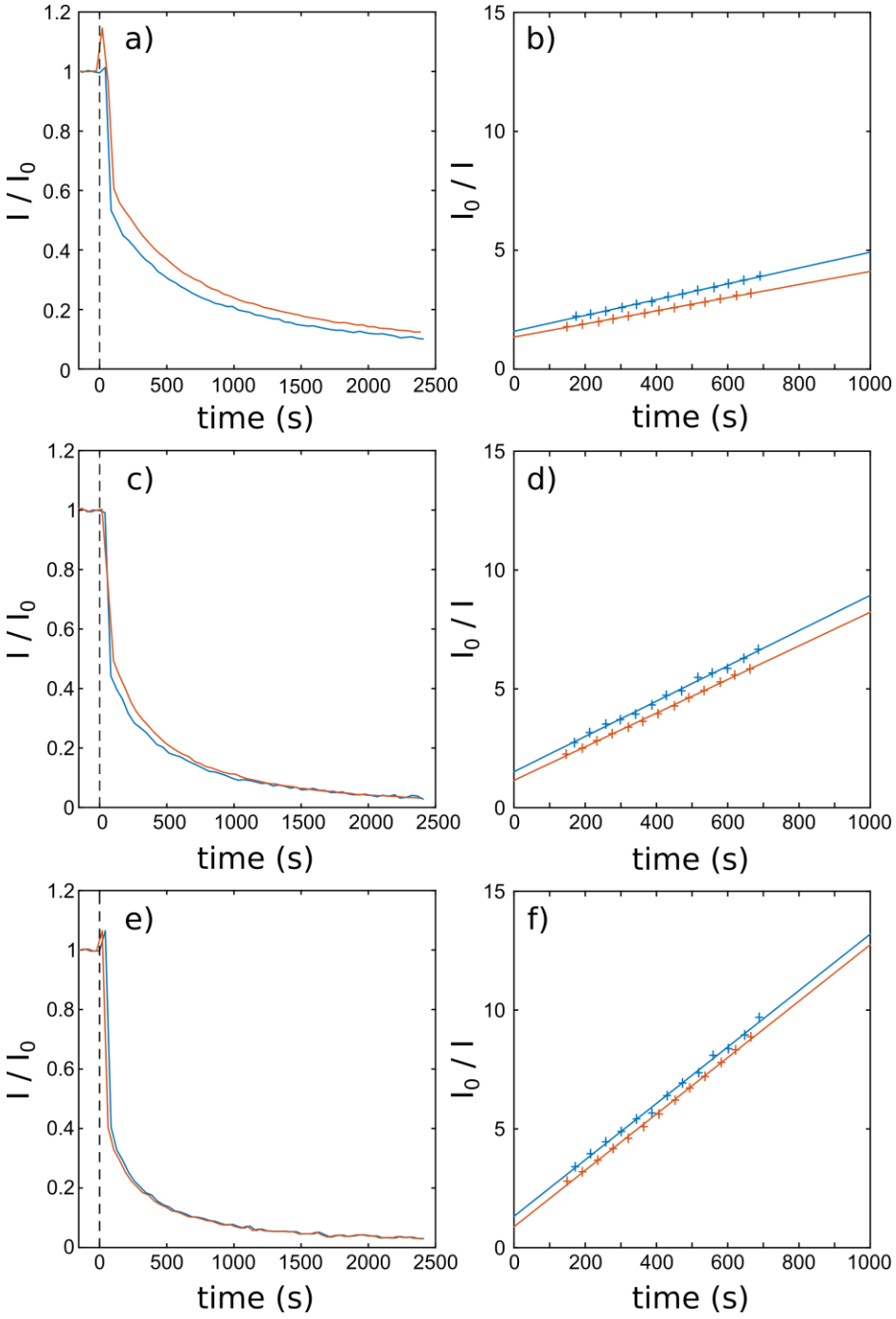

Figure 79: (a, c, e) Evolution of ethyl acetate $CH_3(CO)$ peak integral as a function of time for saponification at 25°C (a), 35°C(c) and 45°C (e). Blue lines correspond to results obtained with UF experiments and red lines correspond to results obtained with 1D ^{1}H experiments. (b, d, f) Fit of the data for times between 150 and 700 s. Blue crosses and lines respectively corresponds to the experimental values and to the fit of results obtained with UF results and red crosses and lines correspond to the experimental values and to the fit of results obtained with 1D ^{1}H experiments

present (solvent of the added NaOH solution) that can lead to the formation of sodium acetate, that is not soluble in acetonitrile.

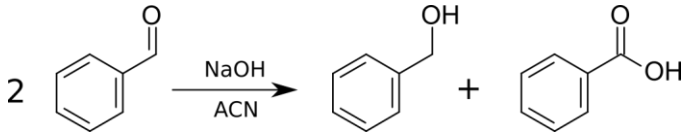

Scheme 5: Cannizzaro reaction of benzaldehyde.

The last reaction tested was an amination of benzaldehyde followed by a cyclisation as shown on Scheme 6. The reaction is done on acidic conditions. However, when the reaction was done, a precipitation occurred. It is supposed that the amine protonates and is not soluble anymore. One solution would be to add the acid of the amine slowly using a pouring bulb, but (i) kinetic information would be difficult to extract and (ii) the setup would not be feasible at this time.

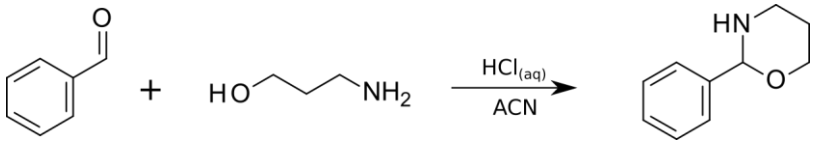

Scheme 6: Imination reaction of benzaldehyde followed by cyclisation.

Unfortunately, none of the reactions contemplated led to exploitable results. However, now that the ductless fume hood has been installed, it will possible to study reaction in solvent that can only be handled under a fume hood.

4.7 Preliminary results with diffusion experiments

Spatial encoding of diffusion could also be useful for reaction monitoring to see the evolution of diffusion coefficients of reactants and products all along the reactions. It could also provide information on the binding of reactants with catalysts, for example.

Diffusion experiments encode Brownian motion using pulsed-field gradients, as explained in section 2.2. Standard DOSY experiments work well when the sample is completely still. Moreover, it was demonstrated that convection, which would lead to artifact in standard experiments, can be compensated thanks to the use of a double stimulated echo. In the case of the flow tube, the situation is different as it is a flow and not convection. First, we wanted to see if conventional DOSY experiments, with and without convention compensation, could give good results on a flowing sample. Conventional STE and DSTE experiments were done on a flowing sample of alcohols flowing with a flow rate of 1 mL /min. For reference, the experiments were also done without flow. Calculated diffusion coefficient for STE and DSTE for diffusion along Z, X and Y-axis are displayed on Table 8 and Table 9.

Table 8: Diffusion coefficient obtained with conventional STE experiments with and without flow

	$D.10^{10}$ ($m^2.s^{-1}$) without flow			$D.10^{10}$ ($m^2.s^{-1}$) flow rate = 1 mL/min		
Axis	Z	X	Y	Z	X	Y
HOD	8.11	16.08	15.76	1.70	18.06	18.28
MeOH	5.54	10.25	9.89	2.22	12.52	12.57
EtOH	4.32	7.60	7.28	1.40	10.12	10.10
n-PrOH	3.74	6.95	6.78	1.97	8.94	9.11

Table 9: Diffusion coefficient obtained with conventional DSTE experiments with and without flow

	$D.10^{10}$ ($m^2.s^{-1}$) without flow			$D.10^{10}$ ($m^2.s^{-1}$) flow rate = 1 mL/min		
Axis	Z	X	Y	Z	X	Y
HOD	15.15	16.34	15.97	15.51	16.31	15.99
MeOH	10.47	11.23	11.04	10.92	11.00	10.96
EtOH	8.65	8.59	8.25	8.75	8.33	8.38
n-PrOH	7.43	7.44	7.44	7.49	7.45	7.40

As expected, the results of STE experiments along Z-axis lead to non-sensical values of diffusion coefficients. The values calculated for transversal diffusion differ with and without flow. These differences are not explained yet. With DSTE experiments though, the values with and without flow are very similar. Differences can be seen depending on the axis on which the diffusion has been done. The differences of diffusion coefficients values between longitudinal and transversal axes could come from the Z-axis gradient non uniformity (see section 5.5 for more details). Based on these results we expect that we will be able to use DOSY experiments for reaction monitoring. However, DSTE experiments are long because of the need to increment gradient values and because of the phase cycling that necessitate 16 scans. In order to reduce the duration of the DSTE experiment, we added orthogonal CTP selection gradients on the DSTE pulse program. As a result, data can be acquired with a single scan per gradient value, as in the Oneshot pulse sequence, and we will use the term oneshot here. However, in this case the equation for the fit does not need to be adapted, as there is no cross term between diffusion-encoding and CTP selection gradients.

When the experiments were done, aberrant points were noticed. An example is displayed on Figure 80. An important loss of intensity can clearly be seen on the fourth point. Several experiments were done and it was noticed that this kind of artifacts randomly appeared on oneshot DSTE experiments. In order to correctly suppress the convection artifacts in DSTE experiments, it is assumed that the velocity of the fluid is the same in the two diffusion delays of the sequence. One explanation to the artifacts we observed could be a difference of velocity during the two delays. This idea led to the imaging experiments described in section 4.4. The artifacts did not appear in the previous experiments because of the number of scans that smoothed them.

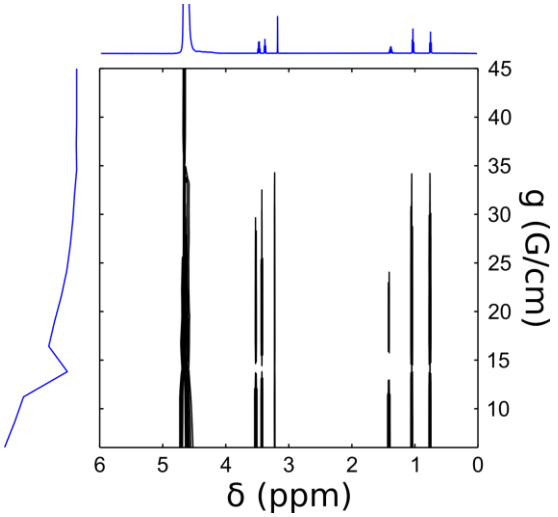

Figure 80: 2D DOSY data representation. Blue lines correspond to projection of the 2D data in both dimensions.

As conventional DSTE experiments were mostly working, except for the random artifacts, it was decided to do spatial encoded experiments. As for the ufCOSY experiments, spatial encoding along longitudinal and transversal axis were done. However, to this day, no repeatable experiments were obtained.

4.8 Conclusion

In this chapter, the use of the flowtube for reaction monitoring has been introduced. The use of this equipment will be useful for reaction monitoring as doing the reaction inside the spectrometer is not always possible, for example for photocatalyzed reaction, and may lead to different results due to the different conditions in terms of stirring or heat transfer.

It was shown for the first time that it was possible to use spatially encoded experiments for reaction monitoring under flow conditions at high field. This way, it will be possible to monitor fast reactions with multidimensional experiments, for reactions carried out in realistic conditions. It can also be used in order to identify compounds with short lifetimes such as reaction intermediates. Moreover, it was shown that kinetic information could be extracted using this method, that would have led to different results if the reaction had been done inside the spectrometer or to less detailed results if the reaction had been done in realistic conditions and sampled several times.

In addition, a phenomenon of interferences between velocity variation and chemical shift spatial encoding has been described. When flow rate increases several peak integrals display high losses and possibly variation. These losses depend on the chemical shift of the peak in the spatial dimension, on the way the chirp pulses sweep and on the spatial encoding pulse sequence that is used. This phenomenon only happens if the spatial encoding is done on the same axis as the flow direction. It was also shown that it is possible to do the experiments with a spatial encoding along a transversal axis to avoid the intensity losses.

5 Acceleration of 3D DOSY NMR by Spatial Encoding of the Chemical Shift

5.1 Introduction

Nuclear magnetic resonance is an essential analytical technique for chemistry. It is used in many applications such as structural identification, quantification, metabolomics, structural biology, interaction probing and many others. One of the most useful experiments for mixture analysis is the DOSY experiment that can be compared to a virtual chromatography. It allows separating the total spectrum in the spectra of the components of the mixture. However, unlike chromatography, there is no physical separation of the molecules.

The principle of DOSY experiments is to encode diffusion information using a pair of pulsed field gradients separated by a "diffusion delay". A series of spectra are acquired with increasing values of gradients, leading to an intensity decrease of the signals. This decay is then fitted to the Stejskal Tanner equation:

$$S = S_0 \, e^{-D\gamma^2\delta^2 g^2 \Delta'}, \tag{5.1}$$

where S and S_0 are the intensity or integration of the signal with and without the diffusion encoding gradients, D is the diffusion coefficient of the compound, γ is the gyromagnetic ratio of the observed nuclei, Δ' is the corrected delay between encoding and decoding gradients, δ is the duration of the encoding gradient and g is the intensity of the encoding/decoding gradients.

DOSY experiments are most of the time used to separate 1D spectra. It works usually well if signals are well separated, but if signals overlap, the fitting becomes more complicated. Multi-exponential fitting and multivariate processing can be used in order to separate spectra. However, we will focus here on another solution to reduce peak overlap to keep a simple mono-exponential fitting. As said earlier, DOSY is usually used to separate 1D spectra, but it can also be used to separate arbitrary nD spectra. DOSY has already been used in combination with COSY, NOESY, HSQC and several others. Despite the usefulness of these experiments, the approach of combining DOSY with spectra with dimensionality higher than one is limited by the duration of the experiment. Indeed, to separate nD spectra, a n+1D experiment has to be acquired, leading to long experiment duration as the number of increments becomes high. This long duration that can go from one hour to more than a day depending on the experiment, can be a problem when the sample is evolving over time. It would not be possible to monitor reactions or to observe compounds that are not stable enough with this kind of experiments. As explained in section 1.4, different approaches have been used to accelerate multidimensional experiments, such as Hadamard spectroscopy,[162] sparse[112] or accordion sampling.[163] It was shown that the method that leads to the highest acceleration is spatial encoding.[6,7,115] It was already shown that spatial encoding of the diffusion information could be used in order to drastically

reduce the duration of a 3D DOSY-COSY experiment.[149] We will show here how spatial encoding of the chemical shift can be used to accelerate even more DOSY-COSY and DOSY-DQS experiments.

The concept and implementation of 3D DOSY-UF2DNMR will first be described. The trueness of the calculation of the diffusion coefficient and the impact of spatial apodisation on it will then be studied. Finally, the limitations of the method will be discussed.

5.2 Experimental part

5.2.1 Samples

Two model mixtures of small molecules were prepared. The first mixture is composed of L-valine (7.2 mg), methanol (2.4 µL), ethanol (3.4 µL) and n-propanol (4.5 µL) solubilized in 590 µL of D_2O. The solution was shaken until complete dissolution of valine and filtered to remove any solid particles. The concentration is near 100 mM for each compound. The second mixture is composed of ethanol (35 µL) and propanol (45 µL) solubilized in 520 µL of D_2O. The concentration is near 1 M for each compound.

5.2.2 Acquisition

All the experiments were carried out on a Bruker Avance III spectrometer operating at a ^1H Larmor frequency of 600.13 MHz and equipped with a room-temperature 5 mm TXI $^1H/^{13}C/^{15}N$ probe with triple-axis gradients. The gradients were calibrated along each axis using a Shigemi tube filled with doped water (1 % H_2O + 0.1 % $CuSO_4$ in D_2O) and a restricted sample length of 10 mm. The temperature inside the probe was calibrated with a standard methanol sample and then set to a value of 298 K with airflow of 535 L/h. All the experiments were done without sample rotation.

Conventional 2D DOSY spectra were recorded using a stimulated echo sequence with bipolar gradient pulses (stebpgp1s Bruker sequence with additional lock stabilization gradients).

For 3D SPEN experiments, conventional parameters for DOSY were used: a diffusion delay of 100 ms (Δ) and a duration of the encoding pulse (δ) of 1.5 ms on Z-axis and 2 ms on X-axis. For COSY-DOSY the diffusion-encoding gradient values consisted of a linear ramp ranging from 10.32 G/cm to 55.04 G/cm with 16 increments when diffusion gradients were applied on Z-axis and from 7.62 to 40.62 G/cm when diffusion gradients were applied on X-axis. For DQS-DOSY the diffusion-encoding gradient values consisted of a linear ramp ranging from 6.88 to 55.04 G/cm with 8 increments when diffusion gradients were applied on Z-axis and from 5.08 to 40.62 G/cm when diffusion gradients were applied on X-axis

For the spatial encoding part of 3D ufCOSY-DOSY, an encoding gradient of 1.12 G/cm was used combined with a 15 ms chirp pulse with a 12 kHz bandwidth. Acquisition parameters were a 48.16 G/cm acquisition gradient strength with 128 gradient loops of 180 points each and a 0.767 µs dwell time. A recycle delay (D1) of 10 s, 2 dummy scans and 1 scan per gradient increment were used, resulting in an experimental time of 2 min 55 s.

For the spatial encoding part of 3D ufDQS-DOSY, an encoding gradient of 0.52 G/cm was used combined with a 15 ms chirp pulse with a 12 kHz bandwith. Acquisition parameters were a 48.16 G/cm acquisition gradient strength with 128 gradient loops of 180 points each and a 0.767 µs dwell time. A recycle delay (D1) of 10s, 2 dummy scans and 4 scans per gradient increment were used, resulting in an experimental time of 5 min 49 s.

For 3D conventional experiments, the same parameters than the previous ones were used: a diffusion delay of 100 ms (Δ) and a duration of the encoding pulse (δ) of 1.5 ms on Z-axis. For COSY-DOSY the diffusion-encoding gradient values consisted of a linear ramp ranging from 10.32 G/cm to 55.04 G/cm with 16 increments with diffusion gradients on Z-axis.

5.2.3 Processing

The processing of 3D experiments with chemical shift spatial encoding consists in importing the data in MATLAB before reshaping the linear data in 3D data. The first dimension corresponds to the k dimension, the second corresponds to the time dimension, and the last one corresponds to the gradient dimension. First, the data were Fourier transformed in the k dimension. Apodisation was done using a Gaussian window in the spatial dimension, and with a sine window for the time dimension. Then, the data were double Fourier transform along the time and spatial dimensions. It results in a series of UF2D spectra with increasing diffusion gradients. The spectrum with the lowest diffusion gradient was plotted and the selection of peak integration regions was done. Integration was done on all the spectra of the series and the plotted as a function for the diffusion gradient intensity. The decay curves were then fitted with Stejskal Tanner equation. Finally, a 3D dataset was reconstructed in which the first and second dimensions are spectral and k dimension, and the third dimension is the diffusion dimension. Slices were extracted from the 3D data set and plotted.

The processing of conventional 3D experiments consists in importing the data in MATLAB before reshaping the linear data in 3D data. The first dimension corresponds to the direct time dimension, the second corresponds to the indirect time dimension, and the last one corresponds to the gradient dimension. Apodisation was done using a sine window for both direct and indirect time dimension. Then, the data were double Fourier transform along direct and indirect time dimensions. It results in a series of 2D spectra with increasing diffusion gradients. The spectrum with the lowest diffusion gradient was plotted and the selection of peak integration regions was done. The integration was done on all the spectra of the series and plotted as a function of the diffusion gradient intensity. The decay curves were then fitted to Stejskal-Tanner equation. Finally, a 3D dataset was reconstructed in which the first and second dimensions are direct and indirect spectral dimensions and the third dimension is the diffusion dimension. Slices were extracted from the 3D data set and plotted.

Spatially encoded experiments were carried out with standard 5 mm tube, while conventional DOSY experiments were carried out once using a standard 5 mm tube and once using a 5 mm Shigemi tube with a restricted sample length of 10 mm.

5.3 DOSY-ufCOSY

The simplest way to convert a 2D experiment in its 3D DOSY equivalent is to concatenate the 2D pulse program with the DOSY pulse program. In this case, the pulse sequence of the 2D will follow the pulse sequence of the DOSY. The opposite is also possible (following the 2D pulse sequence by the DOSY experiment) but we will not study this case. Indeed, in chemical shift spatially encoded experiments, diffusions lead to a loss of intensity that is much higher than for conventional experiment. For conventional diffusion experiments, the spatial phase is created with a first gradient, then diffusion attenuation occurs; before a second pulse that refocuses the spatial phase. In this case, the spatial phase is independent of chemical-shift offsets. In chemical-shift spatial encoded experiments, the spatial phase depends of the spins' chemical shift. If chemical-shift spatial encoding is performed before the diffusion block, this will result in an additional, chemical-shift dependent attenuation, which will reduce sensitivity and make data analysis more complicated.

It was shown that in several cases, the pulse program could be simplified using the gradient already used in the 2D experiment to turn them into diffusion gradients that are used to create the diffusion dimension.[86,88] We will see both cases and the possible limitations.

5.3.1 Classical pulse program

The "classical" pulse program used to acquire 3D DOSY COSY is displayed in Figure 81 a). The version shown in the figure below uses orthogonal coherence selection gradients around the refocusing pulse, to remove the need for phase cycling. Using orthogonal gradients, the fitting does not have to be adapted as it would if a single gradient probe were used.[113] This pulse program can be converted in its spatially encoded version by replacing the t_1 evolution delay by a spatial encoding block, and the acquisition part by an EPSI block, as shown in Figure 81 b).

The spatially encoded experiment was acquired on the model sample 1 (alcohols and valine) with 16 gradient increments and 1 scan per increment. Then the ufCOSY spectrum with the lowest encoding gradient was plotted and the integration regions were defined as shown in Figure 82 a). The evolutions of integrals were plotted as a function of the diffusion gradient intensity as shown in Figure 82 b).

Finally, after the diffusion coefficient has been calculated for each peak, a 3D dataset was reconstructed with the third dimension being the diffusion coefficient. Then slices were extracted from the 3D dataset and plotted in Figure 83. All the compounds of the mixture are well separated showing the validity of the method. Moreover, as a one-shot version of the DOSY is used, the total experiment duration is less than 3 minutes, an acceleration of more than one order of magnitude compared to its conventional equivalent that takes at least several hours.

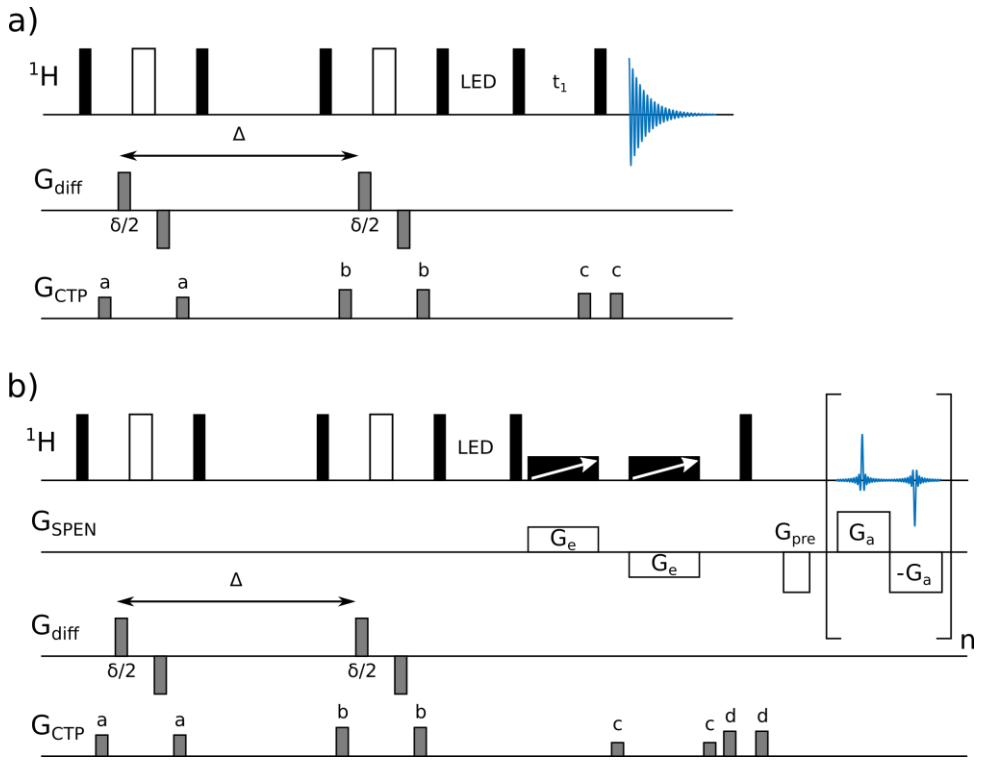

Figure 81: Pulse sequence for conventional (a) and chemical shift spatially encoded (b) COSY-DOSY.

5.3.2 Interlaced versions and limitations

As mentioned previously, the "classical" pulse sequence is not the only way to create the 3D DOSY experiment. Another way is using the gradients that are already used in the pulse sequence to turn them into diffusion-encoding gradients. For example, in some COSY pulse sequences, the last pulse before acquisition is surrounded by gradients that are used as coherence transfer pathway gradients. They are usually close to each other in order to reduce the losses due to diffusion. If we increase the delay between the gradients, it is possible to turn them into diffusion-encoding gradients. Then a series of COSY spectra will be acquired with incremented diffusion gradients.[86] The advantage

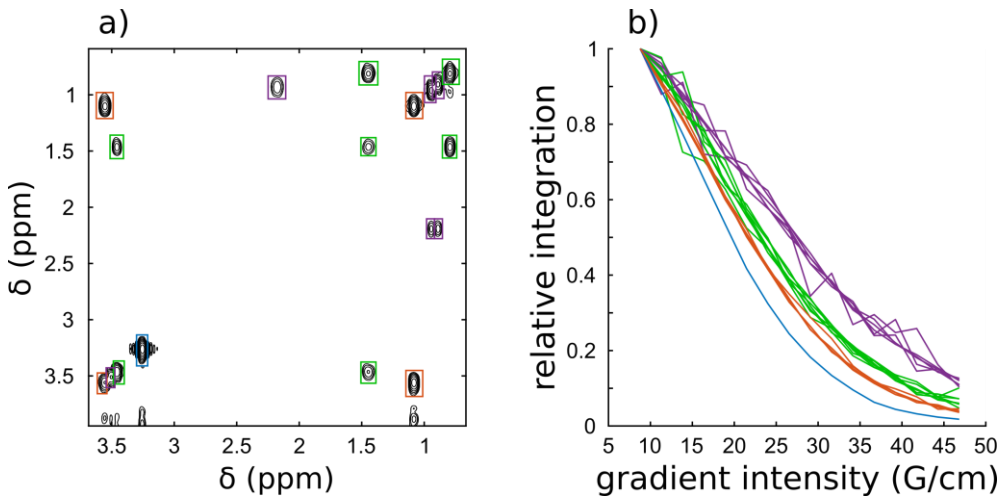

Figure 82: ufCOSY spectrum with the lowest diffusion gradient intensity extracted from the 3D experiment (a) and evolution of selected peaks integrals as a function of diffusion gradient intensity (b).

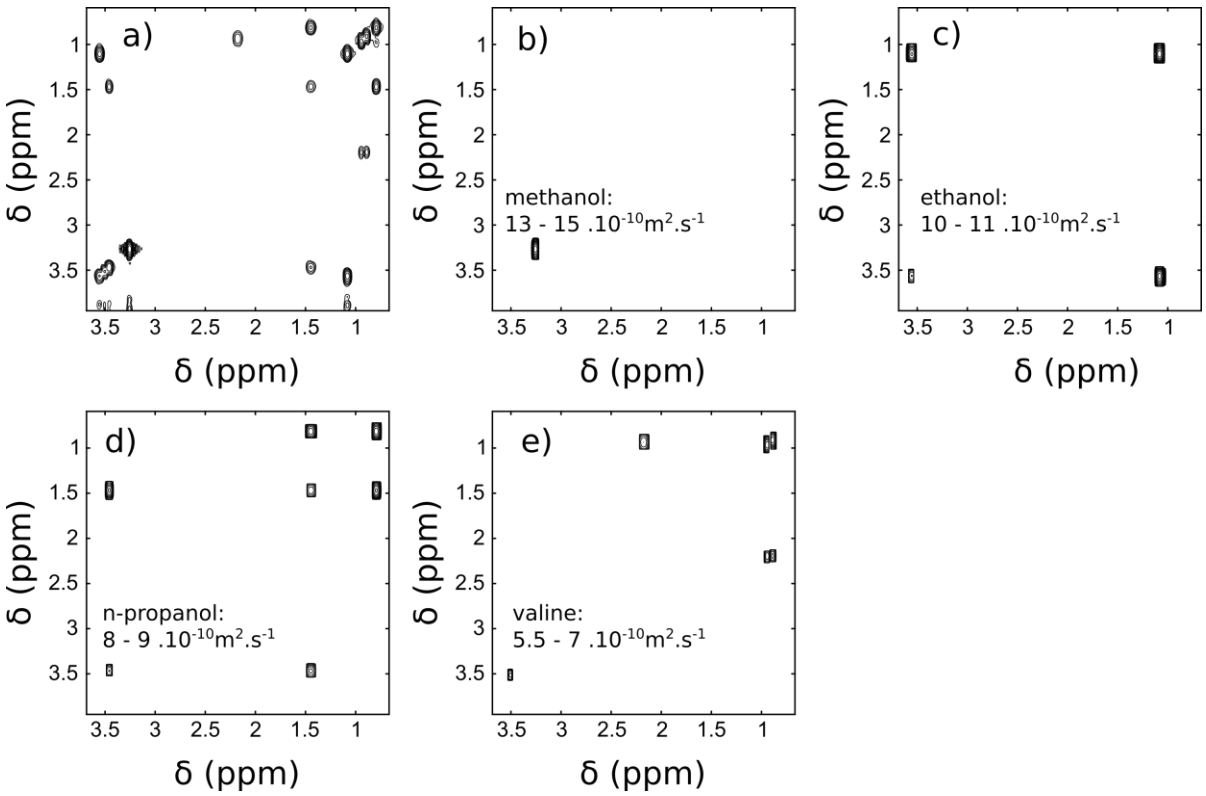

Figure 83: 3D DOSY-ufCOSY of a model mixture of three short chain alcohols and amino acid. (a) is the ufCOSY spectra from the 3D with the lowest gradient intensity. (b)–(e) slices extracted from the 3D spectra. The name of the compound and the selected range of D *is shown on each figure. One valine cross peak is missing in for the valine spectra due to sensitivity losses.*

of this approach is that, as it does not involve a stimulated echo, there are no intensity losses by a factor of 2, leading to a better signal to noise ratio. However, the gradients have to be intense enough so that the echo and anti-echo spectra are well separated. This is why the 3D experiments have been obtained with a gradient ramp whose initial value is 15 % of the maximum gradient intensity whereas conventional DOSY usually starts with an initial gradient between 5 and 10 %.

The method that consists in using the gradient of a nD pulse sequence in order to turn it in a n+1 DOSY experiment is usually called iDOSY method. The pulse sequence of the COSY-iDOSY is displayed on Figure 84 a). To turn this sequence in its ultrafast equivalent, it is possible to replace the t_1 delay by a spatial encoding block, and the acquisition part by an EPSI block, as it is shown in Figure 84 b). However, when an experiment was acquired with this pulse program, pronounced intensity losses were noted. This is the same reason why we did not study the 3D pulse program version where the DOSY block comes after the COSY block. As said earlier, diffusion will lead to important losses when using chemical shift spatial encoded experiments if encoding and decoding are separated by a long delay. In order to be able to combine the iDOSY method with spatial encoding, the SPEN block has to be shifted inside the diffusion delay, leading to a loss of symmetry of the diffusion delay. Moreover, due to the addition of the gradient used for CTP around the second chirp pulse, the diffusion gradient cannot anymore be used as CTP gradients, so gradients have been added around the final pulse of the COSY as shown on Figure 84 c). If the axis on which spatial encoding is done is the

same as the diffusion encoding axis, the diffusion curves obtained lead to nonsensical values of diffusion coefficients. This is due to interferences between the phase induced by the spatial encoding block and the phase induced by the diffusion gradient that is not compensated for, in contrast to the DOSY-ufCOSY. Hence, this last pulse sequence can be used only with a triple axis gradient probe.

A 3D COSY-iDOSY experiment was acquired with the pulse sequence in Figure 84 c) with spatial encoding on the Z-axis and diffusion-encoding on the X-axis. The results are very similar to those obtained with the first experiment. The difference between the DOSY and iDOSY experiments is that the relative peak intensities are different due to J-modulation. It can lead to situations where peak almost disappear as shown in Figure 85 that can be a problem for structure elucidation.

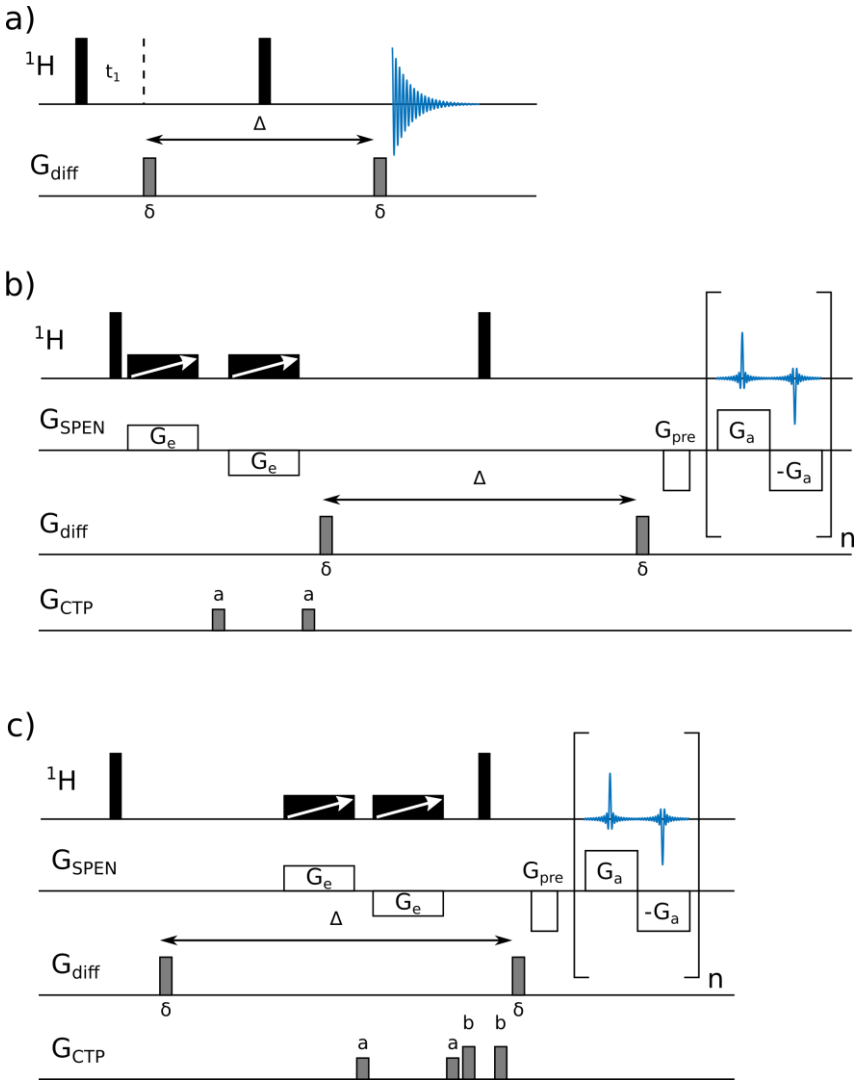

Figure 84: Pulse sequence of the conventional COSY-iDOSY (a) and first (b) and second (c) version of the ufCOSY-iDOSY.

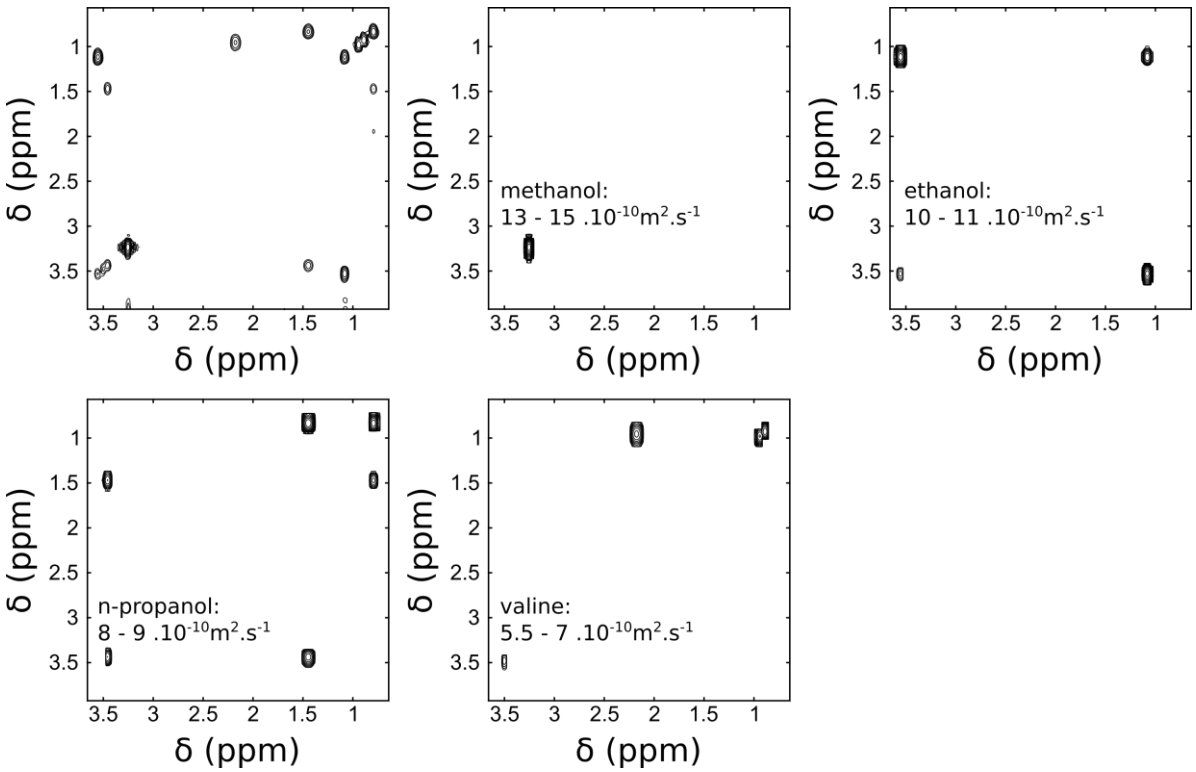

Figure 85: 3D ufCOSY-iDOSY of a model mixture of three short chain alcohols and amino acid. (a) is the ufCOSY spectra from the 3D with the lowest gradient intensity. (b)–(e) slices extracted from the 3D spectra. The name of the compound and the selected range of D *is shown on each figure*

5.4 DOSY-ufDQS

Another 2D experiment that can be very interesting for mixture analysis is Double Quantum Spectroscopy. It was shown that it can be useful for the analysis of complex samples such as biofluids[124,164] and the INADEQUATE experiment is a version of this experiment on ^{13}C. It can lead to less crowded spectra than COSY, but it has also been shown in section 3.3.2.1 that in some cases it can lead to more complicated spectra. As it was done for the 3D COSY-DOSY, the two ways to build the pulse program will be studied.

5.4.1 Classical pulse program

As previously, the pulse sequence for the 3D DQS-DOSY can be written by following the DOSY pulse sequence by the DQS one as shown on the Figure 86 a). As previously, in order to turn it into its chemical shift spatially encoded equivalent, we replaced the t_1 delay by a spatial encoding block and the acquisition part by an EPSI block, as shown on Figure 86 b).

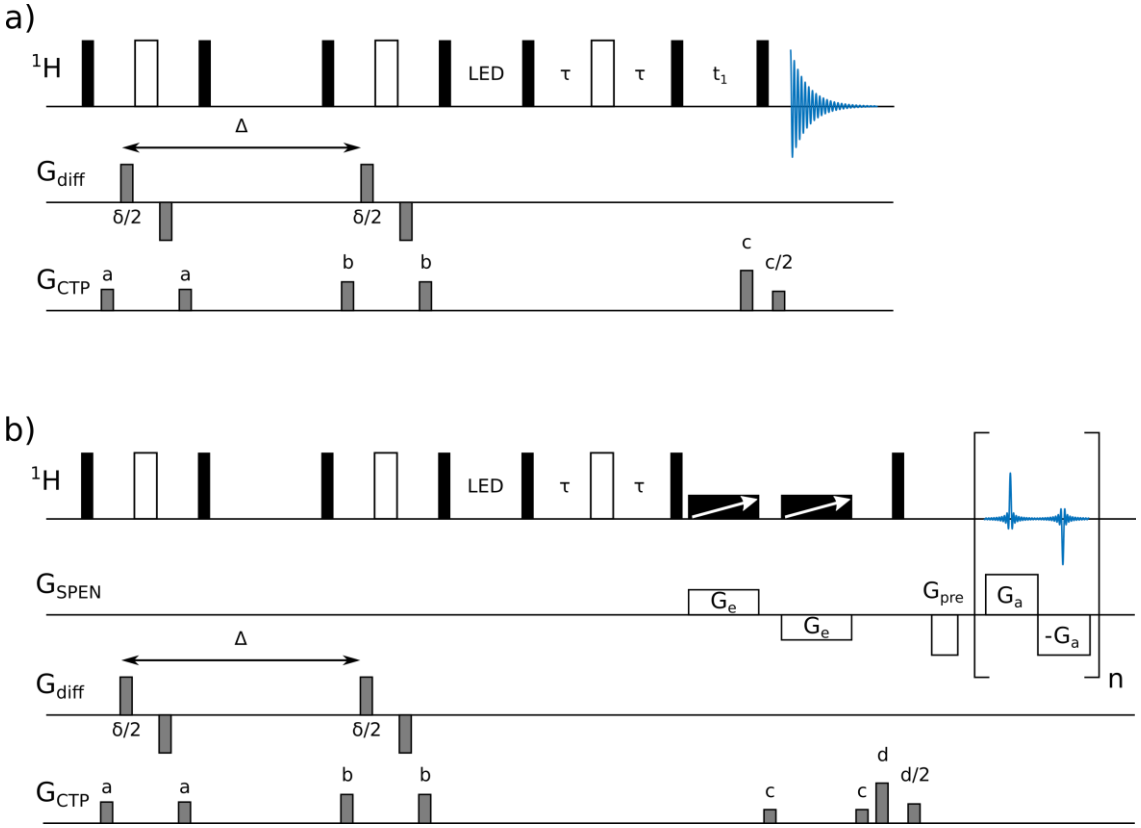

Figure 86: Pulse sequence for conventional (a) and chemical shift spatially encoded (b) DQS-DOSY.

First, a 3D ufDQS-DOSY experiment was acquired on the first model mixture used previously. However, almost no signal was obtained. After several tests, we managed to acquire a good dataset on the second mixture that is a solution of ethanol and n-propanol at a concentration of 1M in D_2O. The results of the acquisition on this second model mixture are shown in Figure 87. In this case, 8 increments of gradient were done with 4 scans for each. Good quality data are obtained and the two components of the mixture are well separated in an acquisition of only 6 minutes. Unfortunately, the sensitivity losses are becoming very high. This is probably due to the combination of several factors such as spatial encoding, the use of a stimulated echo, and the fact that double quantum coherences are more difficult to excite than single quantum ones.

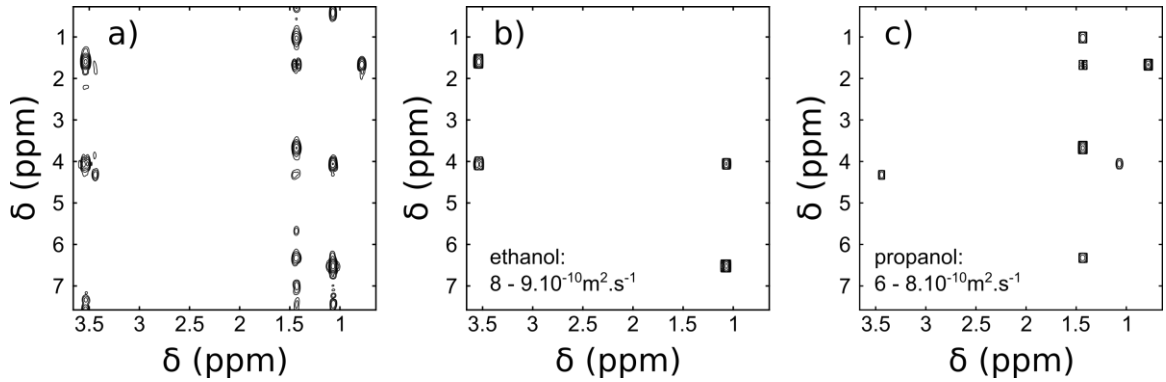

Figure 87: 3D DOSY-ufDQS of a model mixture of three short chain alcohols (a) is the ufDQSY spectra from the 3D with the lowest gradient intensity. (b)–(c) slices extracted from the 3D spectra. The name of the compound and the selected range of D *are shown on each figure.*

5.4.2 Interlaced version

As it was done for 3D COSY-DOSY, it was shown that it was possible to turn the DQS pulse sequence in its 3D iDOSY equivalent.[87] However, unlike the case of the COSY, the gradients that will be used for diffusion are not already in the pulse sequence of the DQS. They will be placed around the 180° hard pulse during the delay that is used to build up the multiple quantum coherences as shown in Figure 88 a). As for the other pulse program the t_1 delay was replaced by a spatial encoding block and the acquisition part by an EPSI block to create the ufDQS-iDOSY pulse sequence that is shown in Figure 88 b). In this case, there are no interferences possible between the spatial encoding block and the diffusion gradients so it can be implemented on a single axis probe. However, in the cases of the DQS-iDOSY (conventional or ultrafast), the diffusion delay Δ is constrained to the value of the optimized 2τ delay. In our case, a value of 100 ms gave good results, but depending on the mixture, it should be adapted.

A 3D ufDQS-iDOSY was acquired on the model mixture 2. The results were very similar to those obtained with the ufDQS-DOSY pulse sequence, including the important intensity losses despite the advantage of the iDOSY version of the method in this domain.

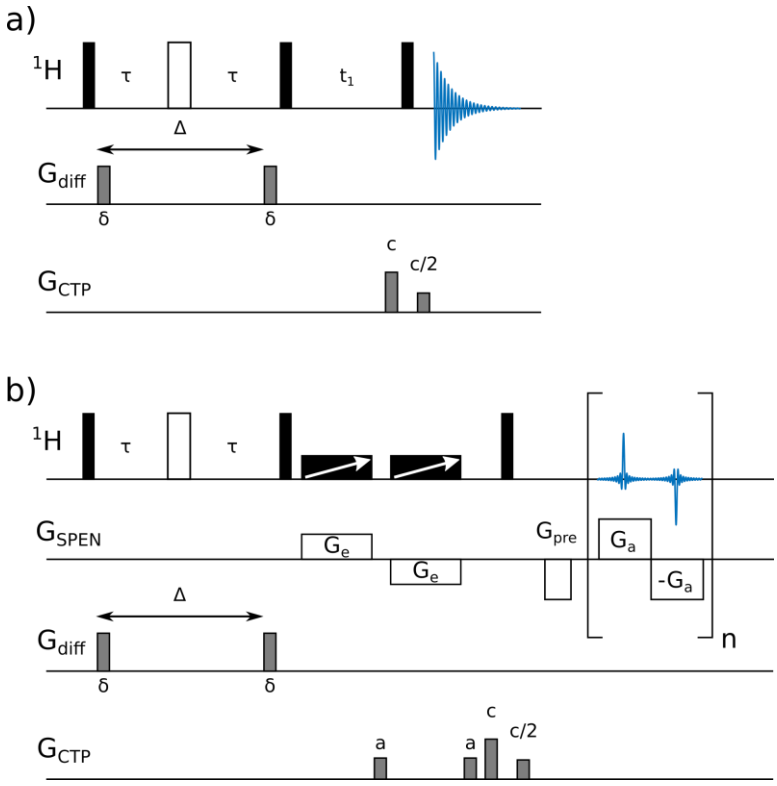

Figure 88: Pulse sequence of the conventional DQS-iDOSY (a) and of the ufCOSY-iDOSY (b).

5.5 3D ufCOSY-DOSY experiments, gradient non-uniformity and diffusion coefficient trueness

It was shown that it was possible to accelerate the acquisition of 3D DOSY experiments by more than one order of magnitude using chemical shift spatial encoding. However, we have not yet compared the diffusion coefficients obtained with the accelerated experiment to the values obtained with conventional DOSY experiments.

The average diffusion coefficients for each compound were extracted from the 3D DOSY-ufCOSY experiment processed with default parameters, and compared with a 2D conventional DOSY, acquired using either a classical NMR tube or a Shigemi tube with a restricted length of 10 mm. The values are shown in Table 10. It can be seen that the values obtained with the UF experiment are in good agreement with those obtained with a Shigemi tube, and that there is a systematic difference with the values obtained with the classical tube. These differences are mostly due to the non-uniformity of the gradient. Indeed, on triple-axis gradient probes, the gradients are more intense at the center of the coil than at the edges. As mentioned earlier, spatial apodisation is used during the processing of ultrafast experiments in order to improve the sensitivity and lineshapes of the spectra. As a result, only the central region of the sample contributes to the processed spectrum. Examples of Gaussian windows usually used for spatial apodisation and their effects are shown in Figure 89 and Figure 90. With the default value of sigma = 3 mm, the selected region corresponds approximately to that present in the Shigemi tube. Note that in this case the values obtained with the Shigemi tube are closer to the true diffusion coefficient than those obtained with a classical tube, since a Shigemi tube was used for gradient calibration.

A more comprehensive comparison was made by acquiring a conventional 3D-DOSY-COSY on the Shigemi tube and a classical tube. The calculated diffusion coefficients are compared peak by peak in Figure 91. As it was seen for the conventional DOSY, the results obtained on the Shigemi tube are closer to the uf-3D than with a classical tube.

Table 10: Comparison of diffusion coefficients obtained on the test sample with conventional DOSY in classic and Shigemi tube and with 3D DOSY-ufCOSY on a classic (unrestricted) tube. Each value here is calculated as the mean of the diffusion coefficient calculated for all signals of one compound.

	$D.10^{-10}$ ($m^2.s^{-1}$)			
Experiment	valine	propanol	ethanol	methanol
DOSY, classical tube	5.09	6.94	7.98	10.59
DOSY, Shigemi tube (L = 10 mm)	6.48	8.99	10.20	13.49
DOSY-ufCOSY	6.13	9.60	10.15	12.97

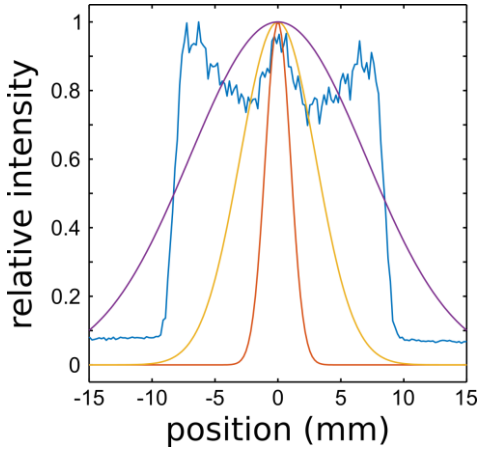

Figure 89: Spatial projection of the 2D spatial-spectral data set resulting from the first increment of the DOSY-ufCOSY experiment. The processing of UF NMR data involved multiplication by a window function in the spatial domain. Three Gaussian windows are shown here, for three values of the width: σ = 1 (red), 3 (yellow) and 7 (purple) mm.

In order to illustrate the consequences of spatial apodisation on the diffusion coefficients, the average diffusion coefficient of each compound was extracted from the 3D ufCOSY-DOSY and plotted as a function of the σ used for the spatial apodisation. The results are displayed in Figure 92.

It can be seen that the standard deviation used for spatial apodisation has a strong impact on the estimated diffusion coefficient. When the standard deviation of the Gaussian used is 3 mm or less, the calculated diffusion coefficients are very close to those obtained with a Shigemi tube (illustrated in Figure 93) with a restricted length of 10 mm. At the opposite, when the Gaussian is wide enough, the whole sample is taken into account, the diffusion coefficient values tend towards the values obtained with conventional DOSY experiments.

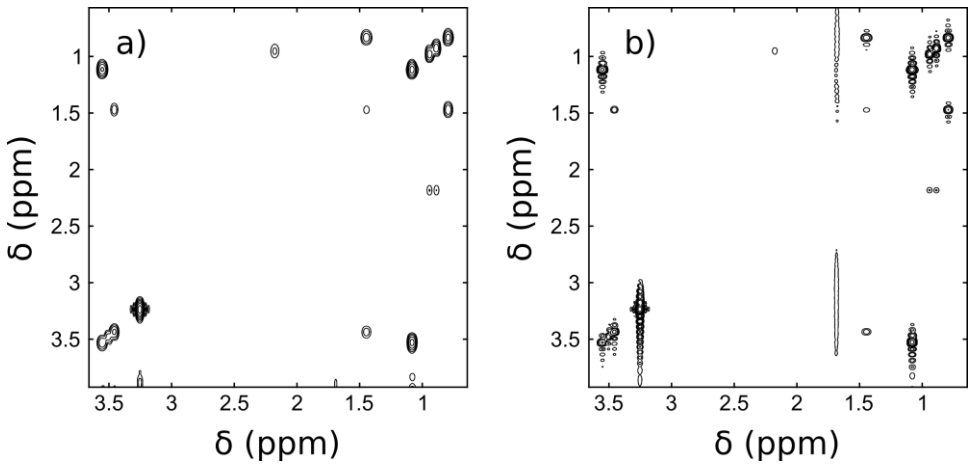

Figure 90: Ultrafast COSY spectra of the model mixture 1 with apodisation a Gaussian with σ = 3 mm (a) and without apodisation (b).

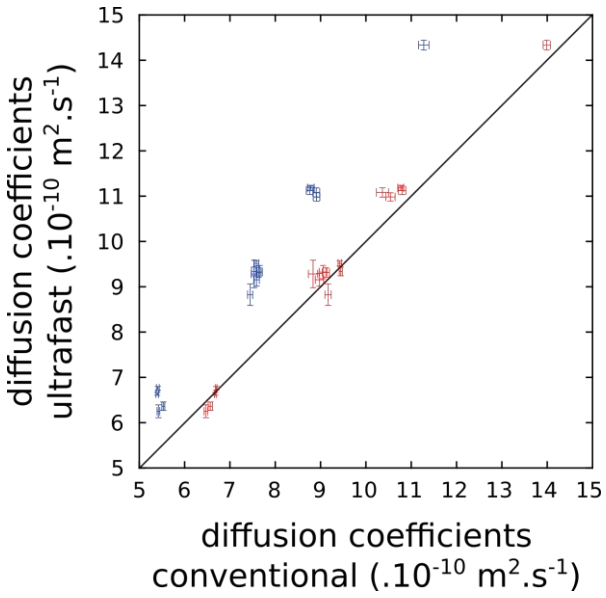

Figure 91: Comparison signal by signal between diffusion coefficients calculated from 3D DOSY-ufCOSY with 3D conventional DOSY-COSY in a classic NMR tube (blue) and in shigemi tube set with L=10 mm (red). The diagonal line is shown as a guide to the eye.

Using a width of the apodisation function of 3 mm or less selects a region of the sample where gradient non uniformity is less pronounced, and give a reasonable estimate of the diffusion coefficients. There would be two more general solutions to this problem, that have not been used yet. The first would be to make a map of the gradient on Z-axis. Then, it would be easy to correct the data taken into account the diffusion gradient that spins actually underwent. The second solution would be to use a probe that has uniform gradient all along the Z-axis. A single axis probe would fit this description, but due to the number of gradients needed (SPEN, diffusion, CTP) the risk of interferences is high and the implementation would probably be complicated. Another kind of probe

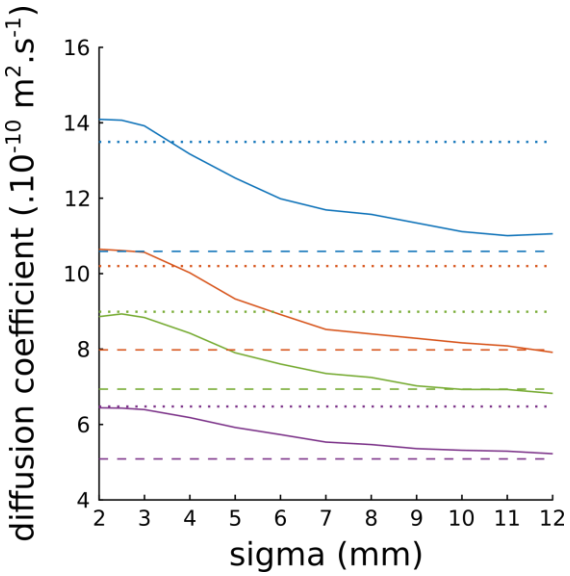

Figure 92: Estimated diffusion coefficients as a function of the spatial apodisation width (sigma) used for the processing of 3D DOSY-ufCOSY data, for a model mixture of methanol (blue), ethanol (red), n-propanol (green) and L-valine (purple). The diffusion coefficients obtained from conventional DOSY with either a conventional tube (dashed lines) or a Shigemi tube set to 10 mm (dots) are displayed for comparison.

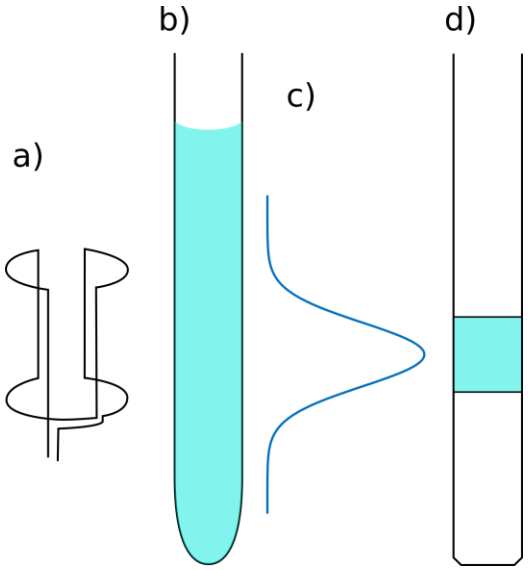

Figure 93: Scheme of a NMR coil a) of a classical NMR tube b), of the spatial apodisation used c) of a Shigemi tube with restricted length that mimic the restriction of length of the spatial apodisiation.

that fits the criterion of uniform gradient is the micro-imaging probe, such as the one that was recently acquired by the laboratory.

5.6 Conclusions

In summary, it was shown that 3D DOSY experiments could be accelerated by more than one order of magnitude using by spatial encoding of chemical shifts. For DOSY-COSY, two pulse sequences have been reported and both give a good separation of the compounds' spectra. However, the iDOSY version, that is more sensitive, cannot be implemented on single-axis gradient probes. For DQS-DOSY, the separation of compounds' spectra was also good and both of the pulse sequences can in theory be implemented on a single-axis gradient probe, but the loss of sensitivity is prohibitive in this case. Finally, it was shown that despite being able to separate the signal of the compounds, the calculated diffusion experiments can be influenced do to the spatial apodisation that is applied during the processing and to the gradient non-uniformity. If an accurate value of diffusion coefficient is not sought, this method can be useful for time-limited analysis of mixture. And even if an accurate diffusion coefficient is needed, solutions exist to calculate it.

Conclusion

Throughout this work, it was shown how spatial encoding of chemical shift or diffusion information can be very useful tool for the NMR analysis of mixture and for reaction monitoring.

In the first part, the spatially encoded DOSY experiment was carefully characterized. Several questions were answered such as the influence of parameters including the acquisition gradient, the acquisition duration or the encoding parameters. The influence of the acquisition duration and the encoding parameters were similar to what was expected, but the influence of the acquisition gradient is not fully understood. It was also shown that the sequence could be implemented on single gradient axis probes if precautions are taken. Finally, the feasibility of convection compensation on spatially encoded experiments has been shown. This method may also help to compensate for flow for online monitoring experiments.

In the second part, the possibility to spatially encode coherence orders higher than two has been demonstrated. This method can be very useful for the analysis of aromatic mixtures, provided that the pulse sequence delays are optimized beforehand. These ultrafast experiments were also used in order to monitor an organic reaction. The sensitivity of ufMQS experiments is unfavorable. However, for reaction monitoring, the sensitivity is not such a big problem as the concentration of the molecules are usually high compared to other applications.

A commercial flowtube has been set up in the laboratory, for online monitoring, and the use of UF2DNMR on a flowing sample has been investigated. Results on the interferences between the flow and the spatial encoding of chemical shifts have been obtained. First, it was shown with 1D images that the HPLC pump creates velocity changes. Then, it seems that when the flow rate is high and if the spatial encoding is done along the Z-axis, the peak intensities in ultrafast experiments are subjected to losses as a function of their chemical shift in the spatial dimension, for all the spatial encoding block used in this document. The solution we chose to use is to spatially encode chemical shifts along a transversal axis. There are still small losses when the flow rate increases but they are not linked to the peak's chemical shift in the spatial dimension. Finally, it was shown that the combination of flow and ultrafast experiments could be used in order to monitor a saponification reaction and lead to the same kinetic results as if the monitoring was done using 1D ^{1}H spectra.

In the last part of the document, it was shown that it was possible to accelerate 3D-DOSY experiments by more than one order of magnitude using spatial encoding of chemical shifts. A clean separation of COSY spectra was obtained in a few minutes. However, for 3D DQS DOSY spectra, the limit of sensitivity is reached. It was also shown that in this kind of experiments, spatial resolution makes it possible, through the use of apodisation to address the effect of gradient non uniformity on the calculated diffusion coefficients.

The next steps are to continue the characterization of the interference between flow and chemical shift spatial encoding and the flow. The micro-imaging probe will also help to obtained spatially

encoded experiments with higher resolution thanks to the possibility to have long acquisition durations. The reaction monitoring will also continue with more interesting reactions as the monitoring of the model reaction showed that it was possible to obtained good results with ultrafast spectra.

Annexes

Pulse sequence for SPEN STE

```
;LG_ufSTEph

;$CLASS=HighRes
;$DIM=2D
;$TYPE=
;$SUBTYPE=
;$COMMENT=

#include <Avance.incl>
#include <Grad.incl>
#include <De.incl>
#include <Delay.incl>

"d20=(td*dw/(2*l3))-d6"
"d12=p11"
"DELTA1=d30-p11-2*d4-2*d11-2*p20-2*d16-2*p1-2*p21-2*d16-p22-d16-2*d11-2*d12-4*d4-
2*d5"
"p21=p20*2"
"p2=2*p1"
"d8=p25/2"

1 ze
  20u st0
  30m

2 30m
  d1
  50u UNBLKGRAD
  20u pl1:f1

  p22:gp24*-1
  d16

;excitation

  p1 ph1
  d5

;spatial encoding

  p20:gp20
  d16
  d11
  d4 gron0
  p11:sp1:f1 ph2
  d11
  d4 groff

  p20:gp21
  d16 pl1:f1
```

```
;stimulated echo

  d5
  p1 ph1

  p21:gp26*-1
  d16

  d4 gron1
  d12
  d11
  d4 groff

  p22:gp24
  d16
  DELTA1

  d4 gron1
  d12
  d11
  d4 groff

  p21:gp27*-1
  d16

  p1 ph4

;decoding period
  d5
  p20:gp22
  d16
  d11
  d4 gron0
  p11:sp1:f1 ph2
  d11
  d4 groff

  p20:gp23
  d16
  d5

; Prephasing

  p25:gp25

  d7 pl1:f1

  p14:gp14
  p2 ph3
  p14:gp14

  d7

  d8
```

```
;acquisition

  ACQ_START(ph30,ph31)
  1u DWELL_GEN:f1
3 d20 gron2
  d6 groff
  d20 gron3
  d6 groff
  lo to 3 times l3
  rcyc=2
  30m mc #0 to 2 F1QF(id2)
  100u BLKGRAD
  d17
exit

;phase cycling

ph1=0
ph2=0
ph3=0
ph5=0
ph4=0
ph29=0
ph30=0
ph31=0


;pl1 : f1 channel - power level for pulse (default)
;sp1: shaped pulse power level for selective detection
;p1 : f1 channel - 90 degree high power pulse
;p11: duration of the encoding chirp
;p20 :1ms coherence-selection delay
;p21 :20ms coherence-selection delay
;p14:1ms
;spnam1 : shaped pulse for spatial encoding
;d1: relaxation delay; 1-5 * T1
;d2: ramping period for gradient pulse (25us)
;d3: delay 10us
;d5: 5us
;d7:1ms
;d8:[0-200]u
;d16: gradient recovery delay (200us)
;d30: diffusion time (big DELTA)
;d6: gradient ramp off during acauisition
;d20 + d6 : acquisition gradient duration
;GPZ0 : strength for excitation gradient [-100-0]
;GPZ1 : strength for acquisition gradient [0-100]
;GPZ2 : strength for reversed acquisition gradient GPZ3 = -GPZ2
;GPZ20 and GPZ21: coherence-selection gradients encoding (GPZ20=-GPZ21)
; GPZ22 : strength for diffusion delay gradient [0-100]
;GPNAM20=GPNAM21= GPNAM22=SINE.100
;NS: 1 (or more if necessary)
;l3=number of loops for acquisition
;IMPORTANT: set d20 + d6 = DW x TD(f3)/(2xL3)
```

Pulse sequence for SPEN STE

```
;LG_ufDSTEphpr(17/12/13)
#include <Avance.incl>
#include <Grad.incl>
#include <De.incl>
#include <Delay.incl>

"d20=(td*dw/(2*l3))-d6"
"DELTA1=d30/2-p11-2*d4-2*d11-2*p20-5*d16-p22-2*d14-2*p1"
"p2=p1*2"
"d14=p16"
"d8=p25/2"

1 ze

  30m pl14:f2
  20u st0

2 30m
  d1 cw:f2 ph29
  4u do:f2
  50u UNBLKGRAD
  20u pl1:f1

;excitation

  p1 ph1
  d14
  d16
;spatial encoding

  p20:gp20
  d16 pl0:f1
  d11
  d4 gron0
  p11:sp1:f1 ph2
  d11
  d4 groff

  p20:gp21
  d16 pl1:f1
   d14
   d16


; first spin echo
  p1 ph1

  p22:gp14
  d16
  DELTA1

  p1 ph1
;decoding period
```

```
 d14
 d16

  p20:gp22
  d16 pl0:f1
  d11
  d4 gron0
  p11:sp1:f1 ph2
  d11
  d4 groff

  p20:gp23
  d16 pl1:f1

;Middle 180 pulse

  p16:gp16
  d16
  p2 ph3
  p16:gp16
  d16
;spatial encoding

  p20:gp26
  d16 pl0:f1
  d11
  d4 gron0
  p11:sp1:f1 ph2
  d11
  d4 groff

  p20:gp27
  d16 pl1:f1

  d14
  d16

;second spin echo

  p1 ph1

  p22:gp15
  d16
  DELTA1

  p1 ph1

   d14
   d16

;decoding period

  p20:gp28
  d16 pl0:f1
  d11
```

```
  d4 gron0
  p11:sp1:f1 ph2
  d11
  d4 groff

  p20:gp29
  d16

   d14
   d16
; Prephasing

  p25:gp25

  d7 pl1:f1

  p14:gp30
  d16
  p2 ph3
  p14:gp31
  d16
  d7

  d8

;acquisition

  ACQ_START(ph30,ph31)
  1u DWELL_GEN:f1
3 d20 gron2
  d6 groff
  d20 gron3
  d6 groff
  lo to 3 times l3
  rcyc=2
  30m mc #0 to 2 F1QF(id2)
  100u BLKGRAD
  d17
exit

;phase cycling

ph1=0
ph2=0
ph3=0
ph4=0
ph29=0
ph30=0
ph31=0



;pl1 : f1 channel - power level for pulse (default)
;sp1: shaped pulse power level for selective detection
;p1 : f1 channel - 90 degree high power pulse
```

```
;p11: duration of the encoding chirp
;p20 :1ms coherence-selection delay
;p21 :20ms coherence-selection delay
;spnam1 : shaped pulse for spatial encoding
;d1: relaxation delay; 1-5 * T1
;d2: ramping period for gradient pulse (25us)
;d3: delay 10us
;d5: 5us
;d16: gradient recovery delay (200us)
;d30: diffusion time (big DELTA)
;d6: gradient ramp off during acauisition
;d20 + d6 : acquisition gradient duration
;GPZ0 : strength for excitation gradient [-100-0]
;GPZ1 : strength for acquisition gradient [0-100]
;GPZ2 : strength for reversed acquisition gradient GPZ3 = -GPZ2
;GPZ20 and GPZ21: coherence-selection gradients encoding (GPZ20=-GPZ21)
; GPZ22 : strength for diffusion delay gradient [0-100]
;GPNAM20=GPNAM21= GPNAM22=SINE.100
;NS: 1 (or more if necessary)
;l3=number of loops for acquisition
;IMPORTANT: set d20 + d6 = DW x TD(f3)/(2xL3)
```

Pulse sequence for ultrafast MQ experiment for observation of even order of coherences without refocusing

```
; MGCufmqsprds_even
;modifed by Corentin Jacquemmoz
;modifed by Maria Grazia Concilio (last modified on 180201)
;UFDQS with constant-time phase encoding
;DS can be used, presat only during d3

;$CLASS=HighRes
;$DIM=2D
;$TYPE=
;$SUBTYPE=
;$COMMENT=

#include <Avance.incl>
#include <Grad.incl>
#include <De.incl>
#include <Delay.incl>

"d0=3u"
"d11=30m"
"d12=20u"
"d13=4u"
"p15=(td*dw/(2*l3))-d6"
"p24=p15"
;"d2=3u + 60*(p15-d6/2)"
"p2=2*p1"
;"d4=1s/(4*cnst1)"
;"d4=d5"
;"in2=2*(p15+d6)/td1"
"p26=p23"
"p21=p20"
"TAU = d1-d3"

1 ze
  d11 pl14:f2
  20u st0

2 30m
  TAU
  d3 cw:f2 ph29
  4u do:f2
  100u UNBLKGRAD
  20u pl1:f1

;excitation

  p1 ph1
  d4
  p2 ph2
  d4
  p1 ph4
```

```
;spatial encoding
  20u gron0
  p11:sp1:f1 ph1
  20u groff
  p20:gp20
  20u gron1
  p11:sp1:f1 ph2
  20u groff
  p21:gp21

;pre-mixing gradient
  10u
  p24:gp24
  10u

;mixing
  p23:gp23
  10u
  5u pl1:f1
  p10 ph2
  10u
  p26:gp26

;post-mixing gradient
  10u
  p24:gp25
  10u

  d2

;acquisition
  ACQ_START(ph30,ph31)
  1u DWELL_GEN:f1
3 p15:gp15
  d6
  p15:gp16
  d6
  lo to 3 times l3
  100u BLKGRAD
  rcyc=2
  100u UNBLKGRAD
;purge gradient
  p27:gp27
  100u BLKGRAD
  30m mc #0 to 2 F1QF(id2)
  d17
exit

ph1=0
ph2=0
ph4=0
ph3=0
ph29=0
ph30=0
```

ph31=0

;pl1 : f1 channel - power level for pulse (default)
;sp1: shaped pulse power level for selective detection
;p1 : f1 channel - 90 degree high power pulse
;p23: coherence-selection gradients for mixing(p23=p26)
;p26: coherence-selection gradients for mixing(p23=p26)
;p20: coherence-selection gradients for spatial encoding(p20=p21)
;p21: coherence-selection gradients for spatial encoding(p20=p21)
;spnam1 : shaped pulse for selective detection
;d1 : relaxation delay; 1-5 * T1
;p15 + d6 : acquisition gradient duration
;p25 : post-mixing gradient duration
;d17 : delay after experiment (not necessary)
;gpz0 : strength for excitation gradient [0-100]
;gpz1 : strength for reversed excitation gradient GPZ1 = -GPZ0
;gpz15 : strength for acquisition gradient [0-100]
;gpz16 : strength for reversed acquisition gradient GPZ16 = -GPZ15
;gpz20: coherence-selection gradients for spatial encoding (GPZ20=GPZ21)
;pgz21: coherence-selection gradients for spatial encoding (GPZ20=GPZ21)
;gpz24: pre- and post-mixing gradients
;gpz25: pre- and post-mixing gradients
;NS: 1 (or more if necessary)
;l3=number of loops for acquisition
;IMPORTANT: set p15 + d6 = DW x TD(F2)/(2xL3)

Pulse sequence for ultrafast MQ experiment for observation of odd order of coherences without refocusing

```
; MGCufmqsprds_odd
;modifed by Corentin Jacquemmoz
;modifed by Maria Grazia Concilio (last modified on 180201)
;DS can be used, presat only during d3

;$CLASS=HighRes
;$DIM=2D
;$TYPE=
;$SUBTYPE=
;$COMMENT=

#include <Avance.incl>
#include <Grad.incl>
#include <De.incl>
#include <Delay.incl>

"d0=3u"
"d11=30m"
"d12=20u"
"d13=4u"
"p15=(td*dw/(2*l3))-d6"
"p24=p15"
;"d2=3u + 60*(p15-d6/2)"
"p2=2*p1"
;"d4=1s/(4*cnst1)"
;"in2=2*(p15+d6)/td1"
"p26=p23"
"p21=p20"
"TAU = d1-d3"

1 ze
  d11 pl14:f2
  20u st0

2 30m
  TAU
  d3 cw:f2 ph29
  4u do:f2
  100u UNBLKGRAD
  20u pl1:f1

;excitation

  p1 ph1
  d4
  p2 ph2
  d4
  p1 ph4

;spatial encoding
  20u gron0
```

```
  p11:sp1:f1 ph1
  20u groff
  p20:gp20
  20u gron1
  p11:sp1:f1 ph2
  20u groff
  p21:gp21

;pre-mixing gradient
  10u
  p24:gp24
  10u

;mixing
  p23:gp23
  10u
  5u pl1:f1
  p10 ph2
  10u
  p26:gp26

;post-mixing gradient
  10u
  p24:gp25
  10u

          d2

;acquisition
  ACQ_START(ph30,ph31)
  1u DWELL_GEN:f1
3 p15:gp15
  d6
  p15:gp16
  d6
  lo to 3 times l3
  100u BLKGRAD
  rcyc=2
  100u UNBLKGRAD
;purge gradient
  p27:gp27
  100u BLKGRAD
  30m mc #0 to 2 F1QF(id2)
  d17
exit

ph1=0
ph2=0
ph4=1
ph3=0
ph29=0
ph30=0
ph31=0
```

;pl1 : f1 channel - power level for pulse (default)
;sp1: shaped pulse power level for selective detection
;p1 : f1 channel - 90 degree high power pulse
;p20: coherence-selection gradients for spatial encoding(p20=p21)
;p21: coherence-selection gradients for spatial encoding(p20=p21)
;spnam1 : shaped pulse for selective detection
;d1 : relaxation delay; 1-5 * T1
;d24 : pre-mixing gradient duration
;d25 : post-mixing gradient duration
;d17 : delay after experiment (not necessary)
;gpz0 : strength for excitation gradient [0-100]
;gpz1 : strength for reversed excitation gradient GPZ1 = -GPZ0
;gpz15 : strength for acquisition gradient [0-100]
;gpz16 : strength for reversed acquisition gradient GPZ16 = -GPZ15
;gpz20: coherence-selection gradients for spatial encoding (GPZ20=GPZ21)
;pgz21: coherence-selection gradients for spatial encoding (GPZ20=GPZ21)
;gpz24: pre- and post-mixing gradients
;gpz25: pre- and post-mixing gradients
;NS: 1 (or more if necessary)
;l3=number of loops for acquisition
;IMPORTANT: set d20 + d6 = DW x TD(F2)/(2xL3)

Pulse sequence for ultrafast MQ experiment for observation of even order of coherences with refocusing

```
; MGCufmqsprds_even_refocgp
;modifed by Corentin Jacquemmoz
;modifed by Maria Grazia Concilio (last modified on 180201)
;DS can be used, presat only during d3

;$CLASS=HighRes
;$DIM=2D
;$TYPE=
;$SUBTYPE=
;$COMMENT=

#include <Avance.incl>
#include <Grad.incl>
#include <De.incl>
#include <Delay.incl>

"d0=3u"
"d11=30m"
"d12=20u"
"d13=4u"
"p15=(td*dw/(2*l3))-d6"
"p24=p15"
;"d2=3u + 60*(p15-d6/2)"
"p2=2*p1"
;"d4=1s/(4*cnst1)"
;"d4=d5"
;"in2=2*(p15+d6)/td1"
"p26=p23"
"p21=p20"
"TAU = d1-d3"

1 ze
  d11 pl14:f2
  20u st0

2 30m
  TAU
  d3 cw:f2 ph29
  4u do:f2
  100u UNBLKGRAD
  20u pl1:f1

;excitation

  p1 ph1
  d4
  p2 ph3
  d4
  p1 ph4

;spatial encoding
```

```
  20u gron0
  p11:sp1:f1 ph1
  20u groff
  p20:gp20
  20u gron1
  p11:sp1:f1 ph2
  20u groff
  p21:gp21

;pre-mixing gradient
  10u
  p24:gp24
  10u

;mixing
  p23:gp23
  10u
  5u pl1:f1
  p10 ph2
  10u
  p26:gp26

;refocus
  d5
  p28:gp28
  d16
  p2 ph5
  d16
  p28:gp28
  d5

;post-mixing gradient
  10u
  p24:gp25
  10u

  d2

;acquisition
  ACQ_START(ph30,ph31)
  1u DWELL_GEN:f1
3 p15:gp15
  d6
  p15:gp16
  d6
  lo to 3 times l3
  100u BLKGRAD
  rcyc=2
  100u UNBLKGRAD
;purge gradient
  p27:gp27
  100u BLKGRAD
  30m mc #0 to 2 F1QF(id2)
  d17
exit
```

```
ph1=0
ph2=0
ph4=0
ph3=0
ph5=1
ph29=0
ph30=0
ph31=0

;pl1 : f1 channel - power level for pulse (default)
;sp1: shaped pulse power level for selective detection
;p1 : f1 channel - 90 degree high power pulse
;p20: coherence-selection gradients for spatial encoding(p20=p21)
;p21: coherence-selection gradients for spatial encoding(p20=p21)
;spnam1 : shaped pulse for selective detection
;d1 : relaxation delay; 1-5 * T1
;d24 : pre-mixing gradient duration
;d25 : post-mixing gradient duration
;d17 : delay after experiment (not necessary)
;gpz0 : strength for excitation gradient [0-100]
;gpz1 : strength for reversed excitation gradient GPZ1 = -GPZ0
;gpz15 : strength for acquisition gradient [0-100]
;gpz16 : strength for reversed acquisition gradient GPZ16 = -GPZ15
;gpz20: coherence-selection gradients for spatial encoding (GPZ20=GPZ21)
;pgz21: coherence-selection gradients for spatial encoding (GPZ20=GPZ21)
;gpz24: pre- and post-mixing gradients
;gpz25: pre- and post-mixing gradients
;NS: 1 (or more if necessary)
;l3=number of loops for acquisition
;IMPORTANT: set d20 + d6 = DW x TD(F2)/(2xL3)
```

Pulse sequence for ultrafast MQ experiment for observation of odd order of coherences without refocusing

```
;MGCufmqsprds_odd_refocgp
;modifed by Corentin Jacquemmoz
;modifed by Maria Grazia Concilio (last modified on 180201)
;DS can be used, presat only during d3

;$CLASS=HighRes
;$DIM=2D
;$TYPE=
;$SUBTYPE=
;$COMMENT=

#include <Avance.incl>
#include <Grad.incl>
#include <De.incl>
#include <Delay.incl>

"d0=3u"
"d11=30m"
"d12=20u"
"d13=4u"
"p15=(td*dw/(2*l3))-d6"
"p24=p15"
;"d2=3u + 60*(p15-d6/2)"
"p2=2*p1"
;"d4=1s/(4*cnst1)"
;"d4=d5"
;"in2=2*(p15+d6)/td1"
"p26=p23"
"p21=p20"
"TAU = d1-d3"

1 ze
  d11 pl14:f2
  20u st0

2 30m
  TAU
  d3 cw:f2 ph29
  4u do:f2
  100u UNBLKGRAD
  20u pl1:f1

;excitation

  p1 ph1
  d4
  p2 ph3
  d4
  p1 ph4

;spatial encoding
```

```
  20u gron0
  p11:sp1:f1 ph1
  20u groff
  p20:gp20
  20u gron1
  p11:sp1:f1 ph2
  20u groff
  p21:gp21

;pre-mixing gradient
  10u
  p24:gp24
  10u

;mixing
  p23:gp23
  10u
  5u pl1:f1
  p10 ph2
  10u
  p26:gp26

;refocus
  d5
  p28:gp28
  d16
  p2 ph5
  d16
  p28:gp28
  d5

;post-mixing gradient
  10u
  p24:gp25
  10u

  d2

;acquisition
  ACQ_START(ph30,ph31)
  1u DWELL_GEN:f1
3 p15:gp15
  d6
  p15:gp16
  d6
  lo to 3 times l3
100u BLKGRAD
  rcyc=2
  100u UNBLKGRAD
;purge gradient
  p27:gp27
  100u BLKGRAD
  30m mc #0 to 2 F1QF(id2)
  d17
exit
```

```
ph1=0
ph2=0
ph4=1
ph3=0
ph5=1
ph29=0
ph30=0
ph31=0


;pl1 : f1 channel - power level for pulse (default)
;sp1: shaped pulse power level for selective detection
;p1 : f1 channel - 90 degree high power pulse
;p20: coherence-selection gradients for spatial encoding(p20=p21)
;p21: coherence-selection gradients for spatial encoding(p20=p21)
;spnam1 : shaped pulse for selective detection
;d1 : relaxation delay; 1-5 * T1
;d24 : pre-mixing gradient duration
;d25 : post-mixing gradient duration
;d17 : delay after experiment (not necessary)
;gpz0 : strength for excitation gradient [0-100]
;gpz1 : strength for reversed excitation gradient GPZ1 = -GPZ0
;gpz15 : strength for acquisition gradient [0-100]
;gpz16 : strength for reversed acquisition gradient GPZ16 = -GPZ15
;gpz20: coherence-selection gradients for spatial encoding (GPZ20=GPZ21)
;pgz21: coherence-selection gradients for spatial encoding (GPZ20=GPZ21)
;gpz24: pre- and post-mixing gradients
;gpz25: pre- and post-mixing gradients
;NS: 1 (or more if necessary)
;l3=number of loops for acquisition
;IMPORTANT: set d20 + d6 = DW x TD(F2)/(2xL3)
```

Pulse sequence for ultrafast COSY experiments with presaturation and excitation sculpting

```
;CJufcosyes
;Version with crushers around both chirp pulses
;modified by Corentin Jacquemmoz 29/11/2017
;UFCOSY with constant-time phase encoding

;$CLASS=HighRes
;$DIM=2D
;$TYPE=
;$SUBTYPE=
;$COMMENT=

#include <Avance.incl>
#include <Grad.incl>
#include <De.incl>
#include <Delay.incl>

"d0=3u"
"p2=2*p1"
"d11=30m"
"p15=(td*dw/(2*l3))-d6"
"p24=p15"
"d2=3u"
"in2=2*(p15+d6)/td1"
"DELTA = d1-d3"
"TAU=de+p1*2/3.1416+50u"

1 ze
  d11 pl9:f2
  20u st0

2 30m
  10u ;reset:f1:f2
  DELTA
  d3 cw:f2 ph29
  4u do:f2
  100u UNBLKGRAD
  20u pl1:f1

;excitation

  p1 ph1
  d10
  p20:gp20
  20u gron0
  p11:sp1:f1 ph1
  20u groff
  p20:gp21
  20u gron1
  p11:sp1:f1 ph2
  20u groff
  p20:gp22
```

```
;pre-mixing gradient
  20u
  p24:gp24
  10u

;mixing
  p23:gp23
  10u
  5u pl1:f1
  p1 ph1
  10u
  p26:gp26
  10u

;Excitation sculpting
  p6:gp7
  d16 pl0:f2
  (p12:sp2 ph2:r):f2
  4u
  d12 pl1:f1

  p2 ph3

  4u
  p6:gp7
  d16
  TAU
  p6:gp8
  d16 pl0:f1
  (p12:sp2 ph4:r):f2
  4u
  d12 pl1:f1

  p2 ph3

  4u
  p6:gp8
  d16

;post-mixing gradient
  10u
  p24:gp25
  10u

;acquisition
  ACQ_START(ph30,ph31)
  1u DWELL_GEN:f1
3 p15:gp15
  d6
  p15:gp16
  d6
  lo to 3 times l3
  100u BLKGRAD
  rcyc=2
```

```
  100u UNBLKGRAD
  p27:gp27
  100u BLKGRAD
  30m mc #0 to 2 F1QF(id2)
  d17
exit

ph1=0
ph2=0 1
ph3=0
ph4=0
ph29=0
ph30=0
ph31=0 2


;pl1 : f1 channel - power level for pulse (default)
;sp1: shaped pulse power level for selective detection
;p1 : f1 channel - 90 degree high power pulse
;p23 and p26: coherence-selection gradients for mixing(p23=p26)
;p20 and p21: coherence-selection gradients for spatial encoding(p20=p21)
;spnam1 : shaped pulse for selective detection
;d1 : relaxation delay; 1-5 * T1
;d3 : presaturation delay, MUST BE < D1
;d24 : pre-mixing gradient duration
;d25 : post-mixing gradient duration
;d17 : delay after experiment (not necessary)
;GPZ0 : strength for excitation gradient [0-100]
;GPZ1 : strength for reversed excitation gradient GPZ1 = -GPZ0
;GPZ15 : strength for acquisition gradient [0-100]
;GPZ16 : strength for reversed acquisition gradient GPZ16 = -GPZ15
;GPZ20 and GPZ21: coherence-selection gradients for spatial encoding (GPZ20=GPZ21)
;GPZ23 and GPZ26: coherence-selection gradients for mixing (GPZ26=-GPZ23)
;GPZ24 and GPZ25: pre- and post-mixing gradients
;GPNAM20=GPNAM21=GPNAM23=GPNAM26=SINE.100
;NS: 1 (or more if necessary)
;l3=number of loops for acquisition
;IMPORTANT: set d20 + d6 = DW x TD(F2)/(2xL3)
```

Pulse sequence for ultrafast COSY experiments with presaturation and WET

```
;CJufcosywetdc.gron
;avance-version (02/05/31)
;Version with crushers around both chirp pulses
;modified by patrick giraudeau 04/10/10
;modified by Corentin Jacquemmoz 29/11/2017
;UFCOSY with constant-time phase encoding

;$CLASS=HighRes
;$DIM=2D
;$TYPE=
;$SUBTYPE=
;$COMMENT=

#include <Avance.incl>
#include <Grad.incl>
#include <De.incl>
#include <Delay.incl>

"d0=3u"
"p2=2*p1"
"d11=30m"
"d15=(td*dw/(2*l3))-d6"
"p24=d15"
"d2=3u"
"in2=2*(p15+d6)/td1"
"DELTA = d1-d3"
"TAU=de+p1*2/3.1416+50u"

1 ze
  d11 pl9:f2
  20u st0

2 30m
  10u pl9:f2 ;reset:f1:f2
  DELTA
  d3 cw:f2 ph29
  4u do:f2

;WETdc
  50u UNBLKGRAD
  d12 pl0:f2
  20u cpd2:f3
  (p12:sp7 ph5):f2
  4u
  p16:gp11
  d16 pl0:f2
  (p12:sp8 ph6):f2
  4u
  p16:gp12
  d16 pl0:f2
  (p12:sp9 ph6):f2
  4u
  p16:gp13
```

```
  d16 pl0:f2
  (p12:sp10 ph6):f2
  4u do:f3
  p16:gp14
  d16
  10m pl1:f1

;excitation

  p1 ph1
  d10
  p20:gp20
  20u gron0
  p11:sp1:f1 ph1
  20u groff
  p20:gp21
  20u gron1
  p11:sp1:f1 ph2
  20u groff
  p20:gp22

;pre-mixing gradient
  20u
  p24:gp24
  10u

;mixing
  p23:gp23
  10u
  5u pl1:f1
  p1 ph1
  10u
  p26:gp26
  10u

;post-mixing gradient
  10u
  p24:gp25
  10u

;acquisition
  ACQ_START(ph30,ph31)
  5u cpd2:f3
  1u DWELL_GEN:f1
3 d15 gron15
  d6 groff
  d15 gron16
  d6 groff
  lo to 3 times l3
  100u BLKGRAD
  rcyc=2
  100u UNBLKGRAD
  p27:gp27
  100u BLKGRAD
  20u do:f3
```

```
  30m mc #0 to 2 F1QF(id2)
  d17
exit

ph1=0
ph2=0 1
ph3=0
ph4=0
ph5=0
ph6=1
ph29=0
ph30=0
ph31=0 2


;pl1 : f1 channel - power level for pulse (default)
;sp1: shaped pulse power level for selective detection
;p1 : f1 channel - 90 degree high power pulse
;p12: f1 channel -  90 degree shaped pulse

;p23 and p26: coherence-selection gradients for mixing(p23=p26)
;p20 and p21: coherence-selection gradients for spatial encoding(p20=p21)
;spnam1 : shaped pulse for selective detection
;d1 : relaxation delay; 1-5 * T1
;d3 : presaturation delay, MUST BE < D1
;d15 + d6 : acquisition gradient duration
;d24 : pre-mixing gradient duration
;d25 : post-mixing gradient duration
;d17 : delay after experiment (not necessary)
;GPZ0 : strength for excitation gradient [0-100]
;GPZ1 : strength for reversed excitation gradient GPZ1 = -GPZ0
;GPZ15 : strength for acquisition gradient [0-100]
;GPZ16 : strength for reversed acquisition gradient GPZ15 = -GPZ16
;GPZ20 and GPZ21: coherence-selection gradients for spatial encoding (GPZ20=GPZ21)
;GPZ23 and GPZ26: coherence-selection gradients for mixing (GPZ26=-GPZ23)
;GPZ24 and GPZ25: pre- and post-mixing gradients
;for z-only gradients for WET:
;gpz11: 80%
;gpz12: 40%
;gpz13: 20%
;gpz14: 10%
;NS: 1 (or more if necessary)
;l3=number of loops for acquisition
;IMPORTANT: set d15 + d6 = DW x TD(F2)/(2xL3)
```

Pulse sequence for ultrafast 3D DOSY-COSY experiments with presaturation

```
;CJbpledufcosy

;$CLASS=HighRes
;$DIM=3D
;$TYPE=
;$SUBTYPE=
;$COMMENT=

#include <Avance.incl>
#include <Grad.incl>
#include <De.incl>
#include <Delay.incl>

define list<gradient> diff=<Difframp>

"p2=p1*2"
"p7=2*p6"
"p21=p20"
"d0=3u"
"p15=(td*dw/(2*l3))-d6"
"p24=p15"
"d2=3u"
;"in2=2*(p15+d6)/td1"
"DELTA1=d20-p30*2-d16*7-p2-p6*2-p1*2-p7*2-p19-15u"
"TAU = d1-d3"

aqseq 321

1 ze
2 30m pl9:f2
  TAU
  d3 cw:f2 ph29
  5u do:f2
  5u pl2:f2
  50u UNBLKGRAD

  p19:gp7*-1
  d16

; excitation
  p1 ph1

; diffusion encoding with xy ctp gradients
  5u
  p6:gp10
  d16
  p30:gp6*diff
  d16
  p2 ph2
  5u
  p30:gp6*-1*diff
  d16
  p6:gp10
```

```
  d16

; storage
  p1 ph3
  5u
  p7:gp17*-1
  d16
  p19:gp7
  d16

  DELTA1

  p7:gp18*-1
  d16
; excitation
  p1 ph4

; diffusion decoding with xy ctp gradients
  5u
  p6:gp10
  d16
  p30:gp6*diff
  d16
  p2 ph2
  5u
  p30:gp6*-1*diff
  d16
  p6:gp10
  d16
  p1 ph5

;LED
  d21

;last excitation and spatial encoding
  p1 ph4
  20u ;d10
  20u gron0
  p11:sp1:f1 ph1
  20u groff
  p20:gp20
  20u gron1
  p11:sp1:f1 ph1
  20u groff
  p21:gp21

;pre-mixing gradient
  20u
  p24:gp24
  10u

;mixing
  p23:gp23
  10u
  5u pl1:f1
```

```
  p1 ph1
  10u
  p26:gp26

;post-mixing gradient
  10u
  p24:gp25
  10u

;acquisition
  ACQ_START(ph30,ph31)
  1u DWELL_GEN:f1
3 p15:gp15
  d6
  p15:gp16
  d6
  lo to 3 times l3
  100u BLKGRAD
  rcyc=2
  100u UNBLKGRAD
  100u BLKGRAD
  30m mc #0 to 2
          F1QF(id2)
          F2QF(igrad diff)
exit


ph1= 0
ph2= 0
ph3= 0
ph4= 0
ph5=0
ph29=0
ph30=0
ph31=0



;pl1 : f1 channel - power level for pulse (default)
;sp1: shaped pulse power level for selective detection
;p1 : f1 channel - 90 degree high power pulse
;p2 : f1 channel - 180 degree high power pulse
;p15 : Acquisition gradient
;p23 and p26: coherence-selection gradients for mixing(p23=p26)
;p20 and p21: coherence-selection gradients for spatial encoding(p20=p21)
;p19: gradient pulse 2 (spoil gradient)
;p30: gradient pulse (little DELTA * 0.5)
;spnam1 : shaped pulse for spatial encoding
;d1 : relaxation delay; 1-5 * T1
;d16: delay for gradient recovery
;d20 : Diffusion delay (BIG delta)
;d24 : pre-mixing gradient duration
;d25 : post-mixing gradient duration
;d17 : delay after experiment (not necessary)
;GPZ0 : strength for excitation gradient [0-100]
```

```
;GPZ1 : strength for reversed excitation gradient GPZ1 = -GPZ0
;GPZ15 : strength for acquisition gradient [0-100]
;GPZ16 : strength for reversed acquisition gradient GPZ15 = -GPZ16
;GPZ17 : Spoil
;GPZ18 : Spoil
;GPZ20 and GPZ21: coherence-selection gradients for spatial encoding (GPZ20=GPZ21)
;GPZ23 and GPZ26: coherence-selection gradients for mixing (GPZ26=-GPZ23)
;GPZ24 and GPZ25: pre- and post-mixing gradients
;NS: 1 (or more if necessary)
;l3=number of loops for acquisition
;IMPORTANT: set p15 + d6 = DW x TD(F2)/(2xL3)

;use AU-program dosy to calculate gradient-file Difframp
```

Pulse sequence for ultrafast 3D COSY i-DOSY experiments with presaturation

```
; CJufcosy_idosypr
;3D UFCOSY-iDOSY with constant-time phase encoding

;$CLASS=HighRes
;$DIM=3D
;$TYPE=
;$SUBTYPE=
;$COMMENT=

#include <Avance.incl>
#include <Grad.incl>
#include <De.incl>
#include <Delay.incl>

define list<gradient> diff=<Difframp>

"d0=3u"
"d11=30m"
"p15=(td*dw/(2*l3))-d6"
"p24=p15"
"in2=2*(p15+d6)/td1"
"TAU = d1-d3"
"DELTA1 = d20-p30-d16*3-p11*2-p20-p21-p24-p6*2-p1-105u"

aqseq 321

1 ze
  d11 pl9:f2
  20u st0
2 30m
  10u ;reset:f1:f2
  TAU
  d3 cw:f2 ph29
  4u do:f2
  100u UNBLKGRAD
  20u pl1:f1

;excitation

  p1 ph1
  20u

;Diffusion
  p30:gp6*diff
  d16
  DELTA1

;Spatial encoding
  20u gron0
  p11:sp1:f1 ph1
  20u groff
```

```
  p20:gp20
  20u gron1
  p11:sp1:f1 ph1
  20u groff
  p21:gp21

;pre-mixing gradient
  10u
  p24:gp24
  10u

;mixing
  5u pl1:f1
  p6:gp7
  d16
  p1 ph2
  4u
  p6:gp7
  d16

;diffusion decoding
p30:gp6*diff

;post-mixing gradient
  10u
  p24:gp25
  10u

  d2

;acquisition
  ACQ_START(ph30,ph31)
  1u DWELL_GEN:f1
3 p15:gp15
  d6
  p15:gp16
  d6
  lo to 3 times l3
  100u BLKGRAD
  rcyc=2
  100u UNBLKGRAD
  p27:gp27
  100u BLKGRAD
  30m mc #0 to 2
          F1QF(id2)
          F2QF(igrad diff)
  d17
exit

ph1=0 2 1 3
ph2=0 0 1 1
ph29=0 2 1 3
ph30=0 0 1 1
ph31=0 2 1 3
```

```
;pl1 : f1 channel - power level for pulse (default)
;sp1: shaped pulse power level for selective detection
;p1 : f1 channel - 90 degree high power pulse
;p15 : Acquisition gradient
;p23 and p26: coherence-selection gradients for mixing(p23=p26)
;p20 and p21: coherence-selection gradients for spatial encoding(p20=p21)
;spnam1 : shaped pulse for spatial encoding
;d1 : relaxation delay; 1-5 * T1
;d20 : Diffusion delay (BIG delta)
;d24 : pre-mixing gradient duration
;d25 : post-mixing gradient duration
;d17 : delay after experiment (not necessary)
;GPZ0 : strength for excitation gradient [0-100]
;GPZ1 : strength for reversed excitation gradient GPZ1 = -GPZ0
;GPZ15 : strength for acquisition gradient [0-100]
;GPZ16 : strength for reversed acquisition gradient GPZ16 = -GPZ15
;GPZ20 and GPZ21: coherence-selection gradients for spatial encoding (GPZ20=GPZ21)
;GPZ23 and GPZ26: coherence-selection gradients for mixing (GPZ26=-GPZ23)
;GPZ24 and GPZ25: pre- and post-mixing gradients
;NS: 1 (or more if necessary)
;l3=number of loops for acquisition
;IMPORTANT: set p15 + d6 = DW x TD(F2)/(2xL3)
```

Pulse sequence for ultrafast 3D DQS i-DOSY experiments with presaturation

```
;CJufdqs_idosy_3d
;3D sequence
;modified by Corentin Jacquemmoz
;UFDQSiDOSY with constant-time phase encoding
;with presaturation only during d3

;$CLASS=HighRes
;$DIM=3D
;$TYPE=
;$SUBTYPE=
;$COMMENT=

#include <Avance.incl>
#include <Grad.incl>
#include <De.incl>
#include <Delay.incl>

define list<gradient> diff=<Difframp>

"d0=3u"
"d11=30m"
"d12=20u"
"d13=4u"
"p15=(td*dw/(2*l3))-d6"
"p24=p15"
"p2=2*p1"
"d4=1s/(4*cnst1)"
"in2=2*(p15+d6)/td1"
"p26=p23"
"p21=p20"
"DELTA1 = d4-p30-d16"
"TAU = d1 - d3"

aqseq 321

1 ze
  d11 pl14:f2
  20u st0

2 30m
  TAU
  d3 cw:f2 ph29
  4u do:f2
  100u UNBLKGRAD
  20u pl1:f1

;excitation
  p1 ph1
; 1st diffusion gradient
  p30:gp6*diff
  d16
; build up of double-quanta coherence & big delta
  DELTA1
```

```
  p2 ph2
  DELTA1
; 2nd diffusion gradient
  p30:gp6*diff
  d16
; excitation of multiple-quanta coherences
  p1 ph2

;spatial encoding
  20u gron0
  p11:sp1:f1 ph1
  20u groff
  p20:gp20
  20u gron1
  p11:sp1:f1 ph2
  20u groff
  p21:gp21

;pre-mixing gradient
  10u
  p24:gp24
  10u

;mixing
  p23:gp23
  10u
  5u pl1:f1
  p10 ph2
  10u
  p26:gp26

;post-mixing gradient
  10u
  p24:gp25
  10u

  d2

;acquisition
  ACQ_START(ph30,ph31)
  1u DWELL_GEN:f1
3 p15:gp15
  d6
  p15:gp16
  d6
  lo to 3 times l3
  100u BLKGRAD
  rcyc=2
  100u UNBLKGRAD
;purge gradient
  p27:gp27
  100u BLKGRAD
  30m mc #0 to 2
          F1QF(id2)
          F2QF(igrad diff)
```

```
 d17
exit

ph1=0 2
ph2=0
ph3=0
ph29=0
ph30=0
ph31=0 2


;pl1 : f1 channel - power level for pulse (default)
;sp1: shaped pulse power level for selective detection
;p1 : f1 channel - 90 degree high power pulse
;p23: coherence-selection gradients for mixing(p23=p26)
;p26: coherence-selection gradients for mixing(p23=p26)
;p20: coherence-selection gradients for spatial encoding(p20=p21)
;p21: coherence-selection gradients for spatial encoding(p20=p21)
;spnam1 : shaped pulse for selective detection
;d1 : relaxation delay; 1-5 * T1
;d2 : Delay before acquisition
;d3 : delay for presaturation : must be < D1
;d4 : = 1s/(4*cnst1) = BIG DELTA/2
;d20 + d6 : acquisition gradient duration
;d24 : pre-mixing gradient duration
;d25 : post-mixing gradient duration
;d17 : delay after experiment (not necessary)
;gpz0 : strength for excitation gradient [0-100]
;gpz1 : strength for reversed excitation gradient GPZ1 = -GPZ0
;gpz15 : strength for acquisition gradient [0-100]
;gpz16 : strength for reversed acquisition gradient GPZ15 = -GPZ16
;gpz6 : strength for diffusion gradient [100]
;gpz20: coherence-selection gradients for spatial encoding (GPZ20=GPZ21)
;pgz21: coherence-selection gradients for spatial encoding (GPZ20=GPZ21)
;gpz23: coherence-selection gradients for mixing (GPZ26=-GPZ23)
;gpz26: coherence-selection gradients for mixing (GPZ26=-GPZ23)
;gpz24: pre- and post-mixing gradients
;gpz25: pre- and post-mixing gradients
;gpnam6: =SMSQ10.32
;NS: 1 (or more if necessary)
;l3=number of loops for acquisition
;IMPORTANT: set p15 + d6 = DW x TD(F2)/(2xL3)
```

Function to read SPEN DOSY acquisition parameters that will be used later in the program

```
function [complexdata,parameters,inputp,shapepulse]=readdosyparms(inputp)
% This program has been created by Ludmilla Guduff, Jean-Nicolas Dumez,
% Corentin Jacquemmoz and Achille Marchand
% CEISAM, CNRS, Université de Nantes, France
% The authors are not responsible for the results obtained with this
program
% This program can be used, modified and shared as long as the authors are
% credited and the program is share under the same conditions
% Please do not delete this header from the file.
%
%-----------------------

%Read acquisqition parameters

acquparams = readacqus([inputp.pathexp num2str(inputp.diffexpno)
'/acqus']); % structure for acquisition parameter
acquparams2 = readacqus([inputp.pathexp num2str(inputp.diffexpno)
'/acqu2s']);
shapepulse= readacqus([inputp.pathexp num2str(inputp.diffexpno)
'/spnam1']); % Structure of shapepulse

% shapepulse parameters for now only chirp
if isfield(shapepulse,'SHL_SW') == 1
    parameters.BW=shapepulse.SHL_SW(1);
    parameters.tau=shapepulse.SHAPE_LENGTH(1)*10^(-6);
else
    shapeparam = textscan(shapepulse.SHAPE_PARAMETERS, '%s');
    BWind = find(strcmp(shapeparam{1},'[Hz]'),1,'first');
    parameters.BW = str2double(cell2mat(shapeparam{1}(BWind+1)));
    tauind = find(strcmp(shapeparam{1},'[usec]'),1,'first');
    parameters.tau = str2double(cell2mat(shapeparam{1}(tauind+1)))*1e-6;
end

%do not work good for QS yet
 shapepulse_temp=shapepulse.XYPOINTS;
 shapepulse_temp(1:9)=[];
 shapepulse_temp=str2num(shapepulse_temp);
 parameters.chirpfile=[shapepulse_temp(1:2:end);
shapepulse_temp(2:2:end)]';

Gdosy = [acquparams.GPX(3) acquparams.GPY(3) acquparams.GPZ(3)];

if length(Gdosy(Gdosy~=0)) == 1 % Check that acquisition has been done on
only one axis
    if Gdosy(1) >0
        parameters.DOSYaxis = 'X';
    elseif Gdosy(2) >0
        parameters.DOSYaxis = 'Y';
    elseif Gdosy(3) >0
        parameters.DOSYaxis = 'Z';
    end
else
    error('The acquisition has been done on a double axis. This option is
not implemented.')
end

% Merge parameters into the omnistructure of parameters
```

```
parameters.Ni=1; % number of interleaves TD2
parameters.N2 = acquparams.L(4); % number of loops in the acquisition
parameters.SW = acquparams.SW_h;% spectral width
parameters.NP = acquparams.TD/2; % total number of points in one fid
parameters.dw = 1/(parameters.SW); % dwell time
parameters.B0 = acquparams.BF1; % spectrometer frequency
parameters.offsetconv=acquparams.O1/parameters.B0; % offset
parameters.D6=acquparams.D(7); % acquisition gradient duration
parameters.td=acquparams.TD; % time domain size
% offsetconv=acquparams.O1/parameters.B0; % offset
byte_format = acquparams.BYTORDA;
byte_size = acquparams.DTYPA;
[GmaxZ,GmaxY,GmaxX] = gradparlist(acquparams.PROBHD);
switch parameters.DOSYaxis % find witch gradient to include in parameters
    case 'X'
        Gacq = abs(acquparams.GPX(3));
        parameters.Gdmax= GmaxX; %(T/m=10^-2*G/cm) maximum gradient
amplitude
        parameters.GPZ0=acquparams.GPX(1)/100; % strength for excitation
gradient
    case 'Y'
        Gacq = abs(acquparams.GPY(3));
        parameters.Gdmax= GmaxY; %(T/m=10^-2*G/cm) maximum gradient
amplitude
        parameters.GPZ0=acquparams.GPY(1)/100; % strength for excitation
gradient
    case 'Z'
        Gacq = abs(acquparams.GPZ(3));
        parameters.Gdmax= GmaxZ; %(T/m=10^-2*G/cm) maximum gradient
amplitude
        parameters.GPZ0=acquparams.GPZ(1)/100; % strength for excitation
gradient
end


parameters.Ta= ((parameters.NP*parameters.dw)/(2*parameters.N2));
%Acquisiton Time

% parameters.offsetconv=offsetconv;
parameters.B0 = acquparams.BF1; % spectrometer frequency
parameters.Gacq=Gacq; % acquisition gradient
parameters.gamma1H = nuclist(acquparams.NUC1); % rad/s.T
parameters.D30=acquparams.D(31); % diffusion time big DELTA (s)
parameters.P1=acquparams.P(2)*10^(-6); % hard pulse duration in us
parameters.d11= acquparams.D(12); % extra dephasing period (s)
parameters.dscale=1e-10;% diffusion coefficient scale
parameters.spoff=acquparams.SPOFFS(2); % shapulse offset

if isfield(acquparams, 'SPW') == 1
    parameters.SPW1=acquparams.SPW(2); % watt hard pulse
    parameters.PLW1=acquparams.PLW(2); % watt shape pulse

parameters.gammaB1=1/(parameters.P1*4)*(parameters.SPW1/parameters.PLW1)^(1
/2);% pulse strength
else
    parameters.SP1=acquparams.SP(2);% ?
    parameters.PL1=acquparams.PL(2); % ?
    parameters.gammaB1=1/(parameters.P1*4)*10^(-(parameters.SP1-
parameters.PL1)/20);% ??? pulse strength in dB ????
end
```

```
    complexdata_full = readfid([inputp.pathexp num2str(inputp.diffexpno)
'/ser'],byte_format,byte_size); %read the ser and the byte format/size
    complexdata=complexdata_full((inputp.numscan-
1)*parameters.td/2+1:(inputp.numscan)*parameters.td/2);

        complexdata_full = complexdata ;

% Select the region of fitting based on the diffusion axis

switch parameters.DOSYaxis
    case 'Z'
        parameters.fitLengthNeg = inputp.fitLengthLongN;
        parameters.fitLengthPos = inputp.fitLengthLongP;
    case {'X', 'Y'}
        parameters.fitLengthNeg = inputp.fitLengthTransN;
        parameters.fitLengthPos = inputp.fitLengthTransP;
end

% Remove the group delay
    nD=acquparams.GRPDLY;
    chop=floor(nD) ;
    complexdata = circshift(complexdata,-chop);
    parameters.p= (nD-chop);

end
```

Function used in the SPEN DOSY processing to obtain the spectroscopic image

```
function
[rwdata,dispaxisufdosy,ppm_axis,SWconv_axis,parameters]=epsiproc(complexdat
a,parameters,inputp)
% This program has been created by Ludmilla Guduff, Jean-Nicolas Dumez
% Corentin Jacquemmoz and Achille Marchand
% CEISAM, CNRS, Université de Nantes, France
% The authors are not responsible for the results obtained with this
program
% This program can be used, modified and shared as long as the authors are
% credited and the program is share under the same conditions
% Please do not delete this header from the file.
%
% description : processing from raw epsi to spectroscopic imaging data
% it need 2 structure that are shaped previously : inputp and parameters
and
% a set of data " complexdata "
% (in order of use)
% parameters : N2 ; Ni; NP; TA ;B0 ; offsetconv ; SW ; gamma1H ; Gdmax ;
Gacq
% inputp : NBC2 ; alpha ; nZFK ; pathexp ; diffexpno ; pathFig ; figonoff
%*************************************************************************

% Reshape the data
parameters.NT = 2*parameters.N2*parameters.Ni;
parameters.NK = parameters.NP/(2*parameters.N2);
ktdata = reshape(complexdata,parameters.NK,parameters.NT);

% % Remove the offset
DC_offset1=ktdata(1:inputp.NBC2,:);
DC_offset1=mean(DC_offset1,1);
DC_offset1=mean(DC_offset1,2);
ktdata=ktdata-DC_offset1;

% Apodization in uf dimension (k)
procufaxis = linspace(-0.5,0.5,parameters.NK)';
procufaxis=reshape(procufaxis,parameters.NK,1);
ktdata = ktdata.* repmat(((1-
inputp.alpha)+inputp.alpha*cos(2*pi*procufaxis)),1,parameters.NT);

% zero filling in the ultrafast dimension
inputp.nZFK=max(inputp.nZFK,parameters.NK);
ktdatazf = zeros(inputp.nZFK,parameters.NT);
ktdatazf(1+(inputp.nZFK-parameters.NK)/2:parameters.NK+(inputp.nZFK-
parameters.NK)/2,:) = ktdata;

% Process only the odd echoes
ktdataoddseq = ktdatazf(:,1:2:2*parameters.N2*parameters.Ni-1);


if parameters.Ni == 1

    ktdataodd = ktdataoddseq;

else

    % Interleave the data
    ktdataodd = zeros(size(ktdataoddseq));
```

```
    for k = 1:parameters.N2
        for l = 1:parameters.Ni
            ktdataodd(:,(k-1)*parameters.Ni+l) =
ktdataoddseq(:,k+parameters.N2*(l-1));
        end
    end
end

% Shearing step to correct unbalanced acquisition gradients
if  exist ([inputp.pathexp num2str(inputp.diffexpno)
'/shearval.txt'],'file') == 0
    [ktdataodd,shearvalue] = shear_gui(ktdataodd);
    shearfile = fopen([inputp.pathexp num2str(inputp.diffexpno)
'/shearval.txt'],'w');
    fprintf(shearfile, '%f', shearvalue);
    fclose(shearfile);
else
    shearquest = questdlg('Shearing has already been done. Do you want to
use the already existing file ?',...
        'Shearing file', 'Yes', 'No', 'Yes');
    switch shearquest
        case 'Yes'
            shearfile = fopen([inputp.pathexp num2str(inputp.diffexpno)
'/shearval.txt'],'r');
            shearvalue = fscanf(shearfile, '%f');
            fclose(shearfile);
            linshear = linspace(0,shearvalue,size(ktdataodd,2));
            for i=1:size(ktdataodd,2)

                ktdataodd(:,i) = CJshear(ktdataodd(:,i),0,linshear(i));
            end
        case 'No'
            [ktdataodd,shearvalue] = shear_gui(ktdataodd);
            shearfile = fopen([inputp.pathexp num2str(inputp.diffexpno)
'/shearval.txt'],'w');
            fprintf(shearfile, '%f', shearvalue);
            fclose(shearfile);
    end
end


% Window multiplication in the conventional dimension
 switch inputp.phmode
     case 'mc'
        procconvaxis = linspace(0,1,parameters.N2*parameters.Ni);
        ktdataodd = ktdataodd .*
repmat(sin(pi*(procconvaxis)),inputp.nZFK,1);
     case 'pk'
         procconvaxis = linspace(0,1,parameters.N2*parameters.Ni);
         ktdataodd = ktdataodd .* repmat(cos(pi/2*(procconvaxis)).^2,
inputp.nZFK,1);
         ktdataodd(:,1) = 0.5*ktdataodd(:,1);
     otherwise
         errordlg ('inputp.phmode should be either mc or pk')
end

% Zero fill in the conventional dimension "nZFT"
inputp.nZFT = max(inputp.nZFT,parameters.N2*parameters.Ni); %find the size
of matrix
ktdataoddzf = zeros(inputp.nZFK,inputp.nZFT);% create the zero matrix
```

```
ktdataoddzf(:,1:parameters.N2*parameters.Ni) = ktdataodd; % put the data in
this matrix
ktdataodd = ktdataoddzf;

% Fourier tranform
switch inputp.phmode
    case 'mc'
kwdata = fftshift(fft(fftshift(ktdataodd,2),[],2),2);
rwdata = fftshift(fft(fftshift(kwdata,1),[],1),1);
rwdata = abs(rwdata);
    case 'pk'
        kwdata = fftshift(fft(ktdataodd,[],2),2);
rwdata = fftshift(fft(fftshift(kwdata,1),[],1),1);
[rwdataph]=uf_ph_man(rwdata,inputp);
rwdata = real(rwdataph);
 otherwise
         errordlg ('inputp.phmode should be either mc or pk')
end

% ppm Axis for data plotting
SWconv=1/(2*parameters.Ta)/parameters.B0;parameters.SWconv=SWconv;
ppm_axis=linspace(0.5,-0.5,inputp.nZFT)'*SWconv+parameters.offsetconv;
%(ppm)
SWconv_axis=linspace(0.5,-0.5,inputp.nZFT)'*1/(2*parameters.Ta); %(Hz)


%lenght (mm) Axis for data plotting:
dispaxisufdosy = linspace(0.5,-
0.5,inputp.nZFK)'*parameters.SW*2*pi/(parameters.gamma1H*parameters.Gdmax*p
arameters.Gacq/100); % FOV (mm)
dispaxisufdosy=flipud(dispaxisufdosy);

ppm_axis=flipud(ppm_axis);


% Find artefact location
artefact_pos=abs(ppm_axis-parameters.offsetconv);
artefact_ind=find(min((artefact_pos))==artefact_pos);
artefact_range=artefact_ind(1)-10-
(inputp.nZFT/parameters.N2/parameters.Ni):artefact_ind(1)+10+(inputp.nZFT/p
arameters.N2/parameters.Ni);
parameters.artefact_range=artefact_range;


switch inputp.figonoff
    case 'on'
        %Stacked plot representation
        figure;
        %fig.Renderer= 'painters';
        xMat = repmat(ppm_axis, 1, numel(dispaxisufdosy));
        yMat = repmat(dispaxisufdosy',numel(ppm_axis), 1);

plot3(xMat(1:1:end,1:1:end),yMat(1:1:end,1:1:end),rwdata(1:1:end,1:1:end)'/
max(rwdata(:)),'b');
        axis( [ppm_axis(1) ppm_axis(end) dispaxisufdosy(1)
dispaxisufdosy(end) 0 1])
        xlabel('ppm');
        ylabel('Zaxis(m)');
        ax=gca;
        set(ax,'Xdir','reverse');
```

```
        % save the figure
        if nargin>8
            cd(inputp.pathFig);
            saveas(gcf,['diffexpno_' num2str(inputp.diffexpno)
'_wtf_mc.fig'])
        end
    case 'off'
        %'no figure is displayed'

     otherwise
         errordlg ('inputp.figonoff should be either on or off')
end
end
```

Function to fit SPEN DOSY diffusion profiles to Stejskal-Tanner equation

```
function
[peakdata]=uf_fit(dispaxisufdosy_im,rdataufdosy_im,range_im,refdata,paramet
ers,inputp)
% This program has been created by Ludmilla Guduff, Jean-Nicolas Dumez,
% Corentin Jacquemmoz and Achille Marchand
% CEISAM, CNRS, Université de Nantes, France
% The authors are not responsible for the results obtained with this
program
% This program can be used, modified and shared as long as the authors are
% credited and the program is share under the same conditions
% Please do not delete this header from the file.
%
% structure needed parameters with
% .gamma1H;Gdmax;GPZ0;.BW;.pi;.NK;fitfraction;sizeaxis;.omega;Gacq;.spoff;
.fitLengthPos;.fitLengthNeg
% and inputp with .figonoff .fitcode

% Select a region
zaxis_raw=dispaxisufdosy_im(range_im);% Axis

peak_raw=rdataufdosy_im(range_im)'; % data


% Region swept by the chirp during spatial encoding.
sweepsize
=parameters.BW*2*pi/(parameters.gamma1H*parameters.Gdmax*parameters.GPZ0);
R = (parameters.BW*2*pi)/parameters.tau; % rad/s^2
Ge= parameters.Gdmax*parameters.GPZ0; % encoding gradient

% Number of gradient level
ngradlevel=ceil(parameters.NK*sweepsize*parameters.fitfraction/(parameters.
sizeaxis)); % not used?

% Axis correction by offset
axis_omega=parameters.omega/...
    (parameters.gamma1H*parameters.Gdmax*parameters.Gacq/100);
zaxis_rawC=zaxis_raw-axis_omega;


parameters.omega_exc = parameters.omega-parameters.spoff*2*pi;

axis_omega_exc=parameters.omega_exc/...
    (parameters.gamma1H*parameters.Gdmax*parameters.GPZ0);

switch inputp.figonoff
    case 'on'
        axis([-sweepsize/2*0.8 sweepsize/2*0.8 0 1])
    case 'off'
    otherwise
        errordlg('inputp.figonoff need to be on or off ; l 39 uf_fit.m')
        edit
end


%definition of ydata
samplelenght=find(zaxis_rawC<(parameters.fitLengthPos)-axis_omega_exc...
    & zaxis_rawC>(parameters.fitLengthNeg)-axis_omega_exc);

%  Take only the data to be fitted
```

```
zi=samplelenght(1);
zf=samplelenght(end);
% Find the range of z values that are within the user-defined bounds
switch inputp.fitcode
    case 'keeler'
        peak=peak_raw(zi:zf)/peak_raw(zi);
        ydata=peak;
    case 'frydman'
        ydata=peak_raw(zi:zf)/peak_raw(zi);
    case 'QS'
        ydata=peak_raw(zi:zf)/peak_raw(zi);
        %ref=refdata(zi:zf);
        otherwise
        errordlg('inputp.fitcode need to be keeler frydman or QS')
end

zaxis=zaxis_raw(zi:zf);

% optionally correct by the reference profile;
switch parameters.refonoff
    case 'on'
        yrefinterp = interp1(refdata.raxis,refdata.rdata,zaxis);
        yrefinterp = yrefinterp/max(yrefinterp);
        ydata = ydata/max(ydata);
        %plot(zaxis,ydata,'r');
        hold all
        %plot(zaxis_raw(zi:zf),ydata,'r');
        %plot(zaxis,yrefinterp,'b');
        ydata = ydata./yrefinterp;
        plot(zaxis,ydata,'+b');
    case 'off'
        ydata = ydata;
    otherwise
        errordlg('parameters.refonoff should be either on or off')
end


% SPEN parameters
R = (parameters.BW*2*pi)/parameters.tau; % rad/s^2
Ge= parameters.Gdmax*parameters.GPZ0; % encoding gradient

RFlist = parameters.chirpfile;
RFval = RFlist(:,1)';
RFval = RFval*2*pi*parameters.gammaB1/100; % gammaB1(t) in rad/s

%Frequency of RF sweep in  rad/s
tsweep = linspace(-0.5,0.5,length(RFlist));
RFsweep = (R*tsweep*parameters.tau);

% This formula is used with NLS_pulse ranging from ""dv/2 to -dv/2"" %
% additional gradient is used ""after"" the chirp pulse
tflip=parameters.tau.*...
    (1-sqrt(-parameters.gamma1H*Ge.*zaxis_raw./(2*pi*parameters.BW)+0.5));

% Effective gradient
b=parameters.gamma1H*Ge;
tpaxis=linspace(0,parameters.tau,length(RFlist));
listGeff=zeros(length(ydata),length(RFlist));

for z=1:length(zaxis)
    dWeff=(parameters.omega_exc*b-b*RFsweep+b^2*zaxis(z))./...
```

```
        sqrt((parameters.omega_exc+b*zaxis(z)-RFsweep).^2+ RFval.^2);
%dWeff/dz
    listGeff(z,:)=dWeff;
    G(z)=trapz(tpaxis,listGeff(z,:));  % integral
end

Geff=G/(parameters.gamma1H*parameters.tau);

% Effective gradient area
switch inputp.fitcode
    case 'keeler'
        Aeff = Geff*parameters.tau+Ge*parameters.d11;
        xdata =Aeff';
    case 'frydman'
        xdata=2*parameters.gamma1H*Ge^2/R*zaxis+Ge*parameters.d11;
    case 'QS'
        tflip=real(tflip);
        Phase_variation_calc=-parameters.gamma1H*Ge.*(2*parameters.tau-
2*tflip);
        xdata=Phase_variation_calc(zi:zf);
         otherwise
        errordlg('inputp.fitcode need to be keeler frydman or QS')
end

% Exponential function simplification S(z)=S0*exp(-
gamma^2*Aeff.^2*Dtrial*DELTA)
x0=[1 4.93];
if inputp.fitcode == "QS"
    expfactor = (parameters.D30-parameters.tau)*parameters.dscale ;
    F = @(x,xdata)x(1)*exp(-x(2)*expfactor*xdata.^2);

else

    switch inputp.fitmode
        case 'STE'
            expfactor=parameters.gamma1H^2*(parameters.D30-
(parameters.tau+parameters.d11)/2)*parameters.dscale;
            F = @(x,xdata)x(1)*exp(-x(2)*expfactor*xdata.^2);

        case 'DSTE'
            expfactor=parameters.gamma1H^2*(parameters.D30-
(parameters.tau+parameters.d11))*parameters.dscale;
            F = @(x,xdata)x(1)*exp(-x(2)*expfactor*xdata.^2);

        case 'ADSE'
            %adseph
            expfactor_red=parameters.gamma1H^2*parameters.dscale;
            delta_b=parameters.D30-4*parameters.tau;
            delta_a=2*(parameters.tau+parameters.d11)/sweepsize;
            F = @(x,xdata)x(1)*exp(-
x(2)*expfactor_red*(delta_a*zaxis+delta_b).*xdata.^2);

        case 'ASE'
            expfactor=parameters.gamma1H^2*(parameters.D30-
(3*parameters.tau+parameters.d11)/4)*parameters.dscale;
            F = @(x,xdata)x(1)*exp(-x(2)*expfactor*xdata.^2);

        case 'SE'
            expfactor_red=parameters.gamma1H^2*parameters.dscale;
            delta_b=parameters.D30-2*parameters.tau;
            delta_a=(parameters.tau+parameters.d11)/sweepsize;
```

```
            F = @(x,xdata)x(1)*exp(-
x(2)*expfactor_red*(delta_a*zaxis+delta_b).*xdata.^2);
          otherwise
        errordlg('inputp.fitcode need to QS if you use QS with STE
sequence. Otherwise (with keeler and frydman) 5 option are available : STE
DSTE ASE ADSE SE')
    end
end

options = optimoptions(@lsqcurvefit,'Display','off');

[x,resnorm,residual,exitflag,output,lambda,jacobian]=...
    lsqcurvefit(F,x0,xdata,ydata,[],[],options);

CM=full(inv(jacobian'*jacobian));%  covariance matrix
sderr=0;

for jj=1:2
    sderr(jj)=sqrt(resnorm/(length(ydata)-2))*sqrt(CM(jj,jj));
end

sderr=real(sderr);
peakdata.RESIDUAL=residual;
peakdata.outputDATA=F(x,xdata);
peakdata.inputDATA=ydata;
peakdata.originalDATA=rdataufdosy_im(range_im)';
peakdata.originalAXIS=zaxis_raw;
peakdata.npoint=length(ydata);
peakdata.originalnpoint=length(zaxis_raw);
peakdata.FITSTATS=[x(1) sderr(1) x(2) sderr(2)];
peakdata.gradarea=xdata;
peakdata.zposition=zaxis;

switch inputp.figonoff
    case 'on'
        plot(zaxis,ydata,'ro');
        hold on
        plot(zaxis,F(x,xdata),':');
        title(['D = ',num2str(round(x(2),2)), ' STD =
',num2str(round(sderr(2),2))...
            , ' \delta =
',num2str(round(parameters.ppm_index_max,2)),'ppm'])
        %legend('Original data','fitted data')
        xlabel('Z (m)');
        axis([-sweepsize/2*0.8 sweepsize/2*0.8 0 inf])
        ax=gca;
        ax.YLimMode = 'manual';
        %ax.YTick = 0:0.1:1;
    case 'off'
        %'no figure is displayed'

    otherwise

        error('figonoff should be either on or off')
end
```

Function to process uf spectra with spatial encoding of the chemical shift (ufCOSY, ufDQS…)

```
function [kwdata,ufaxis,convaxis] =
ufproc(expno,pathexp,conv2ufscale,conv2ufoffset,delta,n_data)
% This program has been created by Jean-Nicolas Dumez and Corentin
Jacquemmoz,
% CEISAM, CNRS, Université de Nantes, France
% The authors are not responsible for the results obtained with this
program
% This program can be used, modified and shared as long as the authors are
% credited and the program is share under the same conditions
% Please do not delete this header from the file.
%
% UFPROC loads and processes ultrafast NMR data.
% Processing parameters must be given in the function body
% The path to the data must be given as well.
% expno: experiment number in topspin
% conv2ufscale: ratio between the conv and uf dimensions
% conv2ufoddset: difference in offset between the conv and uf dimensions
% delta: relative intensity of the minimum contour level with respect to
% the maximum intensity in the spectrum.
% n_data=number of spectra to process (when they are more then one).

% Define some processing parameters
sigmaproc = 3; % standard deviation of the gaussian window, in mm
muproc = 0; % offset of the gaussian window, in mm
nZFconv = 1024; % zero filling in the conventional dimension
nZFuf = 1024; % zero filling in the ultrafast dimension
convsrppm = 0;
d6cut = 60; % number of points cut to reduce 'd6 atifacts', MUST BE >=0,
NOT USED ANYMORE

% Define the path as in the example:
%pathexp = '/data_Gif/data/corentin/nmr/190107_Melange_alcools/';

if nargin < 6
    n_data=0;
end

% End of the data set
final=expno+n_data;

% Load the data
for expno=expno:final

    % Load the parameters
    acquparams = readacqus([pathexp num2str(expno) '/acqus']);
    acquparams2 = readacqus([pathexp num2str(expno) '/acqu2s']);

    % Some parameters are needed for processing and display
    Ni = acquparams2.TD;  % number of interleaves
    N2 = acquparams.L(4); % number of loops in the acquisition
    SW = acquparams.SW_h; % spectral width
    NP = acquparams.TD/2; % total number of points in one fid
    dw = 1/(SW); % dwell time
    B0 = acquparams.BF1; % spectrometer frequency
    offsetconv=acquparams.O1/B0; % offset
    Gacq =
[abs(acquparams.GPX(16)),abs(acquparams.GPY(16)),abs(acquparams.GPZ(16))];
```

```
    [GmaxZ,GmaxY,GmaxX] = gradparlist(acquparams.PROBHD);
    %Gmax = GmaxZ*100;
    byte_format = acquparams.BYTORDA;
    byte_size = acquparams.DTYPA;

    if length(Gacq(Gacq~=0)) == 1 % Check that acquisition has been done on
only one axis
        if Gacq(1) > 0
            Gacq = Gacq(1);
            Gmax = GmaxX*100;
        elseif Gacq(2) > 0
            Gacq = Gacq(2);
            Gmax = GmaxY*100;
        elseif Gacq(3) > 0
            Gacq = Gacq(3);
            Gmax = GmaxZ*100;
        end
    else
        error('The acquisition has been done on a double axis. This option
is not implemente.')
    end

    % Load the data
    complexdata = readfid([pathexp num2str(expno)
'/ser'],byte_format,byte_size);


% Correct the number of points
    NT = 2*N2*Ni;
    NK = NP/(2*N2);
    complexdata(NT*NK+1:end) = [];

    if acquparams.GRPDLY>1
        nD=acquparams.GRPDLY;
        chop=floor(nD);
        complexdata = circshift(complexdata,-chop);
        parameters.p= (nD-chop);
    end

    % Reshape the data
    ktdata = reshape(complexdata,NK,NT);

    % Remove the offset
    ktdata=ktdata-mean(ktdata(:));

    % Window multiplication and zero filling in the ultrafast dimension
    SWacq = SW;
    FOV = SWacq / (Gmax * (Gacq / 100) * 425.7); % FOV in the uf dimension
    rtdata = fftshift(fft(fftshift(ktdata,1),[],1),1);
    procufaxis = linspace(0,FOV,NK)'-FOV/2;
    rtdata = rtdata .* ...
        repmat(exp(-(procufaxis-muproc).^2/(2*sigmaproc^2)),1,NT);
    nZFuf=max(nZFuf,NK);
    rtdatazf = zeros(nZFuf,NT);
    rtdatazf(1+round((nZFuf-NK)/2):NK+round((nZFuf-NK)/2),:) = rtdata;
    ktdata = fftshift(ifft(fftshift(rtdatazf,1),[],1),1);

    % Process only the odd echoes
    ktdataoddseq = ktdata(:,1:2:2*N2*Ni-1);
    %ktdataoddseq = ktdata(:,2:2:2*N2*Ni);
```

```
    % Interleave the data
    if Ni == 1

        ktdataodd = ktdataoddseq;

    else

        ktdataodd = zeros(size(ktdataoddseq));
        for k = 1:N2
            for l = 1:Ni
                ktdataodd(:,(k-1)*Ni+l) = ktdataoddseq(:,k+N2*(l-1));
            end
        end

    end

    % Window multiplication in the conventional dimension
    procconvaxis = linspace(0,1,N2*Ni);
    ktdataodd = ktdataodd .* repmat(sin(pi*(procconvaxis)),nZFuf,1);

    % Zero fill in the conventional dimension
    nZFconv = max(nZFconv,N2*Ni);
    ktdataoddzf = zeros(nZFuf,nZFconv);
    ktdataoddzf(:,1:N2*Ni) = ktdataodd;
    ktdataodd = ktdataoddzf;

    % Fourier tranform in the conventional dimension
    kwdata = fftshift(fft(fftshift(ktdataodd,2),[],2),2);

    % Magnitude mode
    kwdata = abs(kwdata);

end

% Plot with topspin-like contours
k = 1.8;
ncont = 8;
xmax=max(kwdata(:)); % contour level calculated as fraction of the most
intense peak
positive_contours=delta*xmax*cumprod([1 k*ones(1,ncont-1)]);

% Calculate some plotting parameters
Ta = dw * NP / N2 / 2;
swconv = Ni/(2*Ta)/B0;
swuf = swconv * conv2ufscale;
offsetuf = offsetconv + conv2ufoffset;
ufaxis = linspace(0.5,-0.5,nZFuf)*swuf+offsetuf;
convaxis = linspace(0.5,-0.5,nZFconv)'*swconv+offsetconv+convsrppm;
%ufaxis = ufaxis/4;

% Plot
% New version using the plotuf2D_gui
plotuf2D_gui(kwdata,ufaxis,convaxis);

% Old version
% figure
% h1 = axes;
%contour(convaxis,ufaxis,abs(flipud(kwdata)),positive_contours,'k');
%imagesc(convaxis,ufaxis(1+d6cut:end-d6cut),abs(rot90(kwdata(1+d6cut:end-
d6cut,:),2)));
```

```
%imagesc(convaxis,ufaxis(1+d6cut:end-d6cut),abs(fliplr(kwdata(1+d6cut:end-
d6cut,:))));
% contour(convaxis,ufaxis(1+d6cut:end-d6cut),abs(fliplr(kwdata(1+d6cut:end-
d6cut,:))),positive_contours,'k');
%contour(convaxis,ufaxis(1+d6cut:end-d6cut),abs(rot90(kwdata(1+d6cut:end-
d6cut,:),2)),positive_contours,'k');
% axis square;
% set(h1,'XDir','reverse')
% set(h1,'YDir','reverse')
%setnmraxes

end
```

References

(1) Schanda, P.; Brutscher, B. Very Fast Two-Dimensional NMR Spectroscopy for Real-Time Investigation of Dynamic Events in Proteins on the Time Scale of Seconds. *J. Am. Chem. Soc.* **2005**, *127* (22), 8014–8015. https://doi.org/10.1021/ja051306e.

(2) Kupče, E.; Nishida, T.; Freeman, R. Hadamard NMR Spectroscopy. *Prog. Nucl. Magn. Reson. Spectrosc.* **2003**, *42* (3–4), 95–122. https://doi.org/10.1016/S0079-6565(03)00022-0.

(3) Kupče, Ē.; Freeman, R. Two-Dimensional Hadamard Spectroscopy. *J. Magn. Reson.* **2003**, *162* (2), 300–310. https://doi.org/10.1016/S1090-7807(02)00196-9.

(4) Kupče, Ē.; Freeman, R. Frequency-Domain Hadamard Spectroscopy. *J. Magn. Reson.* **2003**, *162* (1), 158–165. https://doi.org/10.1016/S1090-7807(02)00194-5.

(5) Kazimierczuk, K.; Orekhov, V. Yu. Accelerated NMR Spectroscopy by Using Compressed Sensing. *Angew. Chem. Int. Ed.* **2011**, *50* (24), 5556–5559. https://doi.org/10.1002/anie.201100370.

(6) Frydman, L.; Scherf, T.; Lupulescu, A. The Acquisition of Multidimensional NMR Spectra within a Single Scan. *Proc. Natl. Acad. Sci.* **2002**, *99* (25), 15858–15862. https://doi.org/10.1073/pnas.252644399.

(7) Frydman, L.; Lupulescu, A.; Scherf, T. Principles and Features of Single-Scan Two-Dimensional NMR Spectroscopy. *J. Am. Chem. Soc.* **2003**, *125* (30), 9204–9217. https://doi.org/10.1021/ja030055b.

(8) Stejskal, E. O.; Tanner, J. E. Spin Diffusion Measurements: Spin Echoes in the Presence of a Time-Dependent Field Gradient. *J. Chem. Phys.* **1965**, *42* (1), 288–292. https://doi.org/10.1063/1.1695690.

(9) Guduff, L.; Kuprov, I.; van Heijenoort, C.; Dumez, J.-N. Spatially Encoded 2D and 3D Diffusion-Ordered NMR Spectroscopy. *Chem. Commun.* **2017**, *53* (4), 701–704. https://doi.org/10.1039/C6CC09028A.

(10) Jerschow, A.; Müller, N. Suppression of Convection Artifacts in Stimulated-Echo Diffusion Experiments. Double-Stimulated-Echo Experiments. *J. Magn. Reson.* **1997**, *125* (2), 372–375. https://doi.org/10.1006/jmre.1997.1123.

(11) Manjunatha Reddy, G. N.; Mannina, L.; Sobolev, A. P.; Caldarelli, S. Polyphenols Fingerprinting in Olive Oils Through Maximum-Quantum NMR Spectroscopy. *Food Anal. Methods* **2018**, *11* (4), 1012–1020. https://doi.org/10.1007/s12161-017-1069-x.

(12) Rouger, L.; Gouilleux, B.; Pourchet-Gellez, M.; Dumez, J.-N.; Giraudeau, P. Ultrafast Double-Quantum NMR Spectroscopy with Optimized Sensitivity for the Analysis of Mixtures. *The Analyst* **2016**, *141* (5), 1686–1692. https://doi.org/10.1039/C6AN00089D.

(13) Foley, D. A.; Dunn, A. L.; Zell, M. T. Reaction Monitoring Using Online vs Tube NMR Spectroscopy: Seriously Different Results: Online vs Tube NMR: A Kinetic Evaluation of NMR Reaction Monitoring Approaches. *Magn. Reson. Chem.* **2016**, *54* (6), 451–456. https://doi.org/10.1002/mrc.4259.

(14) Foley, D. A.; Bez, E.; Codina, A.; Colson, K. L.; Fey, M.; Krull, R.; Piroli, D.; Zell, M. T.; Marquez, B. L. NMR Flow Tube for Online NMR Reaction Monitoring. *Anal. Chem.* **2014**, *86* (24), 12008–12013. https://doi.org/10.1021/ac502300q.

(15) Khajeh, M.; Bernstein, M. A.; Morris, G. A. A Simple Flowcell for Reaction Monitoring by NMR. *Magn. Reson. Chem.* **2010**, *48* (7), 516–522. https://doi.org/10.1002/mrc.2610.

(16) Blackmond, D. G. Kinetic Profiling of Catalytic Organic Reactions as a Mechanistic Tool. *J. Am. Chem. Soc.* **2015**, *137* (34), 10852–10866. https://doi.org/10.1021/jacs.5b05841.

(17) Brecker, L.; Urdl, P.; Schmid, W.; Griengl, H.; Ribbons, D. W. Simple Device to Monitor Aerobic Biotransformations by in Situ 1H-NMR. *Biotechnol. Lett.* **2000**, *22*, 1135–1141.

(18) Wang, Y.; Pedersen, C. M.; Qiao, Y.; Deng, T.; Shi, J.; Hou, X. In Situ NMR Spectroscopy: Inulin Biomass Conversion in ZnCl 2 Molten Salt Hydrate Medium—SnCl 4 Addition Controls Product Distribution. *Carbohydr. Polym.* **2015**, *115*, 439–443. https://doi.org/10.1016/j.carbpol.2014.09.011.

(19) Amato, M. E.; Ansanelli, G.; Fisichella, S.; Lamanna, R.; Scarlata, G.; Sobolev, A. P.; Segre, A. Wheat Flour Enzymatic Amylolysis Monitored by in Situ ^{1} H NMR Spectroscopy. *J. Agric. Food Chem.* **2004**, *52* (4), 823–831. https://doi.org/10.1021/jf035188v.
(20) Sahoo, S. K.; Liu, W.; Samuelson, L. A.; Kumar, J.; Cholli, A. L. Biocatalytic Polymerization of *p* -Cresol: An in-Situ NMR Approach To Understand the Coupling Mechanism. *Macromolecules* **2002**, *35* (27), 9990–9998. https://doi.org/10.1021/ma021142b.
(21) Stanisavljev, D.; Begović, N.; Žujović, Z.; Vučelić, D.; Bačić, G. ^{1} H NMR Monitoring of Water Behavior during the Bray−Liebhafsky Oscillatory Reaction. *J. Phys. Chem. A* **1998**, *102* (35), 6883–6886. https://doi.org/10.1021/jp980803x.
(22) Mills, A.; O'Rourke, C. In Situ, Simultaneous Irradiation and Monitoring of a Photocatalyzed Organic Oxidation Reaction in a TiO_2 -Coated NMR Tube. *J. Org. Chem.* **2015**, *80* (20), 10342–10345. https://doi.org/10.1021/acs.joc.5b01001.
(23) Ferreira Gomes, B.; Ferreira da Silva, P.; Silva Lobo, C. M.; da Silva Santos, M.; Colnago, L. A. Strong Magnetoelectrolysis Effect during Electrochemical Reaction Monitored in Situ by High-Resolution NMR Spectroscopy. *Anal. Chim. Acta* **2017**, *983*, 91–95. https://doi.org/10.1016/j.aca.2017.06.008.
(24) Bussy, U.; Giraudeau, P.; Silvestre, V.; Jaunet-Lahary, T.; Ferchaud-Roucher, V.; Krempf, M.; Akoka, S.; Tea, I.; Boujtita, M. In Situ NMR Spectroelectrochemistry for the Structure Elucidation of Unstable Intermediate Metabolites. *Anal. Bioanal. Chem.* **2013**, *405* (17), 5817–5824. https://doi.org/10.1007/s00216-013-6977-z.
(25) Stepanov, A. G.; Arzumanov, S. S.; Ernst, H.; Freude, D. 1H MAS NMR Monitoring of the 13C-Labeled Carbon Scrambling for Propane in Zeolite H-ZSM-5. *Chem. Phys. Lett.* **2006**, *420* (4–6), 574–576. https://doi.org/10.1016/j.cplett.2005.12.070.
(26) Nunes, L. M. S.; Moraes, T. B.; Barbosa, L. L.; Mazo, L. H.; Colnago, L. A. Monitoring Electrochemical Reactions in Situ Using Steady-State Free Precession 13C NMR Spectroscopy. *Anal. Chim. Acta* **2014**, *850*, 1–5. https://doi.org/10.1016/j.aca.2014.05.022.
(27) Shapiro, M. J.; Kumaravel, G.; Petter, R. C.; Beveridge, R. 19F NMR Monitoring of a SNAr Reaction on Solid Support. *Tetrahedron Lett.* **1996**, *37* (27), 4671–4674. https://doi.org/10.1016/0040-4039(96)00960-4.
(28) Salvino, J. M.; Patel, S.; Drew, M.; Krowlikowski, P.; Orton, E.; Kumar, N. V.; Caulfield, T.; Labaudiniere, R. Synthesis of a New Fluoro-Wang Resin for Solid-Phase Reaction Monitoring by ^{19} F NMR Spectroscopy. *J. Comb. Chem.* **2001**, *3* (2), 177–180. https://doi.org/10.1021/cc000076r.
(29) Portnoy, M.; Milstein, D. Mechanism of Aryl Chloride Oxidative Addition to Chelated Palladium(0) Complexes. *Organometallics* **1993**, *12* (5), 1665–1673. https://doi.org/10.1021/om00029a026.
(30) Bancroft, D. P.; Lepre, C. A.; Lippard, S. J. Platinum-195 NMR Kinetic and Mechanistic Studies of Cis- and Trans-Diamminedichloroplatinum(II) Binding to DNA. *J. Am. Chem. Soc.* **1990**, *112* (19), 6860–6871. https://doi.org/10.1021/ja00175a020.
(31) Chan-Huot, M.; Lesot, P.; Pelupessy, P.; Duma, L.; Bodenhausen, G.; Duchambon, P.; Toney, M. D.; Reddy, U. V.; Suryaprakash, N. "On-the-Fly" Kinetics of Enzymatic Racemization Using Deuterium NMR in DNA-Based Chiral Oriented Media. *Anal. Chem.* **2013**, *85* (9), 4694–4697. https://doi.org/10.1021/ac4004002.
(32) Foley, D. A.; Wang, J.; Maranzano, B.; Zell, M. T.; Marquez, B. L.; Xiang, Y.; Reid, G. L. Online NMR and HPLC as a Reaction Monitoring Platform for Pharmaceutical Process Development. *Anal. Chem.* **2013**, *85* (19), 8928–8932. https://doi.org/10.1021/ac402382d.
(33) Brächer, A.; Hoch, S.; Albert, K.; Kost, H. J.; Werner, B.; von Harbou, E.; Hasse, H. Thermostatted Micro-Reactor NMR Probe Head for Monitoring Fast Reactions. *J. Magn. Reson.* **2014**, *242*, 155–161. https://doi.org/10.1016/j.jmr.2014.02.013.
(34) Brächer, A.; Behrens, R.; von Harbou, E.; Hasse, H. Application of a New Micro-Reactor 1 H NMR Probe Head for Quantitative Analysis of Fast Esterification Reactions. *Chem. Eng. J.* **2016**, *306*, 413–421. https://doi.org/10.1016/j.cej.2016.07.045.
(35) von Harbou, E.; Behrens, R.; Berje, J.; Brächer, A.; Hasse, H. Studying Fast Reaction Kinetics with Online NMR Spectroscopy. *Chem. Ing. Tech.* **2017**, *89* (4), 369–378. https://doi.org/10.1002/cite.201600068.

(36) Marquez, B.; Fey, M.; Colson, K. L.; Krull, R.; Bez, E.; Piroli, D.; Maas, W. E. NMR REACTION MONITORING FLOW CELL. US Patent 2012/0092013 A1, April 19, 2012.
(37) Hall, A. M. R.; Dong, P.; Codina, A.; Lowe, J. P.; Hintermair, U. Kinetics of Asymmetric Transfer Hydrogenation, Catalyst Deactivation, and Inhibition with Noyori Complexes As Revealed by Real-Time High-Resolution FlowNMR Spectroscopy. *ACS Catal.* **2019**, *9* (3), 2079–2090. https://doi.org/10.1021/acscatal.8b03530.
(38) Hall, A. M. R.; Broomfield-Tagg, R.; Camilleri, M.; Carbery, D. R.; Codina, A.; Whittaker, D. T. E.; Coombes, S.; Lowe, J. P.; Hintermair, U. Online Monitoring of a Photocatalytic Reaction by Real-Time High Resolution FlowNMR Spectroscopy. *Chem. Commun.* **2018**, *54* (1), 30–33. https://doi.org/10.1039/C7CC07059D.
(39) Maiwald, M.; Fischer, H. H.; Kim, Y.-K.; Albert, K.; Hasse, H. Quantitative High-Resolution on-Line NMR Spectroscopy in Reaction and Process Monitoring. *J. Magn. Reson.* **2004**, *166* (2), 135–146. https://doi.org/10.1016/j.jmr.2003.09.003.
(40) Bernstein, M. A.; Štefinović, M.; Sleigh, C. J. Optimising Reaction Performance in the Pharmaceutical Industry by Monitoring with NMR. *Magn. Reson. Chem.* **2007**, *45* (7), 564–571. https://doi.org/10.1002/mrc.2007.
(41) Farley, K. A.; Reilly, U.; Anderson, D. P.; Boscoe, B. P.; Bundesmann, M. W.; Foley, D. A.; Lall, M. S.; Li, C.; Reese, M. R.; Yan, J. Utilizing On- and off-Line Monitoring Tools to Follow a Kinetic Resolution Step during Flow Synthesis: Utilizing on- and off-Line Monitoring Tools during Flow Synthesis. *Magn. Reson. Chem.* **2017**, *55* (4), 348–354. https://doi.org/10.1002/mrc.4494.
(42) Zientek, N.; Laurain, C.; Meyer, K.; Kraume, M.; Guthausen, G.; Maiwald, M. Simultaneous 19F–1H Medium Resolution NMR Spectroscopy for Online Reaction Monitoring. *J. Magn. Reson.* **2014**, *249*, 53–62. https://doi.org/10.1016/j.jmr.2014.10.007.
(43) Jacquemmoz, C.; Giraud, F.; Dumez, J.-N. Online Reaction Monitoring by Single-Scan 2D NMR under Flow Conditions. *The Analyst* **2020**, *145* (2), 478–485. https://doi.org/10.1039/C9AN01758E.
(44) Jones, A. C.; Sanders, A. W.; Sikorski, W. H.; Jansen, K. L.; Reich, H. J. Reactivity of the Triple Ion and Separated Ion Pair of Tris(Trimethylsilyl)Methyllithium with Aldehydes: A RINMR Study. *J. Am. Chem. Soc.* **2008**, *130* (19), 6060–6061. https://doi.org/10.1021/ja8003528.
(45) Chance, B. THE ACCELERATED FLOW METHOD FOR RAPID REACTIONS. Part 2. *J. Frankl. Inst.* **1940**, *229* (6), 737–766. https://doi.org/10.1016/S0016-0032(40)90963-2.
(46) Kühne, R. O.; Schaffhauser, T.; Wokaun, A.; Ernst, R. R. Study of Transient Chemical Reactions by NMR. Fast Stopped-Flow Fourier Transform Experiments. *J. Magn. Reson. 1969* **1979**, *35* (1), 39–67. https://doi.org/10.1016/0022-2364(79)90077-5.
(47) Christianson, M. D.; Tan, E. H. P.; Landis, C. R. Stopped-Flow NMR: Determining the Kinetics of [*Rac* -(C_2H_4(1-Indenyl)$_2$)ZrMe][MeB(C_6F_5)$_3$]-Catalyzed Polymerization of 1-Hexene by Direct Observation. *J. Am. Chem. Soc.* **2010**, *132* (33), 11461–11463. https://doi.org/10.1021/ja105107y.
(48) Dunn, A. L.; Landis, C. R. Stopped-Flow NMR and Quantitative GPC Reveal Unexpected Complexities for the Mechanism of NHC-Catalyzed Lactide Polymerization. *Macromolecules* **2017**, *50* (6), 2267–2275. https://doi.org/10.1021/acs.macromol.6b02139.
(49) McGarrity, J. F.; Prodolliet, J.; Smyth, T. Rapid Injection NMR: A Simple Technique for the Observation of Reactive Intermediates. *Org. Magn. Reson.* **1981**, *17* (1), 59–65. https://doi.org/10.1002/mrc.1270170114.
(50) Denmark, S. E.; Williams, B. J.; Eklov, B. M.; Pham, S. M.; Beutner, G. L. Design, Validation, and Implementation of a Rapid-Injection NMR System. *J. Org. Chem.* **2010**, *75* (16), 5558–5572. https://doi.org/10.1021/jo100837a.
(51) Jones, A. C.; Sanders, A. W.; Bevan, M. J.; Reich, H. J. Reactivity of Individual Organolithium Aggregates: A RINMR Study of *n* -Butyllithium and 2-Methoxy-6-(Methoxymethyl)Phenyllithium. *J. Am. Chem. Soc.* **2007**, *129* (12), 3492–3493. https://doi.org/10.1021/ja0689334.
(52) Plessel, K. N.; Jones, A. C.; Wherritt, D. J.; Maksymowicz, R. M.; Poweleit, EricT.; Reich, H. J. A Rapid Injection NMR Study of the Reaction of Organolithium Reagents with Esters, Amides, and Ketones. *Org. Lett.* **2015**, *17* (10), 2310–2313. https://doi.org/10.1021/acs.orglett.5b00650.

(53) Thomas, A. A.; Denmark, S. E. Pre-Transmetalation Intermediates in the Suzuki-Miyaura Reaction Revealed: The Missing Link. *Science* **2016**, *352* (6283), 329–332. https://doi.org/10.1126/science.aad6981.
(54) Fratila, R. M.; Velders, A. H. Small-Volume Nuclear Magnetic Resonance Spectroscopy. *Annu. Rev. Anal. Chem.* **2011**, *4* (1), 227–249. https://doi.org/10.1146/annurev-anchem-061010-114024.
(55) Olson, D. L.; Peck, T. L.; Webb, A. G.; Magin, R. L.; Sweedler, J. V. High-Resolution Microcoil 1H-NMR for Mass-Limited, Nanoliter-Volume Samples. *Science* **1995**, *270* (5244), 1967–1970. https://doi.org/10.1126/science.270.5244.1967.
(56) Gomez, M. V.; Verputten, H. H. J.; Díaz-Ortíz, A.; Moreno, A.; de la Hoz, A.; Velders, A. H. On-Line Monitoring of a Microwave-Assisted Chemical Reaction by Nanolitre NMR-Spectroscopy. *Chem. Commun.* **2010**, *46* (25), 4514. https://doi.org/10.1039/b924936b.
(57) Carret, G.; Berthelot, T.; Berthault, P. Inductive Coupling and Flow for Increased NMR Sensitivity. *Anal. Chem.* **2018**, *90* (19), 11169–11173. https://doi.org/10.1021/acs.analchem.8b01775.
(58) Cerofolini, L.; Giuntini, S.; Barbieri, L.; Pennestri, M.; Codina, A.; Fragai, M.; Banci, L.; Luchinat, E.; Ravera, E. Real-Time Insights into Biological Events: In-Cell Processes and Protein-Ligand Interactions. *Biophys. J.* **2019**, *116* (2), 239–247. https://doi.org/10.1016/j.bpj.2018.11.3132.
(59) Tabatabaei Anaraki, M.; Dutta Majumdar, R.; Wagner, N.; Soong, R.; Kovacevic, V.; Reiner, E. J.; Bhavsar, S. P.; Ortiz Almirall, X.; Lane, D.; Simpson, M. J.; Heumann, H.; Schmidt, S.; Simpson, A. J. Development and Application of a Low-Volume Flow System for Solution-State *in Vivo* NMR. *Anal. Chem.* **2018**, *90* (13), 7912–7921. https://doi.org/10.1021/acs.analchem.8b00370.
(60) Jeener, J. Ampere Summer School, 1971.
(61) Aue, W. P.; Bartholdi, E.; Ernst, R. R. Two-dimensional Spectroscopy. Application to Nuclear Magnetic Resonance. *J. Chem. Phys.* **1976**, *64* (5), 2229–2246. https://doi.org/10.1063/1.432450.
(62) Davis, D. G.; Bax, A. Assignment of Complex Proton NMR Spectra via Two-Dimensional Homonuclear Hartmann-Hahn Spectroscopy. *J. Am. Chem. Soc.* **1985**, *107* (9), 2820–2821. https://doi.org/10.1021/ja00295a052.
(63) Bax, A.; Freeman, R.; Kempsell, S. P. Natural Abundance Carbon-13-Carbon-13 Coupling Observed via Double-Quantum Coherence. *J. Am. Chem. Soc.* **1980**, *102* (14), 4849–4851. https://doi.org/10.1021/ja00534a056.
(64) Rance, M.; Sørensen, O. W.; Leupin, W.; Kogler, H.; Wüthrich°, K.; Ernst, R. R. Uniform Excitation of Multiple-Quantum Coherence. Application to Two-Dimensional Double-Quantum Spectroscopy. *J. Magn. Reson. 1969* **1985**, *61* (1), 67–80. https://doi.org/10.1016/0022-2364(85)90268-9.
(65) Baishya, B.; Reddy, G. N. M.; Prabhu, U. R.; Row, T. N. G.; Suryaprakash, N. Simplifying the Complex ^{1} H NMR Spectra of Fluorine-Substituted Benzamides by Spin System Filtering and Spin-State Selection: Multiple-Quantum−Single-Quantum Correlation. *J. Phys. Chem. A* **2008**, *112* (42), 10526–10532. https://doi.org/10.1021/jp8055174.
(66) G. N., M. R.; Caldarelli, S. Demixing of Severely Overlapping NMR Spectra through Multiple-Quantum NMR. *Anal. Chem.* **2010**, *82* (8), 3266–3269. https://doi.org/10.1021/ac100009y.
(67) Reddy, G. N. M.; Caldarelli, S. Maximum-Quantum (MaxQ) NMR for the Speciation of Mixtures of Phenolic Molecules. *Chem. Commun.* **2011**, *47* (14), 4297. https://doi.org/10.1039/c1cc10226e.
(68) Manjunatha Reddy, G. N.; Mannina, L.; Sobolev, A. P.; Caldarelli, S. Polyphenols Fingerprinting in Olive Oils Through Maximum-Quantum NMR Spectroscopy. *Food Anal. Methods* **2018**, *11* (4), 1012–1020. https://doi.org/10.1007/s12161-017-1069-x.
(69) Aue, W. P.; Karhan, J.; Ernst, R. R. Homonuclear Broad Band Decoupling and Two-dimensional J-resolved NMR Spectroscopy. *J. Chem. Phys.* **1976**, *64* (10), 4226–4227. https://doi.org/10.1063/1.431994.
(70) Ludwig, C.; Viant, M. R. Two-Dimensional J-Resolved NMR Spectroscopy: Review of a Key Methodology in the Metabolomics Toolbox. *Phytochem. Anal.* **2010**, *21* (1), 22–32. https://doi.org/10.1002/pca.1186.

(71) Kumar, A.; Wagner, G.; Ernst, R. R.; Wuethrich, K. Buildup Rates of the Nuclear Overhauser Effect Measured by Two-Dimensional Proton Magnetic Resonance Spectroscopy: Implications for Studies of Protein Conformation. *J. Am. Chem. Soc.* **1981**, *103*, 3654–3658.
(72) Davis, D. G.; Bax, A. Separation of Chemical Exchange and Cross-Relaxation Effects in Two-Dimensional NMR Spectroscopy. *J. Magn. Reson. 1969* **1985**, *64* (3), 533–535. https://doi.org/10.1016/0022-2364(85)90119-2.
(73) Maudsley, A. A.; Ernst, R. R. Indirect Detection of Magnetic Resonance by Heteronuclear Two-Dimensional Spectroscopy. *Chem. Phys. Lett.* **1977**, *50* (3), 368–372. https://doi.org/10.1016/0009-2614(77)80345-X.
(74) Bodenhausen, G.; Ruben, D. Natural Abundance Nitrogen-15 NMR by Enhanced Heteronuclear Spectroscopy. *Chem. Phys. Lett.* **1980**, *69* (1), 185–189.
(75) Evans, R. The Interpretation of Small Molecule Diffusion Coefficients: Quantitative Use of Diffusion-Ordered NMR Spectroscopy. *Prog. Nucl. Magn. Reson. Spectrosc.* **2019**, S0079656519300585. https://doi.org/10.1016/j.pnmrs.2019.11.002.
(76) Tanner, J. E. Use of the Stimulated Echo in NMR Diffusion Studies. *J. Chem. Phys.* **1970**, *52* (5), 2523–2526. https://doi.org/10.1063/1.1673336.
(77) Sinnaeve, D. The Stejskal-Tanner Equation Generalized for Any Gradient Shape-an Overview of Most Pulse Sequences Measuring Free Diffusion. *Concepts Magn. Reson. Part A* **2012**, *40A* (2), 39–65. https://doi.org/10.1002/cmr.a.21223.
(78) Morris, K. F.; Johnson, C. S. Diffusion-Ordered Two-Dimensional Nuclear Magnetic Resonance Spectroscopy. *J. Am. Chem. Soc.* **1992**, *114* (8), 3139–3141. https://doi.org/10.1021/ja00034a071.
(79) Gibbs, S. J.; Johnson, C. S. A PFG NMR Experiment for Accurate Diffusion and Flow Studies in the Presence of Eddy Currents. *J. Magn. Reson. 1969* **1991**, *93* (2), 395–402. https://doi.org/10.1016/0022-2364(91)90014-K.
(80) Wu, D. H.; Chen, A. D.; Johnson, C. S. An Improved Diffusion-Ordered Spectroscopy Experiment Incorporating Bipolar-Gradient Pulses. *J. Magn. Reson. A* **1995**, *115* (2), 260–264. https://doi.org/10.1006/jmra.1995.1176.
(81) Swan, I.; Reid, M.; Howe, P. W. A.; Connell, M. A.; Nilsson, M.; Moore, M. A.; Morris, G. A. Sample Convection in Liquid-State NMR: Why It Is Always with Us, and What We Can Do about It. *J. Magn. Reson.* **2015**, *252*, 120–129. https://doi.org/10.1016/j.jmr.2014.12.006.
(82) Jerschow, A.; Müller, N. Convection Compensation in Gradient Enhanced Nuclear Magnetic Resonance Spectroscopy. *J. Magn. Reson.* **1998**, *132* (1), 13–18. https://doi.org/10.1006/jmre.1998.1400.
(83) Wu, D.; Chen, A.; Johnson, Jr., C. S. Three-Dimensional Diffusion-Ordered NMR Spectroscopy: The Homonuclear COSY–DOSY Experiment. *J. Magn. Reson. A* **1996**, *121* (1), 88–91. https://doi.org/10.1006/jmra.1996.0142.
(84) Lucas, L. H.; Otto, W. H.; Larive, C. K. The 2D-J-DOSY Experiment: Resolving Diffusion Coefficients in Mixtures. *J. Magn. Reson.* **2002**, *156* (1), 138–145. https://doi.org/10.1006/jmre.2002.2536.
(85) Barjat, H.; Morris, G. A.; Swanson, A. G. A Three-Dimensional DOSY–HMQC Experiment for the High-Resolution Analysis of Complex Mixtures. *J. Magn. Reson.* **1998**, *131* (1), 131–138. https://doi.org/10.1006/jmre.1997.1332.
(86) Nilsson, M.; Gil, A. M.; Delgadillo, I.; Morris, G. A. Improving Pulse Sequences for 3D DOSY: COSY-IDOSY. *Chem. Commun.* **2005**, No. 13, 1737. https://doi.org/10.1039/b415099f.
(87) Birlirakis, N.; Guittet, E. A New Approach in the Use of Gradients for Size-Resolved 2D-NMR Experiments. *J. Am. Chem. Soc.* **1996**, *118* (51), 13083–13084. https://doi.org/10.1021/ja9627151.
(88) Nilsson, M.; Gil, A. M.; Delgadillo, I.; Morris, G. A. Improving Pulse Sequences for 3D Diffusion-Ordered NMR Spectroscopy: 2DJ-IDOSY. *Anal. Chem.* **2004**, *76* (18), 5418–5422. https://doi.org/10.1021/ac049174f.
(89) Stchedroff, M. J.; Kenwright, A. M.; Morris, G. A.; Nilsson, M.; Harris, R. K. 2D and 3D DOSY Methods for Studying Mixtures of Oligomeric Dimethylsiloxanes. *Phys. Chem. Chem. Phys.* **2004**, *6* (13), 3221. https://doi.org/10.1039/b403960b.

(90) Viel, S.; Caldarelli, S. Improved 3D DOSY-TOCSY Experiment for Mixture Analysis. *Chem. Commun.* **2008**, No. 17, 2013. https://doi.org/10.1039/b802789g.
(91) Vermillion, K.; Price, N. P. J. Stable Isotope-Enhanced Two- and Three-Dimensional Diffusion Ordered 13C NMR Spectroscopy (SIE-DOSY 13C NMR). *J. Magn. Reson.* **2009**, *198* (2), 209–214. https://doi.org/10.1016/j.jmr.2009.02.008.
(92) Trefi, S.; Gilard, V.; Balayssac, S.; Malet-Martino, M.; Martino, R. The Usefulness of 2D DOSY and 3D DOSY-COSY 1H NMR for Mixture Analysis: Application to Genuine and Fake Formulations of Sildenafil (Viagra). *Magn. Reson. Chem.* **2009**, *47* (S1), S163–S173. https://doi.org/10.1002/mrc.2490.
(93) Delsuc, M. A.; Malliavin, T. E. Maximum Entropy Processing of DOSY NMR Spectra. *Anal. Chem.* **1998**, *70* (10), 2146–2148. https://doi.org/10.1021/ac9800715.
(94) Antalek, B.; Windig, W. Generalized Rank Annihilation Method Applied to a Single Multicomponent Pulsed Gradient Spin Echo NMR Data Set. *J. Am. Chem. Soc.* **1996**, *118* (42), 10331–10332. https://doi.org/10.1021/ja962172v.
(95) Pons, J.-L.; Malliavin, T.; Delsuc, MarcA. Gifa V. 4: A Complete Package for NMR Data Set Processing. *J. Biomol. NMR* **1996**, *8* (4). https://doi.org/10.1007/BF00228146.
(96) Nilsson, M. The DOSY Toolbox: A New Tool for Processing PFG NMR Diffusion Data. *J. Magn. Reson.* **2009**, *200* (2), 296–302. https://doi.org/10.1016/j.jmr.2009.07.022.
(97) Schanda, P.; Van Melckebeke, H.; Brutscher, B. Speeding Up Three-Dimensional Protein NMR Experiments to a Few Minutes. *J. Am. Chem. Soc.* **2006**, *128* (28), 9042–9043. https://doi.org/10.1021/ja062025p.
(98) Kupče, E.; Freeman, R. Fast Multidimensional NMR by Polarization Sharing. *Magn. Reson. Chem.* **2007**, *45* (1), 2–4. https://doi.org/10.1002/mrc.1931.
(99) Vitorge, B.; Bodenhausen, G.; Pelupessy, P. Speeding up Nuclear Magnetic Resonance Spectroscopy by the Use of SMAll Recovery Times – SMART NMR. *J. Magn. Reson.* **2010**, *207* (1), 149–152. https://doi.org/10.1016/j.jmr.2010.07.017.
(100) Haase, A.; Frahm, J.; Matthaei, D. FLASH Imaging. Rapid NMR Imaging Using Low Flip-Angle Pulses. *J. Magn. Reson.* **1986**, *67* (2), 258–266. https://doi.org/10.1016/0022-2364(86)90433-6.
(101) Barna, J. C. J.; Laue, E. D.; Mayger, M. R.; Skilling, J.; Worrall, S. J. P. Exponential Sampling, an Alternative Method for Sampling in Two-Dimensional NMR Experiments. *J. Magn. Reson. 1969* **1987**, *73* (1), 69–77. https://doi.org/10.1016/0022-2364(87)90225-3.
(102) Schmieder, P.; Stern, A. S.; Wagner, G.; Hoch, J. C. Improved Resolution in Triple-Resonance Spectra by Nonlinear Sampling in the Constant-Time Domain. *J. Biomol. NMR* **1994**, *4* (4), 483–490. https://doi.org/10.1007/BF00156615.
(103) Kupče, Ē.; Freeman, R. Projection−Reconstruction of Three-Dimensional NMR Spectra. *J. Am. Chem. Soc.* **2003**, *125* (46), 13958–13959. https://doi.org/10.1021/ja038297z.
(104) Kim, S.; Szyperski, T. GFT NMR, a New Approach To Rapidly Obtain Precise High-Dimensional NMR Spectral Information. *J. Am. Chem. Soc.* **2003**, *125* (5), 1385–1393. https://doi.org/10.1021/ja028197d.
(105) Orekhov, V. Y.; Ibraghimov, I. V.; Billeter, M. MUNIN: A New Approach to Multi-Dimensional NMR Spectra Interpretation. *J. Biomol. NMR* **2001**, *20*, 49–60.
(106) Kazimierczuk, K.; Koźmiński, W.; Zhukov, I. Two-Dimensional Fourier Transform of Arbitrarily Sampled NMR Data Sets. *J. Magn. Reson.* **2006**, *179* (2), 323–328. https://doi.org/10.1016/j.jmr.2006.02.001.
(107) Barna, J. C. J.; Laue, E. D. Conventional and Exponential Sampling for 2D NMR Experiments with Application to a 2D NMR Spectrum of a Protein. *J. Magn. Reson. 1969* **1987**, *75* (2), 384–389. https://doi.org/10.1016/0022-2364(87)90047-3.
(108) Schmieder, P.; Stern, AlanS.; Wagner, G.; Hoch, JeffreyC. Application of Nonlinear Sampling Schemes to COSY-Type Spectra. *J. Biomol. NMR* **1993**, *3* (5). https://doi.org/10.1007/BF00174610.
(109) Hyberts, S. G.; Heffron, G. J.; Tarragona, N. G.; Solanky, K.; Edmonds, K. A.; Luithardt, H.; Fejzo, J.; Chorev, M.; Aktas, H.; Colson, K.; Falchuk, K. H.; Halperin, J. A.; Wagner, G. Ultrahigh-Resolution ^{1}H− ^{13}C HSQC Spectra of Metabolite Mixtures Using Nonlinear

Sampling and Forward Maximum Entropy Reconstruction. *J. Am. Chem. Soc.* **2007**, *129* (16), 5108–5116. https://doi.org/10.1021/ja068541x.
(110) Lustig, M.; Donoho, D.; Pauly, J. M. Sparse MRI: The Application of Compressed Sensing for Rapid MR Imaging. *Magn. Reson. Med.* **2007**, *58* (6), 1182–1195. https://doi.org/10.1002/mrm.21391.
(111) Windig, W.; Antalek, B. Direct Exponential Curve Resolution Algorithm (DECRA): A Novel Application of the Generalized Rank Annihilation Method for a Single Spectral Mixture Data Set with Exponentially Decaying Contribution Profiles. *Chemom. Intell. Lab. Syst.* **1997**, *37* (2), 241–254. https://doi.org/10.1016/S0169-7439(97)00028-2.
(112) Urbańczyk, M.; Koźmiński, W.; Kazimierczuk, K. Accelerating Diffusion-Ordered NMR Spectroscopy by Joint Sparse Sampling of Diffusion and Time Dimensions. *Angew. Chem. Int. Ed.* **2014**, *53* (25), 6464–6467. https://doi.org/10.1002/anie.201402049.
(113) Pelta, M. D.; Morris, G. A.; Stchedroff, M. J.; Hammond, S. J. A One-Shot Sequence for High-Resolution Diffusion-Ordered Spectroscopy. *Magn. Reson. Chem.* **2002**, *40* (13), S147–S152. https://doi.org/10.1002/mrc.1107.
(114) Mansfield, P. Spatial Mapping of the Chemical Shift in NMR. *Magn. Reson. Med.* **1984**, *1* (3), 370–386. https://doi.org/10.1002/mrm.1910010308.
(115) Pelupessy, P. Adiabatic Single Scan Two-Dimensional NMR Spectrocopy. *J. Am. Chem. Soc.* **2003**, *125* (40), 12345–12350. https://doi.org/10.1021/ja034958g.
(116) Tal, A.; Shapira, B.; Frydman, L. A Continuous Phase-Modulated Approach to Spatial Encoding in Ultrafast 2D NMR Spectroscopy. *J. Magn. Reson.* **2005**, *176* (1), 107–114. https://doi.org/10.1016/j.jmr.2005.05.009.
(117) Pelupessy, P.; Duma, L.; Bodenhausen, G. Improving Resolution in Single-Scan 2D Spectroscopy. *J. Magn. Reson.* **2008**, *194* (2), 169–174. https://doi.org/10.1016/j.jmr.2008.06.023.
(118) Shrot, Y.; Frydman, L. Spatial/Spectral Encoding of the Spin Interactions in Ultrafast Multidimensional NMR. *J. Chem. Phys.* **2009**, *131* (22), 224516. https://doi.org/10.1063/1.3266422.
(119) Giraudeau, P.; Akoka, S. A New Detection Scheme for Ultrafast 2D J-Resolved Spectroscopy. *J. Magn. Reson.* **2007**, *186* (2), 352–357. https://doi.org/10.1016/j.jmr.2007.03.007.
(120) Gouilleux, B.; Rouger, L.; Giraudeau, P. Ultrafast 2D NMR: Methods and Applications. In *Annual Reports on NMR Spectroscopy*; Elsevier, 2018; Vol. 93, pp 75–144. https://doi.org/10.1016/bs.arnmr.2017.08.003.
(121) Mishkovsky, M.; Frydman, L. Interlaced Fourier Transformation of Ultrafast 2D NMR Data. *J. Magn. Reson.* **2005**, *173* (2), 344–350. https://doi.org/10.1016/j.jmr.2005.01.007.
(122) Giraudeau, P.; Akoka, S. Sensitivity and Lineshape Improvement in Ultrafast 2D NMR by Optimized Apodization in the Spatially Encoded Dimension. *Magn. Reson. Chem.* **2011**, *49* (6), 307–313. https://doi.org/10.1002/mrc.2746.
(123) Giraudeau, P. Quantitative 2D Liquid-State NMR: Quantitative 2D NMR. *Magn. Reson. Chem.* **2014**, *52* (6), 259–272. https://doi.org/10.1002/mrc.4068.
(124) Rouger, L.; Gouilleux, B.; Pourchet-Gellez, M.; Dumez, J.-N.; Giraudeau, P. Ultrafast Double-Quantum NMR Spectroscopy with Optimized Sensitivity for the Analysis of Mixtures. *The Analyst* **2016**, *141* (5), 1686–1692. https://doi.org/10.1039/C6AN00089D.
(125) Giraudeau, P.; Massou, S.; Robin, Y.; Cahoreau, E.; Portais, J.-C.; Akoka, S. Ultrafast Quantitative 2D NMR: An Efficient Tool for the Measurement of Specific Isotopic Enrichments in Complex Biological Mixtures. *Anal. Chem.* **2011**, *83* (8), 3112–3119. https://doi.org/10.1021/ac200007p.
(126) Shapira, B.; Karton, A.; Aronzon, D.; Frydman, L. Real-Time 2D NMR Identification of Analytes Undergoing Continuous Chromatographic Separation. *J. Am. Chem. Soc.* **2004**, *126* (4), 1262–1265. https://doi.org/10.1021/ja0389422.
(127) Queiroz Júnior, L. H. K.; Queiroz, D. P. K.; Dhooghe, L.; Ferreira, A. G.; Giraudeau, P. Real-Time Separation of Natural Products by Ultrafast 2D NMR Coupled to on-Line HPLC. *The Analyst* **2012**, *137* (10), 2357. https://doi.org/10.1039/c2an16208c.

(128) Gal, M.; Mishkovsky, M.; Frydman, L. Real-Time Monitoring of Chemical Transformations by Ultrafast 2D NMR Spectroscopy. *J. Am. Chem. Soc.* **2006**, *128* (3), 951–956. https://doi.org/10.1021/ja0564158.
(129) Herrera, A.; Fernández-Valle, E.; Martínez-Álvarez, R.; Molero, D.; Pardo, Z. D.; Sáez, E.; Gal, M. Real-Time Monitoring of Organic Reactions with Two-Dimensional Ultrafast TOCSY NMR Spectroscopy. *Angew. Chem. Int. Ed.* **2009**, *48* (34), 6274–6277. https://doi.org/10.1002/anie.200902387.
(130) Fernández, I.; Fernández-Valle, M. E.; Martínez-Álvarez, R.; Molero-Vílchez, D.; Pardo, Z. D.; Sáez-Barajas, E.; Sánchez, Á.; Herrera, A. Discovering Mechanistic Insights by Application of *Tandem* Ultrafast Multidimensional NMR Techniques. *J. Org. Chem.* **2014**, *79* (17), 8086–8093. https://doi.org/10.1021/jo5012834.
(131) Boisseau, R.; Bussy, U.; Giraudeau, P.; Boujtita, M. *In Situ* Ultrafast 2D NMR Spectroelectrochemistry for Real-Time Monitoring of Redox Reactions. *Anal. Chem.* **2015**, *87* (1), 372–375. https://doi.org/10.1021/ac5041956.
(132) Gouilleux, B.; Charrier, B.; Danieli, E.; Dumez, J.-N.; Akoka, S.; Felpin, F.-X.; Rodriguez-Zubiri, M.; Giraudeau, P. Real-Time Reaction Monitoring by Ultrafast 2D NMR on a Benchtop Spectrometer. *The Analyst* **2015**, *140* (23), 7854–7858. https://doi.org/10.1039/C5AN01998B.
(133) Frydman, L.; Blazina, D. Ultrafast Two-Dimensional Nuclear Magnetic Resonance Spectroscopy of Hyperpolarized Solutions. *Nat. Phys.* **2007**, *3* (6), 415–419. https://doi.org/10.1038/nphys597.
(134) Mishkovsky, M.; Frydman, L. Progress in Hyperpolarized Ultrafast 2D NMR Spectroscopy. *ChemPhysChem* **2008**, *9* (16), 2340–2348. https://doi.org/10.1002/cphc.200800461.
(135) Giraudeau, P.; Shrot, Y.; Frydman, L. Multiple Ultrafast, Broadband 2D NMR Spectra of Hyperpolarized Natural Products. *J. Am. Chem. Soc.* **2009**, *131* (39), 13902–13903. https://doi.org/10.1021/ja905096f.
(136) Daniele, V.; Legrand, F.-X.; Berthault, P.; Dumez, J.-N.; Huber, G. Single-Scan Multidimensional NMR Analysis of Mixtures at Sub-Millimolar Concentrations by Using SABRE Hyperpolarization. *ChemPhysChem* **2015**, *16* (16), 3413–3417. https://doi.org/10.1002/cphc.201500535.
(137) Thrippleton, M. J.; Loening, N. M.; Keeler, J. A Fast Method for the Measurement of Diffusion Coefficients: One-Dimensional DOSY. *Magn. Reson. Chem.* **2003**, *41* (6), 441–447. https://doi.org/10.1002/mrc.1195.
(138) Loening, N. M.; Keeler, J.; Morris, G. A. One-Dimensional DOSY. *J. Magn. Reson.* **2001**, *153* (1), 103–112. https://doi.org/10.1006/jmre.2001.2423.
(139) Shrot, Y.; Frydman, L. Single-Scan 2D DOSY NMR Spectroscopy. *J. Magn. Reson.* **2008**, *195* (2), 226–231. https://doi.org/10.1016/j.jmr.2008.09.011.
(140) Hamdoun, G.; Guduff, L.; van Heijenoort, C.; Bour, C.; Gandon, V.; Dumez, J.-N. Spatially Encoded Diffusion-Ordered NMR Spectroscopy of Reaction Mixtures in Organic Solvents. *The Analyst* **2018**, *143* (14), 3458–3464. https://doi.org/10.1039/C8AN00434J.
(141) Ahola, S.; Zhivonitko, V. V.; Mankinen, O.; Zhang, G.; Kantola, A. M.; Chen, H.-Y.; Hilty, C.; Koptyug, I. V.; Telkki, V.-V. Ultrafast Multidimensional Laplace NMR for a Rapid and Sensitive Chemical Analysis. *Nat. Commun.* **2015**, *6* (1). https://doi.org/10.1038/ncomms9363.
(142) Guduff, L.; Kurzbach, D.; van Heijenoort, C.; Abergel, D.; Dumez, J.-N. Single-Scan ^{13}C Diffusion-Ordered NMR Spectroscopy of DNP-Hyperpolarised Substrates. *Chem. - Eur. J.* **2017**, *23* (66), 16722–16727. https://doi.org/10.1002/chem.201703300.
(143) Guduff, L.; Berthault, P.; van Heijenoort, C.; Dumez, J.; Huber, G. Single-Scan Diffusion-Ordered NMR Spectroscopy of SABRE-Hyperpolarized Mixtures. *ChemPhysChem* **2019**, *20* (3), 392–398. https://doi.org/10.1002/cphc.201800983.
(144) Mankinen, O.; Hollenbach, J.; Ahola, S.; Matysik, J.; Telkki, V.-V. Ultrafast Laplace NMR with Hyperpolarized Xenon Gas. *Microporous Mesoporous Mater.* **2018**, *269*, 75–78. https://doi.org/10.1016/j.micromeso.2017.10.024.
(145) Herrera, A.; Fernández-Valle, E.; Martínez-Álvarez, R.; Molero-Vílchez, D.; Pardo-Botero, Z. D.; Sáez-Barajas, E. Monitoring Organic Reactions by UF-NMR Spectroscopy: Monitoring Organic Reactions by UF-NMR Spectroscopy. *Magn. Reson. Chem.* **2015**, *53* (11), 952–970. https://doi.org/10.1002/mrc.4240.

(146) Shrot, Y.; Frydman, L. Spatial Encoding Strategies for Ultrafast Multidimensional Nuclear Magnetic Resonance. *J. Chem. Phys.* **2008**, *128* (5), 052209. https://doi.org/10.1063/1.2834733.
(147) Valette, J.; Lethimonnier, F.; Lebon, V. About the Origins of NMR Diffusion-Weighting Induced by Frequency-Swept Pulses. *J. Magn. Reson.* **2010**, *205* (2), 255–259. https://doi.org/10.1016/j.jmr.2010.05.007.
(148) Dumez, J.-N. Spatial Encoding and Spatial Selection Methods in High-Resolution NMR Spectroscopy. *Prog. Nucl. Magn. Reson. Spectrosc.* **2018**, *109*, 101–134. https://doi.org/10.1016/j.pnmrs.2018.08.001.
(149) Guduff, L.; Kuprov, I.; van Heijenoort, C.; Dumez, J.-N. Spatially Encoded 2D and 3D Diffusion-Ordered NMR Spectroscopy. *Chem. Commun.* **2017**, *53* (4), 701–704. https://doi.org/10.1039/C6CC09028A.
(150) Gouilleux, B.; Charrier, B.; Akoka, S.; Felpin, F.-X.; Rodriguez-Zubiri, M.; Giraudeau, P. Ultrafast 2D NMR on a Benchtop Spectrometer: Applications and Perspectives. *TrAC Trends Anal. Chem.* **2016**, *83*, 65–75. https://doi.org/10.1016/j.trac.2016.01.014.
(151) Tal, A.; Frydman, L. Single-Scan Multidimensional Magnetic Resonance. *Prog. Nucl. Magn. Reson. Spectrosc.* **2010**, *57* (3), 241–292. https://doi.org/10.1016/j.pnmrs.2010.04.001.
(152) Renzi, P.; Hioe, J.; Gschwind, R. M. Enamine/Dienamine and Brønsted Acid Catalysis: Elusive Intermediates, Reaction Mechanisms, and Stereoinduction Modes Based on in Situ NMR Spectroscopy and Computational Studies. *Acc. Chem. Res.* **2017**, *50* (12), 2936–2948. https://doi.org/10.1021/acs.accounts.7b00320.
(153) Poli, R. THE ELUCIDATION OF MECHANISMS IN HOMOGENEOUS CATALYSIS. *Comments Inorg. Chem.* **2009**, *30* (5–6), 177–228. https://doi.org/10.1080/02603590903423942.
(154) Danieli, E.; Perlo, J.; Duchateau, A. L. L.; Verzijl, G. K. M.; Litvinov, V. M.; Blümich, B.; Casanova, F. On-Line Monitoring of Chemical Reactions by Using Bench-Top Nuclear Magnetic Resonance Spectroscopy. *ChemPhysChem* **2014**, *15* (14), 3060–3066. https://doi.org/10.1002/cphc.201402049.
(155) Hall, A. M. R.; Chouler, J. C.; Codina, A.; Gierth, P. T.; Lowe, J. P.; Hintermair, U. Practical Aspects of Real-Time Reaction Monitoring Using Multi-Nuclear High Resolution FlowNMR Spectroscopy. *Catal. Sci. Technol.* **2016**, *6* (24), 8406–8417. https://doi.org/10.1039/C6CY01754A.
(156) Maciejewski, M. W.; Qui, H. Z.; Rujan, I.; Mobli, M.; Hoch, J. C. Nonuniform Sampling and Spectral Aliasing. *J. Magn. Reson.* **2009**, *199* (1), 88–93. https://doi.org/10.1016/j.jmr.2009.04.006.
(157) Bodenhausen, G.; Ernst, R. R. The Accordion Experiment, a Simple Approach to Three-Dimensional NMR Spectroscopy. *J. Magn. Reson. 1969* **1981**, *45* (2), 367–373. https://doi.org/10.1016/0022-2364(81)90137-2.
(158) Fernández-Valle, M. E.; Martínez-Álvarez, R.; Molero-Vílchez, D.; Pardo, Z. D.; Sáez-Barajas, E.; Herrera, A. 2D Ultrafast HMBC ^{1}H, ^{31}P: Obtaining Mechanistic Details on the Michaelis–Arbuzov Reaction. *J. Org. Chem.* **2015**, *80* (2), 799–805. https://doi.org/10.1021/jo502253p.
(159) Queiroz, L. H. K.; Giraudeau, P.; dos Santos, F. A. B.; Oliveira, K. T.; Ferreira, A. G. Real-Time Mechanistic Monitoring of an Acetal Hydrolysis Using Ultrafast 2D NMR: Real-Time Mechanistic Monitoring of an Acetal Hydrolysis Using Ultrafast 2D NMR. *Magn. Reson. Chem.* **2012**, *50* (7), 496–501. https://doi.org/10.1002/mrc.3827.
(160) Shrot, Y.; Tal, A.; Frydman, L. New Developments in the Spatial Encoding of Spin Interactions for Single-Scan 2D NMR. *Magn. Reson. Chem.* **2009**, *47* (5), 415–422. https://doi.org/10.1002/mrc.2403.
(161) Gal, M.; Frydman, L. Ultrafast Multidimensional NMR: Principles and Practice of Single-Scan Methods. In *Encyclopedia of Magnetic Resonance*; Harris, R. K., Wasylishen, R., Eds.; John Wiley & Sons, Ltd: Chichester, UK, 2008; p emrstm1024. https://doi.org/10.1002/9780470034590.emrstm1024.
(162) Viel, S.; Caldarelli, S. Improved 3D DOSY-TOCSY Experiment for Mixture Analysis. *Chem. Commun.* **2008**, No. 17, 2013. https://doi.org/10.1039/b802789g.

(163) Millet, O.; Pons, M. A New Method for Measuring Diffusion Coefficients by 2D NMR Using Accordion Spectroscopy. *J. Magn. Reson.* **1998**, *131* (1), 166–169. https://doi.org/10.1006/jmre.1997.1351.
(164) Guennec, A. L.; Giraudeau, P.; Caldarelli, S.; Dumez, J.-N. Ultrafast Double-Quantum NMR Spectroscopy. *Chem. Commun.* **2015**, *51* (2), 354–357. https://doi.org/10.1039/C4CC07232D.

DOCTORAT MATIERE BRETAGNE MOLECULES LOIRE ET MATERIAUX

UNIVERSITÉ DE NANTES

Titre : RMN MULTIDIMENSIONNELLE ULTRARAPIDE POUR LE SUIVI DE RÉACTIONS CHIMIQUES

Mots clés : Résonance magnétique nucléaire, encodage spatial, suivi de réaction

Résumé : La RMN est un outil particulièrement puissant pour l'analyse de composés organiques et pour le suivi de réaction. De nombreuses expériences multidimensionnelles existent, mais, de par leur durée, ne peuvent pas être utilisées pour le suivi de réaction rapides. Cette thèse s'est intéressée à l'utilisation de l'encodage spatial, qui est la méthode permettant la plus grande accélération pour l'acquisition d'expériences multidimensionnelles. Une méthode très utile pour l'analyse de mélange est l'expérience DOSY (Diffusion Ordered SpectroscopY) qui permet de séparer les signaux en fonction du coefficient de diffusion des molécules. Dans un premier temps, l'influence de certains paramètres de l'expérience DOSY spatialement encodée a été étudiée et la possibilité d'annuler les artefacts dus à la convection a été adaptée sur ce type de séquence. Dans un second temps, un autre type d'expériences 2D a été étudié : les expériences multi quanta qui permettent de simplifier grandement l'analyse de certains mélanges. La possibilité d'encoder spatialement ces expériences a été prouvée et une optimisation de certains délais a été faite. Puis, elles ont été utilisées pour suivre une réaction d'hétéro Diels-Alder. La possibilité d'utiliser des expériences spatialement encodées sur une échantillon en flux a également été étudiée. Les interférences avec le flux ont été caractérisées, puis le suivi d'une réaction modèle a été réalisé ainsi qu'une mesure de sa cinétique. Enfin, il a également été démontré que l'encodage spatial permet d'accélérer certaines expériences de type 3D DOSY. Différentes séquences d'impulsion ont été comparées et l'influence de l'apodisation spatiale et de la non-uniformité des gradients sur le résultat obtenu a été démontrée.

Title: Ultrafast multidimensional NMR for reaction monitoring.

Keywords: Nuclear magnetic resonance, spatial encoding, reaction monitoring

Abstract: NMR is a powerful tool for organic compounds analysis and for reaction monitoring. Numerous multidimensional experiments exist, however, due to their duration, they cannot be used for fast reaction monitoring. This PhD work focused on the use of spatial encoding that is the method that allow the highest acceleration for the acquisition of multidimensional experiments. One experiment well suited for mixture analysis is DOSY (Diffusion ordered SpectroscopY) that separates signals out of the molecule's diffusion coefficients. First, the influence of several spatially encoded DOSY parameters have been studied and the possibility to cancel convection artifacts has been adapted on this spatially encoded experiment. Then, a second family of 2D experiments have been studied: multiple quantum spectra that help simplifying spectra for certain mixture analysis. The possibility to spatially encode this kind of experiment has been proven and an optimization of delays has been done. They also have been in order to monitor a hetero Diels-Alder reaction. The possibility to use spatially encoded experiments on flowing sample was studied. First, the interferences between the encodage and the flow have been characterized, then the reaction monitoring of a model reaction has been done and the kinteic fo the reaction was calculated. Finally, it was also demonstrated that the spatial encoding could be used in order to reduce the duration of 3D-DOSY experiments. Different pulse sequences have been compared, and the influence of spatial apodisation and of the gradient non-uniformity on the calculation of diffusion coefficients has been demonstrated.